INFORMATION TO USERS

This manuscript has been reproduced from the microfilm master. UMI films the text directly from the original or copy submitted. Thus, some thesis and dissertation copies are in typewriter face, while others may be from any type of computer printer.

The quality of this reproduction is dependent upon the quality of the copy submitted. Broken or indistinct print, colored or poor quality illustrations and photographs, print bleedthrough, substandard margins, and improper alignment can adversely affect reproduction.

In the unlikely event that the author did not send UMI a complete manuscript and there are missing pages, these will be noted. Also, if unauthorized copyright material had to be removed, a note will indicate the deletion.

Oversize materials (e.g., maps, drawings, charts) are reproduced by sectioning the original, beginning at the upper left-hand corner and continuing from left to right in equal sections with small overlaps. Each original is also photographed in one exposure and is included in reduced form at the back of the book.

Photographs included in the original manuscript have been reproduced xerographically in this copy. Higher quality 6" x 9" black and white photographic prints are available for any photographs or illustrations appearing in this copy for an additional charge. Contact UMI directly to order.

UMI

A Bell & Howell Information Company
300 North Zeeb Road, Ann Arbor MI 48106-1346 USA
313/761-4700 800/521-0600

A TIME-AVERAGED APPROACH TO WAVE EVOLUTION FROM DEEP WATER TO SHALLOW WATER

by

Jianlu Xu

B.E. (Hohai University) 1984
M.S. (University of Hawaii, Manoa) 1991

A dissertation submitted in partial satisfaction of the
requirements for the degree of

Doctor of Philosophy

in

ENGINEERING:

Civil Engineering

in the

GRADUATE DIVISION

of the

UNIVERSITY of CALIFORNIA, BERKELEY

Committee in charge:

Professor Rodney J. Sobey, Chair
Professor Mostafa A. Foda
Professor William C. Webster

1996

The dissertation of Jianlu Xu is approved :

R. J. Sobey 14 December 95

Chair Date

William G. Melott Dec. 15, 1995

Date

Dec 17, 1995

Date

University of California, Berkeley

1996

TABLE OF CONTENTS

ACKNOWLEDGMENTS

I wish to express my appreciation to the members of my dissertation committee, Professor Rodney J. Sobey, Professor Mostafa A. Foda and Professor William C. Webster, for their review of the manuscript and suggestions. I am particularly grateful to Professor Sobey for his inspiration over the last few years, and for all his assistance and advice during the course of this research.

I also owe a debt of gratitude to Professor Hsieh Wen Shen with whom I have numerous discussions when I was a research assistant. Though these discussions are not directly related to the current research, he taught me many practical and effective research approaches.

I would also like to sincerely thank Ms Dihua Zhao, a visiting scholar at UC Berkeley, for sharing her rich experience in numerical modeling. Also I want to thank fellow students Jingsong Lai and Chiming Huang for their friendship.

Finally, I wish to truly thank my wife, Su Yang, for her unflagging support and patience throughout this entire process.

This work was performed at the University of California, Berkeley, and made possible in part by financial support through the Lee Fellowship, a Graduate Research Assistantship for the Dan Francisco Bay/Delta Model and the Hans Albert Einstein Memorial Fellowship.

1 INTRODUCTION

1.1 Wave Transformation in Coastal Regions

The coastline, the boundary between land and sea, experiences continuous changes in shape and position upon the action of external forces. Depending on the characteristics of the external forcing, this change may have time scales ranging from geological time to a single wind-wave period, and spatial scales ranging from the size of a continent to the wave length of a sand ripple. To coastal engineers, the main concern is the short-term variations caused by small-scale, short-term fluid motions. One of the most common and most important short-term fluid motions of the sea water is wind waves which bring frequent and powerful hydrodynamic forces to the shallow areas of a coast.

In a wind field, waves form and grow by receiving energy from the wind. The scale and strength of the waves depend primarily on three factors: the wind velocity, a fetch length and a wind duration. The wind waves are three-dimensional in nature, and irregular in amplitude, period and direction. After leaving the wind field, the developed wind waves propagate across the ocean, dispersing and losing little of their energy. When the dispersed waves approach the coast, they transform into swells which are almost two-dimensional in shape, with nearly uniform periods and long crest-lines. As the water depth decreases toward the shoreline, swells exhibit characteristic shallow-water behavior similar to those of periodic waves. The shallow-water transformation commences when the waves "feel" the sea bottom and are affected by its presence. This means in return that the sea bottom receives some influences from the wave motion.

The salient features of wave transformation in the shallow sea are refraction and shoaling. Refraction is the consequence of a change in wave celerity with water depth, local

current velocity and wave period. Wave refraction tends to orient crest-lines parallel to bottom contours. Shoaling is the consequence of a change in propagation velocity of the wave energy flux. As the water shallows, the energy flux velocity generally decreases and the wave height increases. A shoaling wave finally breaks at the location where the water depth can not longer sustain the increase in wave height. The wave transformation may be further complicated by the presence of coastal structures and rugged bathymetry which may induce wave diffraction, reflection, and forced breaking.

From breaker line or zone, the waves proceed into the surf zone, a region of dynamic and complex fluid motions and of great energy dissipation. Considerable sand movement can occur in the surf zone, resulting in potentially significant bathymetric changes. On a uniformly sloping beach, waves will continue to break. On a beach where the slope becomes milder after breaking, the fluid motions tend to recover the properties of oscillatory waves (Horikawa 1989). In either case, wave breaking induces secondary motions in the surf zone, particularly turbulence and currents. These secondary motions in the surf zone, when energetic enough, may impact the incident waves in return.

Aside from the wave motion and turbulence, there also exist fluid motions at time scales longer than the wave period. Such fluid motions manifest themselves in the currents driven by either waves or tides or local winds. The nature of these currents is dependent on the forcing and on the local topography. In the surf zone, wave-current interaction becomes significant, and mean water surface elevations vary appreciably.

Wave-driven currents are commonly observed as undertows, longshore currents and rip currents. Besides wave forcing such as "radiation stresses" (Longuet-Higgins and Stewart 1964), the mass transport associated with wave motion (Sobey and Thieke 1989) and the

shoreline constraint all contribute to the formation of wave-driven currents. Though perhaps secondary in magnitude compared to the wave motion, the mean flow currents are of fundamental importance in net sediment and contaminant transport in the nearshore zone.

In summary, wave transformation in the nearshore zone governs the evolution of coastlines and beach profiles. Thus wave field data in a coastal region are essential to coastal engineering practice. It is the objective of this dissertation to develop a model for simulating wave transformation in coastal regions, in particular the evolution of mean flow circulation and wave-averaged parameters such as wave height and mean water surface elevations.

1.2 Methodology

As waves travel into shallow water, their dynamics becomes progressively more nonlinear and dissipative. The nonlinear behavior of wave propagation, coupled with the wave-current and wave-turbulence interactions, makes the nearshore zone, particularly the surf zone, hydrodynamically so complicated that many physical phenomena in the nearshore zone are still not fully understood.

Among various ways to deal with waves which are naturally irregular, the simplest and most convenient method is to reduce them to representative long-crested monochromatic waves, which enable us to use the rich knowledge on periodic waves. Within this broad approach, models for simulating wave propagation may be characterized in terms of model resolution, as phase-averaged models or as phase-resolving models (Battjes 1994). Phase-averaged models seek to represent the evolution of the wave envelope and mean flow circulation. This type of model has the advantage of precluding small-scale fluctuation from consideration while still retaining the dominant physics in the nearshore zone. Phase-

resolving models seek to resolve detailed wave profiles and have particular value in the zone near structures.

In the past decade or so, a number of phase-averaging models have been developed, such as those by Svendsen (1984a, b, c), Stive and Wind (1986), De Vriend et al. (1987). While these models demonstrate the power of the mean flow approach, they are incomplete. The shortcomings of these models are: (1) some (Sevendsen 1984a, b, c) exclude wave-current interaction, simulating wave setup and mean flow circulation from a decoupled wave height model, (2) some (De Vriend 1987) only deal with a bottom layer from the sea bed to the wave trough by simply neglecting the mass transfer across the wave trough and using empirical formula for the momentum transfer across the wave trough, (3) the transient behavior of the wave field is rarely simulated. It is thus desirable to apply more rigorous fluid dynamic analysis to the description of these phenomena. Recently, Sobey and Thieke (1989) have developed a depth-integrated and wave-averaged model based on the conservation of mass, momentum and wave energy. This model is theoretically sound and consistently valid for the entire coastal region, including the surf zone. Comparisons between the model results with experimental data and field observation for steady wave fields showed this model very promising. In addition, this model can be extended to the transient behavior of the mean wave field and for two horizontal directions.

The background to the depth-integrated wave-averaged model follows an analysis technique used in turbulent shear flows, adapted to derive the governing equations for wave height, wave setup and currents. Variables are decomposed into a mean part and a fluctuating residual, as first applied to waves by Longuet-Higgins and Stewart (1964). Subsequently, the conservation equations for mass and momentum are averaged over wave

groups, and integrated over water depth, giving a set of mean flow mass, momentum and wave energy equations. The time-averaging introduces apparent stress- or Reynolds stress-style terms which introduce a closure problem. Fourier approximation wave theory is used to construct closure surfaces on which the dependent variables are related to water depth, wave period and wave height.

This study will modify and extend the Sobey and Thieke's model to simulate transient wave propagation in horizontally extensive coastal regions.

The model was developed from an Eulerian perspective. There is an important distinction as wave averaging differs significantly between the Eulerian and the Lagrangian perspectives. The differences can best be examined by considering the familiar mass transport in wave propagation. Using linear wave theory, the Lagrangian wave-averaged velocity is uniformly distributed from the sea bed to mean water surface, while the Eulerian wave-averaged velocity is confined between the trough and the crest.

Given the nonlinear nature of the mathematical model and the closure problem, it is difficult to solve the system analytically. The system of wave-averaged equations is quasilinear hyperbolic. Numerical solutions are obtained based on the method of characteristics (MOC), which is a well-proven numerical method for quasilinear hyperbolic problems.

As in any numerical simulation for a truncated computational domain, open boundary conditions are a key issue. Though there are analytical open boundary conditions for some linear systems, the specification of open boundary conditions for a nonlinear system largely relies on empiricism. The dependence of open boundary conditions on a problem at hand or even on a specific boundary makes the specification of open boundary conditions an integral

part of any numerical schemes for boundary value problems. To specify physically justified open boundary conditions is one of the major tasks of this study.

1.3 Scope and Major Assumptions

As stated above, the interest of this study centers on the evolution of wave-averaged parameters, such as wave height, wave setup and mean flow circulation. The ultimate goal is to develop a computational framework for simulating the evolution of the wave-averaged parameters.

The physical processes to be represented in the model include shoaling, refraction, diffraction, wave breaking, and wave-current interaction. Though the wave-averaged evolution equations do not preclude wave reflection, the use of a progressive steady wave theory for closure will make the present model inappropriate for modeling wave reflection.

Given the complex dynamics in the nearshore region, it is neither possible nor appropriate to tackle every physical aspect in a single dissertation. To make the problem tractable and to focus on the dominant physics of wave propagation in coastal regions, the following assumptions are adopted for this study:

- The model is based on a two-layer concept. Recognizing that the mass transport associated with wave propagation is confined between the wave trough and crest in an Eulerian framework, it is appropriate to treat mean flow currents below and above the wave trough separately. In this context, the layer between the trough and the crest is defined as a surface layer, and the layer between the sea bed and the trough as a bottom layer. The surface layer is assumed to be dominated by wave motion, and the wave-driven currents (not the wave kinematics) lie only within the bottom layer. Also the

mean flow currents below the trough are assumed to be uniformly distributed.

- Stokes' first definition of phase speed is used in the Fourier approximation wave theory for establishing closure surfaces.
- Turbulence is assumed secondary in significance to wave motion, even in the surf zone. Thus the turbulent Reynolds stresses are not considered in order to focus on the wave dynamics. The turbulence-associated terms are, however, fully considered in the mathematical model.
- The sea bed is assumed to be slowly varying such that wave reflection is negligible and all dependent variables are slowly varying in space.
- Incident wave conditions are slowly varying in time, so that all wave-averaged dependent variables are also slowly varying in time.

1.4 Organization of This Dissertation

In Chapter 2, a depth-integrated, wave-averaged model is developed from the conservation equations of mass, momentum and energy. Chapter 3 reviews the literature on the fluid motion in the nearshore zone, wave transformation modeling, method of characteristics and open boundary conditions. Chapter 4 discusses closure variables and establishment of closure surfaces from the Fourier approximation wave theory. Subsequently, a set of integral equations with closure variables are derived. In Chapter 5, the model is applied to simulating one-dimensional wave propagation. The procedure for deriving compatibility equations in a one dimensional space is introduced, the detailed steps being given in Appendix A. Also discussed is how to specify open boundary conditions. The model is then applied to four schematic problems and to shoal-normal wave propagation

at Egmond Beach, The Netherlands.

Chapter 6 describes the application of this model in two spatial dimensions. The procedure for deriving compatibility equations is briefly discussed, the complete procedure being given in Appendix B. Characteristics of the system are analyzed under an assumed wave environment. Also presented in this chapter are the numerical scheme based on bi-characteristics and open boundary conditions. Finally, this model is applied for three schematic problems: evolution of an initial water mound, normal and obliquely incident wave propagation, and for simulating wave focusing by a submerged shoal under the conditions of Berkhoff's experiment (1982). In Chapter 7, a brief discussion is given on how to simulate wave reflection and coastal sediment transport with wave-averaged models. In Chapter 8, the main aspects of this study are summarized, including the future research necessary to expand the capabilities of this model.

2. MATHEMATICAL FORMULATION

A rigorous approach to developing a predictive model for the hydrodynamics in the nearshore zone must be based on the conservation equations of mass and momentum. To study the evolution of wave-averaged parameters on the wave phase plane, a wave-averaged model is developed first by time averaging the conservation equations over wave groups. Subsequently, the time-averaged equations are integrated over depth to give a set of wave-averaged and depth-integrated mean flow equations. A conservation equation for wave energy is derived by subtracting the mean flow mechanical energy equation from the time-averaged conservation equation of general mechanical energy. The mean-flow continuity and momentum conservation equations coupled with the conservation equation of the wave energy constitute a set of governing equations for mean wave parameters.

2.1 Conservation Equations

The Cartesian coordinate system is located at the still water level (SWL) with z directed vertically upwards and x and y in the horizontal plane. When applied to a coastal region, the x-axis is conventionally directed onshore, and y-axis alongshore in accordance with a right-handed system as shown below.

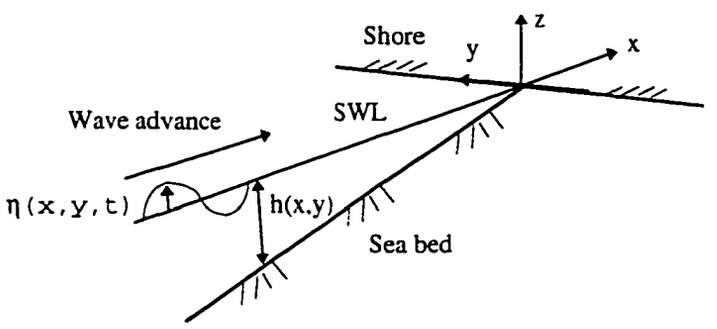

Figure 2-1 Definition Sketch of Coordinate System

The Eulerian continuity equation for an incompressible flow is

$$\frac{\partial u}{\partial x}+\frac{\partial v}{\partial y}+\frac{\partial w}{\partial z}=0 \tag{2.1}$$

and the momentum conservation equations in x, y and z directions are

$$\frac{\partial u}{\partial t}+\frac{\partial (u^2)}{\partial x}+\frac{\partial (uv)}{\partial y}+\frac{\partial (uw)}{\partial z}=-\frac{1}{\rho}\frac{\partial p}{\partial x}+\frac{1}{\rho}[\frac{\partial \tau_{xx}}{\partial x}+\frac{\partial \tau_{yx}}{\partial y}+\frac{\partial \tau_{zx}}{\partial z}] \tag{2.2}$$

$$\frac{\partial v}{\partial t}+\frac{\partial (uv)}{\partial x}+\frac{\partial (v^2)}{\partial y}+\frac{\partial (vw)}{\partial z}=-\frac{1}{\rho}\frac{\partial p}{\partial y}+\frac{1}{\rho}[\frac{\partial \tau_{xy}}{\partial x}+\frac{\partial \tau_{yy}}{\partial y}+\frac{\partial \tau_{zy}}{\partial z}] \tag{2.3}$$

$$\frac{\partial w}{\partial t}+\frac{\partial (uw)}{\partial x}+\frac{\partial (vw)}{\partial y}+\frac{\partial (w^2)}{\partial z}=-\frac{1}{\rho}\frac{\partial p}{\partial z}-g+\frac{1}{\rho}[\frac{\partial \tau_{xz}}{\partial x}+\frac{\partial \tau_{yz}}{\partial y}+\frac{\partial \tau_{zz}}{\partial z}] \tag{2.4}$$

where u(x,y,z,t), v(x,y,z,t), and w(x,y,z,t) are the velocity components in x, y, and z direction, p(x,y,z,t) is the pressure, τ(x,y,z,t) are the viscous stress components, ρ is the water density, and g is the gravitational acceleration.

The kinematic and dynamic boundary conditions at the water surface, η(x,y,t), are

$$\begin{aligned} w-\frac{\partial \eta}{\partial t}-u\frac{\partial \eta}{\partial x}-v\frac{\partial \eta}{\partial y}&=0 \\ p(x,y,t)&=0 \end{aligned} \tag{2.5}$$

The kinematic bottom boundary condition at the sea bed is

$$u\frac{\partial h}{\partial x}+v\frac{\partial h}{\partial y}+w=0 \qquad \text{at} \quad z=-h(x,y) \tag{2.6}$$

where z=-h(x,y) describes the slowly varying bottom topography.

The conservation equation of mechanical energy is

$$\begin{aligned} &\frac{\partial E}{\partial t}+\frac{\partial}{\partial x}[\ u\cdot(\frac{p}{\rho}+E)\ ]+\frac{\partial}{\partial y}[\ v\cdot(\frac{p}{\rho}+E)\ ]+\frac{\partial}{\partial z}[\ w\cdot(\frac{p}{\rho}+E)\ ]= \\ &-gw+\frac{u}{\rho}\frac{\partial(\tau_{xx}+\tau_{yx}+\tau_{zx})}{\partial x}+\frac{v}{\rho}\frac{\partial(\tau_{xy}+\tau_{yy}+\tau_{zy})}{\partial y}+\frac{w}{\rho}\frac{\partial(\tau_{xz}+\tau_{yz}+\tau_{zz})}{\partial z} \end{aligned} \tag{2.7}$$

where

$$E = \frac{1}{2}(u^2 + v^2 + w^2) \tag{2.8}$$

The mechanical energy conservation Equation (2.7) is established as the summation of three momentum conservation Equations (2.2) through (2.4), each multiplied by respective velocity component. In its present form, it is not independent of the momentum equations.

2.2 Wave-Averaged Conservation Equations

Time-averaging is a useful means for directing attention to the longer time scale variation. For instance, in turbulent shear flow, time-averaged flow equations, or mean flow equations, deal specifically with mean flow characteristics by introducing Reynolds stress. The time-averaging technique was initially utilized in wave studies by Longuet-Higgins and Stewart (1964). By using the same concept, Sobey and Thieke (1989) developed a set of mean flow equations for the evolution of wave-averaged parameters. This study will follow the Sobey and Thieke's procedure in deriving conservation equations for mean mass and momentum, and wave energy.

In the nearshore zone, the dominant fluid motion is periodic wave motions. Since the mean flow variation at a time scale greater than the wave period is of interest to this study, the wave period or several wave periods is an appropriate time scale which can truncate from the conservation equations all variations at time scales equal to or shorter than the wave period.

The turbulence in nearshore zone, especially in the surf zone, possesses a time scale generally shorter than the wave period. Hence the time-averaging over the wave period

should remove the turbulent variations as well.

To time-average the conservation equations, each dependent variable (u, v, w, η, p, and τ) is represented as the sum of a mean value and a fluctuating residual. For instance, the velocity component in the x direction, u, is decomposed into:

$$u = \bar{u}(x,y,z) + \tilde{u}(x,y,z,t) \tag{2.9}$$

where $\bar{u}$ is the mean flow velocity in x direction, $\tilde{u}$ the fluctuating residual which includes both wave motion and turbulent motion. Several forms of the mean value, $\bar{u}$, were used in previous studies. Longuet-Higgins and Stewart (1964) and Phillips (1977) defined $\bar{u}$ as the vertically uniform Eulerian current; and Mei (1983) defined $\bar{u}$ as the mass transport velocity which differs from the Eulerian current by a vertically-uniform wave-induced mass transport velocity. Common to these two definitions is that variation of the mean velocity along water depth is not considered, thus $\bar{u}$ may be written in form of $\bar{u}(x,y,t)$. By these definitions, the integration of the conservation equations over depth prior to time-averaging excludes the vertical structure from consideration. However, the vertical structure of the mean flow in the coastal region is a significant phenomenon, as demonstrated in various experimental studies (Nadaoka and Kondoh 1982, Stive and Wind 1982). It is commonly observed that there is a reversal in the flow direction of wave-driven shore-normal currents over water depth. To account for, at least partially, the vertical structure of mean flow parameters, Sobey and Thieke (1989) adopted standard Reynolds averaging in which the mean value is represented as $\bar{u}(x,y,z,t)$. By time-averaging the conservation equations prior to depth integration, the information regarding the vertical profiles of the Eulerian mean quantities is preserved. In this study, this approach is also

used. Other dependent variables are decomposed in the same manner.

The Eulerian definition of a wave-averaged variable, say $\bar{u}$, is

$$\bar{u} = \frac{1}{T}\int_{t_1(z)}^{t_2(z)} u(x, y, z, t)dt \tag{2.10}$$

where T is the wave period, t_1 and t_2 are the lower and upper time limits for integration. For a point located below the wave trough, t_2-t_1=T. But for the elevations above the wave trough, the interval between t_1 and t_2 is shorter than the wave period since they are not constantly submerged. In this case, t_1 and t_2 depend on the vertical position, represent respectively the starting and end times for the point to be submerged within a wave period. In shallow water, wave profile is normally not symmetric about wave crest, thus t_1 and t_2 are not symmetric about the wave crest.

Introducing such decompositions for u, v, and w into the continuity Equation (2.1), time-averaging in the manner of Equation (2.10) and using the Leibniz rule gives the wave-averaged continuity equation:

$$\frac{\partial \bar{u}}{\partial x} + \frac{\partial \bar{v}}{\partial y} + \frac{\partial \bar{w}}{\partial z} - \frac{1}{T}[w(z,t_2)\frac{\partial t_2}{\partial z} - w(z,t_1)\frac{\partial t_1}{\partial z}] = 0 \tag{2.11}$$

The square-bracketed term exists only at elevations above the wave trough for asymmetric waves (Thieke 1988). The two components in the term cancel identically for symmetric wave profiles at elevations above the wave trough, and are both identically zero for symmetric and asymmetric waves below the trough.

Similarly, introducing the decompositions for u, v, w, p and τ, and time averaging the x-momentum conservation Equation (2.2) leads to:

$$\frac{\partial \bar{u}}{\partial t}+\frac{\partial \overline{u}^2}{\partial x}+\frac{\partial \overline{uv}}{\partial y}+\frac{\partial \overline{uw}}{\partial z}-\frac{1}{T}[u(z,t_2)w(z,t_2)\frac{\partial t_2}{\partial z}-u(z,t_1)w(z,t_1)\frac{\partial t_1}{\partial z}]=$$
$$\frac{1}{\rho}\left\{\frac{\partial(-\bar{p}+\bar{\tau}_{xx}-\rho\overline{\tilde{u}\tilde{u}})}{\partial x}+\frac{\partial(\bar{\tau}_{xy}-\rho\overline{\tilde{u}\tilde{v}})}{\partial y}+\frac{\partial(\bar{\tau}_{xz}-\rho\overline{\tilde{u}\tilde{w}})}{\partial z}-\frac{1}{T}[\tau_{xz}(z,t_2)\frac{\partial t_2}{\partial z}-\tau_{xz}(z,t_1)\frac{\partial t_1}{\partial z}]\right\} \quad (2.12)$$

Again the square-bracketed term, appearing in form of $[q(z,t_2)(dt_2/dz)-q(z,t_1)(dt_1/dz)]/T$, is not trivial above the trough if the wave profile is asymmetric about the wave crest. As expected, there remain residual inertial terms involving the wave and turbulent fluctuations which are similar to the Reynolds stresses in turbulent shear flow. These terms account for the contribution of both wave and turbulent fluctuations to the mean flow momentum balance. The existence of these terms presents a closure problem, which will be addressed in Chapter 4.

The wave-averaged y- and z-momentum equations read:

$$\frac{\partial \bar{v}}{\partial t}+\frac{\partial \overline{uv}}{\partial x}+\frac{\partial \overline{v}^2}{\partial y}+\frac{\partial \overline{vw}}{\partial z}-\frac{1}{T}[v(z,t_2)w(z,t_2)\frac{\partial t_2}{\partial z}-v(z,t_1)w(z,t_1)\frac{\partial t_1}{\partial z}]=$$
$$\frac{1}{\rho}[\frac{\partial(\bar{\tau}_{xy}-\rho\overline{\tilde{u}\tilde{v}})}{\partial x}+\frac{\partial(-\bar{p}+\bar{\tau}_{yy}-\overline{\tilde{v}\tilde{v}})}{\partial y}+\frac{\partial(\bar{\tau}_{yz}-\overline{\tilde{v}\tilde{w}})}{\partial z}-\frac{1}{T}[\tau_{yz}(z,t_2)\frac{\partial t_2}{\partial z}-\tau_{yz}(z,t_1)\frac{\partial t_1}{\partial z}]] \quad (2.13)$$

$$\frac{\partial \bar{w}}{\partial t}+\frac{\partial \overline{uw}}{\partial x}+\frac{\partial \overline{vw}}{\partial y}+\frac{\partial \overline{w}^2}{\partial z}-\frac{1}{T}[w^2(z,t_2)\frac{\partial t_2}{\partial z}-w^2(z,t1)\frac{\partial t_1}{\partial z}]=-\bar{g}$$
$$+\frac{1}{\rho}[\frac{\partial(\bar{\tau}_{xz}-\rho\overline{\tilde{u}\tilde{w}})}{\partial x}+\frac{\partial(\bar{\tau}_{yz}-\rho\overline{\tilde{v}\tilde{w}})}{\partial y}+\frac{\partial(-\bar{p}+\bar{\tau}_{zz}-\rho\overline{\tilde{w}\tilde{w}})}{\partial z}-\frac{1}{T}[\tau_{zz}(z,t_2)\frac{\partial t_2}{\partial z}-\tau_{zz}(z,t_1)\frac{\partial t_1}{\partial z}]] \quad (2.14)$$

The time-averaged y-momentum equation is very similar to Equation (2.12). But the mean z-momentum equation includes the gravitational acceleration term, $\bar{g}$. The $\bar{g}$ term is equal to g below the trough, reducing gradually to zero from the trough to the crest.

The time-averaging of energy equation is performed in the same manner. However, the interest of this study is the conservation of wave energy instead of general mechanical

energy. The wave energy equation can be developed by subtracting the product of mean velocity vector and the mean momentum equations from the time-averaged conservation equation of mechanical energy. The conservation equation of kinetic wave energy, k_w

$$k_w = \frac{1}{2}(\overline{\tilde{u}^2} + \overline{\tilde{v}^2} + \overline{\tilde{w}^2}) \tag{2.15}$$

is

$$\begin{aligned}
&\frac{\partial k_w}{\partial t} + \frac{\partial}{\partial x}\left[\frac{\overline{\tilde{p}\tilde{u}}}{\rho} + \frac{1}{2}(\overline{\tilde{u}^3} + \overline{\tilde{u}\,\tilde{v}^2} + \overline{\tilde{u}\,\tilde{w}^2})\right] + \\
&\frac{\partial}{\partial y}\left[\frac{\overline{\tilde{p}\tilde{v}}}{\rho} + \frac{1}{2}(\overline{\tilde{u}^2\tilde{v}} + \overline{\tilde{v}^3} + \overline{\tilde{v}\,\tilde{w}^2})\right] + \frac{\partial}{\partial z}\left[\frac{\overline{\tilde{p}\tilde{w}}}{\rho} + \frac{1}{2}(\overline{\tilde{u}^2\tilde{w}} + \overline{\tilde{v}^2\tilde{w}} + \overline{\tilde{w}^3})\right] = \\
&-(g - \bar{g})\bar{w} + \frac{1}{\rho}(\overline{\tilde{u}\tilde{f}_x} + \overline{\tilde{v}\tilde{f}_y} + \overline{\tilde{w}\tilde{f}_z}) - \bar{u}\frac{\partial k_w}{\partial x} - \bar{v}\frac{\partial k_w}{\partial y} - \bar{w}\frac{\partial k_w}{\partial z} - \overline{\tilde{u}^2}\frac{\partial \bar{u}}{\partial x} - \\
&\overline{\tilde{u}\tilde{v}}\left(\frac{\partial \bar{v}}{\partial x} + \frac{\partial \bar{u}}{\partial y}\right) - \overline{\tilde{u}\tilde{w}}\left(\frac{\partial \bar{w}}{\partial x} + \frac{\partial \bar{u}}{\partial z}\right) - \overline{\tilde{v}^2}\frac{\partial \bar{v}}{\partial y} - \overline{\tilde{v}\tilde{w}}\left(\frac{\partial \bar{w}}{\partial y} + \frac{\partial \bar{v}}{\partial z}\right) - \overline{\tilde{w}^2}\frac{\partial \bar{w}}{\partial z} + \\
&-\frac{1}{T}\left\{\left[\frac{\overline{\tilde{p}\tilde{w}}}{\rho} + \frac{(\overline{\tilde{u}^2\tilde{w}} + \overline{\tilde{v}^2\tilde{w}} + \overline{\tilde{w}^3})}{2}\right]_{z,t_2}\frac{\partial t_2}{\partial z} - \left[\frac{\overline{\tilde{p}\tilde{w}}}{\rho} + \frac{(\overline{\tilde{u}^2\tilde{w}} + \overline{\tilde{v}^2\tilde{w}} + \overline{\tilde{w}^3})}{2}\right]_{z,t_1}\frac{\partial t_1}{\partial z}\right\}
\end{aligned} \tag{2.16}$$

where

$$f_i = \frac{\partial \tau_{ij}}{\partial x_j} \qquad i, j = x, y, z \tag{2.17}$$

The potential energy inherent in the free surface fluctuations is included in the time-averaged pressure terms $\overline{\tilde{p}\tilde{u}}/\rho$ and $\overline{\tilde{p}\tilde{v}}/\rho$. Unlike the energy conservation Equation (2.7), this wave energy equation is mathematically independent of the mean flow momentum equations. This is analogous to the situation in turbulent shear flow where the total mechanical energy equation is dependent on the momentum conservation equations, while the turbulent energy equation is independent of the mean flow momentum equations.

Fox (1970) used a similar set of conservation equations for studying a forced turbulent

plume in a stratified fluid. The independence of the equations of the system will be verified in Chapters 5 and 6 by the fact that the number of distinctive eigen-values equals the number of the equations.

2.3 Depth-Integrated and Wave-Averaged Equations

To focus on the evolution of mean wave parameters on a horizontal plane, the wave-averaged equations are integrated over water depth. Applying the Leibniz rule, the time-averaged kinematic free surface boundary conditions and bottom boundary conditions, the wave-averaged mass, momentum, and wave energy equations are integrated from sea bed to the wave crest. The intermediate steps will not be presented, and only final results are described here. The resulted depth-integrated, mean-flow continuity equation is

$$\frac{\partial \bar{\eta}}{\partial t} + \frac{\partial}{\partial x}\int_{-h}^{\eta_c} \bar{u}\,dz + \frac{\partial}{\partial y}\int_{-h}^{\eta_c} \bar{v}\,dz = 0 \tag{2.18}$$

where $\bar{\eta}$ is the mean water surface elevation (or setup) from still water surface, and η_c is the wave crest elevation. The terms associated with the asymmetry of the wave profile vanish upon depth integration (Thieke 1988). Equation (2.18) is identical to the long wave mass conservation equation, which are applicable to unsteady gradually-varied flow in open channels.

The depth-integrated and wave-averaged x- and y-momentum equations are

$$\begin{aligned} &\frac{\partial}{\partial t}\int_{-h}^{\eta_c} \bar{u}\,dz + \frac{\partial}{\partial x}\int_{-h}^{\eta_c} \bar{u}^2\,dz + \frac{\partial}{\partial y}\int_{-h}^{\eta_c} \overline{uv}\,dz = \\ &\qquad -g(h+\bar{\eta})\frac{\partial \bar{\eta}}{\partial x} + \frac{1}{\rho}\left[\frac{\partial}{\partial x}\int_{-h}^{\eta_c} s_{xx}\,dz + \frac{\partial}{\partial y}\int_{-h}^{\eta_c} s_{xy}\,dz - \tau_{bx}\right] \end{aligned} \tag{2.19}$$

$$\frac{\partial}{\partial t}\int_{-h}^{\eta_c}\bar{v}dz+\frac{\partial}{\partial x}\int_{-h}^{\eta_c}\overline{uv}dz+\frac{\partial}{\partial y}\int_{-h}^{\eta_c}\bar{v}^2dz=$$
$$-g(h+\bar{\eta})\frac{\partial\bar{\eta}}{\partial y}+\frac{1}{\rho}[\frac{\partial}{\partial x}\int_{-h}^{\eta_c}s_{xy}dz+\frac{\partial}{\partial y}\int_{-h}^{\eta_c}s_{yy}dz-\tau_{by}] \quad (2.20)$$

where τ_{bx} and τ_{by} are the respective shear stress component in x and y direction. s_{xx}, s_{xy}, s_{yx}, and s_{yy} are the apparent stresses associated with wave and turbulent motion:

$$s_{xx}=-\Delta p-\rho\overline{\tilde{u}^2}+\rho\overline{\tilde{\omega}^2} \qquad s_{xy}=s_{yx}=-\rho\overline{\tilde{u}\tilde{v}} \qquad s_{yy}=-\Delta p-\rho\overline{\tilde{v}^2}+\rho\overline{\tilde{\omega}^2} \quad (2.21)$$

where Δp is the gravitational term which exists only between the trough and the crest. Again the terms due to the asymmetry of the wave profile vanish upon depth integration. The procedure for deriving these equations is similar to the derivation of the long wave equations, see Thieke (1988) for the details. The key steps include (1) using the time-averaged surface kinematic boundary condition and bottom boundary condition to eliminate terms resulting from the Leibniz rule, (2) integrating the z-momentum conservation equation to provide a vertical distribution of the pressure, which is subsequently substituted into x-and y- momentum equations.

The viscous stresses are assumed to be negligible compared to other terms and are not included in Equations (2.19) and (2.20), which are almost identical to the shallow water wave equations except the apparent stress terms. The depth-integrals of the wave apparent stress terms (S_{xx}, S_{xy} and S_{yy}) are called "radiation stresses" by Longuet-Higgins and Stewart (1964). This terminology does not correctly reflect the dimension of these terms because a "radiation stress" has the dimension of the product of a stress and a length.

The gravitational term in s_{xx}, s_{xy} and s_{yy} are not trivial only between the trough and the crest. The gravitational term at elevations above the mean water surface is defined by

$$\Delta p = \rho g[\frac{1}{T}\int_{t_1(z)}^{t_2(z)} (\eta(t) - z)dt] \qquad \text{for } \overline{\eta} < z < \eta_c \tag{2.22}$$

and between the wave trough and the mean water surface, it is defined by

$$\Delta p = \rho g[\frac{1}{T}\int_{t_1(z)}^{t_2(z)} (\eta(t) - z)dt - (\overline{\eta} - z)] \quad \text{for} \quad \eta_{tr} < z \le \overline{\eta} \tag{2.23}$$

in which $\overline{\eta}$ is the mean water level. Below the wave trough, Δp identically equals zero.

The depth integration of the wave energy Equation (2.16) can be similarly proceeded. For simplicity, the energy losses due to viscous stresses, expressed by $\overline{\tilde{u}\tilde{f}_x}$, $\overline{\tilde{v}\tilde{f}_y}$ and $\overline{\tilde{w}\tilde{f}_z}$, will be neglected since in the nearshore zone, the viscous stresses are generally negligible compared to the wave apparent stresses (Thieke 1988). With the neglect of the viscous energy losses, the depth-integrated wave energy equation becomes

$$\begin{aligned}
&\frac{1}{2}\frac{\partial}{\partial t}[\int_{-h}^{\eta_c}(\overline{\tilde{u}^2} + \overline{\tilde{v}^2} + \overline{\tilde{w}^2})dz + g\overline{\tilde{\eta}^2}] + \frac{\partial}{\partial x}\int_{-h}^{\eta_c}[\frac{\overline{\tilde{p}\tilde{u}}}{\rho} + \frac{1}{2}(\overline{\tilde{u}^3} + \overline{\tilde{u}\,\tilde{v}^2} + \overline{\tilde{u}\,\tilde{w}^2})]dz \\
&-\frac{\partial}{\partial y}\int_{-h}^{\eta_c}[\frac{\overline{\tilde{p}\,\tilde{v}}}{\rho} + \frac{1}{2}(\overline{\tilde{v}\,\tilde{u}^2} + \overline{\tilde{v}^3} + \overline{\tilde{v}\,\tilde{w}^2}]dz = -\frac{\partial}{\partial x}\int_{-h}^{\eta_c}\frac{\overline{u}}{2}(\overline{\tilde{u}^2} + \overline{\tilde{v}^2} + \overline{\tilde{w}^2})dz - \int_{-h}^{\eta_c}\overline{\tilde{u}^2}\frac{\partial \overline{u}}{\partial x}dz \\
&-\int_{-h}^{\eta_c}\overline{\tilde{u}\tilde{v}}(\frac{\partial \overline{v}}{\partial x} + \frac{\partial \overline{u}}{\partial y})dz - \frac{\partial}{\partial y}\int_{-h}^{\eta_c}\frac{\overline{v}}{2}(\overline{\tilde{u}^2} + \overline{\tilde{v}^2} + \overline{\tilde{w}^2})dz - \int_{-h}^{\eta_c}\overline{\tilde{v}^2}\frac{\partial \overline{v}}{\partial y}dz - D_t - D_b
\end{aligned} \tag{2.24}$$

where D_t is the energy dissipation rate per unit area of sea surface due to bottom friction, and D_{wb} is the energy dissipation rate due to wave breaking. The terms of the asymmetry of the wave profile again vanish upon depth integration. The second and third terms on the left hand side represent the energy flux due to wave motion. On the right hand side, the first and fourth terms describe the transport of wave kinetic energy by the mean flow; the second, third and fifth terms represent the interaction between the mean flow and residual fluctuating, which are usually referred as to production terms in the context of the turbulent

shear flow (Tennekes and Lumley 1973).

The depth integration of the energy Equation (2.24) can not be proceeded without simplification as many integrands contain the spatial derivatives of mean velocity components. These spatial derivatives depend on mean flow field which is to be sought. For convenience, these derivatives are assumed to be uniform along the water depth so that they can be taken out of the integration sign. This simplification will not tilt the energy balance among various components because the magnitudes of these terms associated with the spatial derivatives of mean flow currents are much smaller than other terms if the mean flow current is weak (Sobey and Thieke 1989). In this manner, Equation (2.24) can be rewritten as:

$$\begin{aligned}
&\frac{1}{2}\frac{\partial}{\partial t}[\int_{-h}^{\eta_c}(\overline{\tilde{u}^2}+\overline{\tilde{v}^2}+\overline{\tilde{w}^2})dz+g\overline{\tilde{\eta}^2}]+\frac{\partial}{\partial x}\int_{-h}^{\eta_c}[\frac{\overline{\tilde{p}\tilde{u}}}{\rho}+\frac{1}{2}(\overline{\tilde{u}^3}+\overline{\tilde{u}\tilde{v}^2}+\overline{\tilde{u}\tilde{w}^2})]dz \\
&-\frac{\partial}{\partial y}\int_{-h}^{\eta_c}[\frac{\overline{\tilde{P}\tilde{v}}}{\rho}+\frac{1}{2}(\overline{\tilde{v}\tilde{u}^2}+\overline{\tilde{v}^3}+\overline{\tilde{v}\tilde{w}^2}]dz=-\frac{\partial}{\partial x}\int_{-h}^{\eta_c}\frac{\bar{u}}{2}(\overline{\tilde{u}^2}+\overline{\tilde{v}^2}+\overline{\tilde{w}^2})dz-\frac{\partial\bar{u}}{\partial x}\int_{-h}^{\eta_c}\overline{\tilde{u}^2}dz \qquad (2.25)\\
&-(\frac{\partial\bar{v}}{\partial x}+\frac{\partial\bar{u}}{\partial y})\int_{-h}^{\eta_c}\overline{\tilde{u}\tilde{v}}dz-\frac{\partial}{\partial y}\int_{-h}^{\eta_c}\frac{\bar{v}}{2}(\overline{\tilde{u}^2}+\overline{\tilde{v}^2}+\overline{\tilde{w}^2})dz-\frac{\partial\bar{v}}{\partial y}\int_{-h}^{\eta_c}\overline{\tilde{v}^2}dz-D_t-D_b
\end{aligned}$$

In one dimensional steady state wave propagation with the mean velocity $\bar{u}$ being neglected, the above equation further reduces to

$$\frac{d}{dx}\left\{\int_{-h}^{\eta_c}[\frac{\overline{P_d\tilde{u}}}{\rho}+\frac{(\overline{\tilde{u}^3}+\overline{\tilde{u}\tilde{w}^2})}{2}]dz\right\}=-D_t-D_b \qquad (2.26)$$

This is the familiar energy flux equation for wave shoaling.

2.4 Bottom Shear Stresses And Energy Dissipation

In a combined wave-current field, instantaneous bottom friction is approximately

proportional to the square of resultant velocity near the seabed. The wave-averaged bottom shear stress can be obtained by time-averaging the instantaneous shear stress in the manner of Equation (2.10). If mean flow current is relatively weaker in comparison with wave motion, the wave-averaged bottom shear stress in one spatial dimension may be approximated by (Thieke 1988)

$$\tau_b = \frac{1}{2}\rho f_w U_{rms} U_b \tag{2.27}$$

in which τ_b is the wave-averaged bottom shear stress, U_{rms} is the root mean square of wave velocity near the seabed, U_b is the mean flow velocity near the seabed, and f_w is a friction coefficient which can be evaluated from the data of (Jonsson 1966). The U_{rms} is used here to preserve the effects of wave nonlinearity. In a two-dimensional space, the x and y shear stress components can be approximated, respectively, as

$$\tau_{bx} = \frac{1}{2}\rho f_w U_{rms} \cdot u_b \tag{2.28}$$

$$\tau_{by} = \frac{1}{2}\rho f_w U_{rms} \cdot v_b \tag{2.29}$$

where u_b and v_b are the x- and y-component of mean flow velocity at the seabed. Of course, the above formula are a very simplified expression about bottom shear stresses in a coexistent wave-current field. Longuet-Higgins (1970) obtained a similar form by assuming that the incident wave angle is small and that the longshore current is weak compared with the wave orbital velocity.

Energy dissipation during wave propagation in the nearshore zone, in particular in the surf zone, is a very complicated process. Energy may be dissipated through many ways such as white capping, spilling, plunging, surging, bed friction. In general, the energy loss

due to viscous stress is relatively small and can be neglected. Energy dissipation is one of the least understood facets in surf zone hydrodynamics. Empirical formula are used for estimating the rate of wave energy dissipation. In this study, energy dissipation is accounted for by the energy dissipation due to bottom friction and the energy dissipation due to wave breaking.

Jonsson(1966) established a Darcy-Weisbach-type formula for wave energy dissipation due to bottom friction by assuming that the transfer of energy dissipation to heat occurs rapidly and therefore that the dissipated energy can be equated to the dissipation of wave energy without a need to budget the turbulent energy, i.e.

$$D_f = \frac{2}{3\pi} f_w \rho |\overline{\vec{u}_b^3}| \tag{2.30}$$

where the friction factor f_w is identical to that in the formula for the bottom shear stress.

The energy dissipation due to wave breaking is significant in the surf zone. Unfortunately it can not be predicted with certainty. A pragmatic approach, based on dimensional analysis, has been adopted. Choosing the local energy density as the magnitude scale and the frequency as the time scale leads to a predictive equation for the breaking wave dissipation per unit width of the form (Sobey 1989)

$$D_{wb} = f_{wb} \cdot \omega \cdot E_w \tag{2.31}$$

where the constant of proportionality f_{wb} is the wave breaking dissipation coefficient, which would be dependent on dimensionless groups including the water depth and the current and perhaps also on bottom slope. By assuming that the process of wave breaking is hydrodynamically similar to the tidal bore (Le Mehaute 1962, Battjes et al 1978), the proportionality constant can be estimated as

$$f_{wb} = \frac{1}{\pi}(1 + \frac{H_b^2}{H_{rms}^2})\exp(-\frac{H_b^2}{H_{rms}^2}) \qquad (2.32)$$

where H_b is the local breaking wave height, and H_{rms} is the root mean square of incident wave height. This estimator has been successfully used in a range of field and laboratory conditions (Battjes and Stive 1985).

3 LITERATURE REVIEW

This chapter briefly reviews fluid motions in the nearshore zone, wave-transformation modeling, and related computational aspects such as numerical methods and open boundary conditions.

3.1 Fluid Motions In The Nearshore Zone

Fluid motions in a nearshore zone can be broken up into long-period motion, wave motion and turbulence. The long-period motion, according to Shepard and Inman (1950), can be divided into two families: coastal currents and nearshore currents. Coastal currents (ocean currents, tidal currents and wind-induced currents) are not directly associated with the waves in the shallow water, and are mostly directed parallel to the shoreline. Nearshore currents (longshore currents, cross-shore currents and rip currents) are induced by the action of waves.

Munk (1948) and Tucker (1950) are among the earliest to quantitatively demonstrate the existence of a long-period water surface fluctuation in the nearshore zone with a time scale between some tens of seconds and a few minutes, naming this phenomenon "surf beat". Recently, new measurement techniques have detected wave-induced long-period variation in a frequency band from 0.002 Hz to 0.02 Hz in the deep ocean (Filloux and Luther 1991). The nearshore currents may be small in amplitude, but their interaction with the incident short waves may be quite significant in the nearshore zone. The long-period motions cause the wave energy to modulate in space and time and force energy exchange between waves and mean flow (Hamm et al. 1993) .

The long-period variations are normally caused by the spatial gradients of wave

apparent stresses. Far seaward of the breaker zone, the gradients of the apparent stress are small and the mean flow is weak. Approaching and within the surf zone, as energy dissipation increases, the gradients of wave and turbulent apparent stresses increase and the mean flow may be strong. Mean flow velocities of order of 1 m/s are not uncommon (Greenwood et al. 1990).

Energy dissipation in the surf zone is dominated by wave breaking, with bottom friction accounting for no more than 10% of the energy dissipation (Sawaigi and Iwata 1974). A large amount of the potential energy lost in the breaking is first converted into a turbulent kinetic energy of organized large vortices and contributes to the formation of a horizontal roller (Svendsen 1984). The energy contributing to the formation of the surface roller is the energy transfer from the wave motions to the mean flow. Longuet-Higgins (1967) described the surface roller as a gravity current riding down the forward slope of the wave, retaining its identity because the trapping of air bubbles for spilling breakers makes it lighter than the water below. Presence of the surface roller to some extent increases wave energy flux and apparent stress.

Shoreward of the breaker line and for moderate slopes (spilling breakers), the surf zone may be divided (Svendsen et al. 1978) into three sub-zones: an inner breaking region, a transition zone and an outer breaking region. In the inner breaking region or transition zone, breaking waves are transformed into turbulent bores with rapid transitions of the wave shape. In the outer breaking region, waves become very similar to a moving bore and seem to be strongly controlled by local water depth and bed slope. Svendsen (1987) suggested that most turbulent energy be dissipated close to where it is produced.

Though the turbulence is an important feature in the surf zone, periodic motion is still the dominant fluid motion (Battjes et al. 1990). Sobey and Thieke (1990) showed that the wave-induced apparent stresses are an order of magnitude greater than the turbulent apparent stress by analyzing the data of Nadaoka and Kondoh (1982). During wave breaking, the fluid motions below the aerated surface remain periodic (O'Brien 1931). In the measurement of turbulence field for breaking waves, Longuet-Higgins(1967) observed that the highest level of turbulence begins on the forward face of the wave just below the mean water level. Peregrine and Svendsen (1987) also noticed that the turbulent intensity above the trough is much higher than that below the trough.

The nearshore currents are rarely steady. Oltman-Shay et al. (1989) reported oscillations in the longshore current measured on a beach. The unsteadiness and irregularity of the mean flow further complicates the interaction among the mean flow, wave motions and turbulence.

Wave-induced currents exhibit a strong vertical structure in the nearshore zone, as illustrated, for example, in laboratory by Stive and Wind (1986) and in field by Nadaoka and Kondoh (1982) and Greenwood and Osborne(1990). From Eulerian perspective, there is typically a reversal in the vertical profile of the shoal-normal velocity, with the flow in the upper layer directing toward shore and the flow in the lower elevations directing seaward. Skjelberia (1987) observed mass transfer between the upper layer and lower layer. He measured a vertical mass flux across the trough level in the breaking solitary waves, and noticed a strong velocity gradient near the trough. Thieke and Sobey (1990) showed that a vertical mass flux across the layers is an essential part of the mass and momentum balances in the nearshore zone.

The wide swash zone where sheet flow prevails is also important for generating the offshore propagating low frequency waves (Hamm et al. 1993).

3.2 Wave Transformation Modeling

Wave transformation models can be generally grouped into two families: phase-resolving models and phase-averaging models (Battjes 1994). The phase-resolving models seek to follow the instantaneous local motion as it evolves in space and time within wave cycles, computational space and time scales must be of order L/15 and T/15 (L: wave length, T: wave period) respectively to resolve the phase response. Battjes (1994) suggested that the phase-resolving models be necessary only near structures. Boussinesq models (e.g. Peregrine 1967) and the mild-slope equation (Berkhoff 1972) fall into this category.

The phase-averaging models focus attention on the slow variation of integral properties of the local wave field (wave height, setup, undertow, ...) and can operate at much larger space and time scales. Wave-averaged cross-shore models (Battjes and Janssen 1978, Svendsen 1984a and 1984b, Sobey and Thieke 1989) are some examples of this type of model.

In the following review, emphasis centers on phase-averaged models. For a detailed review of phase-resolving models, see Hamm et al. (1993) and Battjes (1994).

Phase-averaged models are normally derived by viewing the horizontal plane as phase space and the vertical coordinate as cross-space, containing the modal structure. The modal structure is determined first, independent of the horizontal variations, and expressed analytically to permit depth integration. Subsequently the depth-integrated

equations are averaged over a wave period, to establish the transport equations describing the horizontal propagation on the phase plane. This procedure has been followed by Phillips (1977), Mei (1983) and Yoo et al. (1986). The sequence of depth integration and time averaging may be exchanged. Also the time-averaging can be performed by using either an ensemble average (Svendsen 1983) or a phase average (Mei 1983, Thieke 1988).

The integral equations so derived in a two dimensional space are not a closed system. Wave direction must be determined since the wave apparent stresses depend on the wave direction. The most popular way to determine the wave direction is based on the irrotationality of a wave number vector.

To provide reasonable results, a phase-averaging model must be able to simulate the following aspects:

- Vertical structure of mean flow currents.
- Nonlinearities.
- Energy dissipation.
- Wave-current interaction.
- Mass and momentum transport due to wave breaking.

Models based on integration over the entire depth (Phillips 1976, Mei 1983) can not accommodate the vertical structure of the mean flow. To consider the vertical structure of mean flow, depth integration may be performed over several sub-layers each with an individual structure (Svendsen 1984, Tshchiya et al. 1988, Sobey and Thieke 1989, Battjes et al. 1990). In this manner, the vertical structure may be approximately preserved and the mass transport above the trough due to wave motion considered.

As waves propagate toward the shore, nonlinearity grows and becomes increasingly significant. Nonlinear wave theory should be preferred over linear wave theory. Sobey and Bando (1991) indicated that the choice of a suitable wave theory to compute wave celerity and wave action is an essential task in shoaling computations. Linear wave theory can provide reliable prediction for small wave steepness if a depth to wave length ratio is less than 0.1, but fails otherwise (Svendsen and Hansen 1977). Thieke (1988) compared the momentum and energy fluxes computed from linear wave theory and from Fourier approximation wave theory. He found that in shallow water the difference between the results from the two wave theories is substantial. The price for using a high-order or nonlinear wave theory is the increasing complexity.

Some wave theories depend on the choice of the definition of wave celerity. Stokes' first definition of wave celerity assumes that the Eulerian mean horizontal fluid velocity at any point is equal to zero. Stoke's second definition assumes that the mass flux over entire water depth is zero. Which definition should be used depends on the problem at hand. For example, in cross-shore steady state wave modeling the second definition should be used because it is more consistent with the physical process being simulated (Thieke 1988). But if the transient behavior is a major concern, it is hard to argue which definition is better. Ease of use becomes a dictating factor.

As discussed in the preceding section, energy dissipation is important for the mean flow circulation since it dramatically increases the gradient of wave apparent stresses. There are numerous estimators for the energy dissipation rate due to wave breaking though none with enduring credibility. Le Mehaute (1962) developed an estimator for the energy dissipation rate based on the resemblance between surf zone waves and bores.

But application of the bore model to the barred profiles or very gentle slopes is problematic since wave breaking ceases after a while (Hamm et al. 1993). A more popular approach is based on parameterization (Battjes and Janssen 1978, Thornton and Guza 1986, Battjes and Stive 1985, Sobey 1989), with a calibrated loss coefficient. According to Battjes (1994), the energy dissipation rate can be realistically predicted with typical relative errors of less than 10%. Energy dissipation is a continuous process, which starts with surface instability and reaches maximum during wave breaking. The concept of a fraction of breaking waves (Battjes and Janssen 1978) is useful in the respect. In the surf zone, the energy dissipation due to bottom friction is much less significant. A pragmatic model is Jonsson (1966).

The present understanding on mass and momentum transport due to wave breaking remains very limited. Svendsen (1984) derived expressions of energy flux and radiation stress in the inner zone by including the effect of the wave shape and of the surface roller considered as a volume of water carried shorewards with the breaker. But these expressions rely on many empirical parameters which are still not well verified.

The phase-averaging models, because of using a wave theory for the closure of the wave-related terms in the time-averaged equations, have difficulty dealing with partial wave reflection. At present, their application must be restricted to weakly reflecting beaches.

3.3 Open Boundary Conditions (OBC)

In the numerical simulation of wave propagation in coastal regions, the physical domain must be truncated to seaward. The truncated solution domain has open

boundaries across which information should be allowed to transmit freely. There should be no numerical reflection at the open boundaries.

The importance of OBC can not be overstated. If an OBC is not properly specified, the interior numerical solutions will be contaminated, in a potentially unrecognizable manner. Numerical instability may even be induced. In addition, the inability to specify correct initial conditions further signifies the importance of OBC. The artificial disturbance-the discrepancy between the imposed initial conditions and true initial conditions-would be reflected back and forth from the open boundaries if they are not "transparent" (Bode and Sobey 1984). For a dissipative system, this disturbance will be attenuated and eventually disappears, with a "calm-down" period depending on the degree of dissipation in the system. For a non-dissipative system, the disturbance persists forever.

Unfortunately, absolutely non-reflecting boundary conditions are available only for some very simple cases, e.g. for one-dimensional, linear wave problems (Verboom et al. 1982). For non-linear systems, only weakly reflecting boundary conditions can be achieved.

The most commonly used OBCs in the literature are listed in Table 3-1. In the table, q represents a dependent variable of interest, C is a wave speed, t is the time, x and y respectively denote an outward normal vector and a tangential vector which form a local coordinate system.

In the sponge-layer method, an artificial damping is imposed within a sponge layer to gradually attenuate outgoing information. The computational domain for this method must be extended such that the area of interest is not affected by the sponge layer.

The Sommerfeld radiation condition (SRC) is another popular OBC which is derived from one dimensional harmonic wave equation. There are many variations in SRC depending on definition of the wave speed C adopted. CLP and GRD are the special forms of SRC with C=0 and C=∞ respectively. SPO is a combination of the sponge-layer method and the Sommerfeld OBC (Israeli and Orszag 1981). HOC (Hedstrom 1979) was initially derived for a one-dimensional nonlinear homogeneous hyperbolic system. Theoretically it has not been successful in extending the HOC to non-linear hyperbolic systems in two spatial dimensions.

Table 3.1 Summary of Open Boundary Conditions

OBC TYPE	ABBR.	REFERENCE
Sponge layer		various
Clamped, q=0	CLP	various
Zero gradient, $\frac{dq}{dx}=0$	GRD	various
Sommerfeld radiation conditions $\frac{\partial q}{\partial t}+C\frac{\partial q}{\partial x}=0$	SRC	various
Mixed sponge layer / free wave propagation	SPO	Israeli and Orszag (1981)
Oblique Radiation, $\frac{\partial q}{\partial t}\frac{\partial^2 q}{\partial x\partial y}+C\left(\frac{\partial q}{\partial x}\right)^2\cdot\left(\frac{\partial q}{\partial y}\right)^2$	ORC	Raymond and Huo (1984)
Invariant along an incoming characteristics $\ell\frac{\partial \vec{q}}{\partial t}=0$, ℓ: left eigenvector corresponding to incoming characteristics.	HOC	Hedstrom (1979)
Highly absorbing local boundary conditions $\left(\frac{d}{dx}-\Gamma(\frac{\partial}{\partial y},\frac{\partial}{\partial t})\sqrt{\frac{\partial^2}{\partial t^2}-\frac{\partial^2}{\partial y^2}}\right)q=0$ $\Gamma\left(\frac{\partial}{\partial y},\frac{\partial}{\partial t}\right)$ is a pseudo-differential operator: $\Gamma\left(y,t,\frac{\partial}{\partial y},\frac{\partial}{\partial t}\right)q=\iint e^{i(\omega y+\xi t)}\Gamma(y,t,i\omega,i\xi)\hat{q}(\omega,\xi)d\xi d\omega$		Engquist and Majda (1976)

The Engquist and Majda OBC in the form presented in Table 3.1 was derived for a scalar wave equation. But open boundary conditions for first order linear symmetric systems can be developed by using a similar approach.

Harper and Sobey (1983), Bode and Sobey(1984), Chapman (1985), Røed and Cooper (1986), among others, have evaluated performance of some OBCs listed in Table 3.1. Røed and Cooper (1986) evaluated CLP, GRD, SRC, ORC, SPO and HOC by using a barotropic, linear model in a rectangular grid under three different forcing conditions: uniform alongshore wind, bell-shaped wind, and moving storms, representing strong, weak and moving forcing at the open boundaries, respectively. They found that HOC is the only OBC which provides a reasonable response in all cases studied, and suggested that CLP and SRC be avoided in most applications. They also pointed out that the choice of OBC is problem dependent.

Besides the OBC's discussed above, there are many OBC's developed for specific problems. For instance, Harper and Sobey (1983) developed an OBC for storm surge modeling, Verboom et al. (1984) designed an OBC for a system consisting of two nonlinear equations with the form of solutions known. Based on the mass conservation at a computational cell, Larsen et al. (1983) also developed an OBC for short wave simulations in terms of the characteristics of incoming waves. But careful examination of the OBC of Larsen et al. shows that it is just a discretized form of the Sommerfeld OBC with a wave speed equal to twice the phase speed.

When studying linearized Navier-Stokes equations. Rudy et al.(1980) extended HOC by adding a spring-effect term to enhance numerical stability and accelerate the convergence of numerical solutions to steady state solutions. This additional term

prevents the numerical solutions from overshooting or undershooting.

There are no analytical non-reflecting boundary conditions for nonlinear systems in a two or three dimensional space. Some of the OBCs listed in the Table 3-1 may be extended for nonlinear systems, but there are no guarantees for weak reflections and numerical stability. The specification of the OBC for nonlinear systems still relies on numerical experiment. In this study, HOC will be used since it has been well proven and is relatively easy to be implemented.

3.4 Numerical Schemes

The integral conservation equations for wave-averaged parameters given in Chapter 2 form a nonlinear and hyperbolic (See Section 5.2 and Section 6.2) system. This system will be solved numerically. This section offers a brief review on numerical methods, aiming to provide a general guideline for selecting an appropriate method for this system.

The most common numerical methods include finite difference method (FDM), finite element method (FEM) and method of characteristics (MOC). Since the information in a hyperbolic system propagates at finite speed, FEM and implicit FDM are physically not appropriate for simulating a hyperbolic system because these methods imply an infinite propagation speed (Potters 1973). Either explicit FDM or MOC can be used for the present model.

FDM is easy to implement numerically, but numerical diffusion can be a significant problem. This is a big concern for simulating wave propagation. To minimize the numerical diffusion, many high-resolution FDM schemes for conservative systems have been developed by using the equations in conservative form; examples are flux-corrected

transport scheme (Book et al. 1974) and total variation diminishing scheme (Yee and Warming 1985). In this manner, the difference equations remain physically consistent with the conservation laws on which the PDE's are based. For this approach, the focus is on the calculation of flux terms. If a dependent variable is specified for a computational cell instead of at grid points, this approach is called a finite volume method (FVM). In this approach, the general boundary condition problem is relegated to the evaluation of the flux across a boundary, which in some cases is easier and thus more favorable.

In MOC, attention is directed to a set of compatibility equations derived by linearly combining the original differential equations weighted by the components of an eigen-vector of the system. Each compatibility equation describes the information propagating at a single speed. The strength of MOC lies in its ability of tracing the information propagation. This feature is especially useful for solving a system with multiple propagation speeds. One significant feature of the compatibility equations is that they are in a solution space of one fewer dimension than the original equations. For example, if a system is defined in x-t space, then the compatibility equations can be defined in a one-dimensional subspace, and the compatibility equations can be written as ordinary differential equations. In two- or three-dimensional physical space, the compatibility equations are still partial differential equations, yet they are defined in a space of one fewer dimension. This reduction in the dimensions of the solution space should simplify numerical simulation significantly, especially for problems in a one-dimensional space. In addition, MOC is capable of dealing with discontinuity problems. The disadvantage of MOC is that in general the compatibility equations in a two or three-dimensional space are formulated in non-conservative forms, thus the corresponding difference equations do

not possess the preservative feature of the original differential system.

Every numerical method has its own advantages and disadvantages. In selecting a numerical method, besides its suitability for the interior domain, consideration should also be given to forming open boundary conditions. The Hedstrom OBC, to be used in this study, is essentially based on MOC. Moreover, all high-resolution schemes of FDM are generally based on MOC, for instance, the very popular Osher et al. (1982) scheme. This means that, even if using FDM the knowledge of the characteristics of a system is still required in order to utilize high-resolution schemes. All factors considered, MOC is most suitable for the model studied here.

MOC has been used extensively in hydrodynamics simulation, i.e., in modeling of tidal propagation by Daubert et al. (1967) and Townson (1974), and of flood wave propagation by Katopodes and Strelkoff (1979). Surprisingly, MOC has not been used for simulating mean flow circulation by coastal engineers.

In a one-dimensional space, the number of characteristics is limited and the compatibility equations are ordinary differential equations. Numerical solutions can be easily obtained by integrating the compatibility equations along the characteristics or characteristic curves. In contrast, MOC is not as convenient in two or three spatial dimensions because the compatibility equations are still partial differential equations. The MOC approach to two-dimensional problems is totally different from that to a one-dimensional problem.

The key to applying MOC in two spatial dimensions is how to take advantage of the infinite sets of compatibility equations. The most popular numerical scheme is based on the integration of compatibility equations along several bi-characteristics which are

defined as the curve of tangency between a characteristic surface with a characteristic conoid which inscribes the characteristic surfaces. This scheme is generally termed as the bi-characteristics method. Since the compatibility equations are still partial differential equations, the integration along the bi-characteristics does not eliminate the differentiation along the other direction, so-called cross derivatives (Katopodes et al. 1979). The stability and accuracy of this numerical scheme depends very much on how to evaluate these cross-derivatives.

For a hyperbolic system with a Jacobian coefficient matrix which could factorize into a quadratic element and a repeated linear element, Bulter (1960) developed a second-order bi-characteristics method, using a continuity equation and compatibility equations along four bi-characteristics. Through algebraic manipulation of these five difference equations, the terms associated with the cross-derivatives were all eliminated. In this manner, MOC becomes completely an integration problem. The solutions at a grid point can be obtained by integrating the compatibility equations along the bi-characteristics which originate from some initial points corresponding to the previous time step. The value of a variable at the starting end of the bi-characteristics segment may be obtained through interpolation from the values at the surrounding grid nodes.

4 APPARENT STRESS CLOSURE

The depth-integrated wave-averaged equations for mass, momentum and wave energy derived in Chapter 2 contain mean and fluctuating parts of velocity and pressure and other unknowns. The number of the unknowns far exceeds the number of the governing equations available. This is the apparent stress closure problem familiar in turbulence. To close the system, a set of closure relationships must be introduced. The number of the closure relationships should be equal to the number of the unknowns minus the number of equations.

Which variables to be closed and how to close them depend on the purpose of a study. Since the objective of this study is to simulate evolution of mean wave parameters, wave height, wave setup and wave-induced mean flow velocity will serve as principal variables, and all other variables should be related to these variables. For instance, in a two-dimensional space, four governing equations allow solving four unknowns, i.e., wave height, wave setup and mean flow velocity components below the wave trough in x and y directions.

All the variables to be closed are involved in some terms which physically represent the fluxes of mass, momentum and energy. Naturally, there are two ways to close this system. One is to close the individual variables and then to compute the flux terms; the other is to close the flux terms, like the Reynolds stress closure in turbulence. Since the present system is comprised by the depth-integrated, wave-averaged equations, closure of individual variables would require tremendous computational work for evaluating the flux terms during simulation. Thus closure of a flux term as a whole is a better choice here, though this closure method may introduce more closure variables than the closure of individual variables.

The fluctuating components of velocity and pressure include both wave motion and turbulence. It is necessary to further decompose the fluctuating component into a turbulence

part and a wave part, as closure hypotheses for the wave motion and turbulence are quite different. The turbulence closure problem has been studied extensively, popular reviews being Bradshaw (1972) and Tennekes and Lumley (1973). The horizontal velocity fluctuation, for example, is further decomposed as

$$\tilde{u} = \tilde{u}_w + u' \tag{4.1}$$

where $\tilde{u}_w$ represents the wave fluctuation and u' the turbulent fluctuation.

This further decomposition does not change the integral continuity Equation (2.18), but it will result in extra terms in the momentum conservation equations and the wave energy equation. In general, the turbulence frequency is much higher than the wave frequency, little correlation is expected between them and none is assumed here. The apparent stress s_{xx} in Equation (2.21), for instance, can be written as

$$s_{xx} = s_{xx,w} + s'_{xx} = -\Delta p_w - \rho\overline{\tilde{u}_w^2} + \rho\overline{\tilde{w}_w^2} - \Delta p' - \rho\overline{u'^2} + \rho\overline{w'^2} \tag{4.2}$$

For terms of third or higher power, such as the energy flux terms in Equation (2.24), this decomposition will not just cause the split of a term into a wave part and a turbulence part, but also include an interaction term between them, typically the transport of turbulent energy by wave motion. As reviewed in Chapter 3, the predominant fluid motion in the nearshore region is wave motion, even after wave breaking. To focus on wave dynamics, in this study the mass, momentum and energy fluxes due to turbulence and the interaction between wave motion and turbulence are all neglected. The turbulence is considered only in evaluating energy dissipation during wave breaking.

In the Eulerian framework, the vertical distribution of the wave-averaged quantity between the wave trough and crest is quite different from that below the wave trough

because the elevation between the trough and the crest is submerged only part of the time. For example, if the velocity between the wave trough and crest is derived through the first order Taylor series expansion based on the velocity at the mean water level from the small-amplitude wave theory, the wave-averaged horizontal velocity is formulated as

$$\bar{u}(z) = \frac{H \cdot \omega}{2 \cdot \pi \cdot \sinh(kh)} \sqrt{1 - (\frac{2z}{H})^2} \qquad for \quad \eta_{tr} \le z \le \eta_c \tag{4.3}$$

where H is the wave height, ω the wave angular frequency, k the wave number, h the still water depth, η_{tr} the wave trough elevation, and η_c the wave crest elevation. The wave-averaged velocity below the trough is identically zero. The vertical distribution of the mean velocity is sketched in Figure 4.1, with a maximum value at the mean water level.

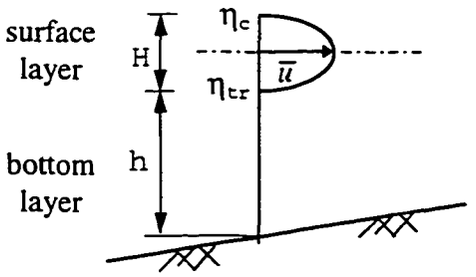

Figure 4.1 Sketch of vertical structure of wave-averaged velocity

To recognize the fact that the wave-averaged variables have different characteristics in the regions below and above the wave trough, these two regions will be treated individually. For convenience, in the following discussions the region between the trough and the crest will be referred to as a surface layer, and the region between the seabed and the trough as a bottom layer. It is further assumed that the water surface kinematics is dominated by wave motion and that the mean velocity in the bottom layer is uniform over the depth. Following this two-layer concept, the depth integration is performed over the surface layer and the bottom layer separately. In this manner, the integral continuity Equation (2.18) is written as

$$\frac{\partial \bar{\eta}}{\partial t}+\frac{\partial}{\partial x}\int_{-h}^{\eta_w}\bar{u}dz+\frac{\partial}{\partial y}\int_{-h}^{\eta_w}\bar{v}dz+\frac{\partial}{\partial x}\int_{\eta_w}^{\eta_c}\bar{u}dz+\frac{\partial}{\partial y}\int_{\eta_w}^{\eta_c}\bar{v}dz=0 \tag{4.4}$$

where $\bar{\eta}$ is the mean water surface elevation from still water level or wave setup. Similarly, the integral x- and y-momentum Equations (2.19) and (2.20) are rewritten as

$$\begin{aligned}&\frac{\partial}{\partial t}(\int_{-h}^{\eta_{tr}}\bar{u}dz+\int_{\eta_{tr}}^{\eta_c}\bar{u}dz)+\frac{\partial}{\partial x}(\int_{-h}^{\eta_{tr}}\bar{u}^2dz+\int_{\eta_{tr}}^{\eta_c}\bar{u}^2dz)+\frac{\partial}{\partial y}(\int_{-h}^{\eta_{tr}}\overline{uv}dz+\int_{\eta_{tr}}^{\eta_c}\overline{uv}dz)=\\&-g(h+\bar{\eta})\frac{\partial\bar{\eta}}{\partial x}+\frac{1}{\rho}[\frac{\partial}{\partial x}(\int_{-h}^{\eta_{tr}}s_{xx}dz+\int_{\eta_{tr}}^{\eta_c}s_{xx}dz)+\frac{\partial}{\partial y}(\int_{-h}^{\eta_{tr}}s_{xy}dz+\int_{\eta_{tr}}^{\eta_c}s_{xy}dz)-\tau_{bx}]\end{aligned} \tag{4.5}$$

$$\begin{aligned}&\frac{\partial}{\partial t}(\int_{-h}^{\eta_w}\bar{v}dz+\int_{\eta_w}^{\eta_c}\bar{v}dz)+\frac{\partial}{\partial x}(\int_{-h}^{\eta_w}\overline{uv}dz+\int_{\eta_w}^{\eta_c}\overline{uv}dz)+\frac{\partial}{\partial y}(\int_{-h}^{\eta_w}\bar{v}^2dz+\int_{\eta_w}^{\eta_c}\bar{v}^2dz)=\\&-g(h+\bar{\eta})\frac{\partial\bar{\eta}}{\partial y}+\frac{1}{\rho}[\frac{\partial}{\partial x}(\int_{-h}^{\eta_w}s_{xy}dz+\int_{\eta_w}^{\eta_c}s_{xx}dz)+\frac{\partial}{\partial y}(\int_{-h}^{\eta_w}s_{yy}dz+\int_{\eta_w}^{\eta_c}s_{xy}dz)-\tau_{by}]\end{aligned} \tag{4.6}$$

And the wave energy Equation (2.24) takes the form

$$\begin{aligned}&\frac{1}{2}\frac{\partial}{\partial t}[\int_{-h}^{\eta_w}(\overline{\tilde{u}^2}+\overline{\tilde{v}^2}+\overline{\tilde{w}^2})dz+\int_{\eta_w}^{\eta_c}(\overline{\tilde{u}^2}+\overline{\tilde{v}^2}+\overline{\tilde{w}^2})dz+g(\overline{\eta}^2+\overline{\tilde{\eta}^2})]+\\&\frac{\partial}{\partial x}\{\int_{-h}^{\eta_w}[\overline{P_d\tilde{u}}/\rho+(\overline{\tilde{u}^3}+\overline{\tilde{u}\tilde{v}^2}+\overline{\tilde{u}\tilde{w}^2})/2]dz+\int_{\eta_w}^{\eta_c}[\overline{P_d\tilde{u}}/\rho+(\overline{\tilde{u}^3}+\overline{\tilde{u}\tilde{v}^2}+\overline{\tilde{u}\tilde{w}^2})/2]dz\}+\\&\frac{\partial}{\partial y}\{\int_{-h}^{\eta_w}[\overline{\tilde{P}_d\tilde{v}/\rho}+(\overline{\tilde{u}^2\tilde{v}}+\overline{\tilde{v}^3}+\overline{\tilde{v}\tilde{w}^2})/2]dz+\int_{\eta_w}^{\eta_c}[\overline{\tilde{P}_d\tilde{v}/\rho}+(\overline{\tilde{u}^2\tilde{v}}+\overline{\tilde{v}^3}+\overline{\tilde{v}\tilde{w}^2})/2]dz\}=\\&-\frac{\partial}{\partial x}\int_{\eta_w}^{\eta_c}\frac{\bar{u}(\overline{\tilde{u}^2}+\overline{\tilde{v}^2}+\overline{\tilde{w}^2})}{2}dz-[\int_{-h}^{\eta_w}(\frac{3\overline{\tilde{u}^2}}{2}+\frac{(\overline{\tilde{v}^2}+\overline{\tilde{w}^2})}{2})dz]\frac{\partial U_b}{\partial x}-\frac{U_b}{2}\frac{\partial}{\partial x}[\int_{-h}^{\eta_w}(\overline{\tilde{u}^2}+\overline{\tilde{v}^2}+\overline{\tilde{w}^2})dz]\\&-\frac{\partial\bar{u}_s}{\partial x}[\int_{\eta_w}^{\eta_c}\overline{\tilde{u}^2}dz]-(\frac{\partial\bar{v}}{\partial x}+\frac{\partial\bar{u}}{\partial y})(\int_{-h}^{\eta_w}\overline{\tilde{u}\tilde{v}}dz+\int_{\eta_w}^{\eta_c}\overline{\tilde{u}\tilde{v}}dz)-\frac{\partial}{\partial y}\int_{\eta_w}^{\eta_c}\frac{\bar{v}}{2}(\overline{\tilde{u}^2}+\overline{\tilde{v}^2}+\overline{\tilde{w}^2})dz\\&-\frac{\partial V_b}{\partial y}\int_{-h}^{\eta_w}(\frac{\overline{\tilde{u}^2}+\overline{\tilde{w}^2}}{2}+\frac{3}{2}\overline{\tilde{v}^2})dz-\frac{\bar{v}_b}{2}\frac{\partial}{\partial y}[\int_{-h}^{\eta_w}(\overline{\tilde{u}^2}+\overline{\tilde{v}^2}+\overline{\tilde{w}^2})dz]-\frac{\partial\bar{v}_s}{\partial y}\int_{\eta_w}^{\eta_c}\overline{\tilde{v}^2}dz-D_t-D_b\end{aligned} \tag{4.7}$$

The mean velocity and flux terms in the surface layer will be treated as closure variables.

The wave height does not explicitly appear in Equations (4.4) through (4.7); it is only implicated as the range of depth integration over the surface layer, i.e., $H=\eta_c-\eta_{tr}$. Since the wave height is one of most informative parameters describing mean wave field, it is desirable to express the wave height explicitly in the governing equations. This can be achieved by introducing a scale parameter when evaluating a flux term in the surface layer. For example, the mass flux in the surface layer can be expressed by

$$\int_{\eta_{tr}}^{\eta_c} \bar{u}(z;x,y,t)dz = \alpha_s U_s H \tag{4.8}$$

where U_s is the scale parameter of $\bar{u}(z;x,y,t)$ in the surface layer, and α_s is a shape factor. The shape factor depends on the vertical structure of $\bar{u}(z;x,y,t)$ in a layer and on the choice of the scale parameters. This approach is also applied to the evaluation of flux terms in the bottom layer. Thieke and Sobey (1990) chose the value at the mean water level as the scale parameter for the surface layer, and the value at the mid-depth as the scale parameter for the bottom layer, and established a set of shape factors corresponding to these scale parameters. Physically, it does not matter how the scale parameters are chosen as long as the shape factors are consistently determined. Thus scale parameters should be so chosen that the algebraic manipulation is simplest. If the mean values in a layer are chosen as the scale parameters, all the corresponding shape factors are identically equal to unity. In addition, this choice does not have to assume that the vertical profile of a closure variable is self-similar (Thieke 988), which is indispensable if the scale parameter is represented by the value at any particular elevation. In this study, the mean values of each layer will be used as the scale parameters.

4.1 Layer-Averaged Scale Parameters In Closure Solution

The closure process is focused along the local wave propagation direction, with vector quantities being resolved into this direction. Such closure solutions can be directly used for wave propagation in a one dimensional space. For a two-dimensional space, the closure solutions can be transformed into solutions for the desirable closure variables, the exact transformation being discussed in Section 4.5. In the direction of wave propagation, the layer-arranged scale parameters must be established for

(1) $\hat{U}_s$, the layer-averaged mean-flow velocity in the surface ("s") layer in the mass and momentum conservation equations.

$$\hat{U}_s = \frac{1}{H}\int_{\eta_{tr}}^{\eta_c} \bar{u}\,dz \tag{4.9}$$

(2) $\hat{U}_s^2$, the layer-averaged mean-flow momentum flux in the surface layer in the momentum conservation equations.

$$\hat{U}_s^2 = \frac{1}{H}\int_{\eta_{tr}}^{\eta_c} \hat{U}_s^{\,2}\,dz \tag{4.10}$$

(3) S_s and S_b, the layer-averaged apparent stresses in the surface ("s") and bottom ("b") layers in the momentum conservation equations.

$$S_s = \frac{1}{H}\int_{\eta_{tr}}^{\eta_c} [-\Delta p + \rho(\overline{\tilde{w}^2} - \overline{\tilde{u}^2})]dz \tag{4.11}$$

$$S_b = \frac{1}{h - \eta_{tr}}\int_{-h}^{\eta_{tr}} \rho(\overline{\tilde{w}^2} - \overline{\tilde{u}^2})dz \tag{4.12}$$

(4) F_s and F_b, the layer-averaged energy fluxes in the surface ("s") and bottom ("b") layers in the wave energy equation.

$$F_s = \frac{1}{H}\int_{\eta_{tr}}^{\eta_c}[\frac{\overline{\tilde{p}\tilde{u}}}{\rho} + \frac{1}{2}(\overline{\tilde{u}\tilde{u}\tilde{u}} + \overline{\tilde{u}\tilde{w}\tilde{w}})]dz \tag{4.13}$$

$$F_b = \frac{1}{h - \eta_{tr}}\int_{-h}^{\eta_{tr}}[\frac{\overline{\tilde{p}\tilde{u}}}{\rho} + \frac{1}{2}(\overline{\tilde{u}\tilde{u}\tilde{u}} + \overline{\tilde{u}\tilde{w}\tilde{w}})]dz \tag{4.14}$$

(5) K_s, the layer-averaged energy flux due to the mean flow current in the surface ("s") layer in the wave energy equation.

$$K_s = \frac{1}{H}\int_{\eta_{tr}}^{\eta_c}\frac{\hat{U}_s}{2}(\overline{\tilde{u}^2} + \overline{\tilde{w}^2})dz \tag{4.15}$$

(6) N_s and N_b, the layer-averaged horizontal momentum flux of wave motion in the surface ("s") and bottom ("b") layers in the wave energy equation.

$$N_s = \frac{1}{H}\int_{\eta_{tr}}^{\eta_c}\overline{\tilde{u}^2}dz \tag{4.16}$$

$$N_b = \frac{1}{h - \eta_{tr}}\int_{-h}^{\eta_{tr}}\overline{\tilde{u}^2}dz \tag{4.17}$$

(7) W_s and W_b, the layer-averaged wave kinetic energy (double) in the surface ("s") and bottom ("b") layers in the wave energy equation.

$$W_s = \frac{1}{H}\int_{\eta_{tr}}^{\eta_c}(\overline{\tilde{u}^2} + \overline{\tilde{w}^2})dz \tag{4.18}$$

$$W_b = \frac{1}{h - \eta_{tr}}\int_{-h}^{\eta_{tr}}(\overline{\tilde{u}^2} + \overline{\tilde{w}^2})dz \tag{4.19}$$

(8) $\overline{\eta^2}$, the wave-averaged value of the square of the water surface displacement in the wave energy equation.

$$\overline{\eta^2} = \frac{1}{T}\int_0^T \tilde{\eta}^2 \, dt \tag{4.20}$$

(9) U_{rms}, the root mean square of velocity near the bed, being used for the calculation of the bottom shear stress in the momentum conservation equations.

$$U_{rms} = \sqrt{\frac{1}{T}\int_0^T \tilde{u}_b^2 \, dt} \tag{4.21}$$

(10) $\overline{U_b^3}$, wave-averaged value of the cubic of the fluctuating velocity near the bed, used for calculating the energy dissipation due to bottom friction in the wave energy equation.

$$\overline{U_b^3} = \frac{1}{T}\int_0^T \left|\tilde{u}_b\right|^3 dt \tag{4.22}$$

In addition to these 14 closure variables which appear explicitly in the depth-integrated, wave-averaged equations, the wave trough elevation, η_{tr}, is also treated as a closure variable.

Given a set of wave height, wave period and water depth, these closure variables can be estimated from a wave theory. If the closure solutions are computed over a comprehensive range of wave height, wave period and water depth, a solution surface can be established. In later computer modeling, the values of the closure variables are interpolated from the solution surface for given wave height, wave period and water depth.

The large number of closure variables suggests that the choice of a wave theory for closure will be a crucial step. The linear wave theory would give explicit forms of solutions for all the closure variables, but the error is significant within and approaching a surf zone (Thieke 1988). Similarly, Stokes' and Cnoidal wave theory are only valid in deep water and in shallow water, respectively, and use of either one would limit the range of applicability of the model. Thus a wave theory consistently valid in deep water and shallow water should be

used for establishing solution surfaces. In this study, the Fourier approximation wave theory (Fenton 1987) is chosen. A brief introduction of this wave theory is given below.

4.2 Fourier Approximation Wave Theory

Fourier approximation wave theory is a hybrid analytical-numerical theory for steady progressive waves, in which the solution is partially analytical in accommodating the field equation, kinematic bottom boundary condition and the periodic lateral boundary conditions, but is completed numerically.

Fourier approximation wave theory can be used with both Stokes' first and second definitions of phase speed. But the use of the second definition needs knowledge of the current in the bottom layer which is one of the unknowns being sought. Only Stokes' first definition of phase speed, with U_E=0, is adopted here.

The stream function in a steady frame (moving with the crest) is represented (Sobey 1989) by the truncated Fourier series:

$$\Psi(X,z) = \overline{U}(h+z) + \frac{g^2}{\omega^3}\sum_{j=1}^{N} B_j \frac{\sinh jk(h+z)}{\cosh(jkh)}\cos(jkX) \qquad (4.23)$$

where the B_j are the dimensionless Fourier coefficients, of which there are N, ω the wave angular frequency, k the wave number, g the gravitational acceleration, h water depth, $\overline{U}$ the current in the steady frame, z the vertical coordinate which is measured positively upward from mean water level, and X the horizontal coordinate. This stream function automatically satisfies the field equation, the kinematic bottom boundary condition (for a locally horizontal bed) and the periodic lateral boundary conditions.

The water surface elevation is defined at M+1 discrete points (identified from 0 to M in

the following description) instead of as a continuous function. The numerical solutions may be obtained through nonlinear, least squares optimization. The objective function is

$$O = \sum_{1}^{2M+6} f_i^2 \tag{4.24}$$

where f_i's are defined as follows

For wave height,

$$f_1 = \eta_0 - \eta_M - H \tag{4.25}$$

For the mean water level

$$f_2 = \frac{1}{2M}(\eta_0 + 2\sum_{i=1}^{M-1}\eta_i + \eta_M) \tag{4.26}$$

For the kinematic free surface boundary condition at each of the free surface nodes,

$$f_i = \Psi(X_i, \eta_i) + Q \quad i = 0, M \tag{4.27}$$

For the dynamic free surface boundary condition also at each of the free surface nodes,

$$f_i = \frac{1}{2}(\frac{\partial\psi(X_i,\eta_i}{\partial x})^2 + \frac{1}{2}(\frac{\partial\psi(X_i,\eta_i)}{\partial z})^2 + g\eta_i - R \quad i = 0, M \tag{4.28}$$

And finally for the Eulerian current

$$f_{2m+5} = \frac{\omega}{k} - \overline{U} - U_E \tag{4.29}$$

or the Stokes drift

$$f_{2m+6} = \frac{\omega}{k} - \frac{Q}{h} - U_s \tag{4.30}$$

where R is the Bernoulli constant, and Q is the mass flux in the steady frame. In solving the system, the wave height, water depth and wave angular frequency are given. All 2M+6 f_i's should be zero in exact solutions.

The unknown variables in a Fourier wave solution are k, U, U_s, Q, R, h_i (i=0,1,...M) and

B_j, of which there are M+N+6. Here U_E is equal to zero, based on Stoke's first definition of wave phase speed. These unknowns are implicitly involved in a set of 2N+6 constraints. So the problem is uniquely defined for M=N and over-specified for M<N. The solutions can be obtained by iteration until the objective function, the sum of the square of f_i functions is within a tolerance limit.

Once these parameters are known, the horizontal and vertical velocities can be established from the stream function (Equation 4.23), and the dynamic pressure from the Bernoulli equation in the steady frame.

4.3 Solution Surfaces

The value of a closure variable is uniquely determined by using the Fourier approximation wave theory for a given set of wave height, wave period and water depth. To organize the solution surfaces, these three dimensional parameters are combined into two dimensionless parameters, a dimensionless water depth ($h\cdot\omega^2/g$) and a dimensionless wave height (H/H_{miche}). Here H_{miche} is the Miche (1950) estimate of wave height limit, $H_{miche}=0.142\cdot L\cdot\tanh(kh)$, where L is the wave length. In establishing the solution surfaces, the base 10 logarithmic value of the dimensionless water depth is plotted as the abscissa, and the dimensionless wave height as the ordinate. The reason beyond using the Miche's wave height limit as a scale factor is to make the range of the ordinate values relatively uniform across the abscissa. The broken wave heights corresponding to shallow water depths are small. Without scaling, the resolution would be compromised for shallow-water portion of the solution surface which is formed by solution nodes on a uniform rectangular mesh.

The closure variables are also transformed into dimensionless variables using a set of

scale parameters. The scale parameters are: ω/g for $\hat{U}_s$ and U_{rms}, ω^2/g^2 for $\hat{U}_s^2$, N_s, N_b, W_s and W_b, ω^4/g^2 for $\overline{\eta^2}$, ω^3/g^3 for F_s, F_b, K_s and $\overline{U_b^3}$, and $\rho\cdot\omega^2/g^2$ for S_s and S_b.

A total of 546 solution points, corresponding to 21 different dimensionless water depths and 26 different dimensionless wave heights, were obtained to construct the solution surfaces. The increase in wave non-linearity with increase in wave height or decrease in water depth required use of different truncation orders (N) in the Fourier approximation for different portions of the solution surfaces, as shown in Figure 4.2. The truncation orders were often higher than absolutely necessary to guarantee a smooth transition between adjacent regions. The solution surfaces are shown in Figures 4.3 through 4.17.

As wave height approaches some limit, numerical instability starts to occur (Fenton 1988). As a rule of thumb, the numerical solutions are reliable for the wave heights within 95% of the limit. The limit of application of the solution surfaces may be determined using some wave breaking criterion consistent with the Fourier approximation wave theory. Williams (1981) gave the ratio of wave height limit to water depth, H_b/h, using high-order Stokes expansions and analytically incorporating the crest singularity. These results can be used as the upper limits of the solution surfaces since they are also based on a high-order wave theory. The Williams' short wave limit is $H_b/L=0.141063$ for deep water waves, and the long wave limit $H_b/h=0.83322$ for solitary waves. Fenton (1988) expressed the wave height limits as a function of the wave length and the water depth based on the Williams' data

$$\frac{H_b}{h} = \frac{0.141063\cdot(L/h) + 0.0095721\cdot(L/h)^2 + 0.0077829\cdot(L/h)^3}{1 + 0.078834\cdot(L/h) + 0.0317567\cdot(L/h)^2 + 0.0093407(L/h)^3} \tag{4.31}$$

The upper boundary based on this criterion is also shown in Figures 4.2 through 4.17.

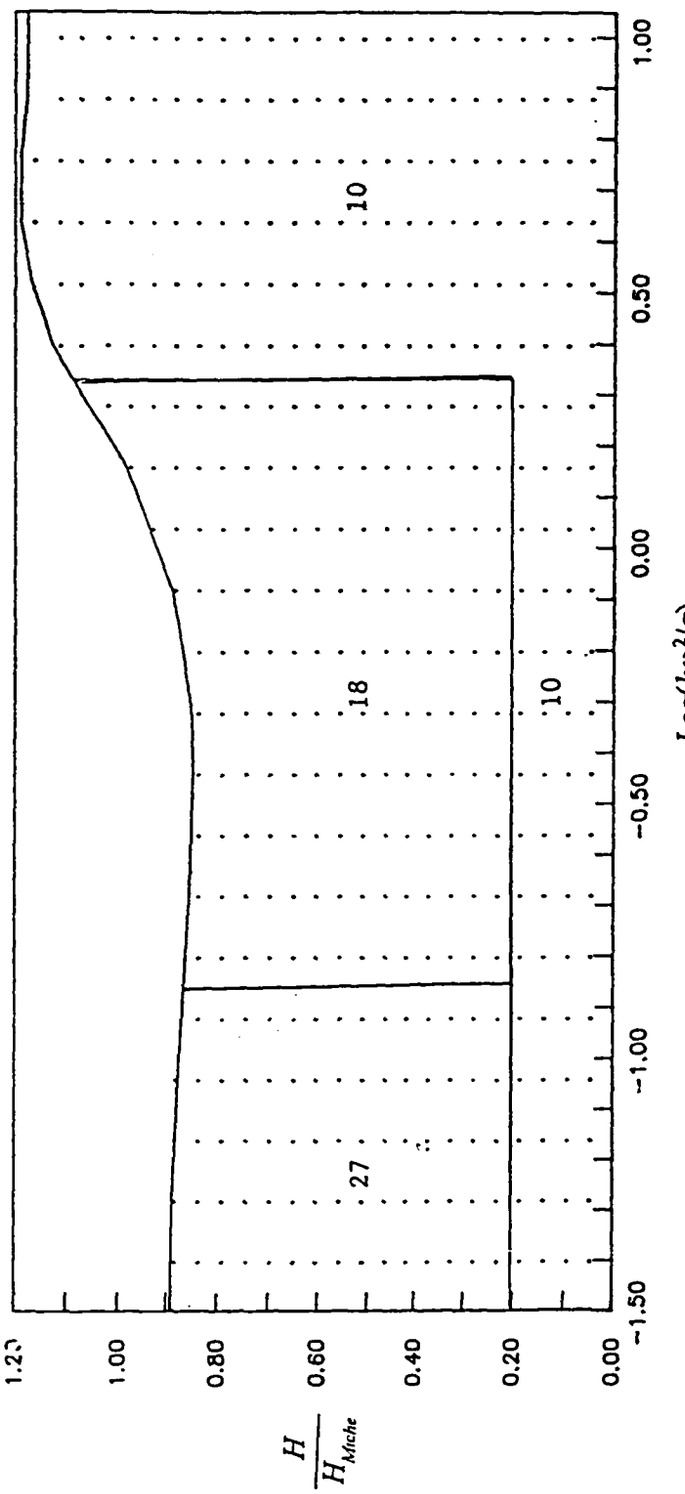

Figure 4-2: Order of Truncation in Fourier Approximation Wave Theory for Establishment of Solution Surfaces

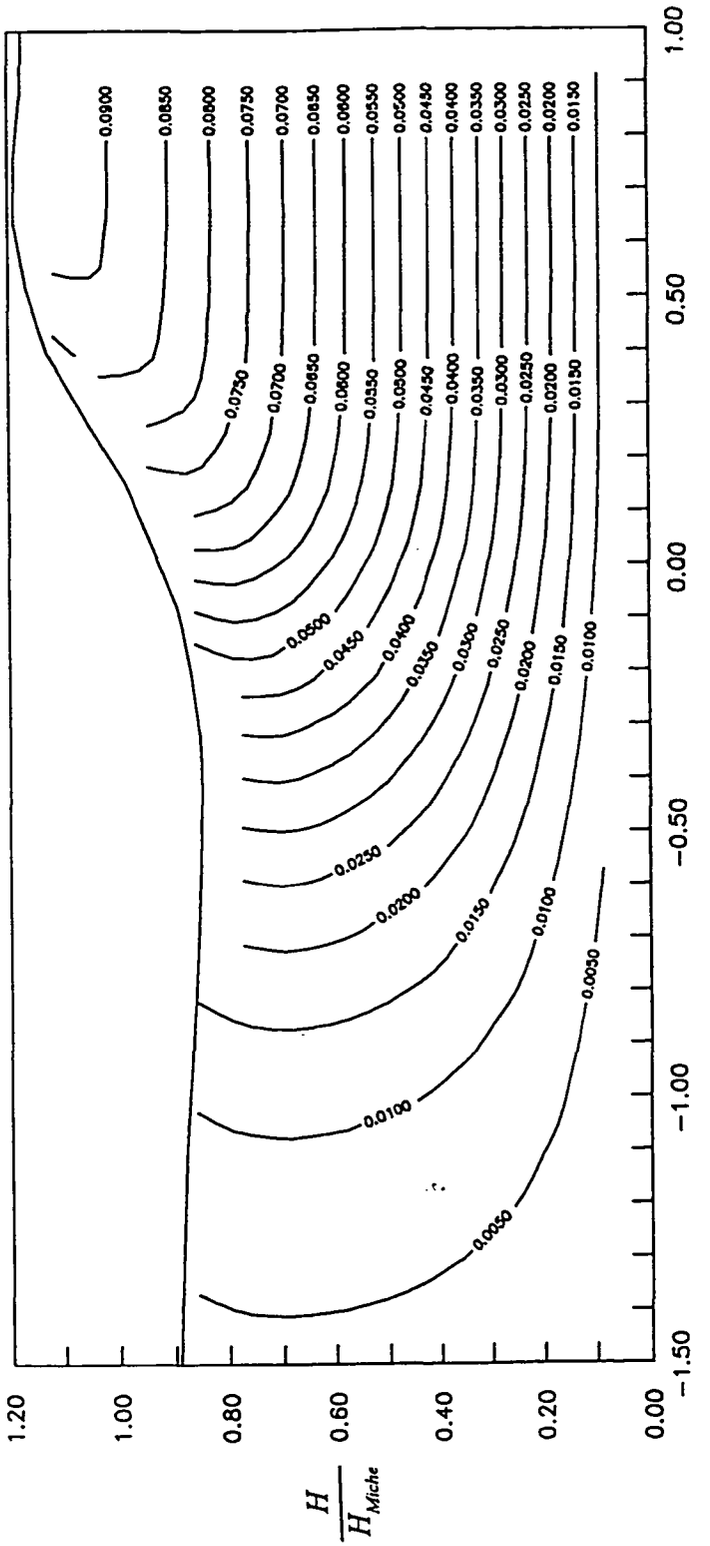

Figure 4 - 3: $\frac{\hat{U},\omega}{g}$ Solution Surface

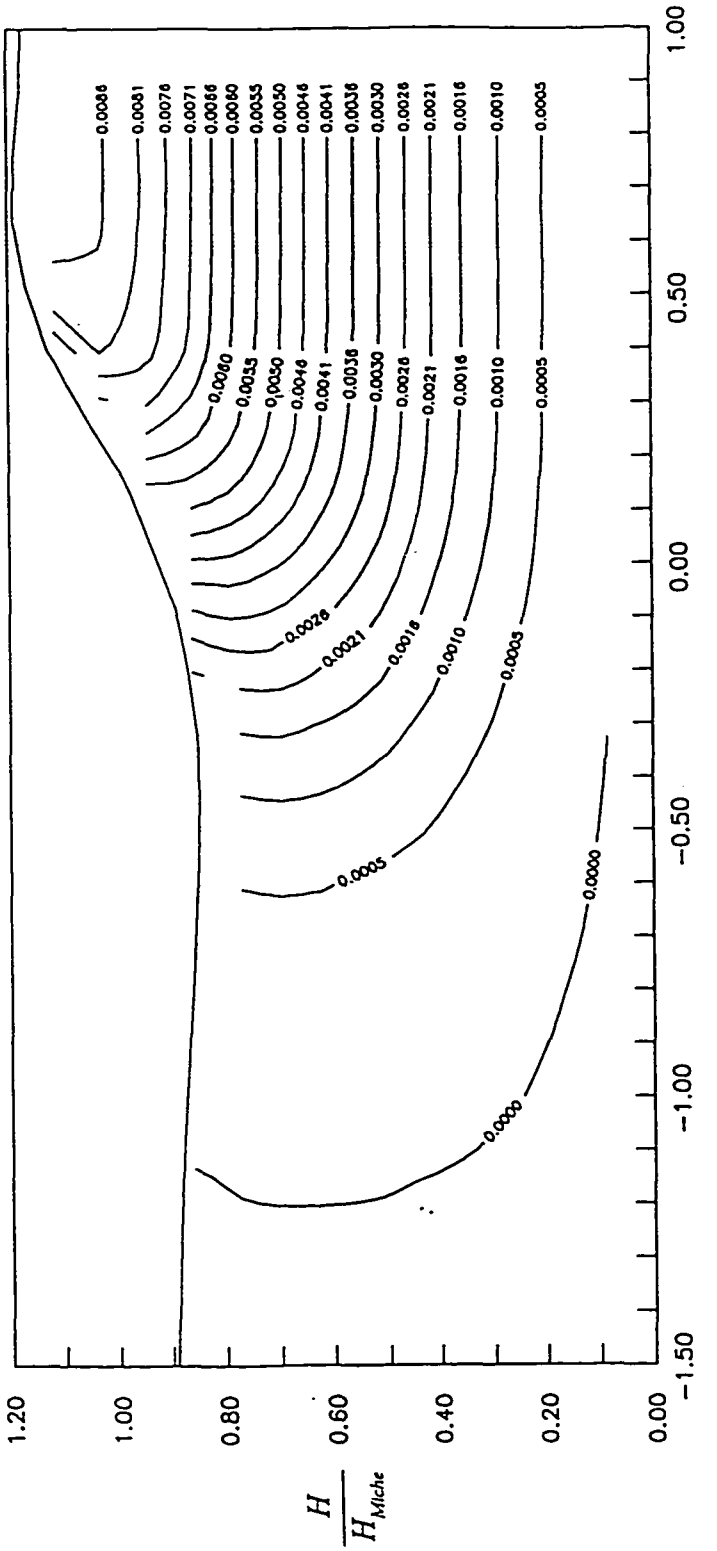

Figure 4 - 4: $\frac{\hat{U}_s^2 \omega^2}{g^2}$ Solution Surface

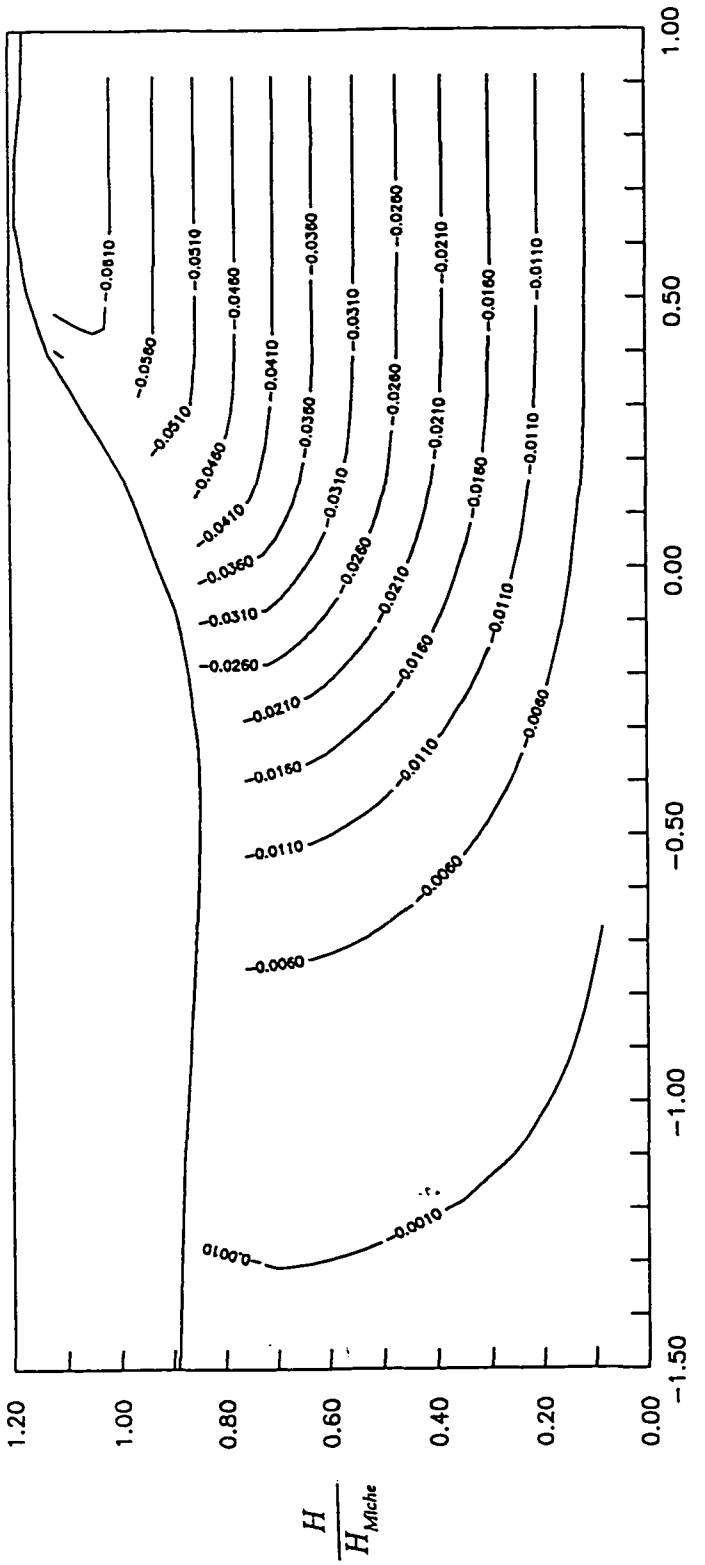

Figure 4-5: $\frac{S_s\omega^2}{g^2}$ Solution Surface

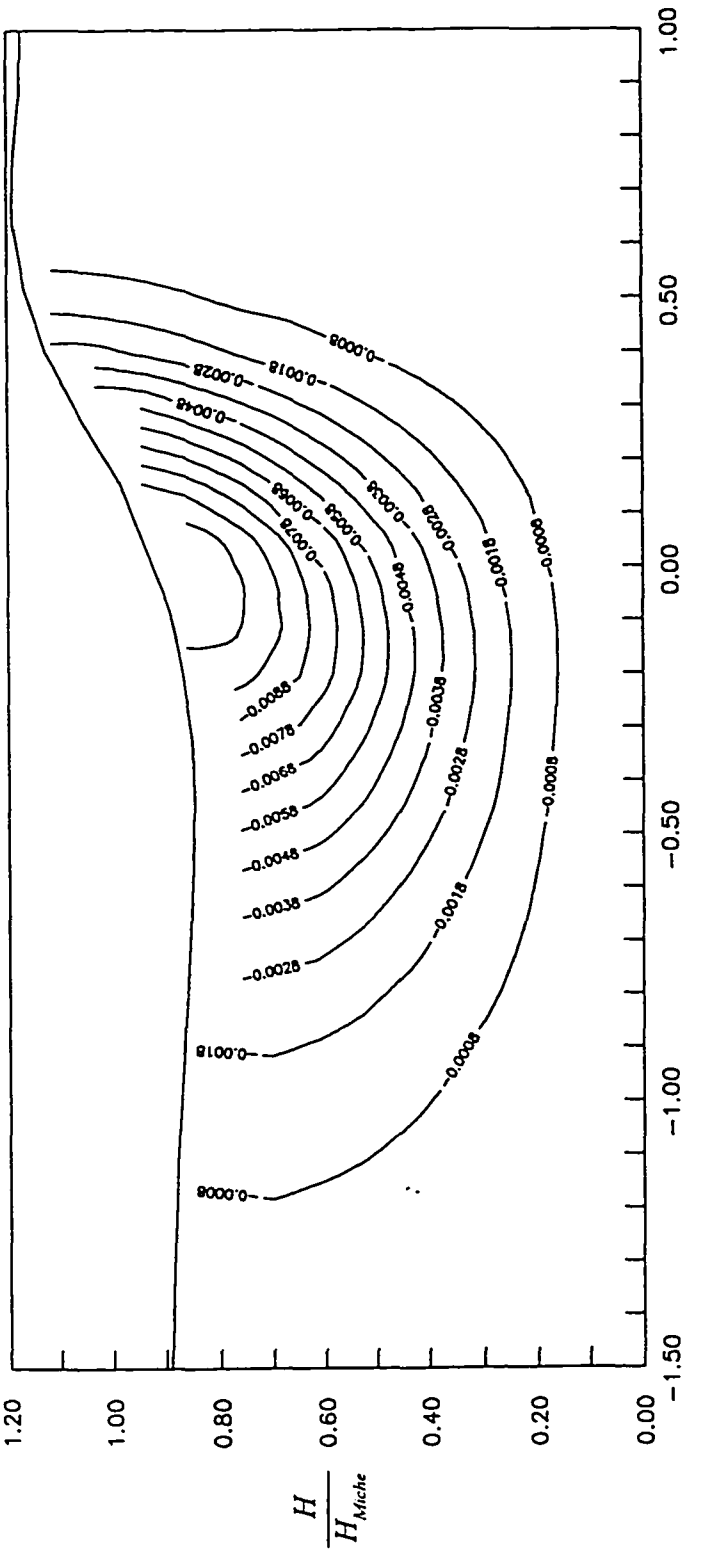

Figure 4-6: $\frac{S_b \omega^2}{g^2}$ Solution Surface

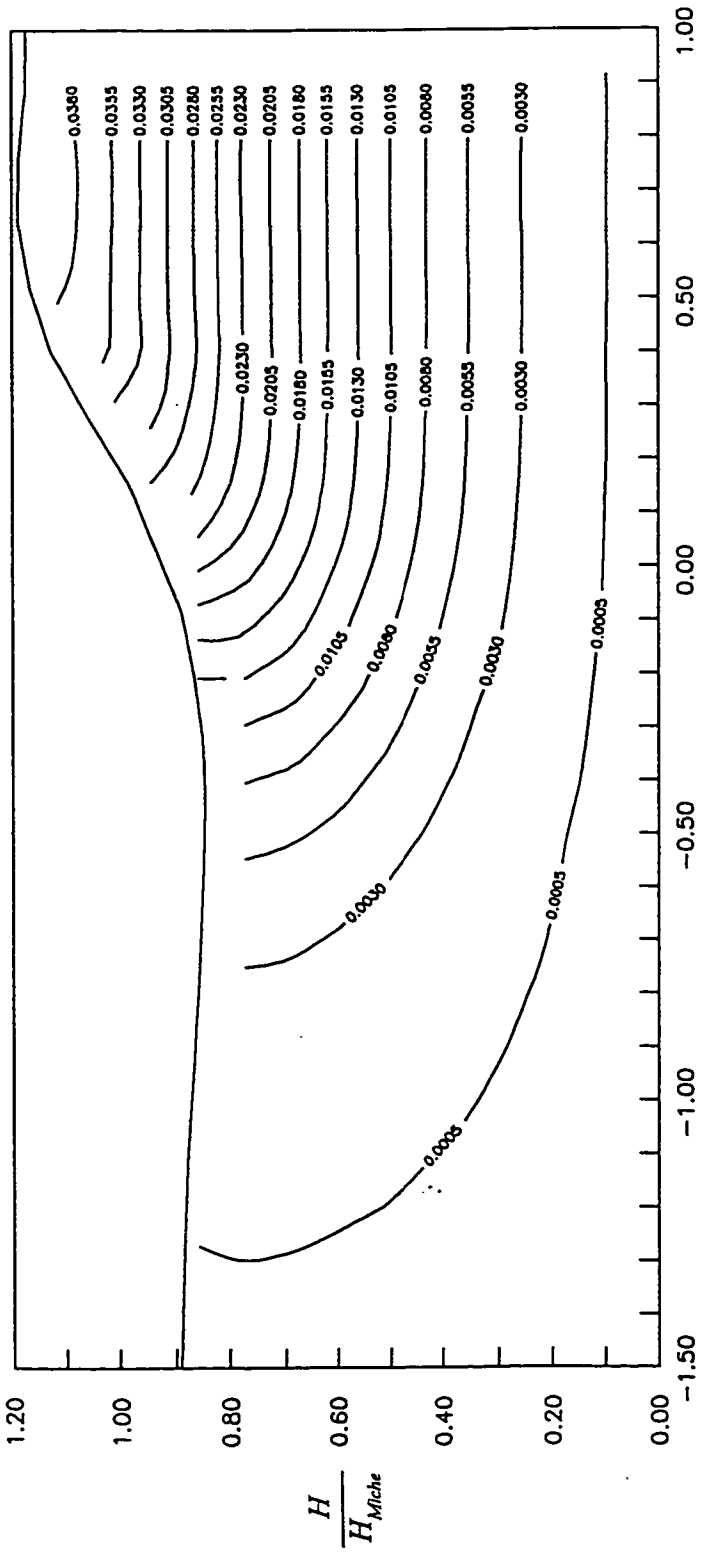

Figure 4 - 7: $\frac{N_1\omega^2}{g^2}$ Solution Surface

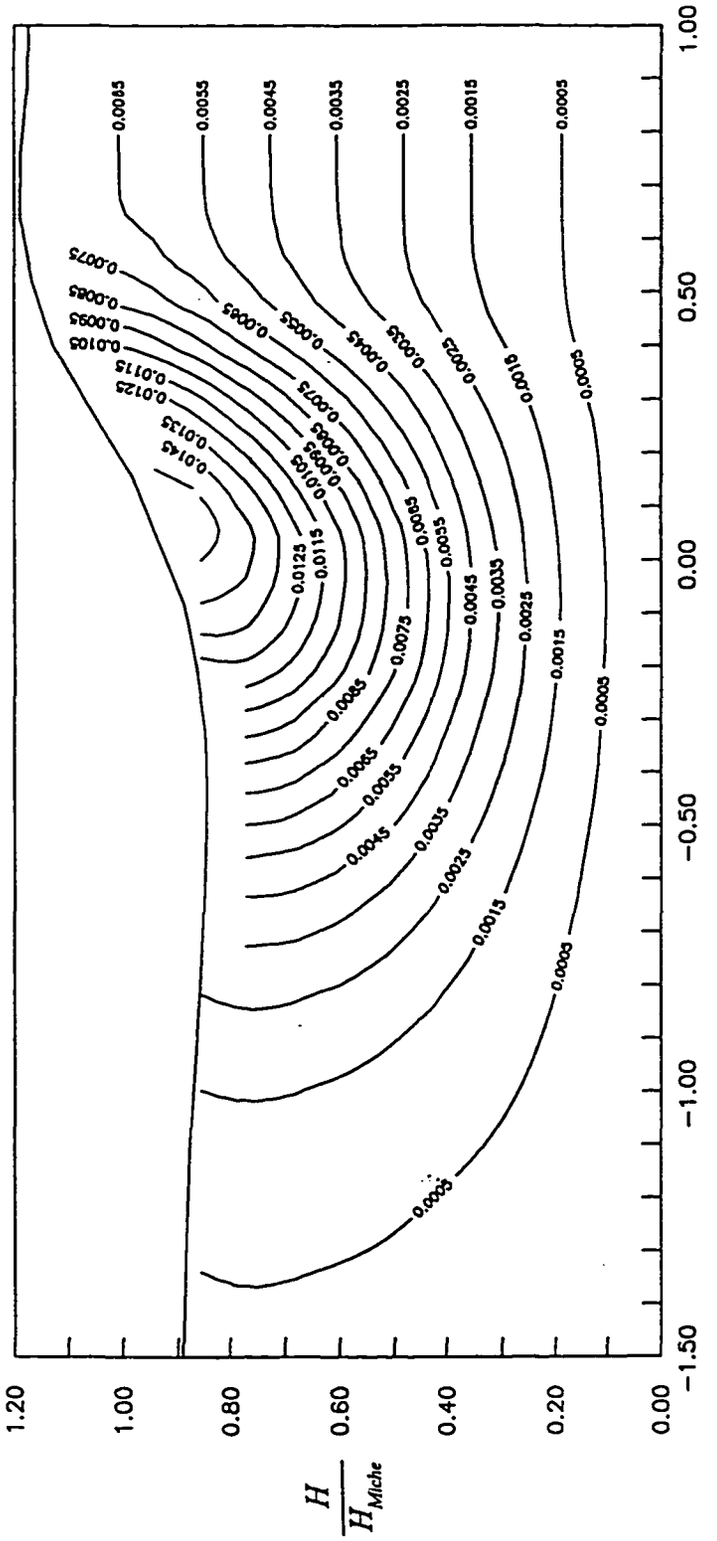

Figure 4 - 8: $\frac{N_b \omega^2}{g^2}$ Solution Surface

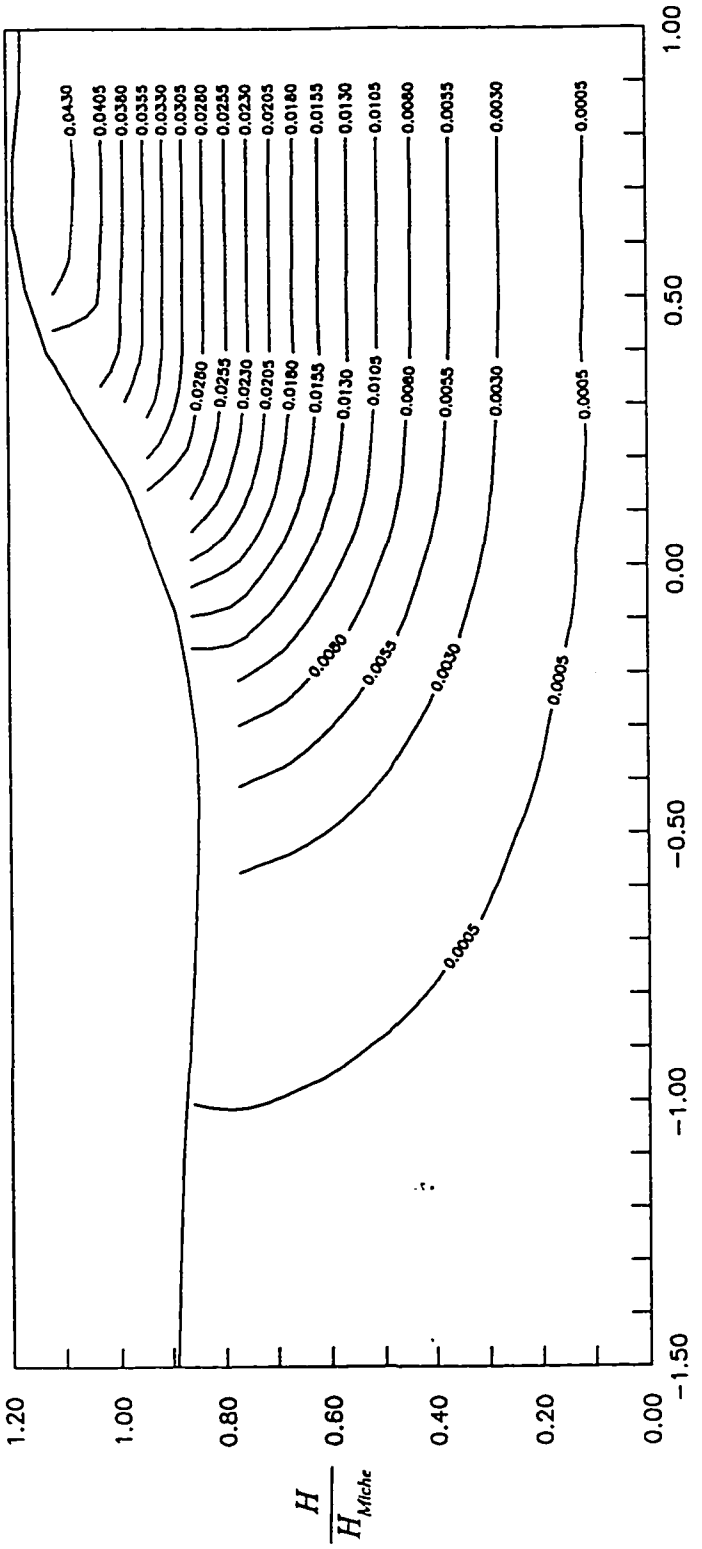

Figure 4-9: $\frac{F_s\omega^3}{g^3}$ Solution Surface

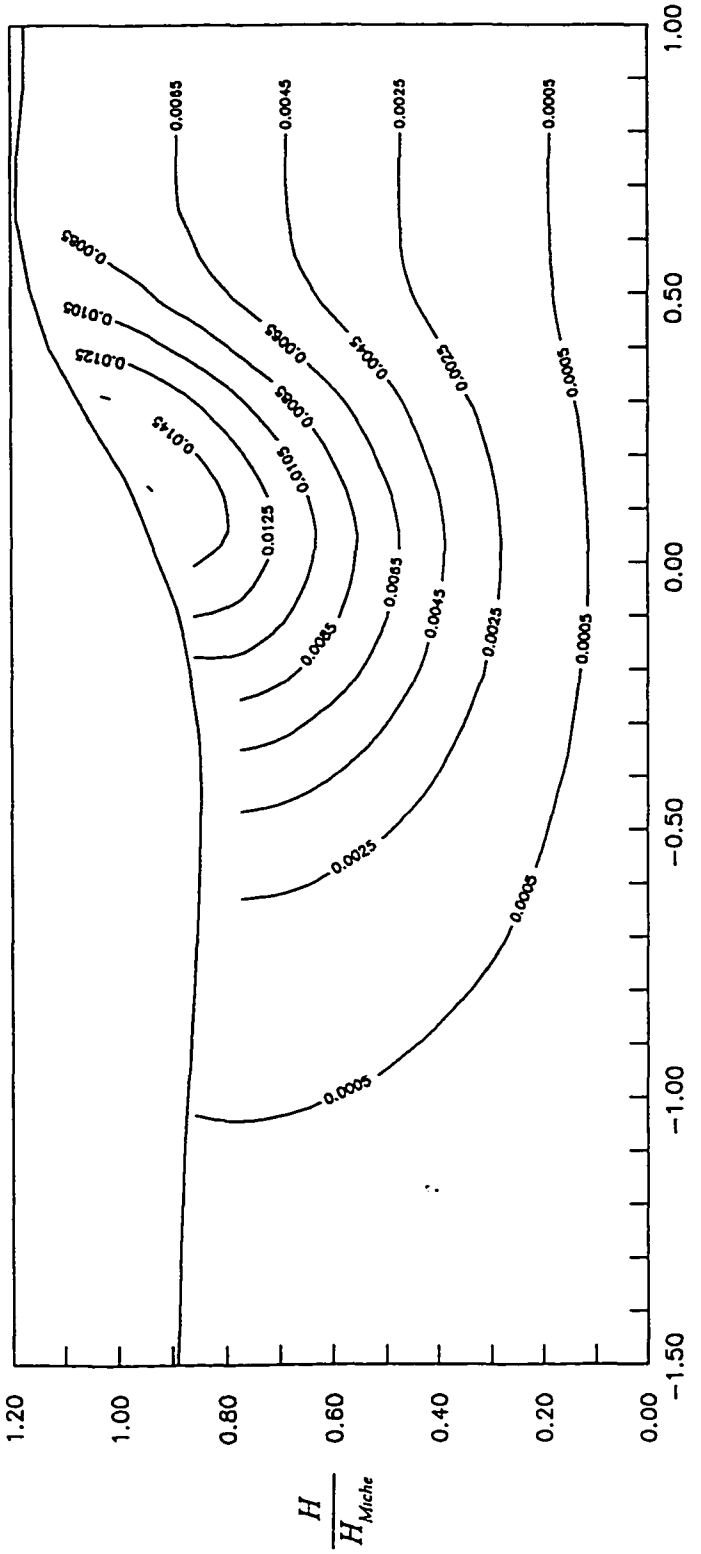

Figure 4-10: $\frac{F_b\omega^3}{g^3}$ Solution Surface

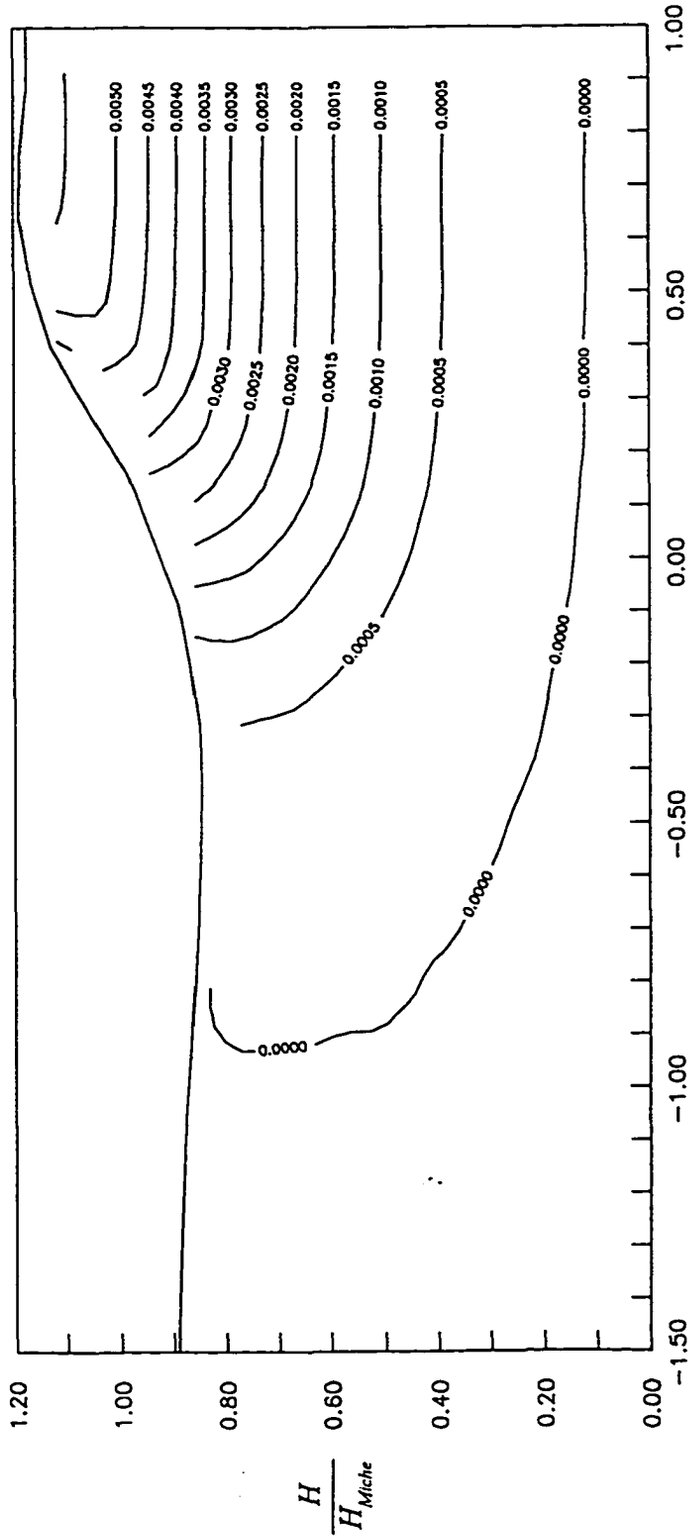

Figure 4-11: $\frac{K_s\omega^3}{g^3}$ Solution Surface

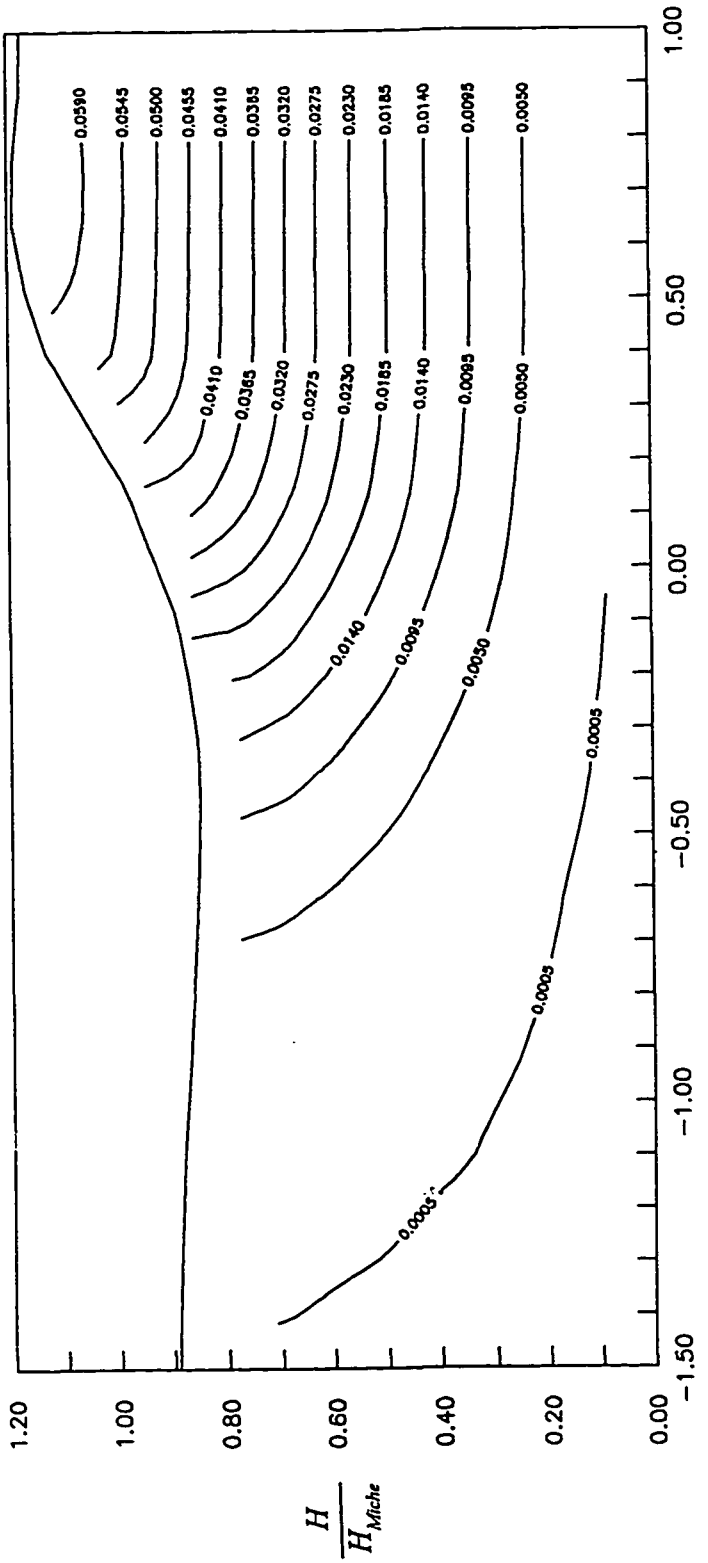

Figure 4-12: $\frac{W_s\omega^2}{g^2}$ Solution Surface

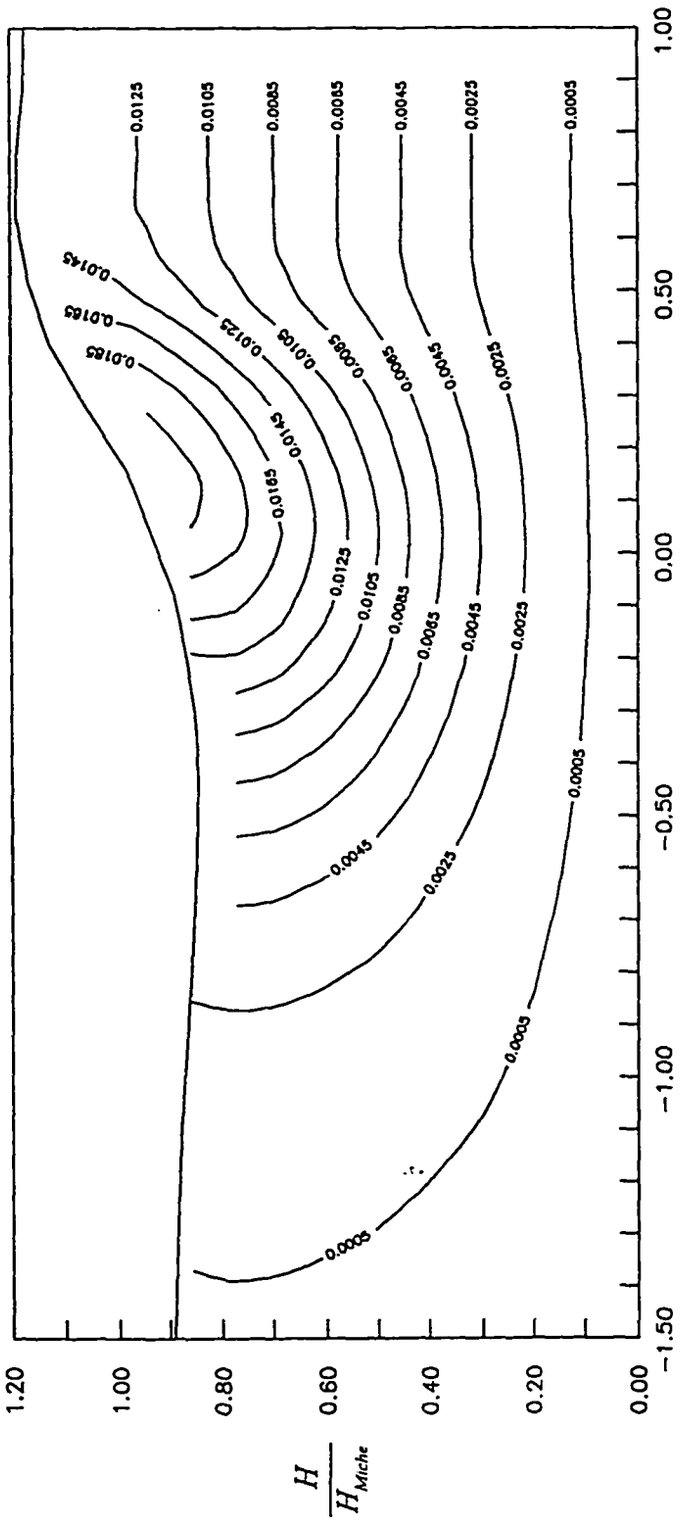

Figure 4-13: $\frac{W_b\omega^2}{g^2}$ Solution Surface

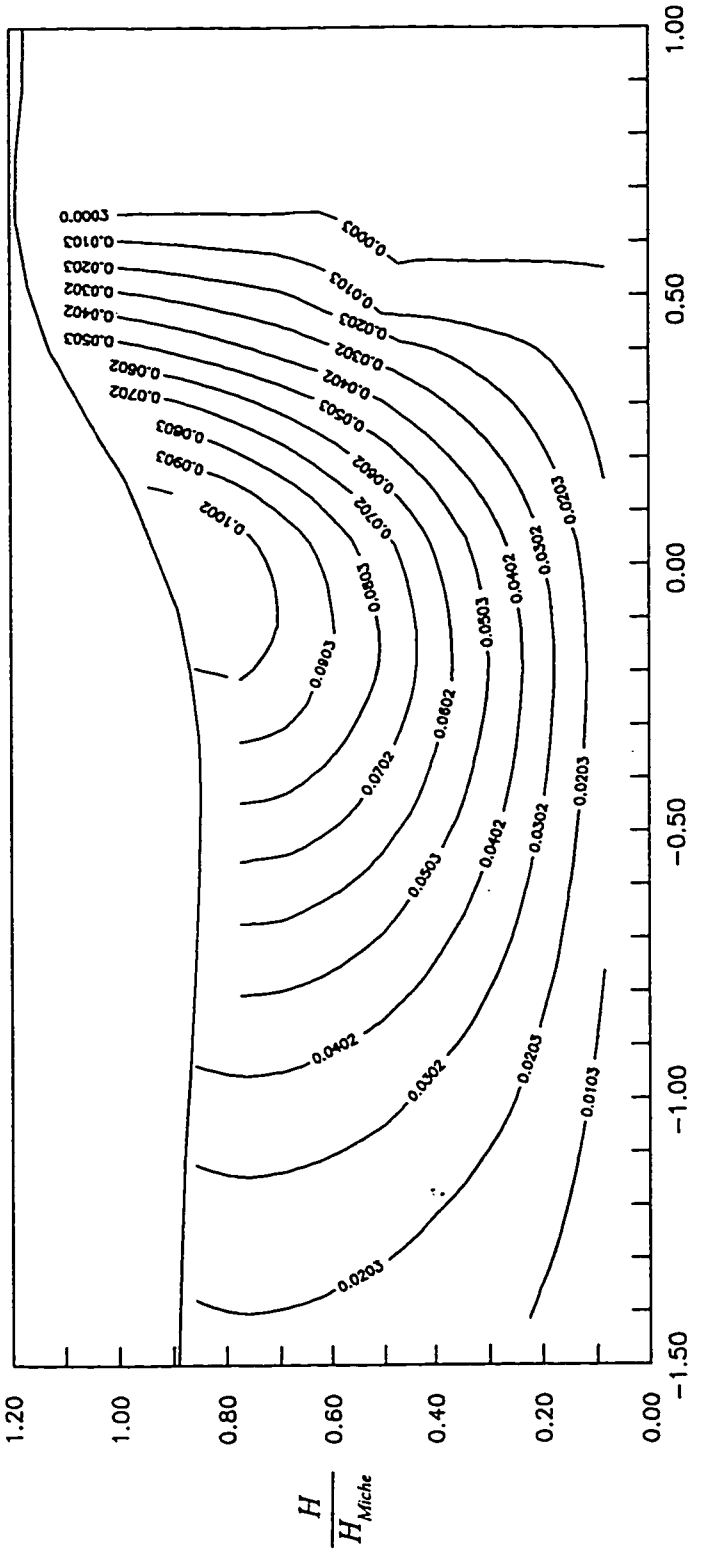

Figure 4-14: $\frac{U_{mis}\omega}{g}$ Solution Surface

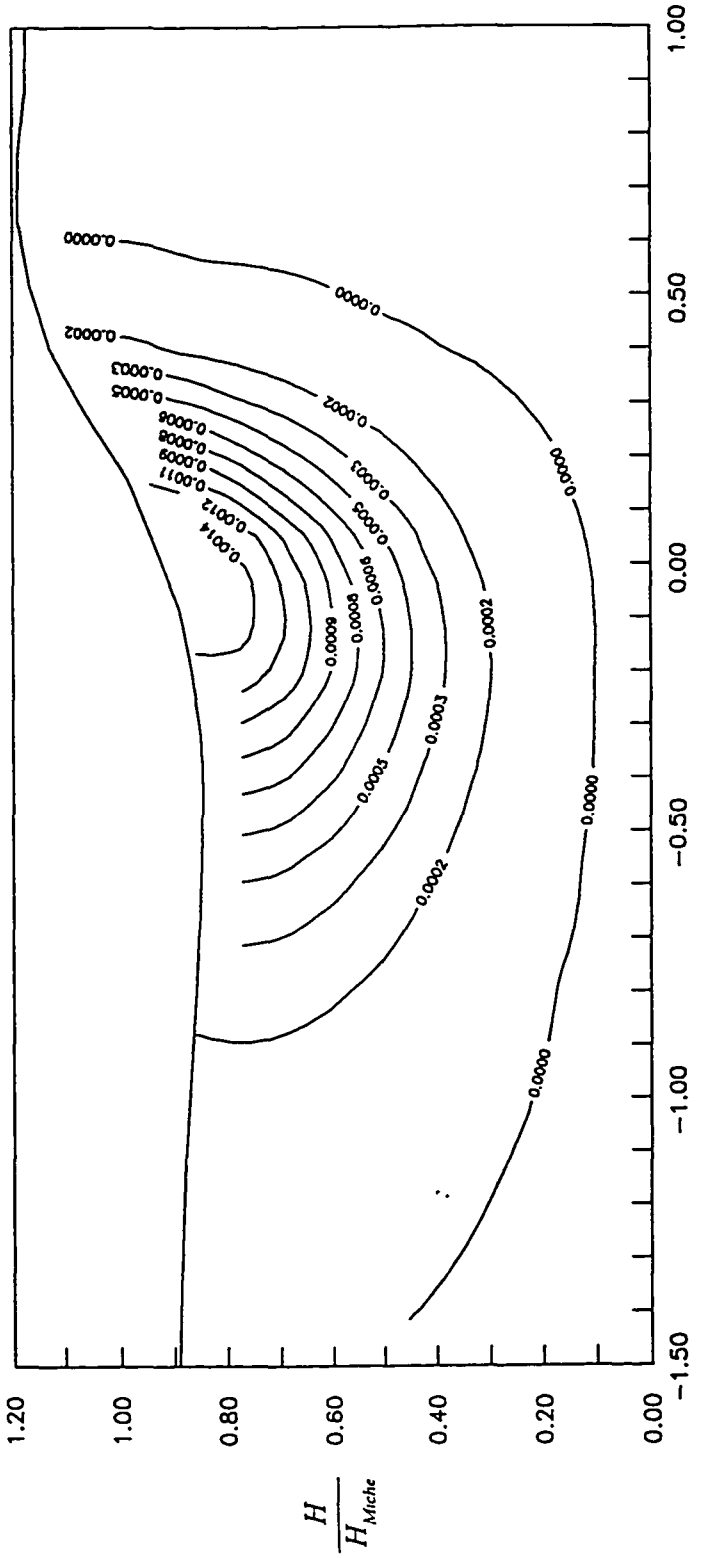

Figure 4-15: $\frac{\hat{U}_b^3 \omega^3}{g^3}$ Solution Surface

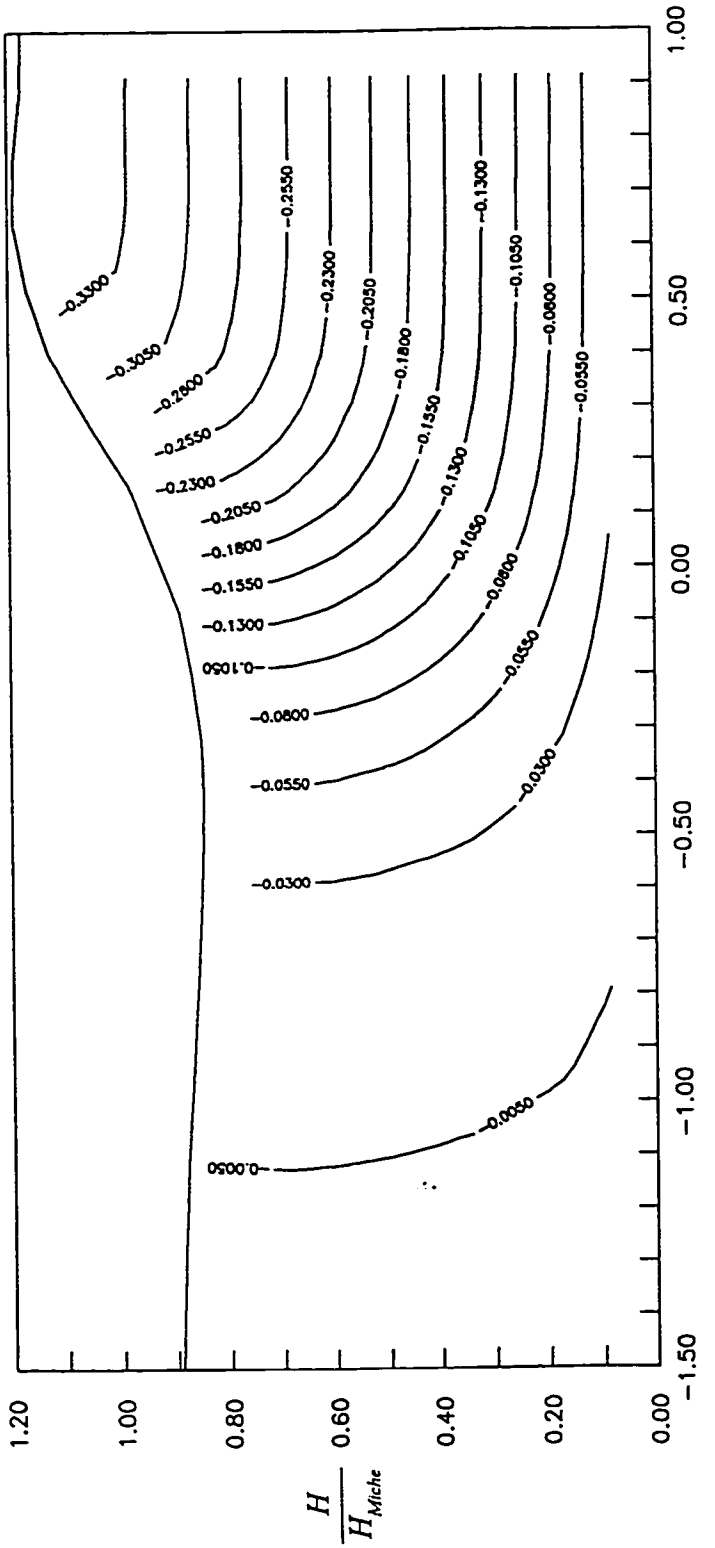

Figure 4-16: $\frac{\eta_{ir}\omega^2}{g}$ Solution Surface

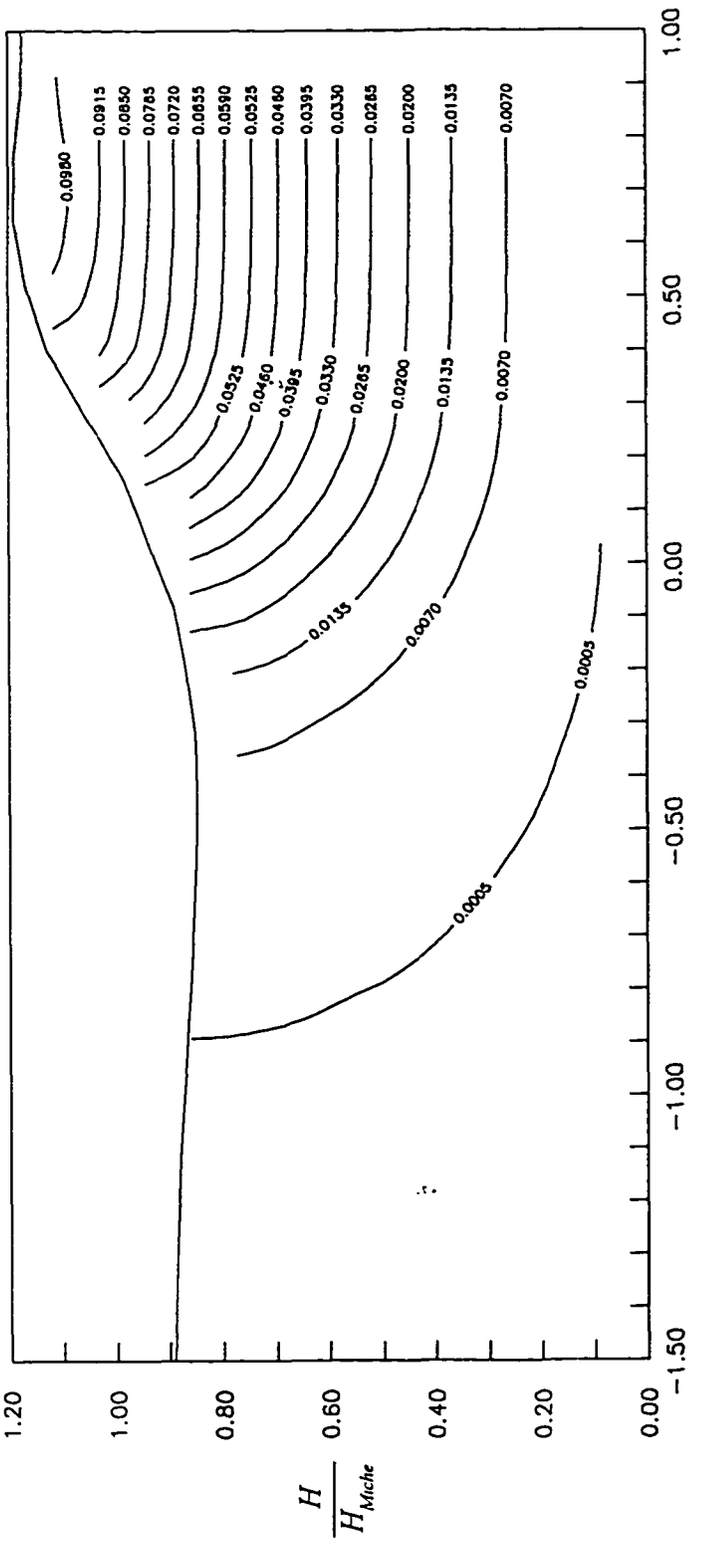

Figure 4-17: $\frac{\overline{\eta^2}\omega^4}{g^2}$ Solution Surface

4.4 Closed Integral Equations In One Spatial Dimension

Non-dimensionalizing the depth-integrated, wave-averaged conservation equations and substituting the dimensionless closure variables give a set of closed integral equations. In a one-dimensional space with x denoting the wave propagation direction, the non-dimensional integral continuity equation is

$$\frac{\partial \bar{\eta}}{\partial t}+\frac{\partial}{\partial x}[H U_s+(h+\bar{\eta}+\eta_{tr}) U_b]=0 \tag{4.32}$$

The dimensionless integral momentum equation becomes

$$\begin{aligned}&\frac{\partial}{\partial t}[H U_s+(h+\bar{\eta}+\eta_{tr}) U_b]+\frac{\partial}{\partial x}[H U_s^2+(h+\bar{\eta}+\eta_{tr}) U_b^2]= \\ &-(h+\bar{\eta})\frac{\partial \bar{\eta}}{\partial x}+\frac{\partial}{\partial x}[H S_s+(h+\bar{\eta}+\eta_{tr}) S_b]-\frac{\tau_{bx}}{\rho}\end{aligned} \tag{4.33}$$

and the dimensionless integral wave energy equation becomes

$$\begin{aligned}&\frac{1}{2}\frac{\partial}{\partial t}[E_p+H * W_s+(h+\bar{\eta}+\eta_{tr}) W_b]+\frac{\partial}{\partial x}[H * F_s+(h+\bar{\eta}+\eta_{tr}) F_b] \\ &=-\frac{\partial}{\partial x}(K_s * H)-H * N_s\frac{\partial U_s}{\partial x}-[(N_b+\frac{W_b}{2}) * (h+\bar{\eta}+\eta_{tr})]\frac{\partial U_b}{\partial x} \\ &-\frac{U_b}{2}\frac{\partial}{\partial x}[W_b * (h+\bar{\eta}+\eta_{tr})]-D_b-D_t\end{aligned} \tag{4.34}$$

4.5 Closed Integral Equations In Two Spatial Dimensions

As stated in Section 4.1, the closure process was focused along with local wave propagation, with vector quantities being resolved into this direction. But the two-dimensional depth-integrated, wave-averaged equations include velocity components in both x and y directions. In this section, it will be illustrated that the solution surfaces established before can still be used for evaluating closure variables in two dimensional cases.

Assigning θ as the angle between the local wave propagation direction and the x axis, the velocity components in the x and y directions are related to the resultant horizontal velocity, $\tilde{U}$, in the direction of wave propagation as follows

$$\begin{aligned} \tilde{u} &= \tilde{U}\cos\theta \\ \tilde{v} &= \tilde{U}\sin\theta \end{aligned} \tag{4.35}$$

where $\tilde{u}$ and $\tilde{v}$ are the x- and y-velocity components of wave motion, respectively. Substituting Equation 4.35 into the mass, momentum and wave energy equations in a two dimensional space, i.e., Equations (2.18), (2.19), (2.20) and (2.24), all the horizontal velocity components will be eliminated. Then the closure problems can be proceeded in the similar manner as in one spatial dimension.

The energy flux in the bottom layer in the x direction, for example, can be related to the defined closure variable, F_b, as follows

$$\begin{aligned} &\frac{1}{h-\eta_{tr}}\int_{-h}^{\eta_{tr}}\left[\ \frac{\overline{\tilde{p}\tilde{u}}}{\rho}+\frac{1}{2}\left(\overline{\tilde{u}\tilde{u}\tilde{u}}+\overline{\tilde{u}\tilde{v}\tilde{v}}+\overline{\tilde{u}\tilde{w}\tilde{w}}\right)\ \right]dz = \\ &\cos\theta\frac{1}{h-\eta_{tr}}\int_{-h}^{\eta_{tr}}\left[\ \left[\frac{\overline{\tilde{p}\tilde{U}}}{\rho}+\frac{1}{2}\overline{\tilde{U}(\tilde{U}\tilde{U}+\tilde{w}\tilde{w})}\right]\ \right]dz = F_b\cdot\cos\theta \end{aligned} \tag{4.36}$$

The energy flux in the bottom layer in the y direction can be similarly obtained as $F_b\cdot\sin\theta$. In this manner, the two dimensional integral equations can be closed with the closure variables being evaluated from the established solution surfaces once wave height, water depth, wave period and wave propagation direction are known.

The results of transforming the flux terms of wave motion into a function of defined closure variables are given below.

$$\int_{-h}^{\eta_c} \overline{\tilde{u}^2} dz = (\cos\theta)^2 [H N_s + (h + \bar{\eta} + \eta_{tr}) N_b] \tag{4.37}$$

$$\int_{-h}^{\eta_c} \overline{\tilde{v}^2} dz = (\sin\theta)^2 [H N_s + (h + \eta_{tr} + \bar{\eta}) N_b)] \tag{4.38}$$

$$\int_{-h}^{\eta_c} s_{xx}\, dz = H \cdot [S_s + N_s (\sin\theta)^2]) + (h + \eta_{tr} + \bar{\eta})[S_b + N_b \cdot (\sin\theta)^2] \tag{4.39}$$

$$\int_{-h}^{\eta_c} s_{xy}\, dz = \sin\theta \cos\theta \left[H \cdot N_S - (h + \bar{\eta} + \eta_{tr}) N_b\right] \tag{4.40}$$

$$\int_{-h}^{\eta_c} s_{yy}\, dz = H \cdot [S_S + N_S (\cos\theta)^2] + (h + \bar{\eta} + \eta_{tr})[S_b + N_b (\cos\theta)^2] \tag{4.41}$$

$$\int_{-h}^{\eta_c} (\overline{\tilde{u}^2} + \overline{\tilde{v}^2} + \overline{\tilde{w}^2}) dz = H \cdot W_s + (h + \bar{\eta} + \eta_{tr}) W_b \tag{4.42}$$

$$\int_{\eta_{tr}}^{\eta_c} \frac{\bar{u}_s}{2} (\overline{\tilde{u}^2} + \overline{\tilde{v}^2} + \overline{\tilde{w}^2}) dz = H \cdot K_s \cdot \cos\theta \tag{4.43}$$

$$\int_{\eta_{tr}}^{\eta_c} \frac{\bar{v}_s}{2} (\overline{\tilde{u}^2} + \overline{\tilde{v}^2} + \overline{\tilde{w}^2}) dz = H \cdot K_s \cdot \sin\theta \tag{4.44}$$

$$\int_{-h}^{\eta_c} [\overline{\frac{p_d \tilde{u}}{\rho}} + \frac{1}{2} (\overline{\tilde{u}^3} + \overline{\tilde{u}\,\tilde{v}^2} + \overline{\tilde{u}\,\tilde{w}^2})] dz = \cos\theta [H F_s + (h + \bar{\eta} + \eta_{tr}) F_b] \tag{4.45}$$

$$\int_{-h}^{\eta_c} [\overline{\frac{p_d \tilde{v}}{\rho}} + \frac{1}{2} (\overline{\tilde{u}^2 \tilde{v}} + \overline{\tilde{v}^3} + \overline{\tilde{v}\,\tilde{w}^2})] dz = \sin\theta [H F_s + (h + \bar{\eta} + \eta_{tr}) F_b] \tag{4.46}$$

Substituting these expressions into non-dimensionalized depth-integrated, wave-averaged mass, momentum and wave energy equations results in four closed integral equations. The integral continuity equation becomes

$$\frac{\partial \bar{\eta}}{\partial t}+\frac{\partial}{\partial x}[(H U_s \cos\theta)+(h+\bar{\eta}+\eta_{tr}) U_b]+\frac{\partial}{\partial y}[(H U_s \sin\theta+(h+\bar{\eta}+\eta_{tr}) V_b]=0 \qquad (4.47)$$

and the closed integral x- and y-momentum equations are

$$\frac{\partial}{\partial t}[HU_s\cos\theta+(h+\bar{\eta}+\eta_{tr}) U_b]+\frac{\partial}{\partial x}[H U_s^2\cos^2\theta+(h+\bar{\eta}+\eta_{tr}) U_b^2+(h+\frac{\bar{\eta}}{2})\bar{\eta}]$$
$$+\frac{\partial}{\partial y}[H U_s^2\frac{\sin 2\theta}{2}+(h+\bar{\eta}+\eta_{tr}) U_b V_b]=-\bar{\eta}\frac{\partial h}{\partial x}+\frac{\partial}{\partial x}[H(S_s+\sin^2\theta N_s) \qquad (4.48)$$
$$+(h+\bar{\eta}+\eta_{tr})(S_b+\sin^2\theta N_b)]-\frac{\partial}{\partial y}[\frac{\sin 2\theta}{2}(H N_s+(h+\bar{\eta}+\eta_{tr}) N_b)]-\frac{\tau_{bx}}{\rho}$$

$$\frac{\partial}{\partial t}[H U_s\sin\theta+(h+\bar{\eta}+\eta_{tr}) V_b]+\frac{\partial}{\partial x}[H U_s^2\cos^2\theta+(h+\bar{\eta}+\eta_{tr}) U_b V_b]$$
$$+\frac{\partial}{\partial y}[H U_s^2\sin^2\theta+(h+\bar{\eta}+\eta_{tr}) V_b^2+(h+\frac{\bar{\eta}}{2})\bar{\eta}]=-\bar{\eta}\frac{\partial h}{\partial y}-\frac{\partial}{\partial x}\{[\frac{\sin 2\theta}{2}(HN_s \qquad (4.49)$$
$$+(h+\bar{\eta}+\eta_{tr}) N_b]\}+\frac{\partial}{\partial y}[H(S_s+\cos^2\theta N_s)+(h+\bar{\eta}+\eta_{tr})(S_b+\cos^2\theta N_b)]-\frac{\tau_{by}}{\rho}$$

Finally, the closed integral wave energy equation is

$$\frac{1}{2}\frac{\partial}{\partial t}[\overline{\eta^2}+HW_s+(h+\bar{\eta}+\eta_{tr}) W_b]+\frac{\partial}{\partial x}\{\cos\theta[H(F_s+K_s)+F_b(h+\bar{\eta}+\eta_{tr})]\}+$$
$$\cos^2\theta H N_s\frac{\partial U_s}{\partial x}+(N_b\cos^2\theta+\frac{W_b}{2})(h+\bar{\eta}+\eta_{tr})\frac{\partial U_b}{\partial x}+\frac{U_b}{2}\frac{\partial}{\partial x}[W_b(h+\bar{\eta}+\eta_{tr})]+$$
$$H N_s\frac{\sin 2\theta}{2}(\frac{\partial U_s}{\partial y}+\frac{\partial V_s}{\partial x})+(h+\bar{\eta}+\eta_{tr}) N_b\frac{\sin 2\theta}{2}(\frac{\partial V_b}{\partial x}+\frac{\partial U_b}{\partial y})+ \qquad (4.50)$$
$$\frac{\partial}{\partial y}\{\sin\theta[H(F_s+K_s)+(h+\bar{\eta}+\eta_{tr}) F_b]\}+(h+\bar{\eta}+\eta_{tr})(N_b\frac{\sin 2\theta}{2}+\frac{W_b}{2})\frac{\partial V_b}{\partial y}+$$
$$\frac{V_b}{2}\frac{\partial}{\partial y}[(h+\bar{\eta}+\eta_{tr}) W_b]+HN_s\sin^2\theta\frac{\partial U_s}{\partial y}=-\frac{2}{3\pi}f_w\overline{U_b^3}-f_{wb}\omega H^2$$

where f_w is the bottom friction factor and f_{wb} is a dimensionless factor for calculating energy dissipation rate due to wave breaking.

5 TRANSIENT WAVE PROPAGATION IN A ONE-DIMENSIONAL SPACE

In this chapter, a numerical scheme based on the method of characteristics is developed for solving the one-dimensional integral equations with apparent stress closure as given in Chapter 4. First, the procedure to derive characteristics and characteristic equations is illustrated, and the characteristics of this system in deep water, intermediate water and shallow water are demonstrated for typical wave conditions. Then a scheme for obtaining numerical solutions of the characteristic equations and open boundary conditions are proposed. The proposed numerical scheme and open boundary conditions are tested for simulating the evolution of mean wave parameters in four cases: evolution of an initial water mound, and wave propagations over a flat beach, over a ripple bed, and over a slope. Finally, the developed model is applied to simulate the cross-shore wave propagation at the Egmond Beach, the Netherlands where limited field data are available for comparison with the numerical results.

5.1 Characteristic Equations

The integral equations with apparent stress closure in one spatial dimension given in Chapter 4 (Equations 4.32 through 4.34), can be generalized to the form

$$\frac{\partial \Phi_i}{\partial t} + \frac{\partial F(\Phi_i)}{\partial x} = Q(x, t, \Phi_i) \tag{5.1}$$

where Φ_i is a vector variable denoting wave setup, flow momentum and wave energy:

$$\begin{aligned} \Phi_1 &= \overline{\eta} \\ \Phi_2 &= HU_s + (h + \overline{\eta} + \eta_{tr})U_b \\ \Phi_3 &= \frac{1}{2}[g\overline{\eta^2} + HW_s + (h + \overline{\eta} + \eta_{tr})W_b] \end{aligned} \tag{5.2}$$

$F(\Phi_i)$ denote fluxes of mass, momentum and wave energy, and $Q(x,t,\Phi_i)$ are the source or sink terms, which may be a function of x, t, and Φ_i, but not of $\partial\Phi/\partial x$.

As discussed in Chapter 3, the method of characteristics (MOC) is appropriate for obtaining numerical solutions of this system. In MOC, the first step is to derive the characteristic equations. Since the information to be sought is mean wave parameters, i.e., wave height, H, wave setup, $\overline{\eta}$, and undertow current, U_b, the integral equations (5.2) are transformed with dependable variable directly in these three parameters

$$\frac{\partial W}{\partial t} + A \bullet \frac{\partial W}{\partial x} = S(x, t, W) \qquad (5.3)$$

where W is a dependent variable vector

$$W = \left[H, \overline{\eta}, U_b\right]^T \qquad (5.4)$$

S is a source or sink vector, and A is a 3×3 Jacobian coefficient matrix. The exact entries of this coefficient matrix are given in Appendix A. Equation (5.3) represents a quasi-linear system.

The nature of information propagation of the system can be described by the characteristics, i.e., eigenvalue and eigenvector, of the coefficient matrix. The eigenvalues, λ, of the coefficient matrix A are defined as the roots of the following polynomial (Wylie and Barrett 1982)

$$\det\left|A - I\lambda\right| = 0 \qquad (5.5)$$

where "det" denotes the determinant, and I is a 3×3 unit matrix for a three-equation system. Equation (5.5) is generally a polynomial in λ of the third power. Three eigenvalues, say, λ_1, λ_2 and λ_3, may be obtained from Equation (5.5). If all three roots are

real and distinct, the system is said to be hyperbolic. Physically, the three eigenvalues λ_1, λ_2 and λ_3 are the speeds at which the system information propagates. A curve defined in the x-t space with a local gradient equal to the eigenvalue describes the information propagation path. This curve is termed as the characteristic curve, or simply the characteristics, of the system (Wylie and Barrett 1982).

Associated with each eigenvalue, there is a characteristic equation in the form

$$\vec{\ell}_i \cdot [\frac{\partial}{\partial t} + A\frac{\partial}{\partial x}]W = \vec{\ell}_i \cdot S \qquad i = 1, 2, 3 \tag{5.6}$$

where $\vec{\ell}_i$ is a left eigenvector of the coefficient matrix A, being defined as

$$\vec{\ell}_i \cdot [A - \lambda I] = 0 \tag{5.7}$$

Equation (5.6) reduces to

$$\vec{\ell}_i \cdot \frac{dW}{dt} = \sum \vec{\ell}_i \cdot S \qquad i = 1, 2, 3 \tag{5.8}$$

along the characteristic curve

$$\frac{d}{dt} = \frac{\partial}{\partial t} + \lambda_i \cdot \frac{\partial}{\partial x} \tag{5.9}$$

In contrast with Equation (5.6), Equation (5.8) is an ordinary differential equation. The numerical solutions can be obtained by integrating the characteristic equation (5.8) along the characteristic curves.

This process can be illustrated by obtaining solutions at point O at the time level t^n, as shown in Figure 5-1. First three eigenvalues at the point O' are calculated based on the values at the time step t^{n-1}. These eigenvalues are approximately used to locate the points at which three characteristic curves through point O intersect with the t^{n-1} line. The x

coordinates of the points, say, P, Q and R, relative to O' are respectively equal to $\lambda_i \cdot \Delta t$, where Δt is the time step.

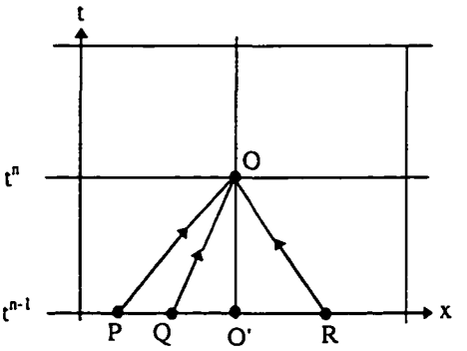

Figure 5.1: Illustration of Solution Process

The region OPR is the domain of dependence for the point O. The value of a variable at P, Q or R is estimated using 3rd order polynomial interpolation from the values at the closest four grid points. Then the characteristic equations are integrated along the three characteristics, resulting in three equations

$$\vec{\ell}_i \cdot (W_o - W_j) = \Delta t \cdot \sum \vec{\ell}_i \cdot S \qquad \text{j=P, Q and R} \tag{5.10}$$

The solutions at point O can be subsequently solved from these equations.

Numerical stability is secured if the domain of dependence for the difference Equations (5.10) covers that of the differential Equations (5.8). This is analogous to the Courant-Friedrichs-Lewy (1928) condition (or CFL number) which was originally developed for a linear system. For a nonlinear system, the CFL condition is only used as a general guideline to estimate the time step corresponding to a given space step

$$C_r = \frac{\Delta t \cdot |\lambda|_{max}}{\Delta x} \leq 1 \tag{5.11}$$

where $|\lambda|_{max}$ is the maximum eigenvalue throughout the entire simulation period and over

the entire computational domain if a constant and uniform time step is to be used. Ultimately, this time step should be adjusted according to numerical experiments.

5.2 Characteristic Properties

In this section, the characteristics of this system will be investigated for different water depths and wave periods. The eigenvalues and eigenvectors for four cases with different combination of water depth and wave period are given in Table 5.1. In the table, H is wave height, h is the water depth, T is the wave period, g is the acceleration of gravity, and L_o is the deep-water wave length, equal to $gT^2/2\pi$.

Table 5.1 Characteristics for Different Water Depths and Wave Periods

Case	H (m)	T (Sec.)	h (m)	h/L_0	$\sqrt{gh}$ (m/s)	Eigenvalue (m/s)	Eigenvector		
							ℓ_1	ℓ_2	ℓ_3
A	0.5	10	1	0.006	3.13	4.13	0.817	1.0	0.133
						2.94	-0.233	1.0	0.206
						-3.16	0.003	1.0	-0.191
B	1.0	10	100	0.64	31.3	31.32	0.005	0.601	1.0
						9.15	1.0	-0.005	-0.002
						-31.32	0.001	-0.601	1.0
C	1.0	10	10	0.064	9.90	10.01	0.297	1.0	0.611
						7.88	1.0	-0.194	-0.098
						-9.90	0.003	1.0	-0.605
D	1.0	12	10	0.045	9.90	10.05	0.348	1.0	0.510
						8.18	1.0	-0.255	-0.115
						-9.91	0.004	1.0	-0.505

In Cases A and D, the ratio of water depth to wave length, h/L_0, is less than 0.05; in Case C, $0.05<h/L_0<0.5$; and in Case B, $h/L_0>0.5$. Thus these fours cases cover from deep-water wave condition to an intermediate water wave condition to shallow water wave conditions (Dean and Dalrymple 1984). The phase speed of long waves, $\sqrt{gh}$, is also given in Table 5.1 for comparison with the eigenvalues. From Table 5.1, the following observations are appropriate:

1. In all cases studied, the three eigenvalues are real and distinct. Thus the system is generally hyperbolic.
2. Except for the very shallow water wave condition, i.e., in case A, the first and third eigenvalues are almost equal to the long-wave speed in magnitude. This suggests that the system to some extent be similar to shallow water wave equations. The third eigenvalue is always negative. The negative sign denotes information propagating in a direction opposite to the x axis. The characteristics corresponding to the eigenvalues of an magnitude approximately equal to the long-wave speed are termed (Katopodes and Strelkoff 1979) as wave characteristics. The wave characteristics may travel in both positive and negative x directions.
3. The second eigenvalue for each case is almost equal to the wave group speed. Thus the corresponding characteristics will be termed as an energy characteristics in this context.
4. As indicated in Equation (5.6), the eigenvector actually measures the degree of cohesiveness among the equations in a system. Under deep water wave conditions (Case B), the first component of the eigenvectors of wave characteristics is always

much smaller compared to other the second and third components, while the first component of the eigenvector for the energy characteristics is much greater than two other components. This means, in deep waters, that the wave characteristic equations are almost independent of the wave energy equation and that the energy characteristic equation is almost independent of the mean-flow mass and momentum equations. Thus the wave setup and undertow current are primarily described by the mean flow equations with the wave height is almost governed by the wave energy equation alone. As water shallows, the first component of the eigenvector of the positive wave characteristics increases. This indicates that in shallow water the mean flow is more influential on the transfer of wave energy, and vice versa.

5. If other conditions remain the same, a larger wave period means that the water is relatively shallower. Thus, the mean flow mass and momentum transfer and wave energy flux are more closely related, as suggested by the comparison of the eigenvectors of Case C and Case D.
6. Regardless of water depth conditions, the first component of the eigenvector corresponding to the negative eigenvalue is always much smaller than two other components. This suggests that the interaction between the transfer of wave energy and the transfer of mean flow mass and momentum is directional. Such an interaction is only significant in the direction of wave propagation.

5.3 Open Boundary Conditions

The numerical simulation of wave propagation normally involves two types of

boundary: open boundary and beach boundary. An open boundary is the boundary where information can pass through freely, and a beach boundary is where water surface intersects beach profile. The location of the open boundary is normally fixed; in contrast, the beach boundary moves back and forth as water surface oscillates up and down. In this section, only open boundary conditions are discussed. The beach boundary conditions will be dealt with in the study of wave propagation over a slope in Section 5.6.

5.3.1 Open Boundary Conditions

The present three-equation system requires three constraints to be specified at the boundary. To permit the interior information crossing the boundary freely, the characteristic equations of the outgoing characteristics should be used as part of the boundary conditions. If the flow is subcritical, there are at most two outgoing characteristics. Additional constraints have to be specified as supplements to the characteristic equations of outgoing characteristics. The number of the additional constraints should equal the number of equations minus the number of outgoing characteristics.

An ideal situation would be to supplement the outgoing characteristic equations with field data. But field data is only rarely available. Accordingly, approximate boundary conditions should be so imposed that no detrimental wave reflection takes place at the boundary.

Hedstrom (1979) developed approximately non-reflecting boundary conditions for a homogeneous, quasi-linear system. The procedure to develop Hedstrom's approximate

open boundary condition is briefly introduced below. For a hyperbolic system with n equations, the n eigenvalues of the system are ranked in acceding order

$$\lambda_1 < \lambda_2 < \ldots < \lambda_n \tag{5.12}$$

Suppose that m eigenvalues are negative at an open boundary and that n-m eigenvalues are positive. If the negative eigenvalues represent outgoing characteristics, then there are m outgoing characteristics and n-m incoming characteristics at the open boundary. The problem of reflection is interesting only if $1 \leq m < n$. This is the case for the present study since the wave-induced mean flow is normally subcritical.

Hedstrom (1979) proved that the following supplemental boundary conditions

$$\vec{\ell}_i \bullet \frac{\partial W}{\partial t} = 0 \qquad (m<i\leq n) \tag{5.13}$$

gives no waves coming into the solution domain from the boundary if there are only simple waves going out. If a shock of strength ε leaves the boundary, condition (5.13) produces an incoming wave of strength $O(\varepsilon^3)$. In Equation (5.13), W is a dependent variable vector, and $\vec{\ell}_i$ is a left eigenvector.

Comparing the general characteristic Equation (5.8) for a homogeneous system (S=0) with Equation (5.13), the condition (5.13) is equivalent to

$$\vec{\ell}_i \bullet \frac{\partial W}{\partial x} = 0 \qquad (m<i\leq n) \tag{5.14}$$

In the linear case with the constant coefficient matrix, the eigenvalues and eigenvectors are constant. The condition (5.13) and (5.14) then become

$$\vec{\ell}_i \bullet W = \text{ constant} \qquad (m<i\leq n) \tag{5.15}$$

This is a Riemann invariant along the incoming characteristics, which states that the characteristic variables corresponding to incoming characteristic curves are constant.

To use conditions (5.13) as approximately non-reflecting boundary conditions, the problem itself should be at most weakly reflective. In the context of wave propagation, the constraint of being weakly reflective requires that the bottom slope is mild and that bottom friction is relatively small.

5.3.2 Typical Boundary Conditions

In one-dimensional wave simulation, the wave period, bathymetry data and the wave height at the offshore boundary are normally given. In the following discussions, the offshore boundary from which waves enter the computational domain is referred as an inflow boundary, and the other boundary from which waves leave the computational domain as an outflow boundary. At the offshore boundary, only two boundary conditions are required since the wave height is known. For a subcritical flow, there is one outgoing characteristics at the inflow boundary (see Table 5.1). The outgoing characteristic equation and condition (5.13) along one incoming characteristics are sufficient to give the two boundary conditions. In this case, there are two incoming characteristics at the inflow boundary, but only one of them is needed. Since the wave height is given at the inflow boundary, the characteristics corresponding to wave energy propagation should not be used to avoid redundancy because the propagation of wave height profile is predominately governed by the energy characteristics. Hence, the condition (5.13) along the incoming wave characteristics should be used.

At an outflow boundary, if no other constraints are given, two outgoing characteristic equations and condition (5.13) along the incoming wave characteristics are sufficient to form the open boundary conditions.

5.4 Case Studies

In this section, the proposed numerical scheme and open boundary conditions will be examined in four case studies. These four cases are: evolution of an initial water mound, wave propagation over a horizontal seabed, wave propagation over a ripple bed and wave propagation over a slope. In all four cases, the wave height and undertow velocity are zero at the beginning of simulation.

Case I - Evolution of An Initial Water Mound

An water mound is initially located in the middle of a computational domain which is 1000 m long and 10 m deep, as sketched in Figure 5.2. The shape of the initial water mound is described by

$$\begin{aligned} \overline{\eta}_{t=0}(x) &= (1-\frac{|x-500|}{150})^2 \quad \text{for} \quad 350 < x < 650 \\ \overline{\eta}_{t=0}(x) &= 0 \qquad\qquad \text{elsewhere} \end{aligned} \tag{5.16}$$

The water mound will evolve with time and eventually propagate out the domain. Thus, both ends of the domain are outflow boundaries. This case study is designed to check the performance of the proposed open boundary conditions and wave propagation speed which should be approximately equal to the long wave phase speed. A spatial step of 10 m and a time step of 1 second are used with a CFL number approximately equal to 1.

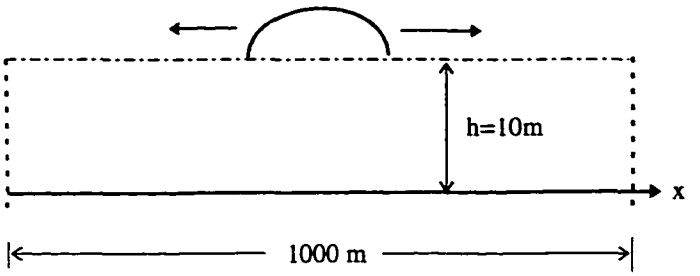

Figure 5.2 Sketch of the Computational Domain of Case I

Figures 5.3 and 5.4 show the time histories of water surface profiles and flow velocity, respectively. As shown in Figure 5.3, the initial water mound first splits into two sub-mounds of the same shape. The two sub-mounds maintain their shape and propagate in opposite directions. These two sub-mounds may be viewed as two wave packets which consist of wave components of various wave lengths. Each wave packet moves at a speed of about 10m/s (estimated from the advancement of the toe of the sub-mound over consecutive time intervals). This speed is almost identical to the phase speed of long waves ($C=\sqrt{gh} = 9.96$ m/s). Thus, the wave propagation speed is correctly simulated by the proposed numerical scheme.

After the two sub-mounds leave the computational domain, the water surface becomes level immediately, which implies that the imposed boundary conditions do not generate appreciable numerical reflection at the boundaries. The flow velocity shown in Figure 5.4 are asymmetric because the two wave packets propagate in the opposite directions. After the two sub-mounds are completely separated, the magnitude of the flow velocity can be approximated by the water particle velocity in the long wave situation, i.e., $u=\eta \cdot C/h$, where η is the water surface elevation.

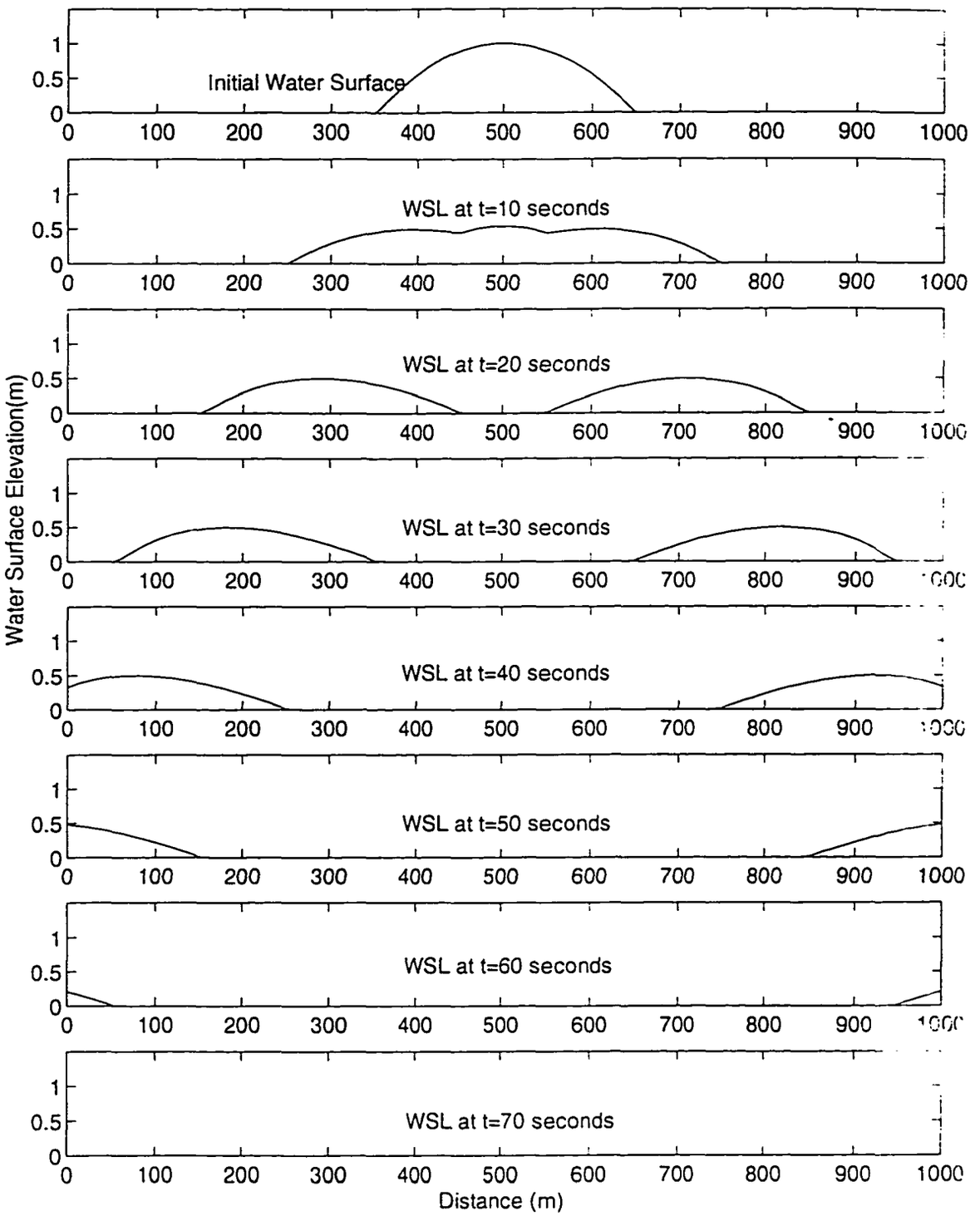

Figure 5.3: Evolution of Water Surface Profile For Case I

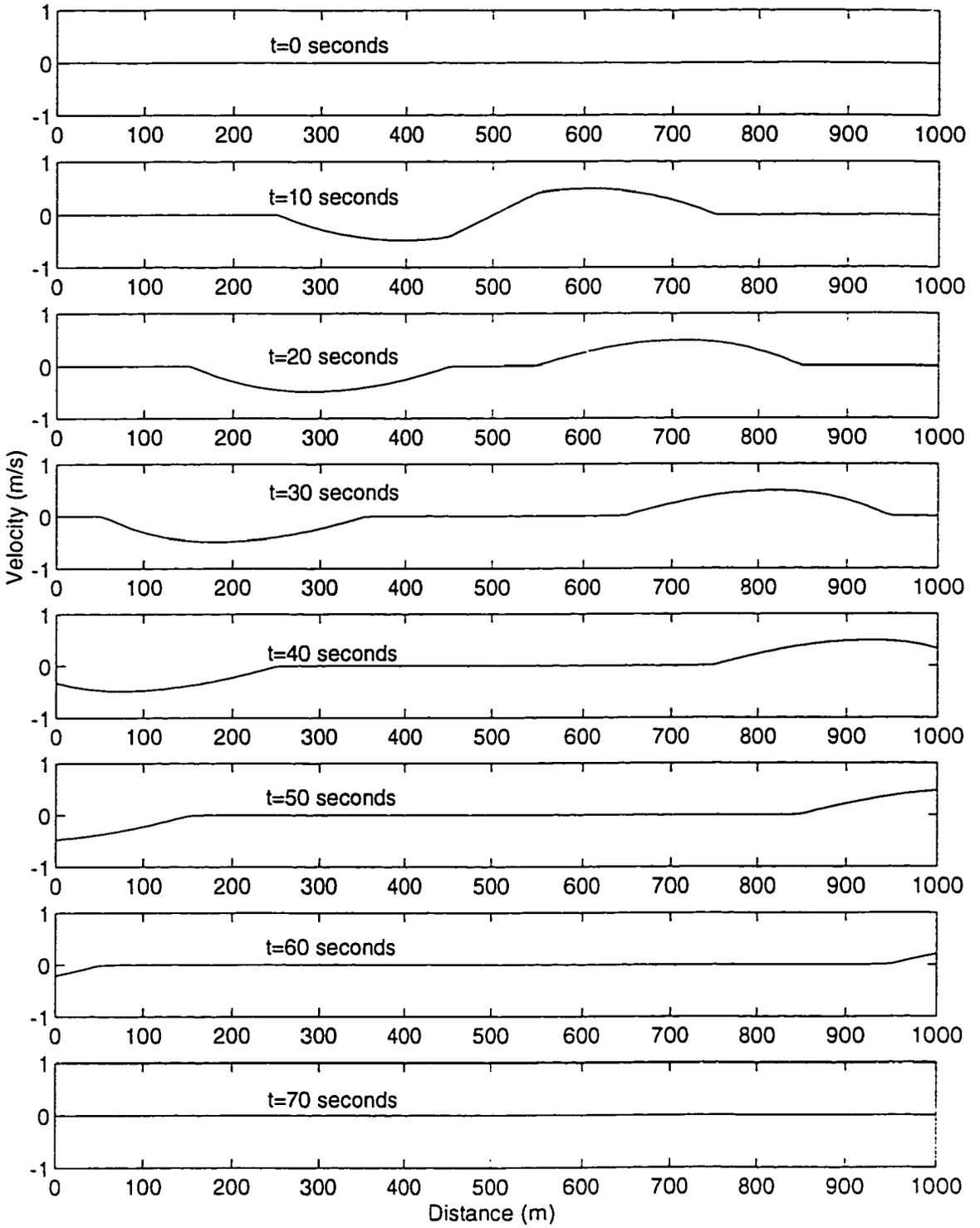

Figure 5.4: Flow Velocity For Case I

Case II - Wave Propagation Over A Horizontal Seabed

A wave train, with a height of 1m and a period of 10 seconds, propagates into a domain of 1000 m long and 10 m deep, as illustrated in Figure 5.5. The wave incident boundary is an inflow boundary and the other boundary is an outflow boundary. This case study aims to test the inflow and outflow boundary conditions, wave phase speed and energy transfer speed.

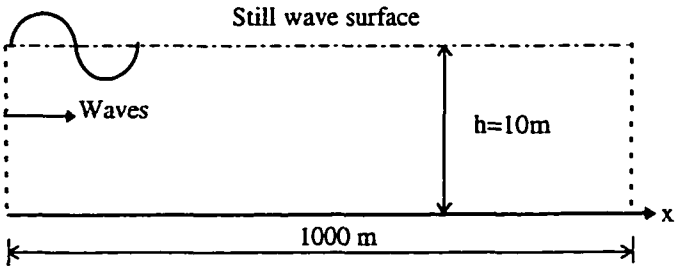

Figure 5.5 Sketch of the Computational Domain of Case II

The wave characteristics and water depth of this case are the same as Case C studied in Section 5.2. The three eigenvalues are 10.01, 7.88 and -9.90. The first and third eigenvalues represent the propagation speed of wave characteristics in the positive and negative x direction, respectively. And the second eigenvalue represents the propagation speed of energy characteristics. A spatial step, Δx=10m, and a time step, Δt=0.95 second, are used with a CFL number of about 0.95. The wave height of 1 m is instantly imposed at the inflow boundary at the beginning of the simulation and maintained so throughout the simulation.

The simulated wave height profiles at eight time levels are presented in Figure 5.6. The wave height profiles advance at a speed of 7.9 m/s (estimated from the advancement

of point A on the wave height profiles) which is close to the wave group speed, C_g, of 8.01 m/s, as estimated from the Fourier approximation wave theory. The rate of lengthening of the wave region must be equal to C_g because the rate of energy input at the inflow boundary is $E \cdot C_g$,(Mei 1983). Also obvious in the wave height profiles is the numerical diffusion on the front part of the wave height profiles. The numerical diffusion is proportional to $\Delta x^2/\Delta t$ (Potter 1973). Use of a larger CFL number may reduce the numerical diffusion, if numerical stability can be ensured .

Figure 5.7 shows the evolution of mean water surface profiles. As waves pass by, the mean water surface rises as a result of wave mass transport. Subsequently, the surface disturbance propagates forward at a speed equal to the eigenvalue of the wave characteristics. Since this speed is faster than the energy transfer speed, thus the zone with the elevated mean water surface will gradually lengthen. The rate of lengthening is equal to $V_{ws} = \lambda_w^+ - \lambda_e^+$, where λ_w^+ and λ_e^+ are the positive eigenvalues of wave and energy characteristics, respectively.

The mean flow velocities below the wave trough at eight time levels are shown in Figure 5.8. The mean flow is generated as a result of wave momentum flux. The magnitude of the velocity is governed by the gradient of wave apparent stresses. Under the present wave conditions, the mean flow velocity is weak, only about 5 cm/s. When the wave field approaches steady state, the mean flow current also disappears.

Figures 5.6 through 5.8 indicate no numerical reflection at both the inflow and outflow boundaries as the wave train passes trough the computational domain.

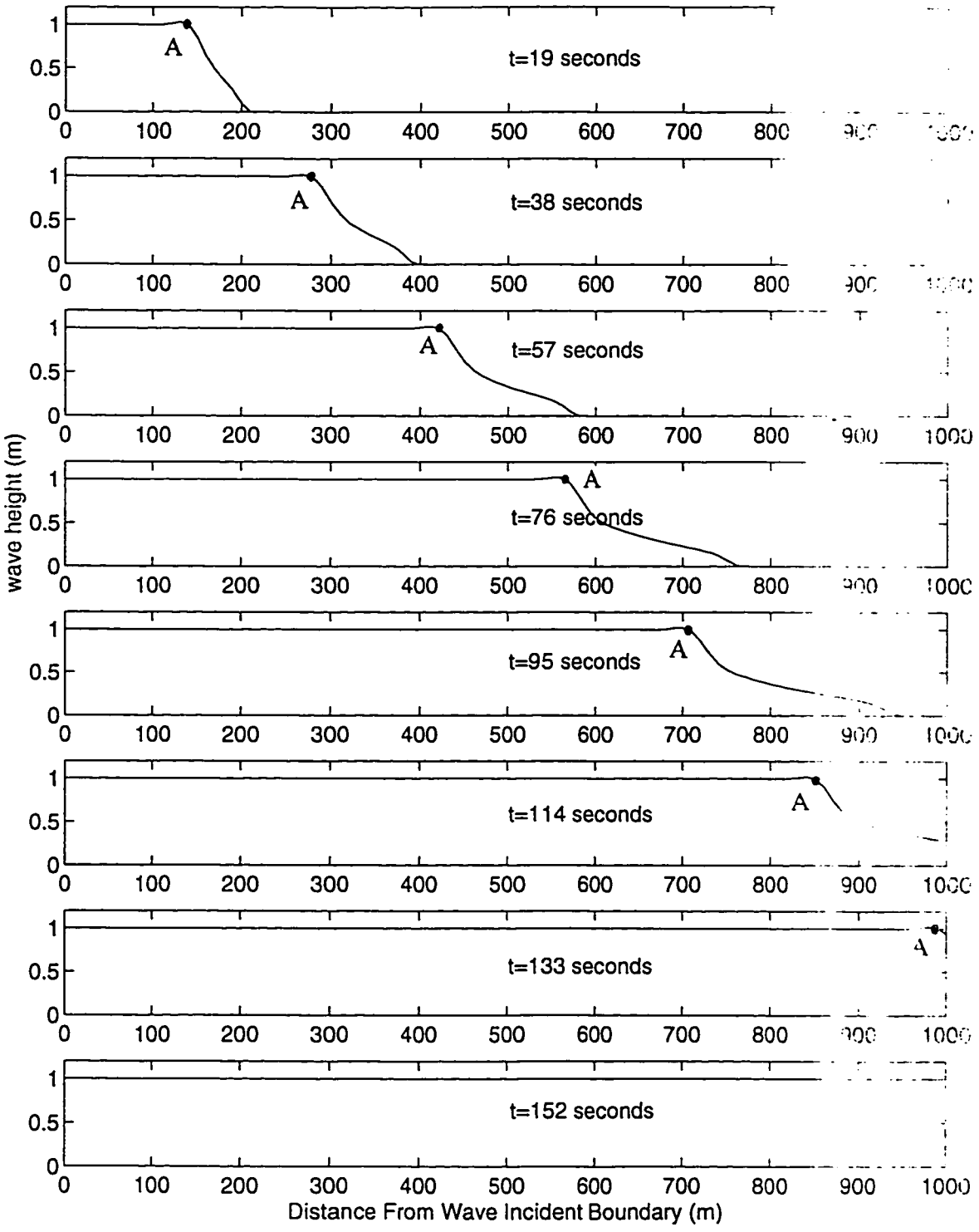

Figure 5.6 Evolution of Wave Height Profile As Waves Advance

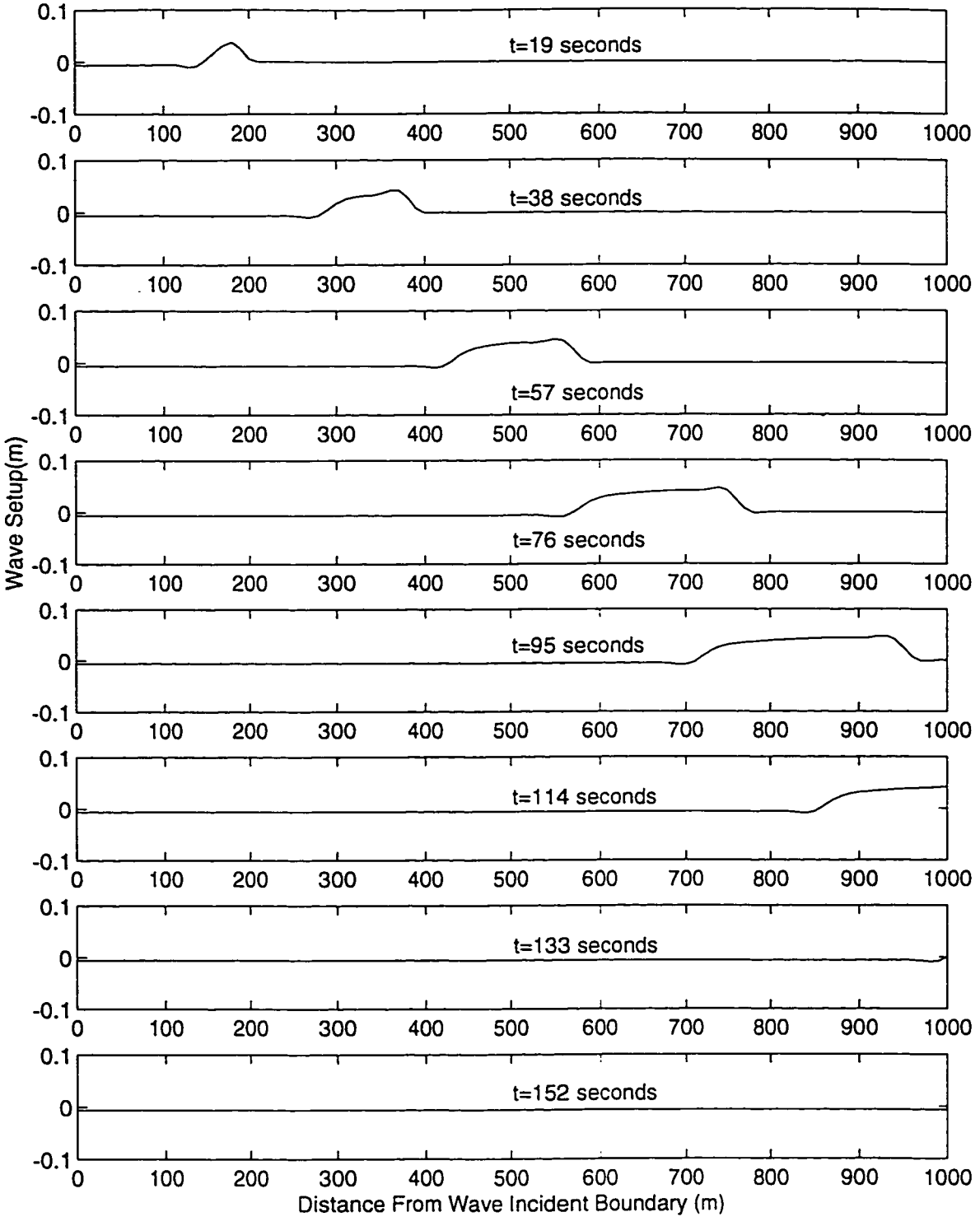

Figure 5.7 Evolution of Mean Water Surface Profiles as Waves Advance

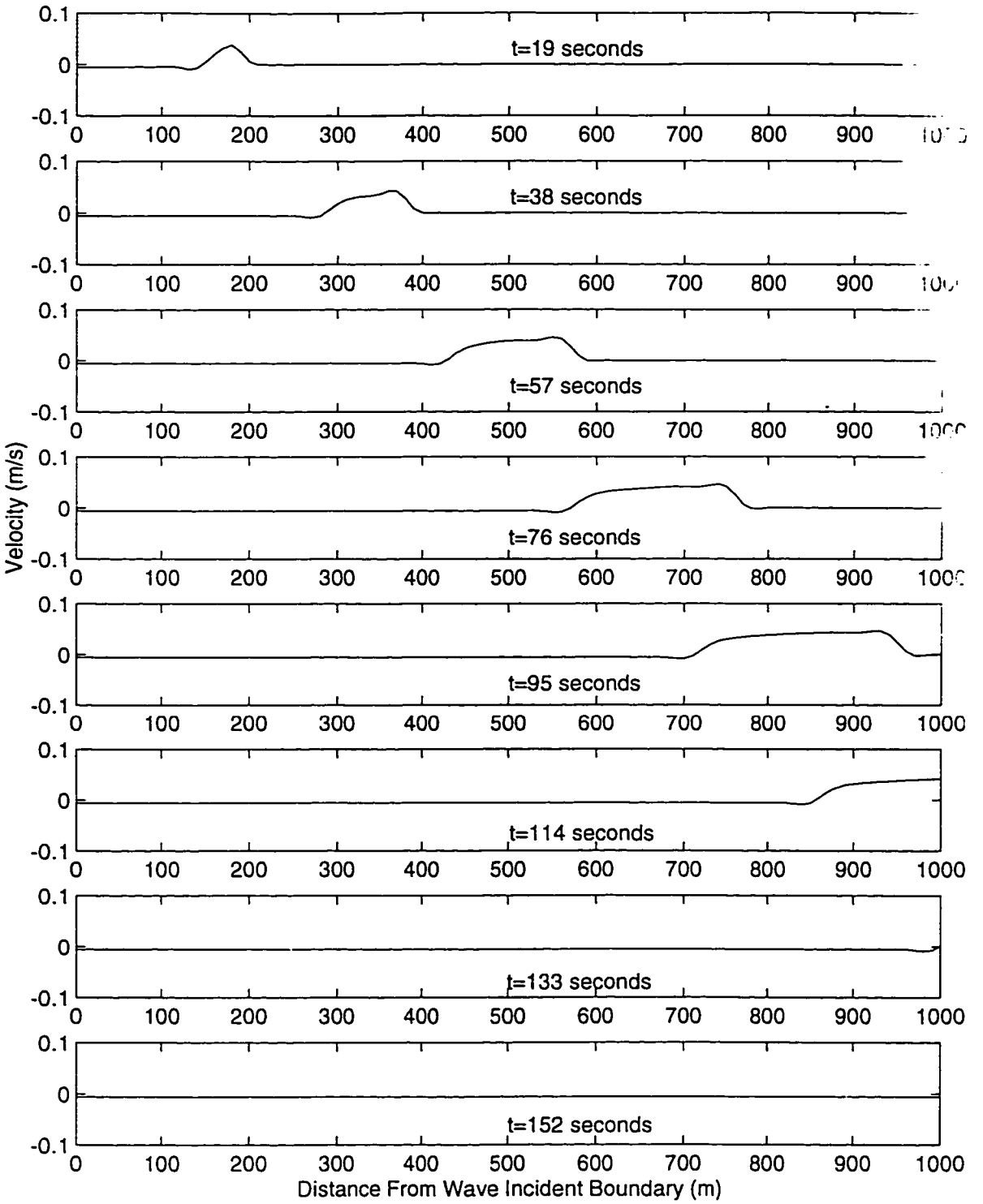

Figure 5.8 Evolution of Mean-Flow Velocity Below Wave Trough as Waves Advance

Case III Wave Propagation Over A Ripple Bed.

This case is designed to study the effect of bathymetric variation on wave propagation. The bed form, shown in Figure 5.9, has an amplitude of 1 m and a wave length of 100 m, with an average water depth of 10 m.

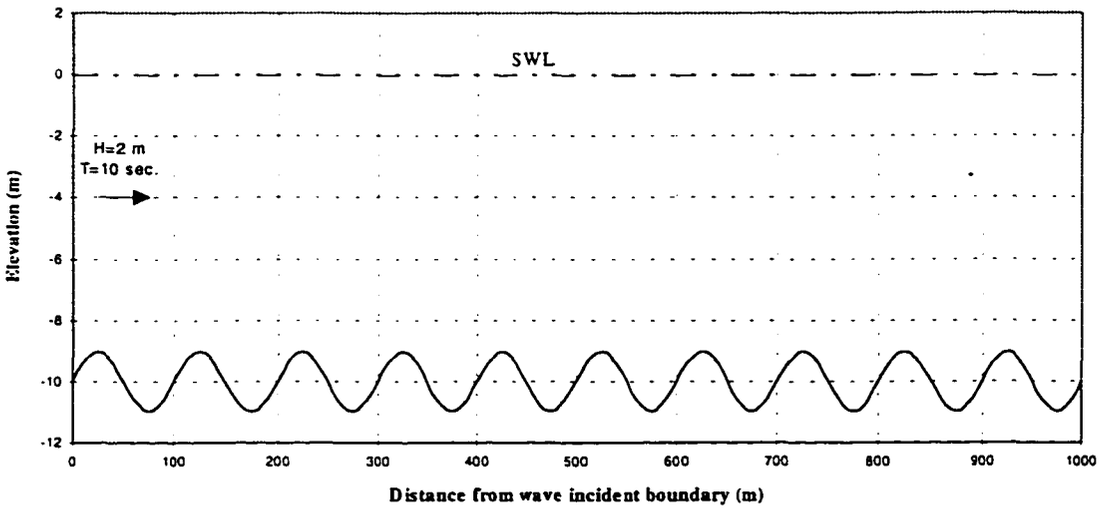

Figure 5.9 Computational Domain For Case III

The incident waves are 2 m height with a period of 10 seconds. In order to make the impact of the bed form appreciable, a greater wave height, compared to Case II, is used.

When surface waves are incident in a region of undulating sea bed topography, it is well known that wave energy may be scattered by the bed forms (Massel 1989). In one spatial dimension, there generally exists the interaction of back-scatter and forward-scatter. The degree of back-scatter depends on the ratio of bed form amplitude to water depth and on the ratio of wave number (assuming horizontal bed) to the bed-form wave number. The back-scatter is maximized when the wave number to bed form wave

number is equal to 0.5 (Mei 1985). In this case, the ratio of bed form amplitude to water depth is equal to 0.1, and the ratio of wave number to bed-form wave number is to 1.08. Thus no significant reflection is expected, and the present model is applicable. A spatial step of 10 m and a time step of 0.95 second are used.

Figures 5.10 through 5.12 show the computed wave height profiles, mean water surfaces and undertow velocities at 8 time levels. Before a steady-state wave field is reached, the evolution of wave height, wave setup and undertow velocity are similar to those in Case II. After the steady state wave field being established, the wave height profiles vary in phase with the bed form, while the wave setup and undertow velocities display an out-of-phase pattern. The in-phase variation of wave height with the bed form is likely caused by wave shoaling. The wave height increases as water depth decreases (In this case, the ratio of water depth to deep water wave length is between 0.0576 and 0 0705), in other words, the wave height increases as the bed rises. On the other hand, the wave setups vary with the gradient of wave mass flux, and the undertow velocities vary with the gradient of wave apparent stresses. The wave mass flux and wave apparent stresses generally increase as wave height increases. Where the wave height increases. the gradients of the mass flux and apparent stress are positive, resulting in a wave setdown and a undertow current in the negative x direction. The spatial variations in the steady state profiles of all three variables are small. This suggests that the propagation of mean wave parameters be only slightly affected by the bed form for the wave conditions studied. The wave height profiles advance at a speed of about 7.85 m/s, which is almost identical to the wave group speed for a uniform depth of 10 m.

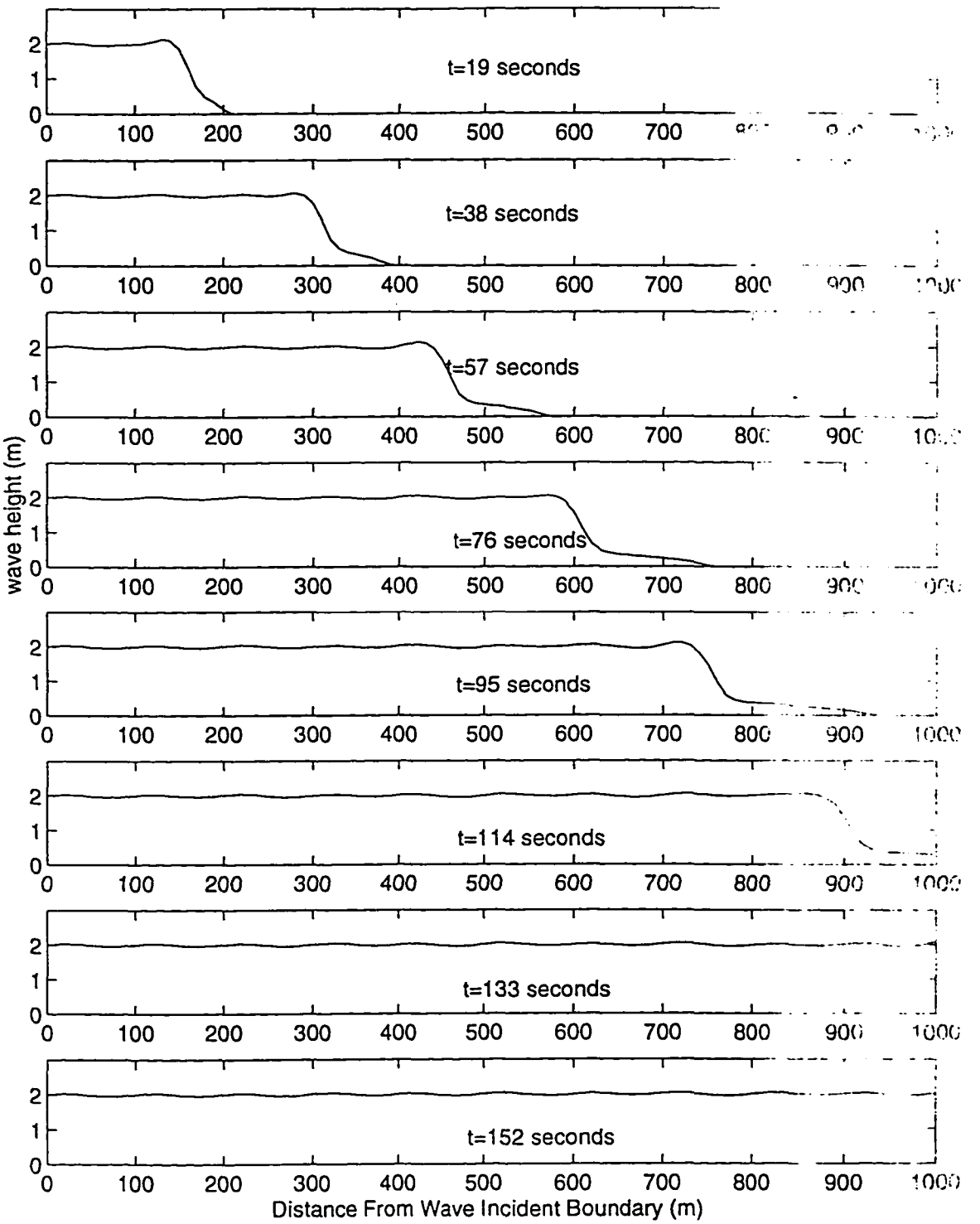

Figure 5.10 Evolution of Wave Height Profiles for Case III

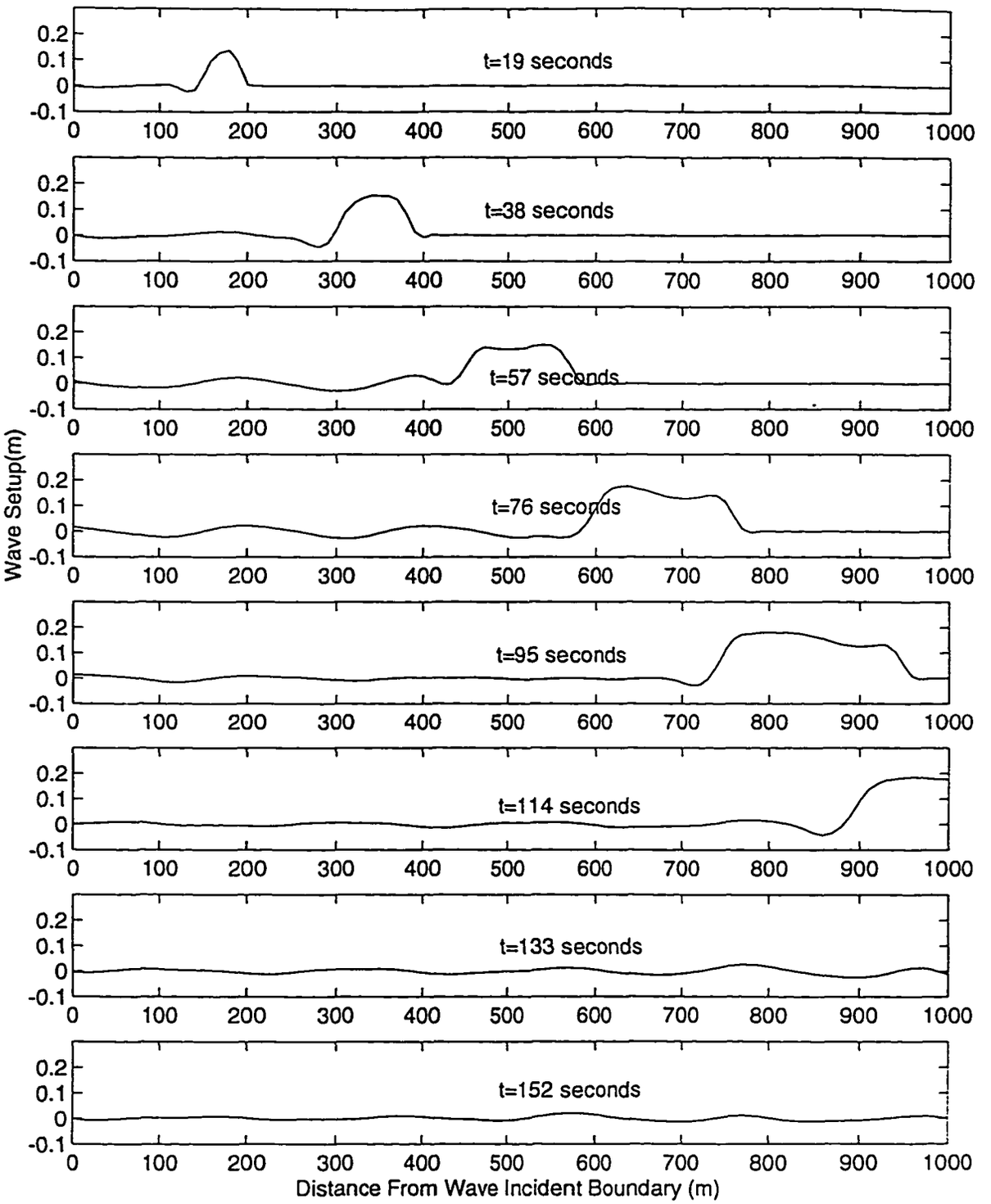

Figure 5.11 Evolution of Mean Water Surface Profiles For Case III

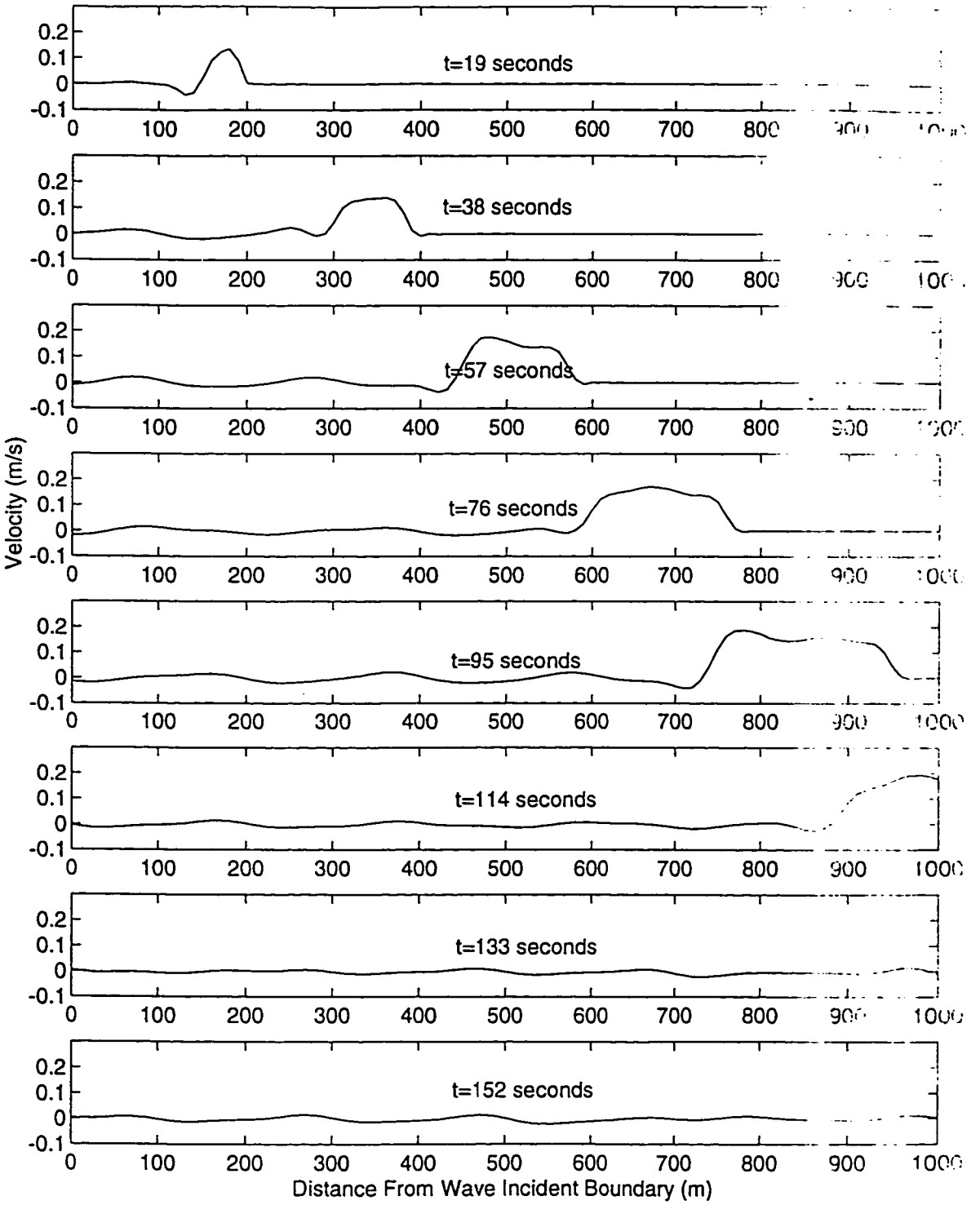

Figure 5.12 Evolution of Mean Flow Velocity For Case III

Case IV Wave Propagation Over A Slope

In this case, both open boundary and beach boundary are present. Thus, the beach boundary conditions have to be specified in addition to the open boundary conditions. The ensuing discussion on the beach boundary conditions centers on slowly varying, dissipative beaches. Strongly reflective boundaries, such as at vertical sea walls, are beyond the scope of this study because the use of a progressive wave theory in the apparent stress closure limits the present model from simulating wave reflection.

In this study, a beach boundary is defined as where the mean water surface intersects with the beach profile. Based on this definition, the water depth at the beach boundary is always zero, and the wave height can legitimately be set to zero. The region around the beach boundary is also called a swash zone. In the swash zone, sheet flow normally prevails. The instantaneous flow velocity at the wave front may be significant. But the mean velocity over a wave period may still be small. To avoid introducing much complexity in dealing with the swash zone, the mean flow velocity is assumed to be zero at the beach boundary.

The wave setup at the beach boundary can be estimated from a lowest order finite difference approximation to the continuity equation for the computational cell bordering the beach boundary, as shown in Figure 5.13.

$$\overline{\eta}_m^{n+1} = \overline{\eta}_m^n + \frac{\Delta t}{\Delta x}[H_{m-1}^n U_{s,m-1}^n + (h_{m-1} + \overline{\eta}_{m-1}^n) U_{b,m-1}^n] \qquad (5.17)$$

where the superscript "n" denotes the previous time step, and the subscript "m" denotes the beach boundary. In this manner, the computational cell is treated as a water storage

the elevation of which rises when water pumps in, or falls when water goes out. This is, of course, a crude approximation which suppresses much of dynamics in the swash zone. But this approach is convenient, besides, it does not prevent the model from correctly simulating wave transformation from deep water up to the swash zone.

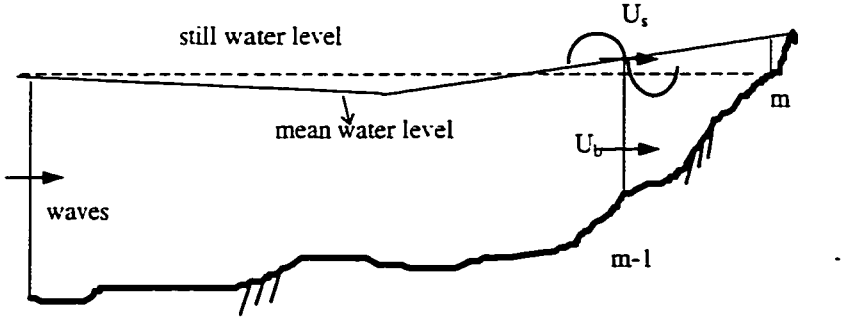

Figure 5.13 Schematics of Beach Boundary Conditions

Unlike an open boundary, the beach boundary moves back and forth as the mean water surface oscillates up and down. The active computational domain has to be adjusted at each time step. A computational cell is deemed being active if it satisfies

$$z + \overline{\eta}^n \geq \Delta \tag{5.18}$$

where z is the bottom elevation, $\overline{\eta}^n$ is the wave setup, and Δ is a small depth cut-off value which is required for the sake of numerical stability. It is set at 0.1 m in this study.

The beach boundary conditions along with the proposed numerical scheme and open boundary conditions are used to simulate wave shoaling over a 1:100 slope, as shown in Figure 5.14. The incident waves are one meter high with a period of ten seconds. The suitability of the present model for simulating wave propagation over the slope is checked by the surf parameter ξ_o, which is defined as (Battjes 1974)

$$\xi_o = \frac{\tan\beta}{(H_o / L_o)^{1/2}} \tag{5.19}$$

where H_o is the incident wave height, L_o the deep water wave length, and $\tan\beta$ is the bottom slope. For the slope, ξ_o is equal to 0.125, so it can be classified as being slowly varying and dissipative. The present model is thus applicable.

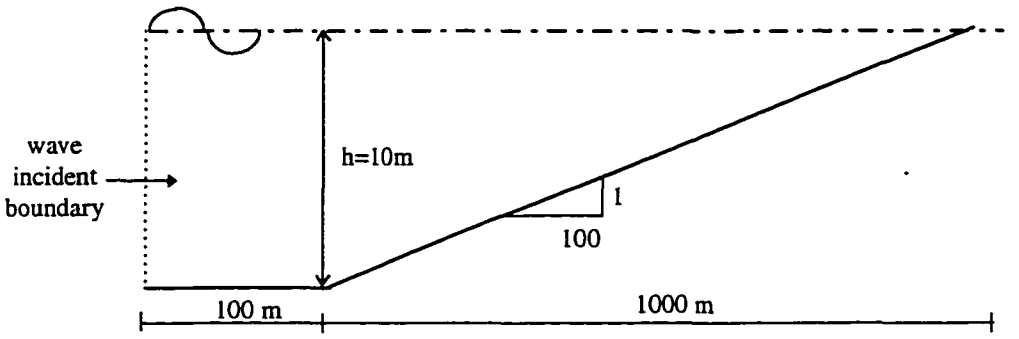

Figure 5.14 Sketch of the Computational Domain for Case IV

The model is set up based on a uniform grid spacing of 10m and a time step of 0.95 second, with a Courant-Friedich-Lewy number of about 0.95 at the deep end of the domain. The energy dissipation due to wave breaking and bottom friction are also included using the models described in Chapter 2. The bottom friction factor is assumed to be equal to 0.04.

Figures 5.15-17 show the evolution of wave height profiles, variation of mean water surfaces and undertow currents at eight time levels. The transients of the wave shoaling process reveal some basic physics in wave propagation in shallow waters. Some of the features are summarized as follows:

- Wave height increases until the energy dissipation rate due to wave breaking exceeds the energy influx. The maximum wave height occurs at water depth 3.8 m, with a height/depth ratio of 0.32, much lower than the theoretical value in the range from 0.7 to 0.8. This is because the energy dissipation was computed based on the fraction of wave breaking (random wave breaking model). Since the beach is dissipative, the wave height near the shoreline has gradually decreased to zero.

- Wave height profiles reach steady state relatively faster than wave setup and undertow current. The length of time for wave setup and undertow currents to approach steady state is about triple the time for wave propagating through the simulation domain.

- As waves approach to the shoreline, the mass transport is predominantly shoreward, causing a significant water surface pulse and shoreward mass transport. After waves reach the shoreline, seaward undertow currents develop. The transient wave setup and undertow current in shallow water are much greater than steady state wave setups and undertow currents. This suggests that the transient dynamics in coastal process could be very important though the transient action only lasts in a short period of time.
- The steady state wave setup at shoreline is 0.12 m. which is consistent with empirical estimates (Dean & Dalrymple 1984) for a breaking wave height to depth ratio (breaker index) of 0.32, rather than the value of 0.7.
- Though wave reflection is excluded by the present model, the reflection of wave setup and undertow current is simulated in Figures 5.16 and 5.17.

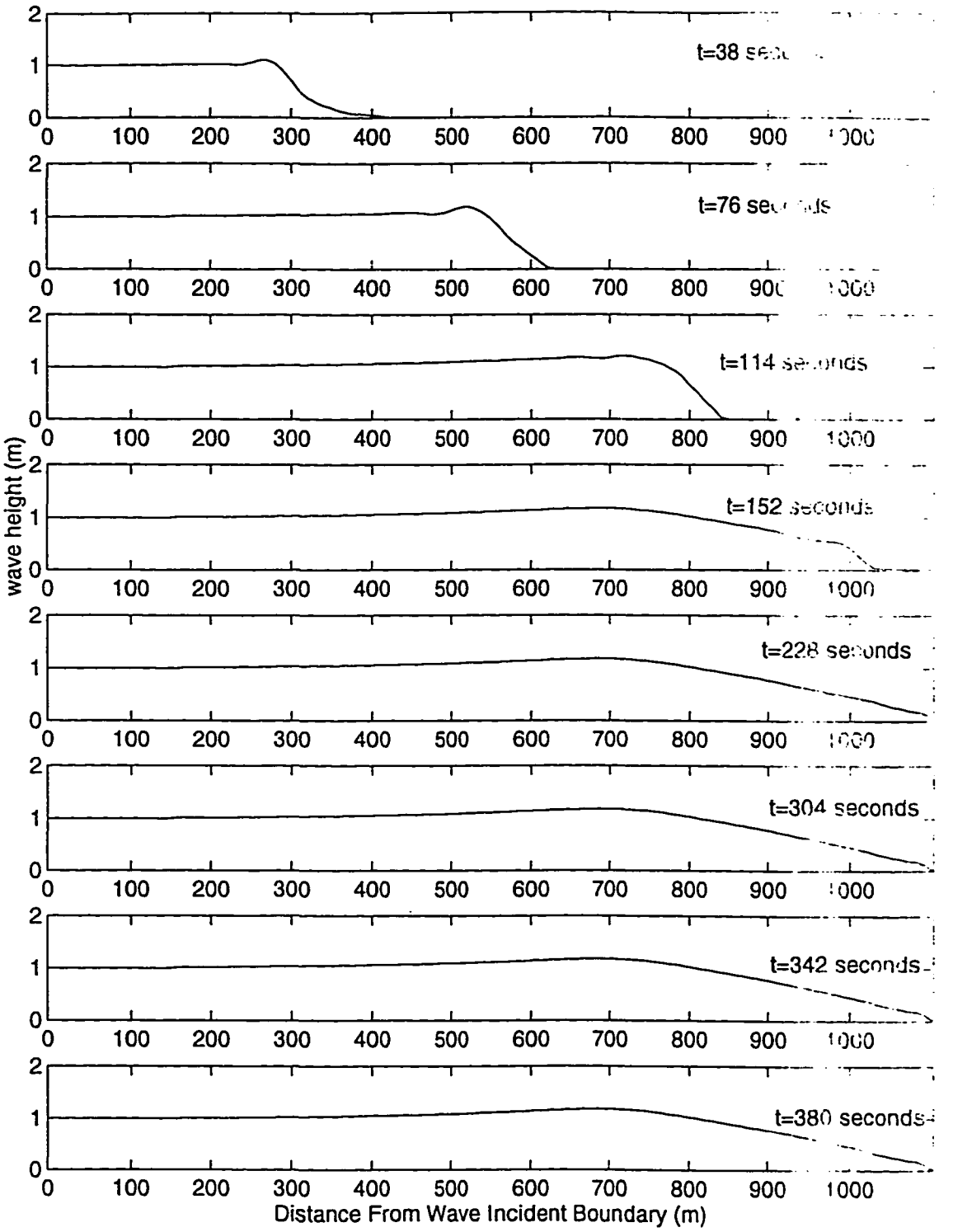

Figure 5.15 Evolution of Wave Height Profiles For Case IV

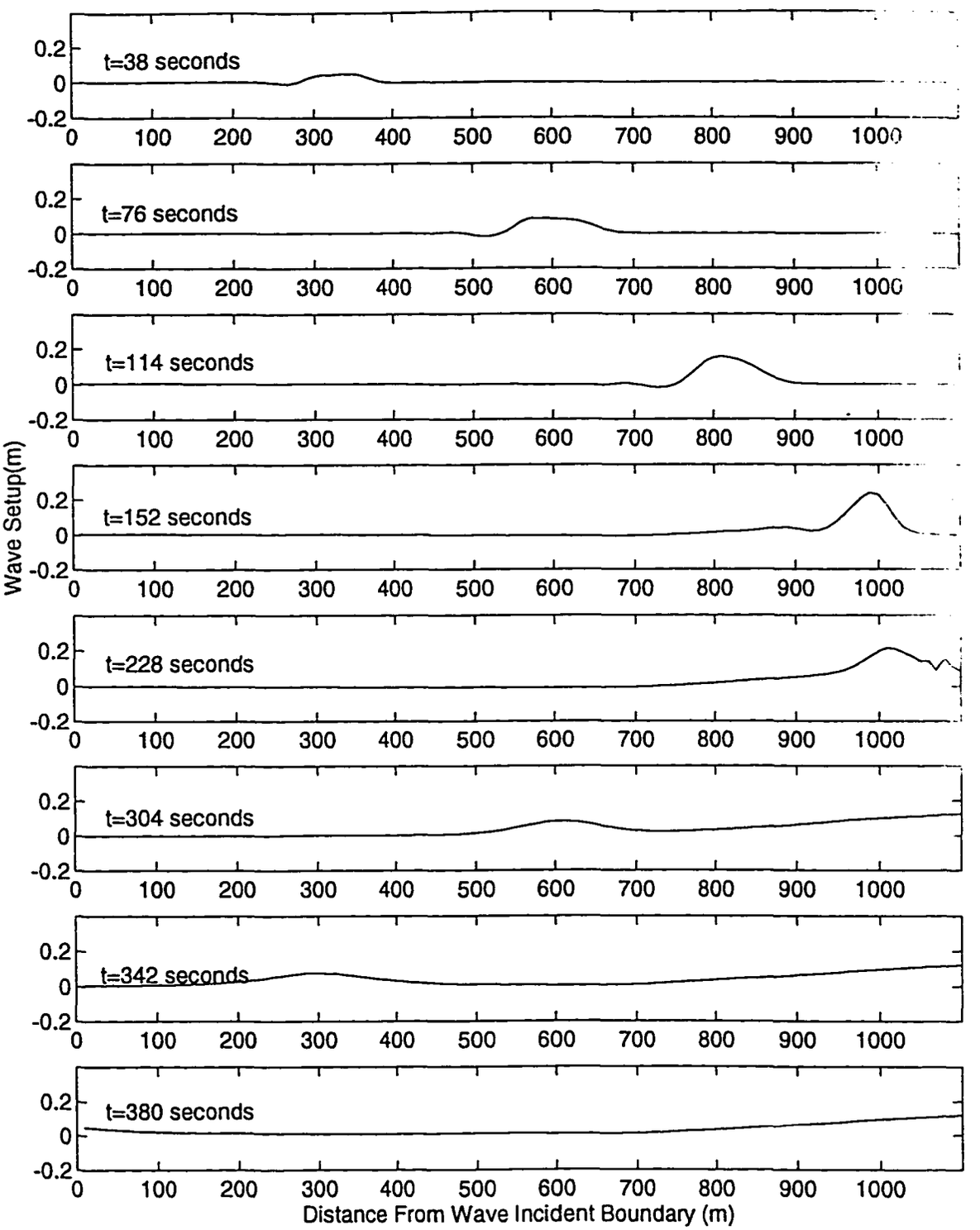

Figure 5.16 Evolution of Mean Water Surface Profiles For Case IV

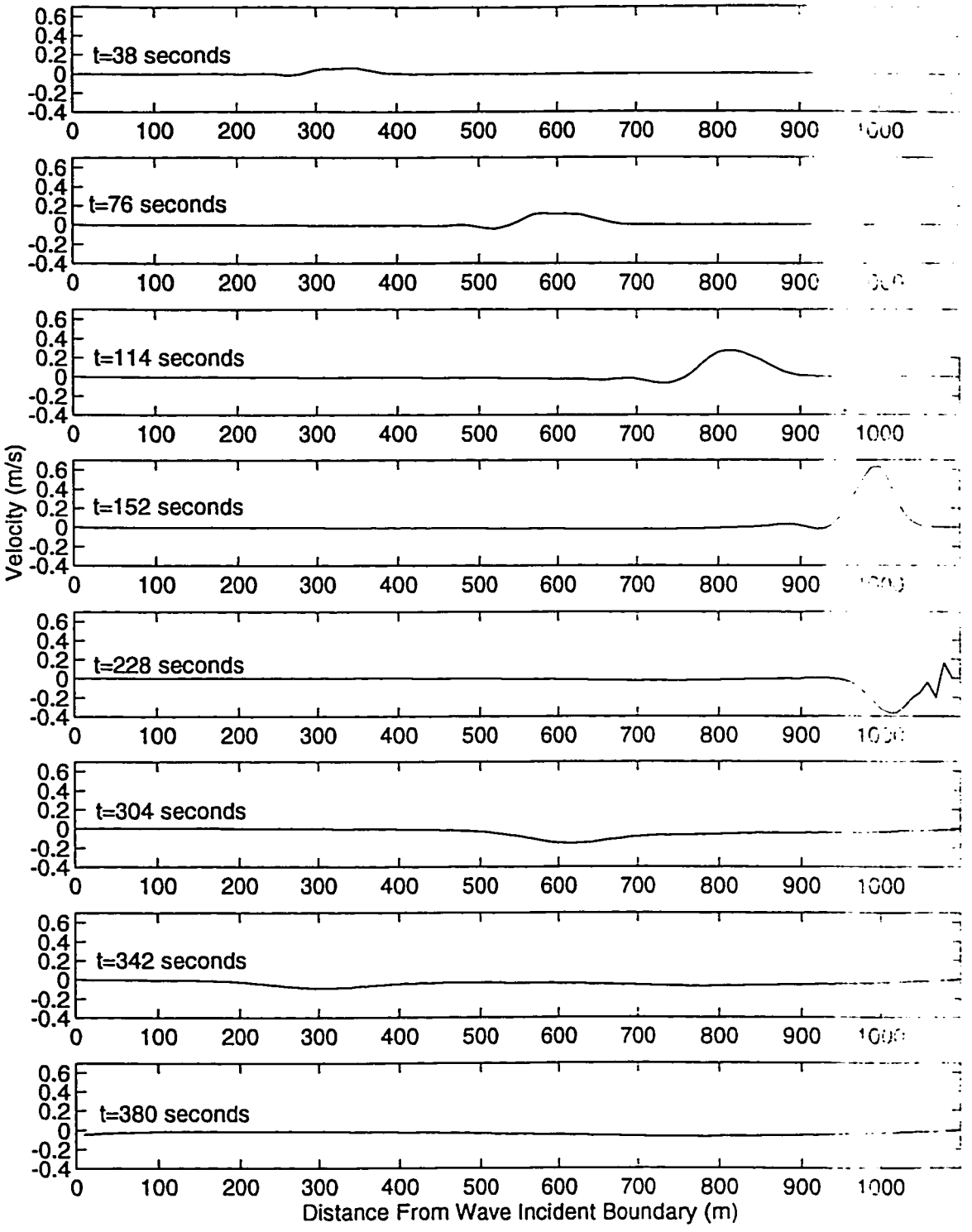

Figure 5.17 Mean Flow Velocity Under Wave Trough For Case IV

5.5 Simulation of Cross-Shore Wave Propagation at Egmond Beach

Egmond beach is located on the North Sea coast of the Netherlands. The contours at the beach are almost parallel to the shoreline and typical wave direction is normal to the shoreline. Given the contour characteristics, a one dimensional model should be adequate for simulating cross-shore wave propagation at the beach.

The beach profile shown in Figure 5.18 is typical in coastal regions, featuring multiple offshore bars. Derks and Stive (1984) observed the wave characteristics at the beach, measuring wave height and wave setup at several nearshore locations. The observed offshore significant wave height is 2.78 m and the significant wave period is 8.7 seconds.

The computational domain is about 3000 m long, with the water depth at the offshore boundary being about 16 m. A uniform spacing of 10 m is used with a corresponding time step of 0.7 second (the Courant-Friedich-Lewis number at the offshore boundary is equal to about unity.

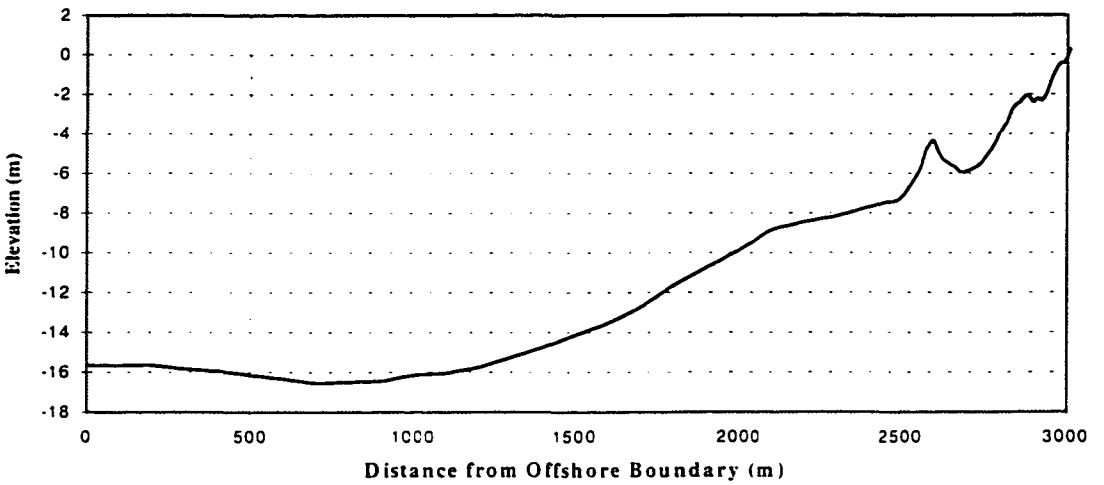

Figure 5-18 Bathymetric Profile At Egmond Beach

The numerical scheme as discussed in Section 5.1 is implemented, the open boundary conditions follows Hedstrom's methodology presented in Section 5.3, and the beach boundary conditions are specified as in Case IV in Section 5.4. Wave forcing is suddenly imposed at the offshore boundary and remains constant thereafter. The system is assumed to be initially quiescent, with wave height, wave setup and undertow current all equal to zero at the beginning of simulation.

The predicted transient wave height profiles at 8 different time levels are shown in Figure 5.19. After seven minutes, a steady state wave height profile is established. The evolution of the mean water surface level and undertow currents are shown in Figures 5.20 and 5.21. It takes about fourteen minutes for the wave setup and undertow currents to reach an equilibrium state. Before the steady state is reached, the characteristics of the evolution of wave height, wave setup and undertow currents are similar to those observed in the simulation of wave propagation over a uniform slope in Section 5.4. Seaward undertow currents start to develop when waves reach the shoreline. The seaward undertow currents then penetrate toward the offshore boundary from the shoreline. Again, the maximum transient wave setup and undertow currents are much greater than the steady state values. The observed wave height and setup are also plotted in Figures 5.19 and 5.20. Good agreement is found for both wave height and wave setup.

The four case studies and the simulation at the Egmond Beach lead to the following conclusions: (1) the numerical scheme is effective for simulating the evolution of mean wave parameters in one spatial dimension; (2) the open boundary conditions work satisfactorily; and (3) the beach boundary conditions are adequate for dissipative beaches.

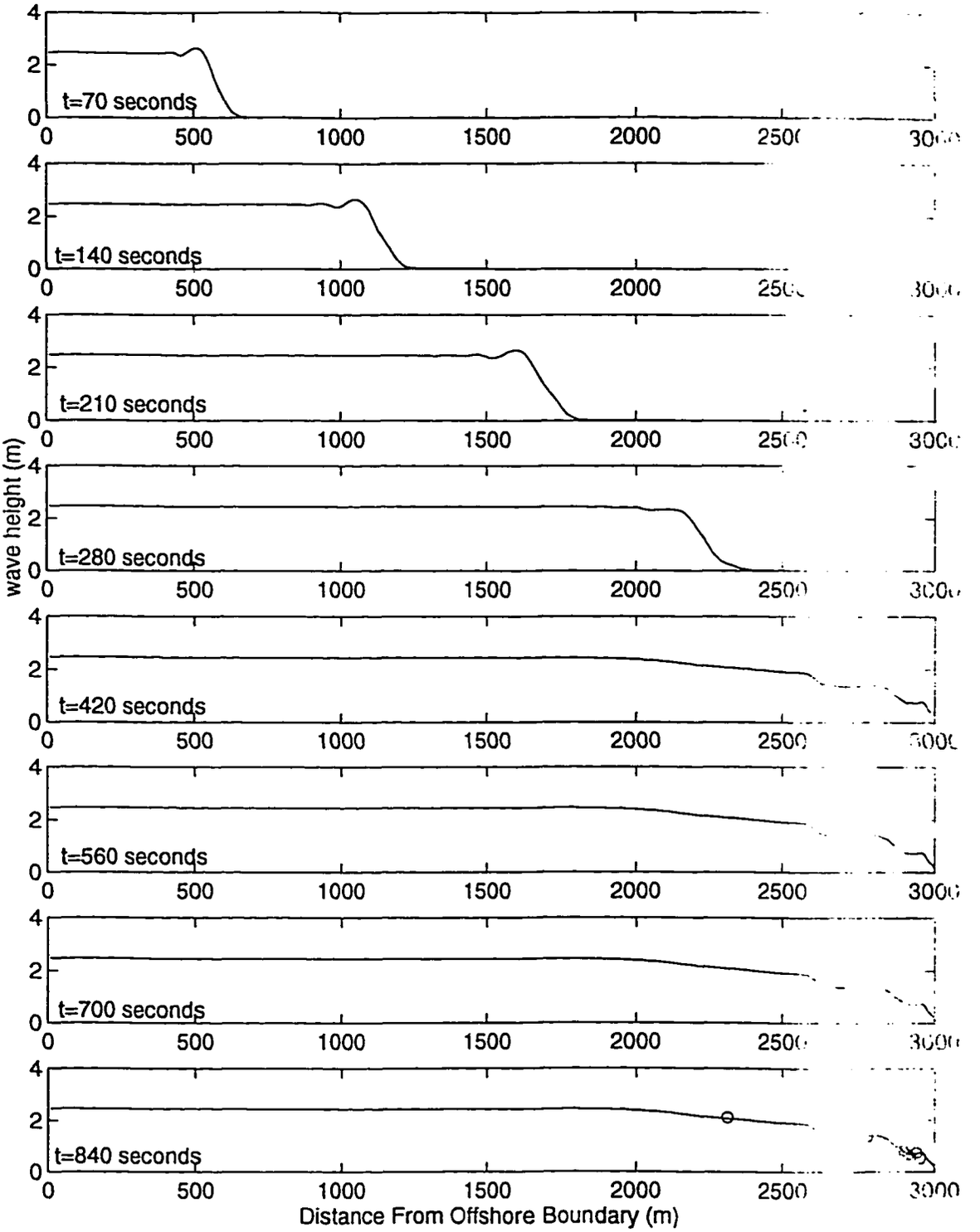

Figure 5.19 Evolution of Wave Height Profiles at Egmond Beach

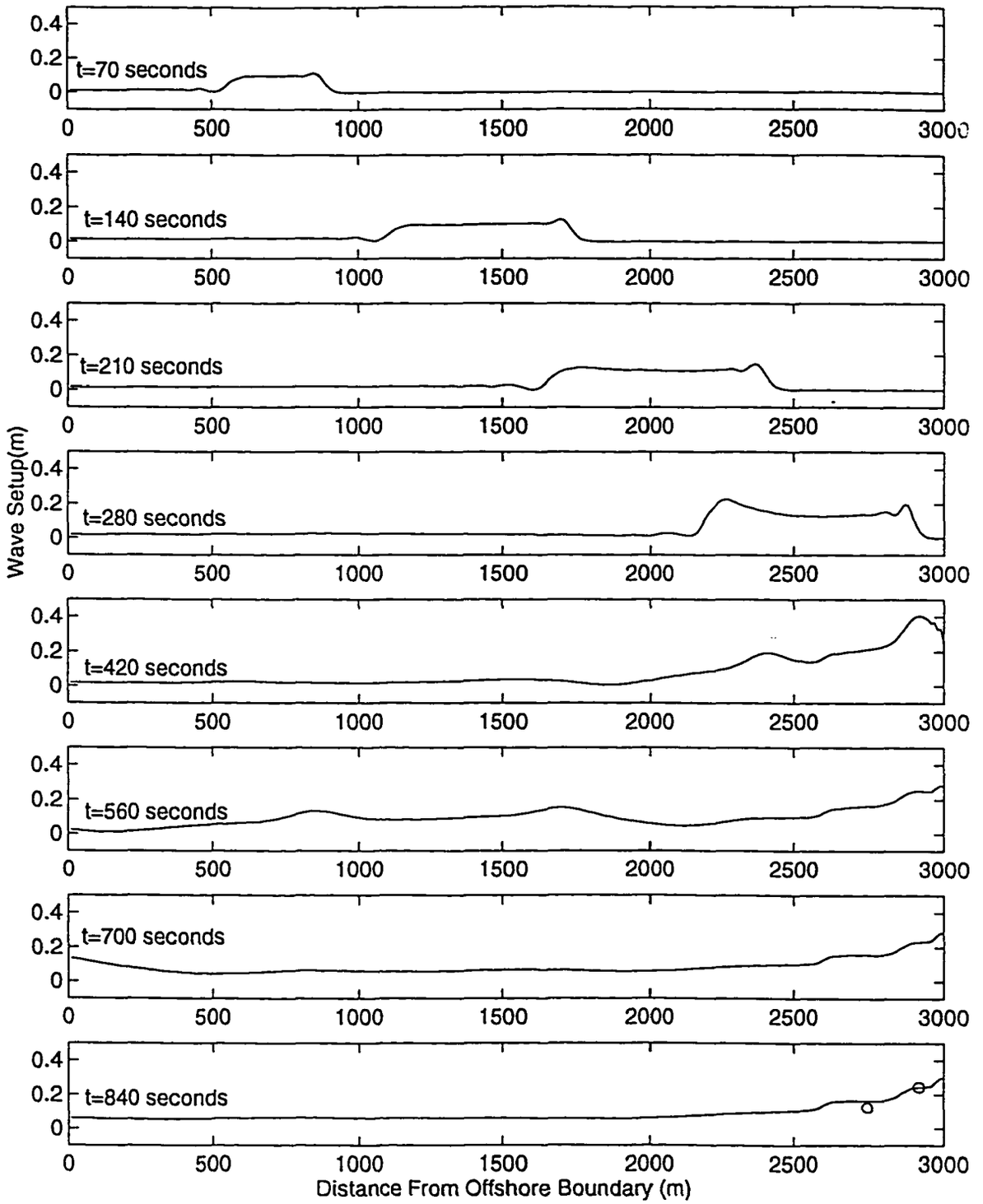

Figure 5.20 Evolution of Mean Water Surface Profiles at Egmond Beach

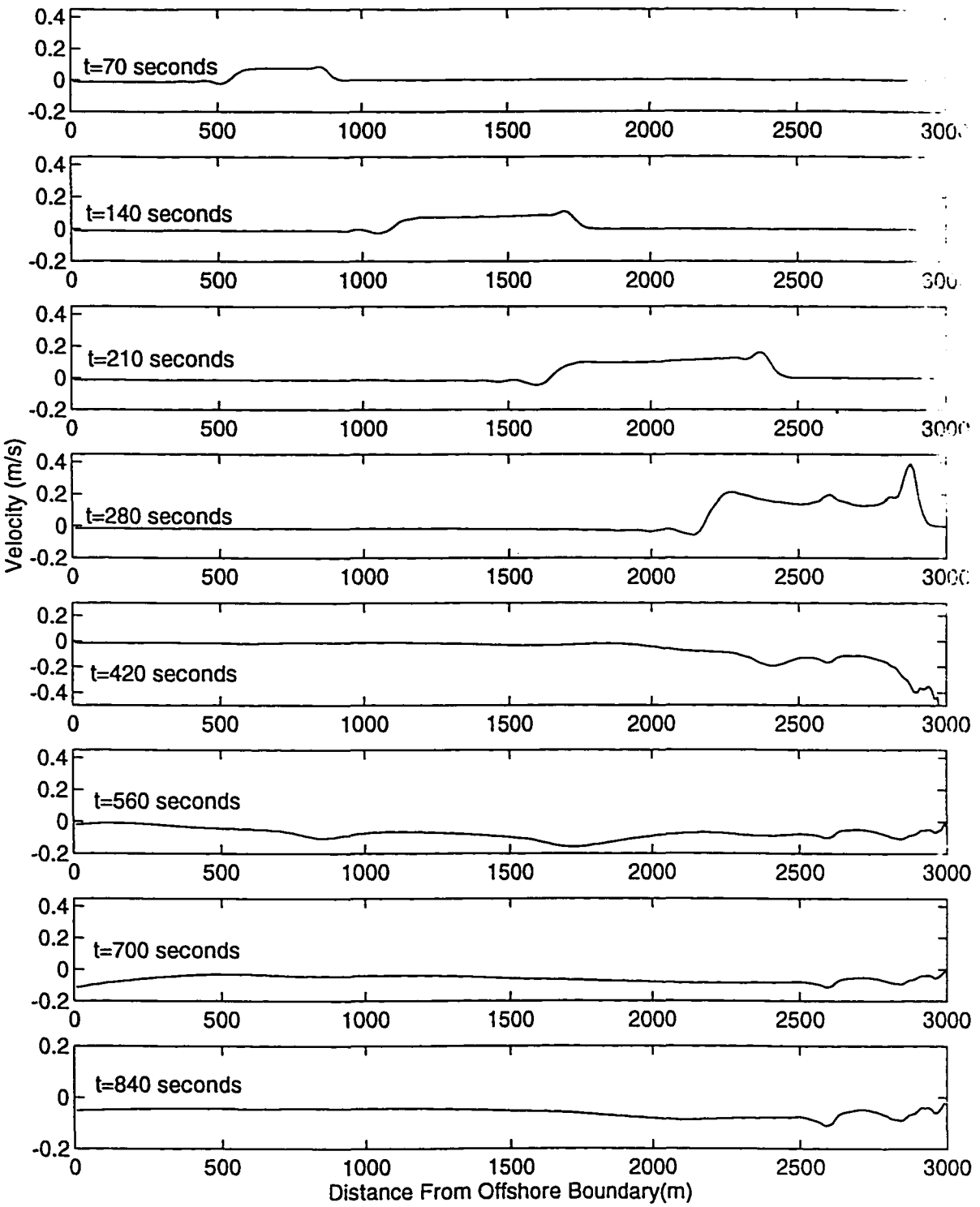

Figure 5.21 Mean Flow Velocity Under Wave Trough at Egmond Beach

6. MODELING OF WAVE PROPAGATION IN TWO SPATIAL DIMENSIONS

This chapter presents a numerical framework for the evolution of wave height, wave setup and wave-induced currents in two horizontal spatial dimensions, based on the method of characteristics. The major issues are (1) estimate of wave propagation direction, which is critical to the evaluation of wave apparent stresses, (2) a numerical scheme taking into account the fact that there are infinite characteristic equations in two spatial dimensions, and (3) open boundary conditions. First, the procedure for deriving characteristic equations is introduced and the characteristics of the system are investigated for typical coastal wave and bathymetric conditions. A numerical scheme based on bi-characteristics is then developed, along with the specification of open boundary conditions. Three case studies demonstrate the performance of the numerical scheme and open boundary conditions. Subsequently, various approaches for modeling wave propagation direction over irregular bathymetry are discussed. Finally, the model is applied to wave focusing by a submerged shoal, under the experimental conditions of Berkhoff et al. (1982).

6.1 Characteristic Equations

The integral model for mean wave parameters in a two-dimensional space was presented in Chapter 4 (Equations 4.42 through 4.45). This model can be written in a vector form

$$\frac{\partial \Phi}{\partial t} + \frac{\partial F_x(\Phi)}{\partial x} + \frac{\partial F_y(\Phi)}{\partial y} = Q(x, t, \Phi) \qquad (6.1)$$

where Φ is a dependent variable vector composed of wave setup, mean-flow momentum

components, and wave energy

$$\begin{aligned} \Phi_1 &= \overline{\eta}, \\ \Phi_2 &= HU_s + (h + \overline{\eta} + \eta_{tr})U_b, \\ \Phi_3 &= HV_s + (h + \overline{\eta} + \eta_{tr})V_b, \\ \Phi_4 &= g\overline{\tilde{\eta}^2} + HW_s + (h + \overline{\eta} + \eta_{tr})W_b \end{aligned} \tag{6.2}$$

$F_x(\Phi)$ and $F_y(\Phi)$ represent mass, momentum and energy fluxes. and $Q(x,t,\Phi)$ are the source or sink terms, being a function of x, t, and Φ, but not of the derivatives of Φ.

To apply the method of characteristics, these equations are transformed a set of quasi-linear equations of $H, \overline{\eta}, U_b$ *and* V_b .

$$\frac{\partial W}{\partial t} + A_x \frac{\partial W}{\partial x} + A_y \frac{\partial W}{\partial y} = Q \tag{6.3}$$

where W is the dependent variable vector

$$W = [H, \overline{\eta}, U_b, V_b] \tag{6.4}$$

and A_x and A_y are the coefficient matrices

$$A_x = \frac{\partial F_x}{\partial w_j}, \qquad A_y = \frac{\partial F_y}{\partial w_j} \tag{6.5}$$

The details on the entries of A_x, A_y and Q are given in Appendix B.

Nonlinear hyperbolic problems are known (Hirsch 1983) to be weakly "dissipative." i.e., the solution may develop spontaneous shocks. Physically, the homogeneous part of such first order quasi-linear partial differential equations admit wave-like solutions. The wave front separates the points already influenced by the propagating disturbance from the points not yet reached by the wave. If $S(x,y) = S_0$ (where S_0 is a constant) is such a phase surface of the wave, a solution of the form

$$W = \hat{W} e^{iS(x,y)} \tag{6.6}$$

represents a general wave. Substituting Equation (6.6) into Equation (6.3) gives

$$\left[I\cdot\frac{\partial S}{\partial t}+A^{x}\frac{\partial S}{\partial x}+A^{y}\frac{\partial S}{\partial y}\right]\hat{W}=0 \tag{6.7}$$

where I is a 4×4 unit matrix.

To have nontrivial solutions for W, the determinant of the square-bracketed matrix must be zero. As the normal vector of the wave front surface, $\bar{n}$, is proportional to gradient of the surface function, ∇S, the necessary and sufficient condition for the existence of non-trivial solutions for W is expressed by

$$\det\left|I\cdot n_{t}+A_{x}n_{x}+A_{y}n_{y}\right|=0 \tag{6.8}$$

Equation (6.8) is an eigenvalue problem. Defining

$$K=A_{x}n_{x}+A_{y}n_{y} \tag{6.9}$$

Then Equation (6.8) may be reduced to

$$\det|K-\lambda I|=0 \tag{6.10}$$

which leads to a fourth order polynomial in λ.

If the four roots of λ are all real and distinct, the system is a hyperbolic system. And each eigenvalue defines a family of characteristic surfaces the normal vector of which is $(-\lambda, n_x, n_y)$. On the characteristic surface, the original system of equations can be reformulated into differential relations with differentiations along the surface only. The first-order system of Equation (6.3) can be transformed through a linear combination of the form,

$$\ell_{j}\left(\frac{\partial W}{\partial t}+A_{x}\frac{\partial W}{\partial x}+A_{y}\frac{\partial W}{\partial y}\right)=\ell_{j}Q_{i}\qquad j=1,,4 \tag{6.11}$$

where ℓ_j is a left eigenvector, which is defined as

$$\ell_i\left(A_x n_x + A_y n_y - \lambda I\right) = 0 \tag{6.12}$$

Since the determinant of the bracketed matrix is zero, an infinite set of solutions may be obtained for ℓ_j from Equation (6.12). On substituting any set of ℓ_j solutions into Equation (6.12), all the differentiations in the equation are performed along the characteristic surfaces.

The analytical expressions for the characteristics and characteristic equations of this system are not available due to the complex form of the integral equations. As indicated in Chapter 2, the mean-flow continuity and momentum equations in the present system are similar to the shallow water wave equations. To assist in appreciating the present system, the characteristics and characteristic equations for the shallow water wave equations are given in Appendix C.

There are some fundamental differences in generalizing the method of characteristics from two independent variables to three. With two independent variables, transforming the governing equations into characteristic equations reduces partial differential equations to ordinary differential equations. For a system of three independent variables, the characteristic equations are still partial differential equations, though of one fewer independent variable. Another significant difference is that for two independent variables, the characteristic curves passing through a point equal the number of equations, whereas for three independent variables the characteristic surfaces passing through a point are infinite. Accordingly, the approaches based on the method of the characteristic in (x-y-t) space are totally different from those in (x-t) space.

6.2 Characteristic Properties

To further appreciate this system, the eigenvalues and eigenvectors are computed numerically for the following conditions: wave direction $\phi=\pi/2$(with x-axis), wave height=1.0 m, water depth h=10 m, mean water elevation $\bar{\eta}=0$, and mean flow velocities under wave trough U_b=0.5 m/s and V_b=0.5 m/s. The eigenvalues depend on a specific direction or azimuth which ranges from 0 to 2π, as shown in Figure 6.1.

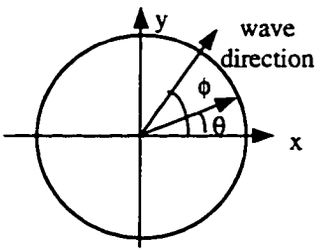

Figure 6.1 Sketch of Direction Domain

The four eigenvalues are plotted in Figure 6.2. Also shown in the figure are the three eigenvalues of the shallow water wave equations under the same conditions along with their analytical expressions, two identified by λ_w denoting wave characteristics, and the other by λ_f denoting flow characteristics (Katopodes 1979). The flow characteristics is

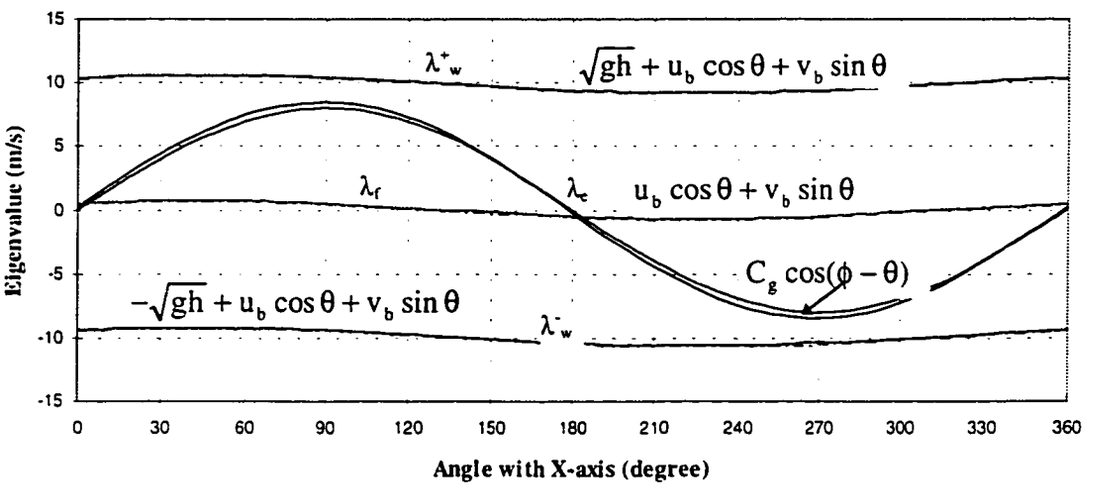

Figure 6-2 Variation Of Eigenvalue λ With Azimuth θ

unique in the two spatial dimensions. The magnitude of the eigenvalue of the flow characteristics is within the order of magnitude of the flow velocity. The eigenvalue labeled by λ_e, is the additional eigenvalue for the present system. This eigenvalue is called an energy characteristics because its value is related to the wave group speed. and physically it is the speed of wave energy transfer. The eigenvectors of the present system in three specific directions are given in the following table.

Table 6.1 Eigenvectors for θ=0, π/4 and π/2

Direction	Eigenvalue	Eigenvector			
	λ (m/s)	ℓ_1	ℓ_2	ℓ_3	ℓ_4
π/2	10.47	0.1726	1.0	0.0	0.5079
	8.47	1.0	-0.230	0.0	-0.1021
	0.5	-0.0383	0.1621	1.0	0.0
	- 9.41	0.0101	1.0	0.0	-0.505
π/4	10.63	0.0384	1.0	0.3576	0.3584
	6.19	1.0	-0.0747	-0.0332	-0.0049
	0.70	-0.0026	0.0014	-0.9995	1.0
	-9.2	0.0214	1.0	-0.3568	-0.3570
0	10.41	-0.0091	1.0	0.506	0.0
	0.5	-0.0123	-0.002	-0.001	1.0
	0.22	1.0	-0.0234	0.0003	0.0
	-9.4	0.0295	1.0	-0.505	0.0

The computed eigenvalues and eigenvectors lead to the following observations

- This system is normally hyperbolic because four eigenvalues in all directions under

the given wave conditions are real and distinct.

- Under the assumed wave conditions, the eigenvalues of wave and flow characteristics of the present system are almost identical to those of shallow water wave equations. As a matter of fact, they can hardly be distinguished in Figure 6.2.
- The eigenvalue of the energy characteristics may be approximated by $C_g \cos(\phi - \theta)$, in which C_g is the plane wave group speed. As indicated in Chapter 5, a negative eigenvalue denotes information propagating in a direction opposite to the azimuth from which the eigenvalue is derived. The eigenvalues of the energy characteristics in a polar coordinate system are sketched in Figure 6.3. Thus information along the energy characteristics can only propagate forward.

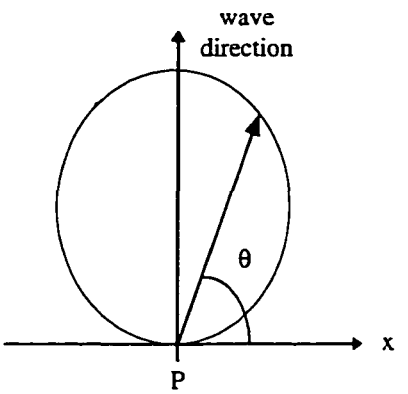

Figure 6.3 Eigenvalue of Energy Characteristics

- The eigenvalues λ_w^+ and λ_w^- of the wave characteristics are identical when considering the entire range of direction $(0, 2\pi)$ since $\lambda_w^+(\theta) = -\lambda_w^-(\theta+\pi)$. Only one of them, conventionally λ_w^+, is used in describing wave characteristics. As shown in Figure 6.2, the eigenvalues of the wave characteristics vary slightly with direction,

which suggests information radiating out to any direction at an almost equal speed.

- As implied in Equation (6.11), the ratios among the components of an eigenvector measure the correlation of the equations in a system. For the energy characteristics, the first component of the eigenvector is much greater than three other components, which indicates that the evolution of wave height is primarily described by the wave energy equation. This is not surprising because the wave energy equation is an equation for the energy of residual fluid motions, while the three other equations are only related to the mean flow. This loose connection between the energy equation and the mean flow equations is also indicated by the fact that the magnitude of the first component of the eigenvectors for wave or flow characteristics is much smaller than other components. In simulating mean wave parameters in one spatial dimension, Svendsen (1984) noticed that wave height is mainly determined from the energy equation while wave setup depends on the momentum equation.

As shown in Figure 6.1, the maximum eigenvalue occurs in the flow direction, here in $\theta=\pi/4$. Since the maximum eigenvalue physically denotes the fastest speed at which information could propagate from a point. This direction and the characteristics in this direction are of particular interest for numerical simulation because the maximum eigenvalue defines the domain of influence or dependence. The flow direction will be termed a principal direction. In the principal direction, the eigenvalues and characteristic equations of the shallow water wave equations in two spatial dimensions are the same as those in one spatial dimension. The details are given in Appendix C.

6.3 Numerical Schemes

As indicated in Section 6.2, there are an infinite sets of characteristics at any solution point. Hence, an infinite number of characteristic equations can be derived. The present system contains four unknowns only. Thus to ensure the uniqueness of the solutions, only four of the equations are independent. In Appendix C, it is shown that only three sets of characteristics are linearly independent for the shallow water wave system of three equations. Physically, this can be explained by the fact that the information propagations in various directions are related to one another.

In this section, a numerical scheme is developed based on bi-characteristics which is defined as the curve of tangency between a characteristic surface and a characteristic conoid. Four equations are formed through combination of the integral continuity equation along a flow path and the characteristic equations integrated along five bi-characteristics. These four equations are used to solve four unknowns at a solution point.

6.3.1 Major Issues

A successful numerical scheme based on the method of characteristics (MOC) should address the following issues:

- **Completeness.** The infinity of characteristic equations provides "freedom" of choice in characteristic equations. But the characteristics in all directions should be reflected in the chosen characteristic equations.
- **Multiplicity.** The current system has three families of characteristics. The behavior of each family of characteristics is different. Thus the characteristic equations of each

family should be included and treated differently. For instance, the information propagates along wave characteristics in all directions at an almost equal speed, while information propagates along an energy or a flow characteristics in a predominant direction. Accordingly, wave characteristic equations in several directions may be needed, but a single energy or flow characteristic equation in the predominant direction should be sufficient.

- **Cross Derivatives.** In two spatial dimensions, the characteristic equations include two partial derivatives, one along the bicharacteristics and the other along a direction more or less perpendicular to the bicharacteristics (Appendix D). The derivative in the direction other than the bi-characteristics is called a cross-derivative (Ransom 1981). Integration of the characteristic equations along the bi-characteristics does not eliminate the cross derivative. The treatment of these cross derivatives directly affects the accuracy of the numerical results.
- **Interpolation.** In obtaining the solutions at a node in, say, a uniform grid system, the characteristic equations are integrated along bi-characteristics segments over a time step. The starting points of the bi-characteristics segments normally do not coincide with the grid nodes. The values at the starting points must be interpolated from the surrounding grid nodes. The way of interpolation has a significant impact on numerical stability and solutions(Townson 1974, Fowell and Ransom et al. 1986).

6.3.2 Bi-Characteristics Method

In this section, the discussion centers on the development of four equations in H, $\overline{\eta}$, U_b and V_b based on bi-characteristics. The four equations consist of one energy

characteristic equation in the direction of wave propagation and three other equations formed by combination of four wave characteristic equation and continuity equation. The choice of energy bi-characteristics reflects the fact that wave energy transfers predominantly in the direction of wave propagation. The flow characteristic equation is not directly involved in forming the four equations because the flow characteristics can be obtained by linear combination of the wave characteristics in two complementary directions, as shown in Appendix C for shallow water wave equations. The procedure is demonstrated by forming the four equations at node P in a uniform grid system, as shown in Figure 6.4. The integration of the energy characteristic equation along the bicharacteristics, say, line 6-P, in the direction of wave propagation gives

$$\ell_1^6 H_p + \ell_2^6 \overline{\eta}_p + \ell_3^6 U_{b,p} + \ell_4^6 V_{b,p} = \ell_1^6 H_6 + \ell_2^6 \overline{\eta}_6 + \ell_3^6 U_{b,6} + \ell_4^6 V_{b,6} + [\, a_6 \frac{\partial H}{\partial x} + b_6 \frac{\partial H}{\partial y} + c_6 \frac{\partial \overline{\eta}}{\partial x} + d_6 \frac{\partial \overline{\eta}}{\partial y} + e_6 \frac{\partial U_b}{\partial x} + f_6 \frac{\partial U_b}{\partial y} + g_6 \frac{\partial V_b}{\partial x} + h_6 \frac{\partial V_b}{\partial y} + S_6 \,] \cdot \Delta t \tag{6.12}$$

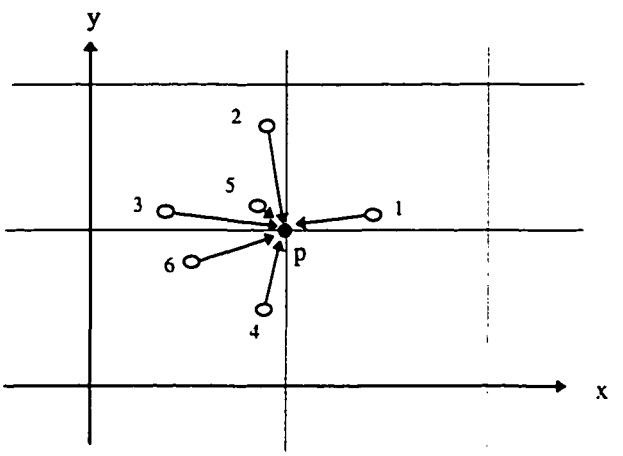

Figure 6.4 Illustration of Bi-characteristics Scheme

The choice of wave bi-characteristics follows Butler(1960). For unsteady plane flow, Bulter (1960) proposed a numerical scheme which could eliminate all cross derivatives

through combining the continuity equation with the characteristic equations in four evenly spaced directions. For the present system, this scheme will not eliminate all the cross derivatives, but it does reduce the magnitudes of these terms significantly. So it is still considered an appropriate method for the present system.

The characteristic equations in directions $\theta=0$, $\pi/2$, π, $3\pi/2$ are integrated along four bi-characteristic curves: 1-P, 2-P, 3-P and 4-P. The four integral equations are

$$\ell^i_1(H_p - H_i) + \ell^i_2(\overline{\eta}_p - \overline{\eta}_i) + \ell^i_3(U_{b,p} - U_{b,i}) + \ell^i_4(V_{b,p} - V_{b,i}) = \left[a_i \frac{\partial H}{\partial x} + b_i \frac{\partial H}{\partial y} + c_i \frac{\partial \overline{\eta}}{\partial x} + d_i \frac{\partial \overline{\eta}}{\partial y} + e_i \frac{\partial U_b}{\partial x} + f_i \frac{\partial U_b}{\partial y} + g_i \frac{\partial V_b}{\partial x} + h_i \frac{\partial V_b}{\partial y} + S_i \right] \cdot \Delta t \qquad i=1,2,3,4 \quad (6.13)$$

where $(\ell^i_1, \ell^i_2, \ell^i_3, \ell^i_4)$ is the eigenvector of wave characteristics in the ith direction, and a_i, b_i, ... are the coefficients of the cross derivatives. A numerical procedure for determining the bi-characteristics and deriving the characteristic equations is given in Appendix E.

Along the streamline 5-p, the continuity equation can be written as

$$\overline{\eta}_p - \overline{\eta}_5 = \left[a_5 \frac{\partial H}{\partial x} + b_5 \frac{\partial H}{\partial y} + c_5 \frac{\partial \overline{\eta}}{\partial x} + d_5 \frac{\partial \overline{\eta}}{\partial y} + e_5 \frac{\partial U_b}{\partial x} + f_5 \frac{\partial U_b}{\partial y} + g_5 \frac{\partial V_b}{\partial x} + h_5 \frac{\partial V_b}{\partial y} + S_5 \right] \cdot \Delta t \qquad (6.14)$$

A set of four linearly independent equations can be extracted from the above six equations in the following manner.

Summing up the four equations included in (6.13) and subtracting it by two times the continuity equation gives

$$
\begin{aligned}
&(\sum_{i=1,4}\ell_1^i)H_p+(\sum_{i=1,4}\ell_2^i-2)\overline{\eta}_p+(\sum_{i=1,4}\ell_3^i)U_{b,p}+(\sum_{i=1,4}\ell_4^i)V_{b,p}=\\
&\Bigg[\sum_{i=1,4}\ell_1^i H_i+(\sum_{i=1,4}\ell_2^i\overline{\eta}_i-2\overline{\eta}_5)+\sum_{i=1,4}\ell_3^i U_{b,i}+\sum_{i=1,4}\ell_4^i V_{b,i}+\\
&(\sum_{i=1,4}a_i)\frac{\partial H}{\partial x}+(\sum_{i=1,4}b_i)\frac{\partial H}{\partial y}+(\sum_{i=1,4}c_i)\frac{\partial\overline{\eta}}{\partial x}+(\sum_{i=1,4}d_i)\frac{\partial\overline{\eta}}{\partial y}+\\
&(\sum_{i=1,4}e_i)\frac{\partial U_b}{\partial x}+(\sum_{i=1,4}f_i)\frac{\partial U_b}{\partial y}+(\sum_{i=1,4}g_i)\frac{\partial V_b}{\partial x}+(\sum_{i=1,4}h_i)\frac{\partial V_b}{\partial y}+(\sum_{i=1,4}S_i)\Bigg]\cdot\Delta t
\end{aligned}
\tag{6.15}
$$

For the shallow water wave equations, the coefficients of H_p, $U_{b,p}$ and $V_{b,p}$ on the left side are equal to zero. The coefficients for the cross derivative terms are also equal to zero. Thus it directly gives the solution for $\overline{\eta}_p$. In the present system, though the coefficients of H_p, $U_{b,p}$ and $V_{b,p}$ are not zero, but their values are at least 2 orders of magnitude smaller than that of $\overline{\eta}_p$. This is verified in the case studies in Section 6.5.

Subtracting the wave characteristic equation in the direction $\theta=0$ from that in the direction $\theta=\pi$ gives

$$
\begin{aligned}
&(\ell_1^1-\ell_1^3)H_p+(\ell_2^1-\ell_2^3)\overline{\eta}_p+(\ell_3^1-\ell_3^3)U_{b,p}+(\ell_4^1-\ell_4^3)V_{b,p}=\\
&\ell_1^1H_1-\ell_1^3H_3+\ell_2^1\overline{\eta}_1-\ell_2^3\overline{\eta}_3+\ell_3^1U_{b,1}-\ell_3^3U_{b,3}+\ell_4^1V_{b,1}-\ell_4^3V_{b,3}+\\
&[(a_1-a_3)\frac{\partial H}{\partial x}+(b_1-b_3)\frac{\partial H}{\partial y}+(c_1-c_3)\frac{\partial\overline{\eta}}{\partial x}+(d_1-d_3)\frac{\partial\overline{\eta}}{\partial y}+(e_1-e_3)\frac{\partial U_b}{\partial x}\\
&+(f_1-f_3)\frac{\partial U_b}{\partial y}+(g_1-g_3)\frac{\partial V_b}{\partial x}+(h_1-h_3)\frac{\partial V_b}{\partial y}+S_1-S_3]\cdot\Delta t
\end{aligned}
\tag{6.16}
$$

In the shallow water wave equations, the coefficients of H_p, $\overline{\eta}_p$ and $V_{b,p}$ on the left side and the coefficients of the derivatives are all zero. Equation (6.16) directly gives the solution for $U_{b,p}$. Similarly, subtracting the characteristic equation in the direction $\theta=\pi/2$ from that in the direction $\theta=3\pi/2$ gives

$$
\begin{aligned}
&(\ell_1^2-\ell_1^4)H_p+(\ell_2^2-\ell_2^4)\overline{\eta}_p+(\ell_3^2-\ell_3^4)U_{b,p}+(\ell_4^2-\ell_4^4)V_{b,p}= \\
&\quad \ell_1^2H_2-\ell_1^4H_4+\ell_2^2\overline{\eta}_2-\ell_2^4\overline{\eta}_4+\ell_3^2U_{b,2}-\ell_3^4U_{b,4}+\ell_4^2V_{b,2}-\ell_4^4V_{b,4}+ \\
&(a_2-a_4)\frac{\partial H}{\partial x}+(b_2-b_4)\frac{\partial H}{\partial y}+(c_2-c_4)\frac{\partial \overline{\eta}}{\partial x}+(d_2-d_4)\frac{\partial \overline{\eta}}{\partial y}+(e_2-e_4)\frac{\partial U_b}{\partial x} \\
&\quad +(f_2-f_4)\frac{\partial U_b}{\partial y}+(g_2-g_4)\frac{\partial V_b}{\partial x}+(h_2-h_4)\frac{\partial V_b}{\partial y}+S_2-S_4]\Delta t
\end{aligned}
\tag{6.17}
$$

In the shallow water wave equations, Equation (6.17) directly gives the solution to $V_{b,p}$. In the present system, the coefficient of $V_{b,p}$. are much greater than the coefficients of other unknowns on the left side, and the coefficients of the derivatives are also very small. Equations (6.12), and (6.15) through (6.17) are used to obtain the solutions for H, $\overline{\eta}$, U_b and V_b at the point P.

In Appendix D, details are given on determining the locations of the starting points of bi-characteristics segments. The results are given here.

$$
\begin{aligned}
&x_{2,4,5}=x-u\Delta t; \qquad x_{1,3}=x-(u\mp C)\Delta t; \qquad x_6=x-\lambda_e\Delta t\cos\phi \\
&y_{2,4,5}=y-v\Delta t; \qquad y_{1,3}=y-(v\mp C)\Delta t; \qquad y_6=y-\lambda_e\Delta t\sin\phi
\end{aligned}
\tag{6.18}
$$

where x,y are the coordinates of the point at which the solutions are sought, u, v, and C are calculated by Equations (D.4) through (D.6), ϕ is the direction of local wave propagation, and λ_e is the eigenvalue of energy characteristics in the direction ϕ.

At a boundary, some bi-characteristics lie outside the computational domain. The above procedure may not be completely applicable. Some corresponding characteristic equations must be replaced by boundary conditions specified in other manner. This problem will be discussed in Section 6.4 on open boundary conditions and in case studies in Section 6.5.

6.3.3 Interpolation Scheme

When integrating the characteristic equations, the values of the dependent variables at the starting ends of the bi-characteristics segments are interpolated from the surrounding grid points. Webster (1968) stressed the importance of the interpolation process. For the shallow water wave equations, he explored three methods of interpolation, each based on nine points centered spatially at the internal points (Points P through Viii in Figure 6.5) and offset at boundaries. These three interpolation schemes were exact polynomial, least squares and orthogonal polynomial surfaces. Indications were that a least squares polynomial was most successful. Townson (1974) found that a first-order least square polynomial scheme was effective and efficient. The first-order least square polynomial scheme will also be used in this study.

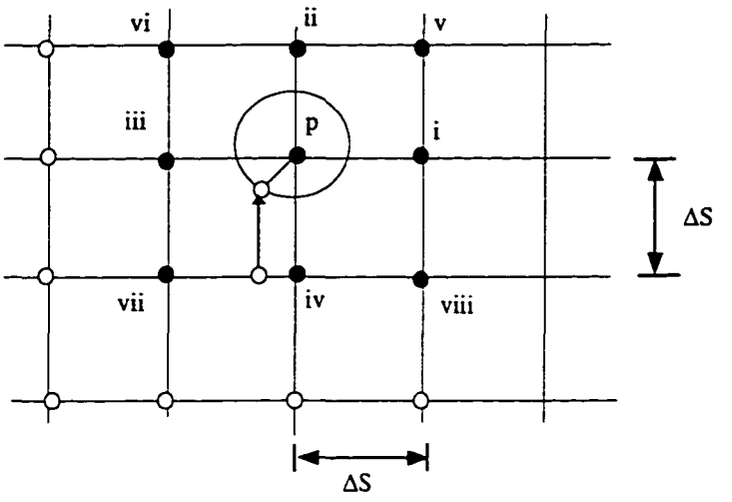

Figure 6.5 Interpolation Scheme

The first order polynomial is a plane $\psi=Ax+By+C$ and as such is compatible with the linear characteristics. Thus ψ becomes the solution surface for H, η, U_b and V_b in turn with x and y taking values from (6.18). The coefficients A, B and C are found by solving

the normal equations of the least squares methods over the five grid points p, i and through iv as sketched in Figure 6.5. With a square grid of size Δs, the coefficients A, B, and C are obtained (Townson 1974) as follows

$$A = \frac{1}{2}(\psi_i - \psi_{iii}) / \Delta s; \qquad B = \frac{1}{2}(\psi_{ii} - \psi_{iv}) / \Delta s$$
$$C = \frac{1}{5}(\psi_i + \psi_{ii} + \psi_{iii} + \psi_{iv} + \psi_p) \tag{6.19}$$

At boundary points, Townson (1974) found that the interpolation scheme is not appropriate since it tends to distort the boundary effect. Instead the use of surrounding four or three points gives more physically reasonable results.

6.3.4 Stability Criterion

Courant, Friedichs and Lewy (1928) established that the necessary condition for convergence of a difference scheme for general hyperbolic problems is that the domain of dependence of the difference scheme must contain the domain of dependence of its differential equation. The domain of dependence for a point is determined by the backward-in-time characteristic cone, as shown in Figure 6.6.

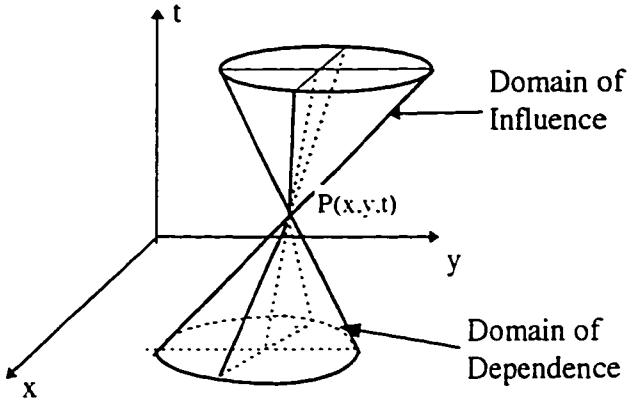

Figure 6. Domain of Influence and Dependence

In two spatial dimensions, the CFL stability condition is (Potters 1973)

$$\frac{C_{max}\Delta t}{\Delta x} < \frac{1}{\sqrt{2}} \tag{6.20}$$

where C_{max} is the maximum speed which could occur over the entire computational domain and throughout the entire simulation. This speed corresponds to the maximum eigenvalue. Equation(6.20) provides an estimate of a time step for a given spatial step.

6.4 Open Boundary Conditions

As in the interior domain, four constraints are needed for solving the four unknowns at a boundary. The bi-characteristics scheme developed in Section 6.3.2 is not applicable at the boundary because some bi-characteristics lie outside the computational domain. Extra boundary conditions must be specified to supplement to characteristic equations of outgoing characteristics. The following discussion is based on general wave incidence at an angle θ with the x-axis, as shown in Figure 6.7.

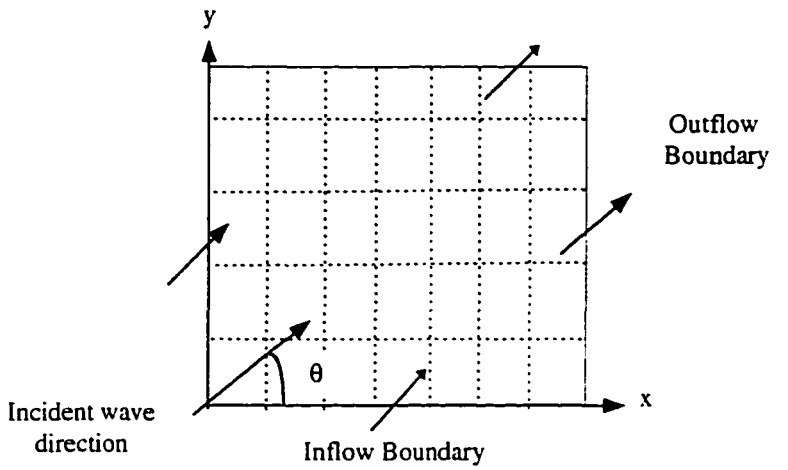

Figure 6.7 Sketch of Open Boundaries

By far there are no exact non-reflecting boundary conditions for a hyperbolic

nonlinear system in two spatial dimensions. In the study of the characteristics of the shallow water wave equations, it is found that the characteristics along a flow path in a two dimensional space behave exactly the same as in a one dimension space. Heuristically, the Hedstrom's open boundary conditions introduced in Section 5.3 may still be valid for two spatial dimensional problems as long as the open boundary conditions are applied in the flow direction.

The four eigen-values in the flow direction at a boundary point are ranked as

$$\lambda_1 < \lambda_2 < \lambda_3 < \lambda_4 \qquad (6.21)$$

If there are M incoming characteristics, then 4-M outgoing characteristic equations may be used to form the boundary conditions. M extra boundary conditions should be specified to supplement to the outgoing characteristic equations. The extra conditions may then use the Hedstrom's approximate boundary conditions in the flow direction (Section 5.3.1), i.e.

$$\tilde{\lambda}_j \bullet \frac{\partial W}{\partial t} = 0 \qquad j = 1..M \qquad (6.22)$$

It should be reminded that in a two dimensional space, information may propagate in or out of the domain at any angle. The open boundary conditions so specified in the flow direction do not guarantee non-reflection at the open boundary.

Also care must be exercised in choosing the characteristic equations to avoid redundancy. For example, if wave height is given at a boundary, then the energy characteristic equation should not be used.

6.5 Case Studies

In this section, three case studies are performed. These three cases are: evolution of an initial water mound over a flat bottom, the advance of normally incident waves over a flat bottom and the advance of obliquely incident waves over a flat bottom. In the first case, there is no incident short-period waves. In the second and third cases, the direction of wave propagation is known by physical intuition. The evaluation of wave direction is not required in either of the three cases. These case studies are designed to test the proposed numerical scheme and open boundary conditions.

Case I Evolution Of An Initial Water Mound

An initial conical water mound is located in the center of a square domain as shown in Figure 6.8. The computational domain is 200 m by 200 m with a uniform water depth of 10 m. The shape of the initial water mound is

$$\eta(x,y)=\begin{cases}1-\dfrac{r}{50}\,(m) & \text{for } r \le 50m \\ 0 & \text{for } r > 50m\end{cases} \tag{6.23}$$

where η is the displacement from mean water surface and r is the distance from the center

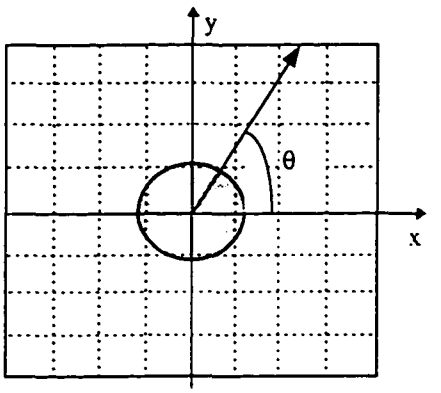

Figure 6.8 Sketch of the Computational Domain For Case I

of the domain (x=100, y=100). A uniform grid is used with Δx=10 m and Δy=10 m. For the given grid spacing, a time step may be estimated using Equation (6.20); The finally chosen time step is 0.5 second.

All four boundaries are outflow boundaries. Open boundary conditions are specified according to the characteristics in a flow direction at the boundary. The flow direction in this case is along the radial line from the center of the domain to a point in question, as shown in Figure 6.8. The three boundary conditions are comprised by one outgoing wave characteristic equation. the Hedstrom boundary condition along the incoming characteristics, and Equation (6.16) for lower and upper boundaries or Equation (6.17) for left or right boundaries. Flow characteristics or the corresponding characteristic equations are not adopted because the flow direction changes with time; the flow characteristics may be an inflow characteristics at one time, and becomes an outflow characteristics at other time.

The computed water surface profiles and velocity fields at six different time levels are shown in Figures 6.9 and 6.10. Figure 6.9 shows the water surface oscillating around the mean water surface while propagating out of the domain. The water surface profile actually consists of a spectrum of wave modes. Spectral analysis is necessary in order to compute wave propagation speeds.

There is no appreciable reflection at all open boundaries. Neither is spurious reflection suggested by the flow fields shown in Figure 6.10. At the simulation time of about 20 seconds, the water surface has returned to quiescence.

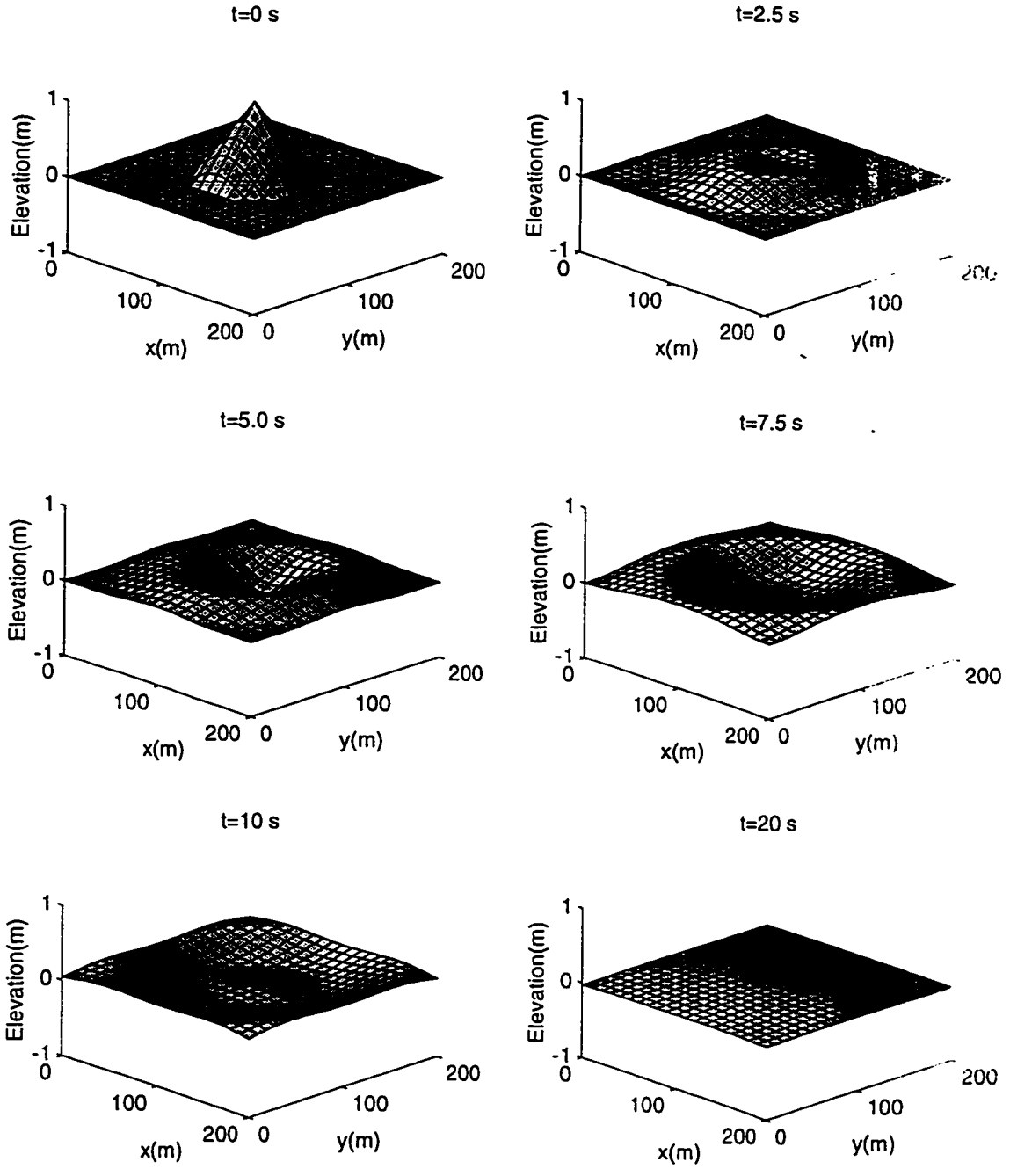

Figure 6.9 Evolution of Water Surface For Case I

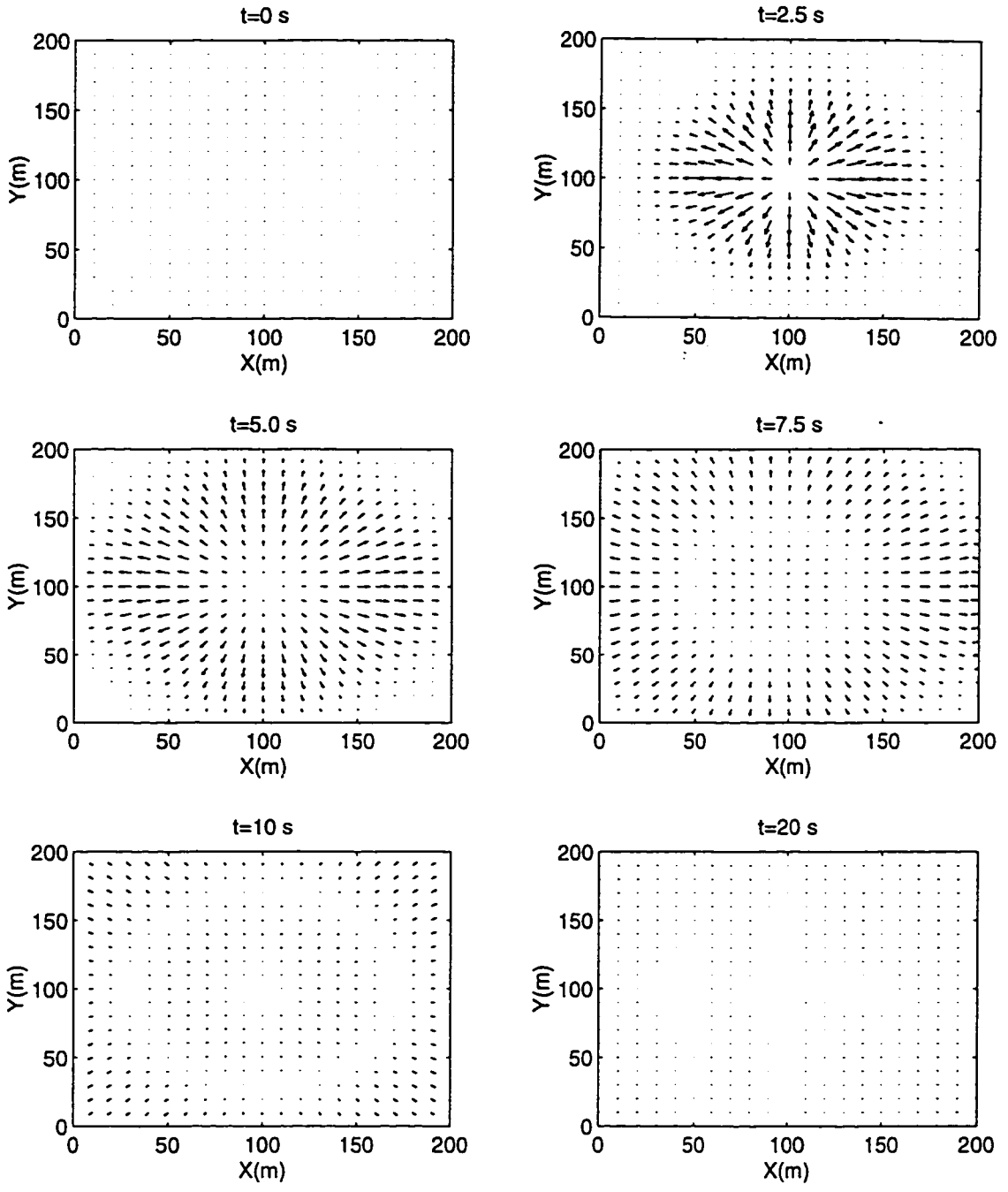

Figure 6.10 Evolution of Velocity Field for Case I

Case II Advance Of Normally Incident Waves

Waves are assumed to propagate into a square domain along the y axis, as shown in Figure 6.11. The computational domain has a uniform water depth of 10 m. The wave height and wave period are 1 m and 10 seconds, respectively. A uniform square grid with Δx=10 m and Δy=10 m is used. Corresponding to the grid spacing, a time step may be estimated using Equation (6.20) with the maximum eigenvalue which is the eigenvalue of

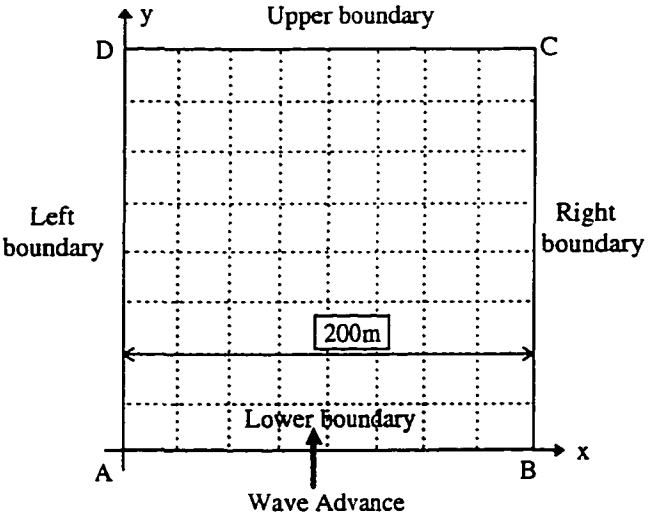

Figure 6.11 Sketch of Computational Domain For Case II

wave characteristics in the direction of wave propagation. After some numerical experiments, the finally adopted time step is 0.5 second with a Courant-Friedrichs-Lewy number equal to 0.7.

Initially, the computational domain is quiescent. The wave height is suddenly imposed at the lower boundary at the beginning of simulation and remains constant thereafter.

In this case, the lower boundary AB is an inflow boundary and the upper boundary CD is an outflow boundary. At the inflow boundary AB, at least one extra boundary

condition is required since there is only one outgoing characteristics for subcritical flow. Wave height is given at this boundary, so that only three boundary conditions are needed. The three boundary conditions are: outgoing wave characteristic equation in the direction $\theta=\pi/2$, Equation (6.22) along the incoming wave characteristics in the same direction, and $U_b=0$ which is obvious from physical intuition.

At the outflow boundary CD, four constraints must be specified. For subcritical flow, there are at least one incoming characteristics, and extra boundary conditions have to be specified. The characteristics from the incident wave conditions show that there are at least two outgoing characteristics, including one wave characteristics and one energy characteristics. Thus the characteristic equations of the outgoing wave characteristics and energy characteristics must be used. $U_b=0$ is Also used for the same reason given above. The fourth constraint is the Hedstrom approximate boundary condition (Equation 6.22) along the incoming wave characteristics.

At the left and right boundaries, the four boundary conditions are: the compatibility equation of energy characteristics in the direction of wave propagation(i.e. $\theta=\pi/2$), $U_b=0$, Equation(6.17) and Equation (6.22) along the incoming wave characteristics in direction $\theta=0$ for the left boundary or in the direction $\theta=\pi$ for the right boundary.

The computed wave height surface, wave setup and mean flow under the trough at six time levels are shown in Figures (6.12) through (6.14). The general behavior is similar to that expected in one spatial dimension. Again, the solutions at all boundaries show no signs of spurious reflection. The proposed open boundary conditions and numerical scheme have been shown to be appropriate.

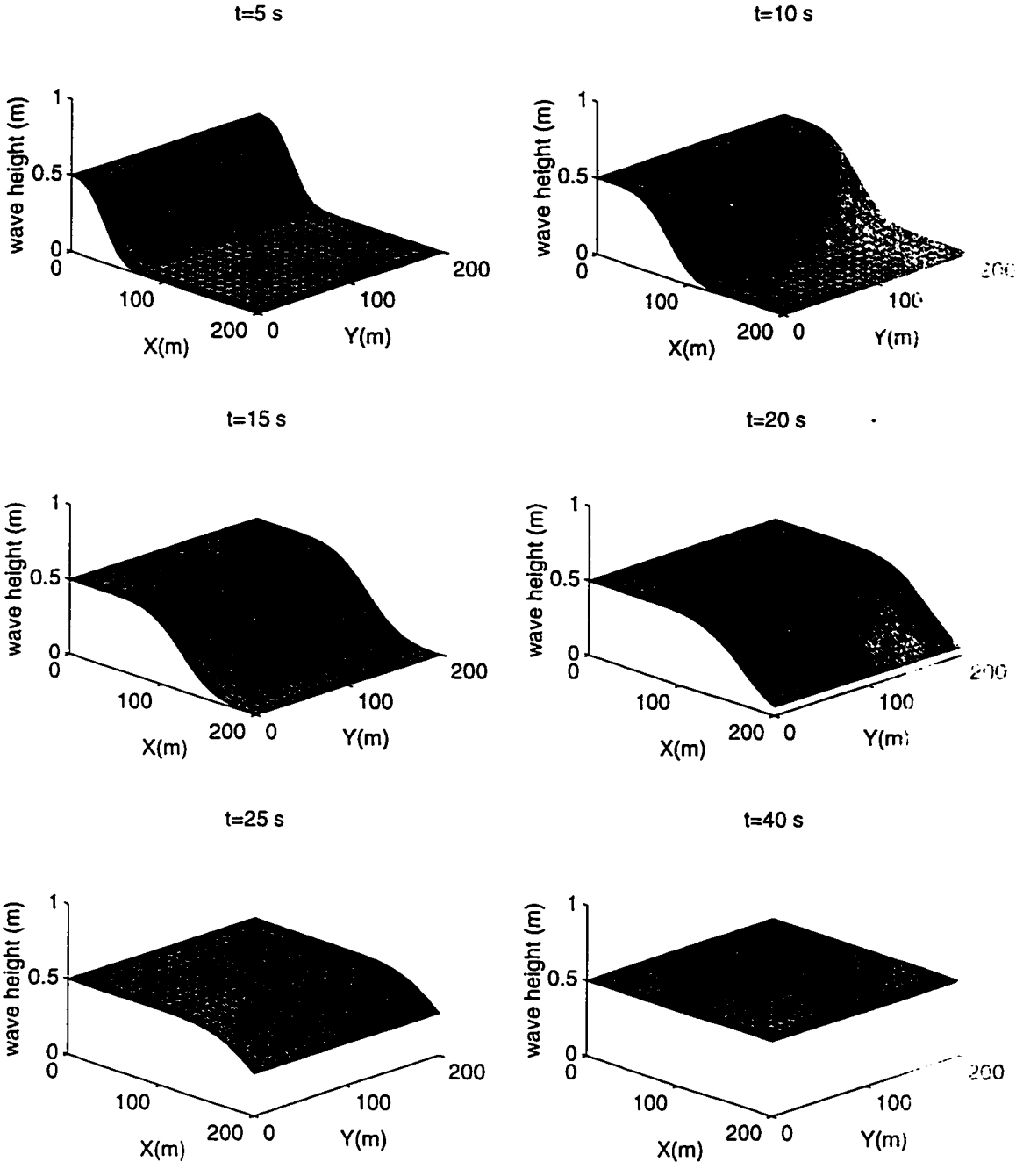

Figure 6.12 Evolution Of Wave Height Profile For Case II

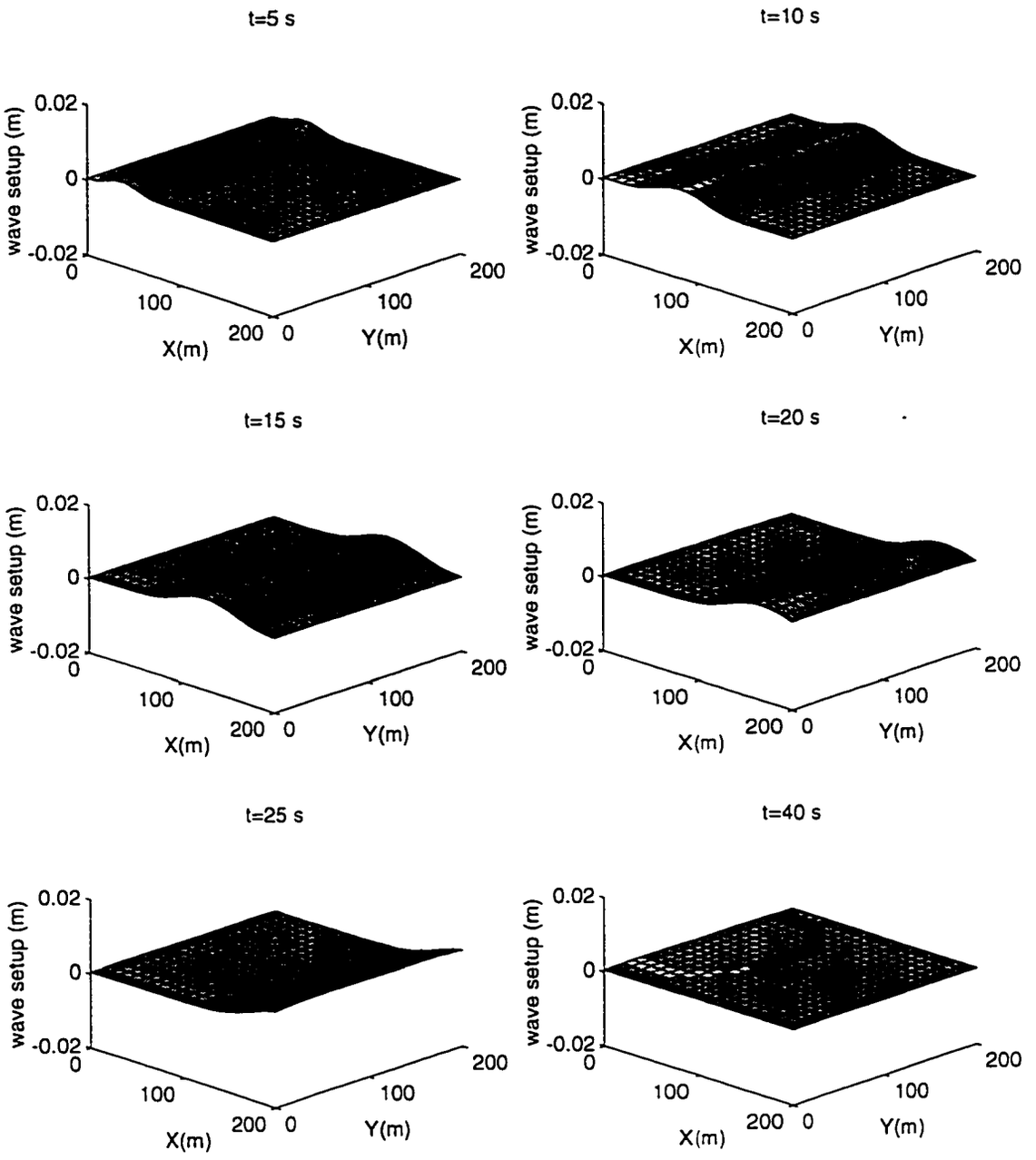

Figure 6.13 Evolution Of Mean Water Surface For Case II

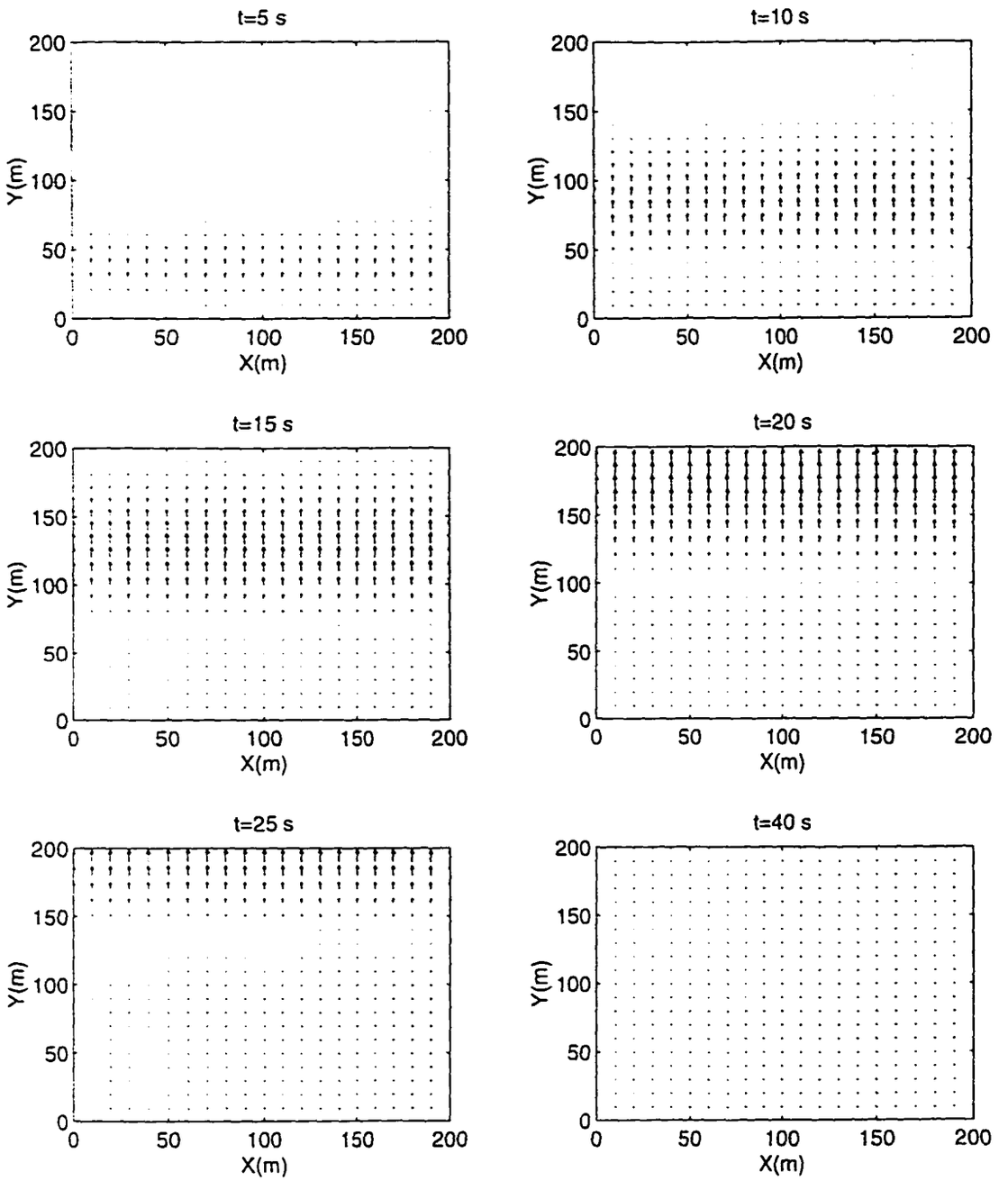

Figure 6.14 Evolution Of Mean Flow Velocity For Case II

Case III Propagation of Obliquely Incident Waves

To test the performance of the numerical scheme and open boundary conditions for oblique wave propagation, waves are assumed to advance into a square domain from the left lower corner at an angle of 45° with the x-axis, as shown in Figure 6.15. The computational domain has a uniform water depth of 10m. The incident waves have a period of 12 seconds and a height of 0.5 m. A uniform grid with $\Delta x=\Delta y=10$m is used, coupling a time step of 0.5 second.

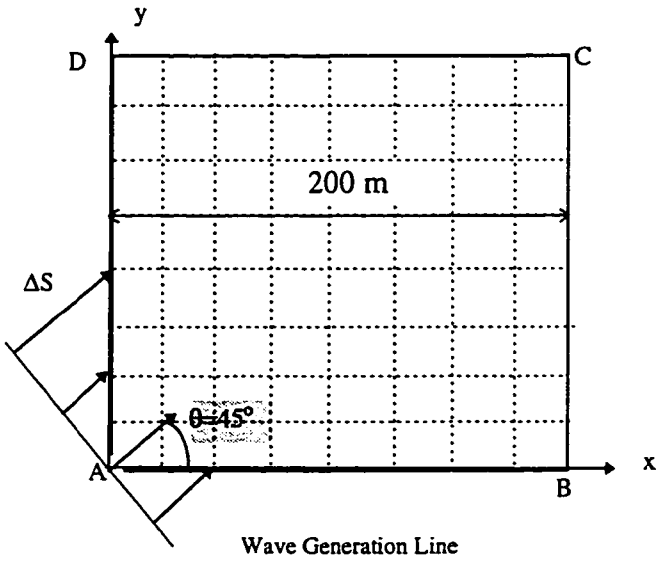

Figure 6-15 Sketch of Computational Domain for Case III

Of the four boundaries, AB and DA are inflow boundaries where the wave height is given, and BC and CD are outflow boundaries where all four boundary conditions need to be specified. The boundary conditions for the inflow and outflow boundaries require locally specific consideration.

To impose wave height at the inflow boundaries AB and DA, draw a wave crest line through A, as shown in Figure 6.15. This line represents a wave crest at the instant waves reach point A. Since the distance from the boundary to the wave generation line

varies with the grid point, the wave height varies with the grid points along a boundary. In this case, the wave forcing is gradually imposed at the boundaries according to the following function

$$H_b(t) = H_i \exp\left[-\left(\frac{\Delta s}{\lambda_w t}\right)^5\right] \tag{6.24}$$

where $H_b(t)$ is the wave height at a boundary point at time t, H_i is the incident wave height at the line of wave generation, Δs is the distance from the boundary point to the wave crest line, and λ_w is the eigenvalue of energy characteristics which physically represents the speed of wave energy transfer. The exponential function smoothes the transition from the boundary to the interior domain because the solutions in the interior domain always include numerical diffusion.

Since wave height is given at the inflow boundaries, only three boundary conditions are required. Physically, the velocity vector should be in the direction of wave incidence, i.e., $U_b=V_b$. The outgoing wave characteristic equation in the direction $\theta=\pi/4$ serves as a boundary condition. The third boundary condition is zero gradient of wave setup along the wave crestline, in the direction $\theta=3\pi/4$. For the uniform square grid with an incident wave angle of $\pi/4$, this boundary condition is expressed as

$$\begin{aligned} \overline{\eta}_{i,1} &= \overline{\eta}_{i-1,2} \quad \text{at the lower boubdary} \\ \overline{\eta}_{1,j} &= \overline{\eta}_{2,j-1} \quad \text{at the left boubdary} \end{aligned} \tag{6.25}$$

The flow characteristics is not used in the formation of boundary conditions because the flow velocity is very small and flow direction changes with time.

At the outflow boundaries BC and CD, the constraint $U_b=V_b$ remains valid. Three additional boundary conditions are comprised by the outgoing wave characteristic

equations and the energy characteristic equation both in the direction of wave incidence, i.e., $\theta=\pi/4$, and the Hedstrom approximate boundary condition (Equation 6.22) along the incoming wave characteristics in the same direction.

The computed wave height surface, mean water surface and mean flow below the trough at six time levels are shown in Figure (6.16) through (6.18), respectively. At time 50 seconds (the last figure), waves have passed through the computational domain, so that wave height is uniform over the entire domain, the mean water surface returns to undisturbed position and the mean flow current is trivial, as expected. The solutions at the inflow and outflow boundaries are smooth at all six time levels, demonstrating again that the imposed boundary conditions do not cause any appreciable numerical reflection at the boundaries.

To further illustrate the wave propagation, the wave height profiles along the diagonal line AC at 8 different time levels are plotted in Figure (6.19a). To estimate the propagation speed, a straight-line is drawn through wave height 0.25 m. The propagation speed is estimated by dividing the distance by the time interval. The estimated speed of energy transfer is 8.25 m/s. The wave group speed estimated from Fourier approximation wave theory is 8.34 m/s, which about 1% greater than the numerical speed of wave energy transfer. Shown in Figure (6.19b) are the wave height profiles along the right open boundary BC at 8 different time levels. Prior to t=15 sec., waves have not yet reached the boundary, so they not labeled. At t=45 sec., the wave field has almost reached the steady state.

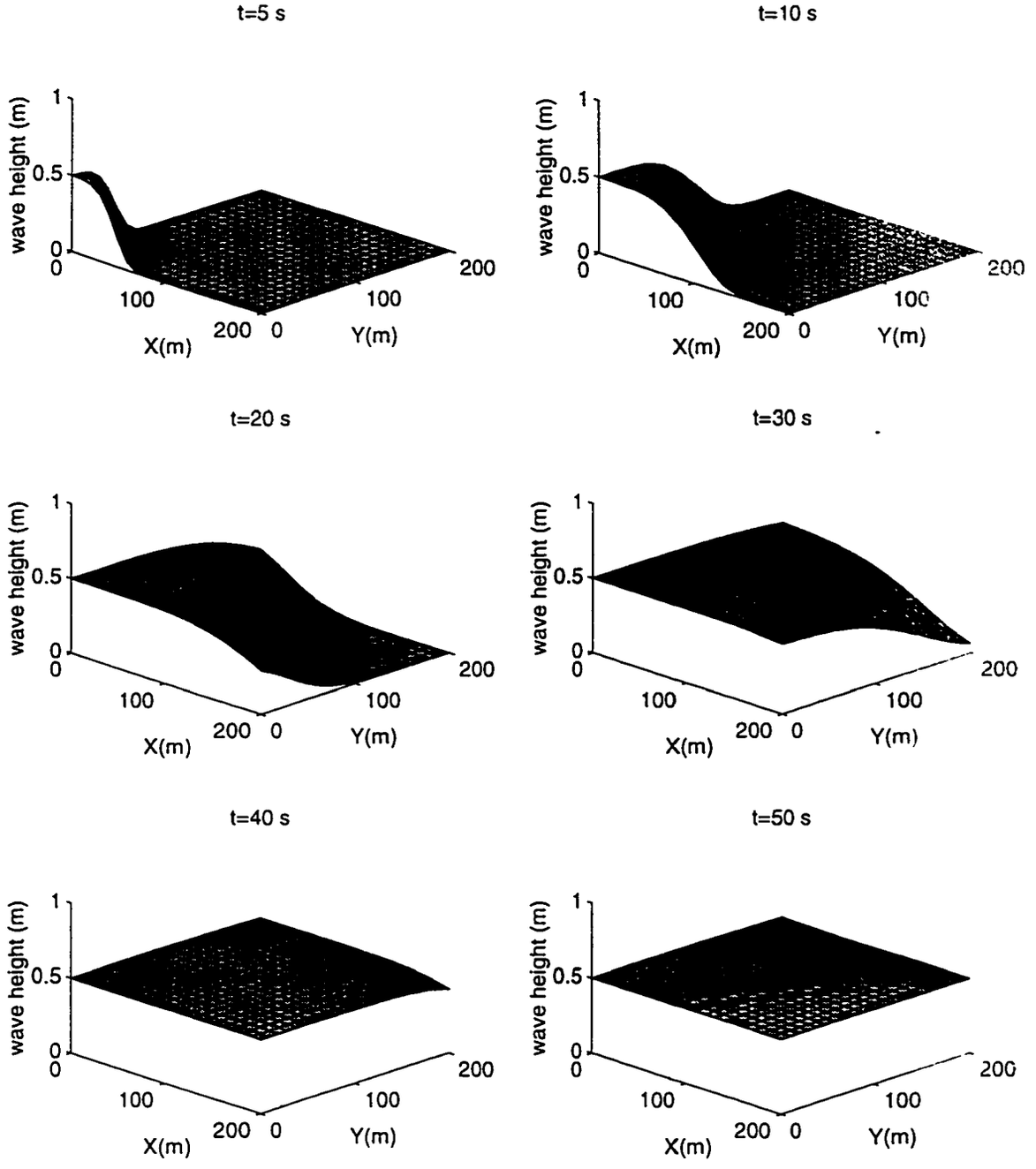

Figure 6.16 Evolution of Wave Height Profile for Case III

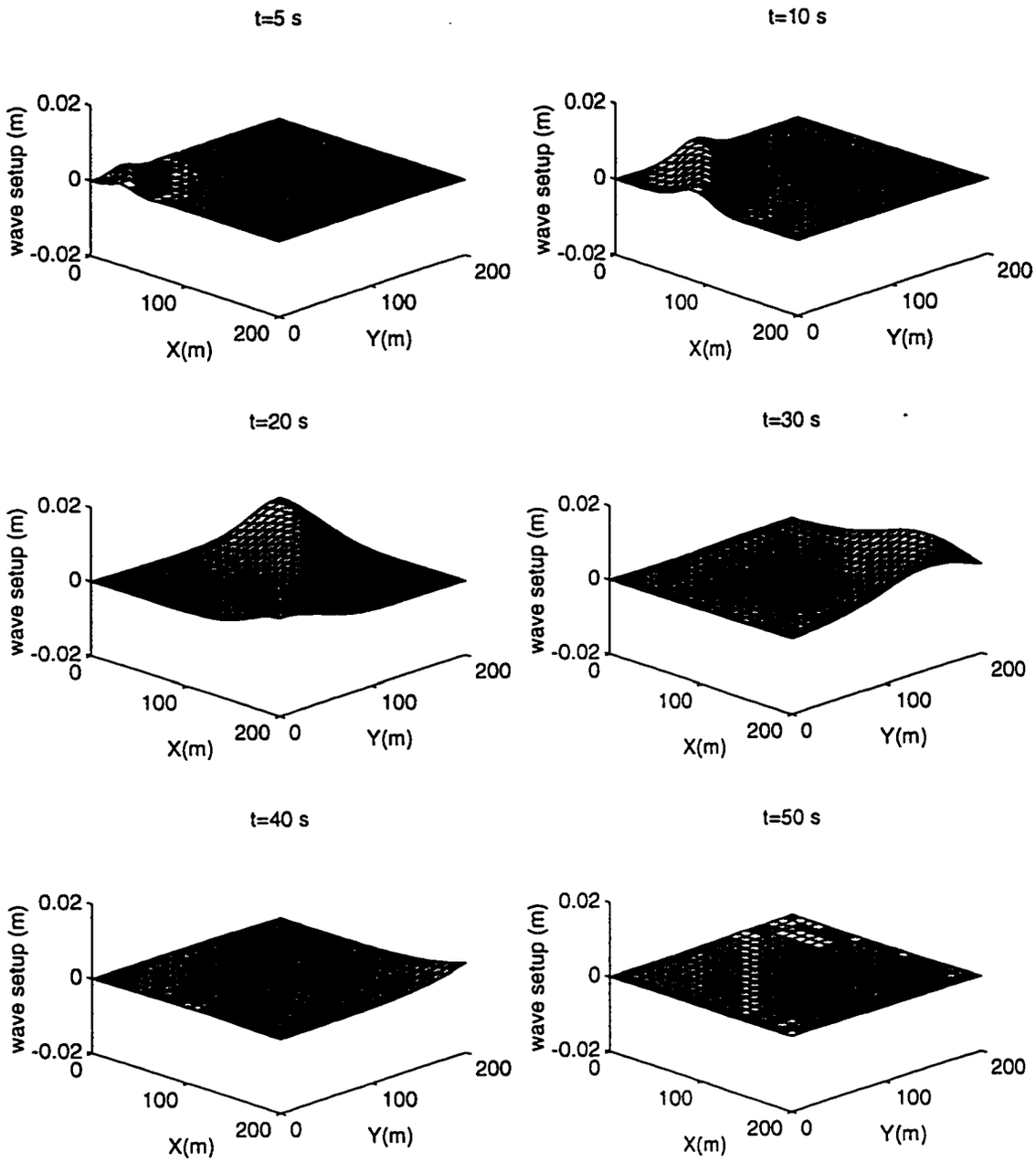

Figure 6.17 Evolution of Mean Water Surface for Case III

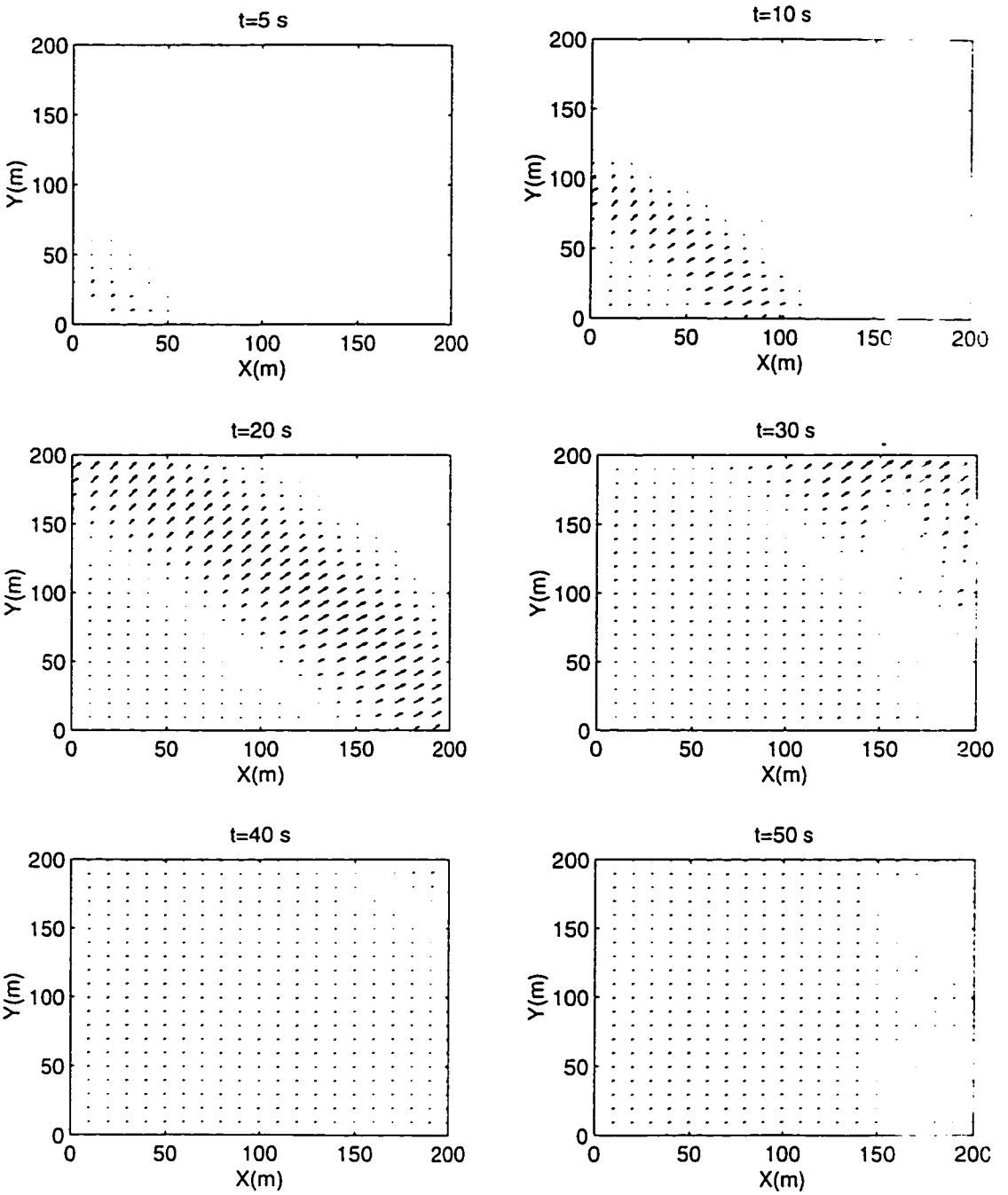

Figure 6.18 Evolution of Mean Flow Velocity for Case III

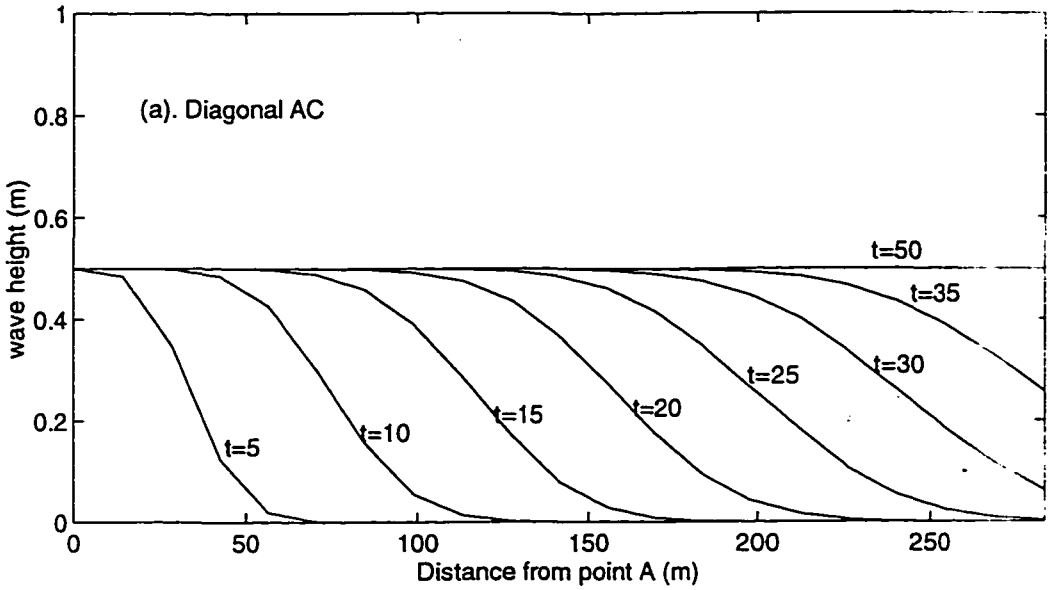

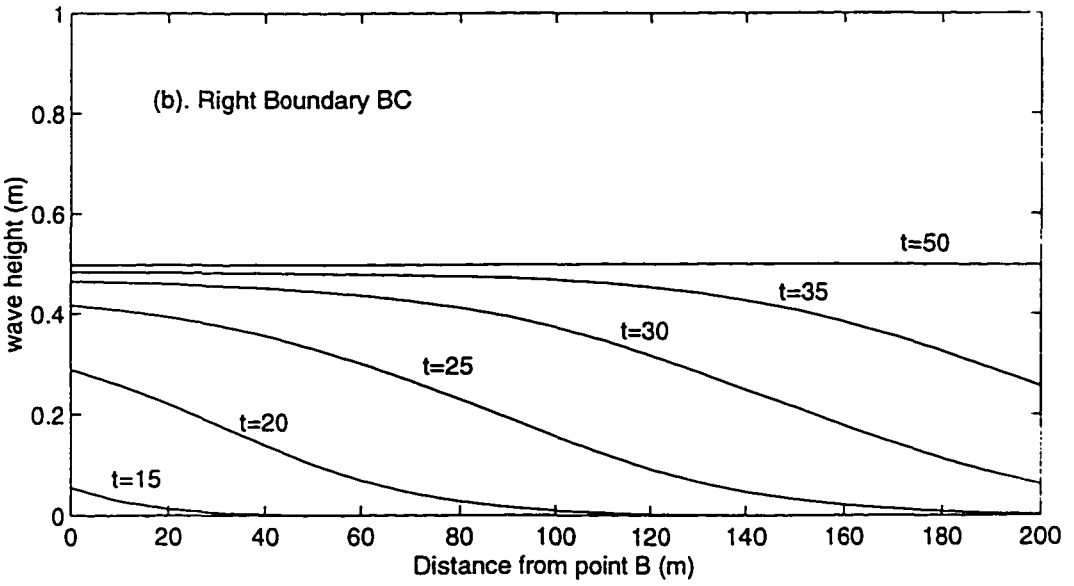

Figure 6.19 Wave Height Profiles Along Diagonal Line and Right Boundary

6.6 Wave Direction

In two spatial dimensions, the direction of wave propagation changes in response to variations in water depth and in the flow field. The local wave field can be characterized by wave height and wave direction. Under the assumption that the kinematics in the surface layer is dominated by wave motion, the velocity vector in the surface layer (from wave trough to crest) is in the same direction of the wave propagation. The mean velocity vector in the bottom layer (from sea bed to the trough) is generally not in the wave propagation direction, as corroborated by wave-generated longshore currents. In this section, two approaches to the modeling of wave direction will be introduced.

(a) Mild Slope Model

If the current is weak, wave direction can be estimated from the coupled eikonal and transport equations that are equivalent to the mild-slope equation (Massel 1989).

$$(\nabla_h S)^2 = k^2 + \frac{1}{CC_g a}\nabla_h(CC_g \nabla a) \tag{6.26}$$

$$\nabla_h(CC_g a^2 \nabla_h S) = 0 \tag{6.27}$$

where S is the phase function, k is the wave number, C is the wave phase speed, C_g is the group speed, a is the wave amplitude, and ∇_h is a horizontal gradient operator. The term with the spatial gradient of wave amplitude describes wave diffraction. $\nabla_h S$ defines the local wave direction.

Without diffraction, Equation (6.26) reduces to refraction approximation

$$\nabla \times \bar{k} = 0 \tag{6-28}$$

Equations (6.26) and (6.27) may be used to solve the two components of $\nabla_h S$. Since the present model uses wave height instead of wave amplitude, for convenience, the wave amplitude is replaced by wave height. The phase speed C and group speed C_g may be estimated from Fourier approximation wave theory, like all other closure variables.

(b) Vertical Mass Flux Model

Since the velocity vector in the surface layer is assumed to be in the same direction of wave propagation, this approach centers on solving the velocity components in the surface layer. The continuity equation in the surface layer is

$$\frac{\partial(HU_s)}{\partial x}+\frac{\partial(HV_s)}{\partial y}=q_t \tag{6.29}$$

where q_t is the vertical mass flux per unit area across the trough. The angle between the wave propagation direction with the x-axis, θ, can be obtained

$$\theta = a\tan^{-1}(\frac{V_s}{U_s}) \tag{6.30}$$

Equation (6.29) includes three unknowns in U_s, V_s and q_t. Besides Equation (6.29), two more constraints must be specified to solve the three unknowns. The resultant velocity in the surface layer may be obtained using the solution surface. If the mass flux across the trough can be estimated, then the system is closed.

To find out what factors q_t depends on, the mass transport in the surface layer in one spatial dimension is studied first. In one spatial dimension, Equation (6.29) can be approximated by

$$\frac{\partial I}{\partial x}=\frac{\partial}{\partial x}(\frac{E}{C})=q_t \tag{6.31}$$

where I is the wave-averaged mass transport, E is the wave energy, and C is the wave phase speed. Substituting $E=\frac{1}{8}\rho g H^2$ into Equation (6.31) gives

$$q_t = \frac{\rho g}{8C}\frac{\partial H^2}{\partial x} - \frac{\rho g H^2}{8C^2}\frac{\partial C}{\partial x} \tag{6.32}$$

where H is the wave height, ρ the water density and g the gravitational acceleration. In deep water, $C=\frac{g}{2\pi}T$, then Equation (6.32) becomes

$$\frac{q_t}{\rho} = \frac{g}{8C}\frac{\partial H^2}{\partial x} = \frac{\omega}{8}\frac{\partial H^2}{\partial x} \tag{6.33}$$

where ω is the wave angular frequency. In shallow water, $C=\sqrt{gh}$ and Equation (6.32) becomes

$$\frac{q_t}{\rho} = \frac{1}{8}\sqrt{\frac{g}{h}}\left(\frac{\partial H^2}{\partial x} - \frac{H^2}{h}\frac{\partial h}{\partial x}\right) = \frac{\sqrt{g}}{8h^{3/2}}\left(h\cdot\frac{\partial H^2}{\partial x} - H^2\frac{\partial h}{\partial x}\right) \tag{6.34}$$

For broken waves, the water depth may be related to wave height by h=H/γ, where γ is a breaking index. Equation (6.34) thus becomes

$$\frac{q_t}{\rho} = \frac{\sqrt{g\gamma/H}}{16}\frac{\partial H^2}{\partial x} \tag{6.35}$$

Equation (6.32) can be generalized in form

$$q_t = \beta\cdot\frac{\partial H^2}{\partial x} \tag{6.36}$$

where β is a constant with the dimension of time. As indicated in Equations (6.33) through (6.35), β depends on water depth and wave characteristics. Dimensional analysis gives that β= αω, where ω is wave angular frequency, and α is a dimensionless constant.

The coefficient α can be calibrated using the numerical results for steady state wave

propagation at Egmond Beach (Thieke and Sobey 1990). A plot of the mass flux versus the gradient of squared wave height is shown in the following Figure.

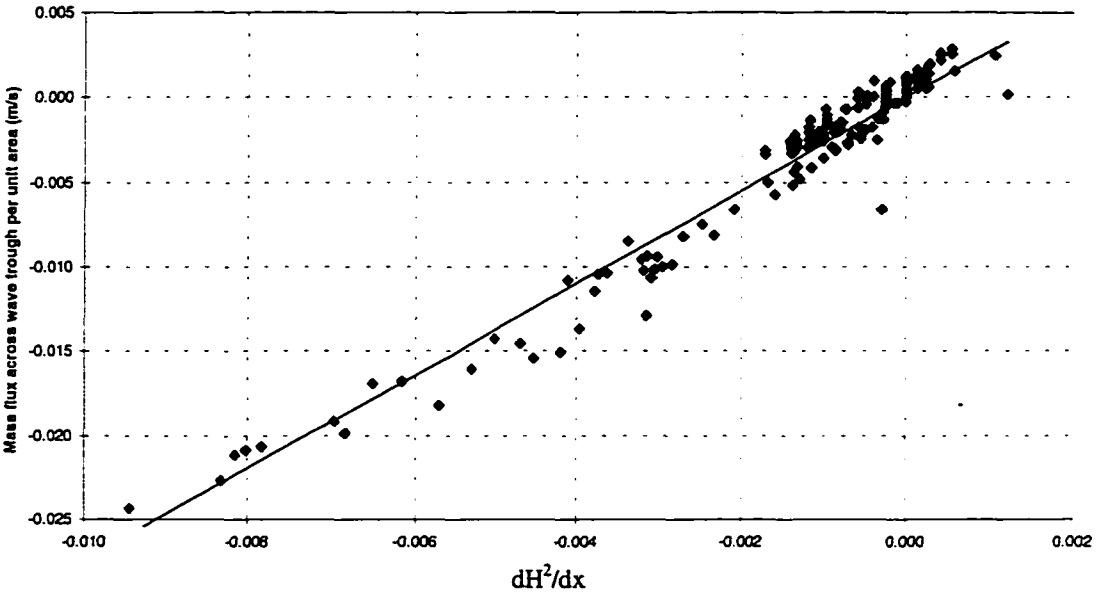

Figure 6.20. The relationship between mass transfer across wave trough and energy gradient in the direction of wave propagation

From this figure, α is approximately equal to 2.08. A difference form of Equation (6.29) is written as

$$\frac{(HU_s)_{i,j} - (HU_s)_{i-1,j}}{\Delta x} + \frac{(HV_s)_{i,j} - (HV_s)_{i,j-1}}{\Delta y} = \bar{q}_t \tag{6.37}$$

where $\bar{q}_t$ is evaluated from the mean value of the wave heights at the four grid points and the gradient of wave height in the wave propagation direction, i.e.

$$\bar{q}_t = \alpha\omega \frac{H_{i,j} + H_{i-1,j} + H_{i,j-1} + H_{i-1,j-1}}{4} \frac{\partial H}{\partial S} \tag{6.38}$$

The directional derivative in the direction of wave propagation is

$$\frac{\partial H}{\partial S} = \cos\theta \frac{\partial H}{\partial X} + \sin\theta \frac{\partial H}{\partial y} \tag{6.39}$$

The derivative of wave height in the x and y directions can be estimated by using the backward difference with the wave height at the previous time step.

6.7 Wave Focusing By A Submerged Shoal

In this section, the model is applied to simulate wave focusing by a submerged shoal under the experimental conditions of Berkhoff et al. (1982). In the model test, normally incident waves are generated at a period of 1 second and with an amplitude of 0.0232 m by a wave paddle at the deep end of the wave tank, and are dissipated by breaking on a gravel beach at the shallow end. Thus wave reflection is not included in the wave transformation process. The experimental topography has an elliptic shoal resting on a plane sloping bottom with a slope of 1:50, as shown in Figure 6.21. The plane slope rises from a region of constant 0.45 m depth, and the entire slope is turned at an angle of 20° to the paddle. The slope is described by

$$h = \begin{cases} 0.45 \quad \text{m} & y' < -5.82\text{m} \\ 0.45 - 0.02(5.82 + y') \quad \text{m} & y' \geq -5.82\text{m} \end{cases} \tag{6.40}$$

where (x',y') is a coordinate system with x' axis parallel the contour, as sketched in Figure 6.22. The boundary of the elliptic shoal is defined by

$$\left(\frac{x'}{4}\right)^2 + \left(\frac{y'}{3}\right)^2 = 1 \tag{6.41}$$

and the depth in the shoal region is modified according to

$$h = h_{slope} - 0.5 \cdot [1 - \left(\frac{x'}{5}\right)^2 - \left(\frac{y'}{3.75}\right)^2]^{1/2} + 0.3 \tag{6.42}$$

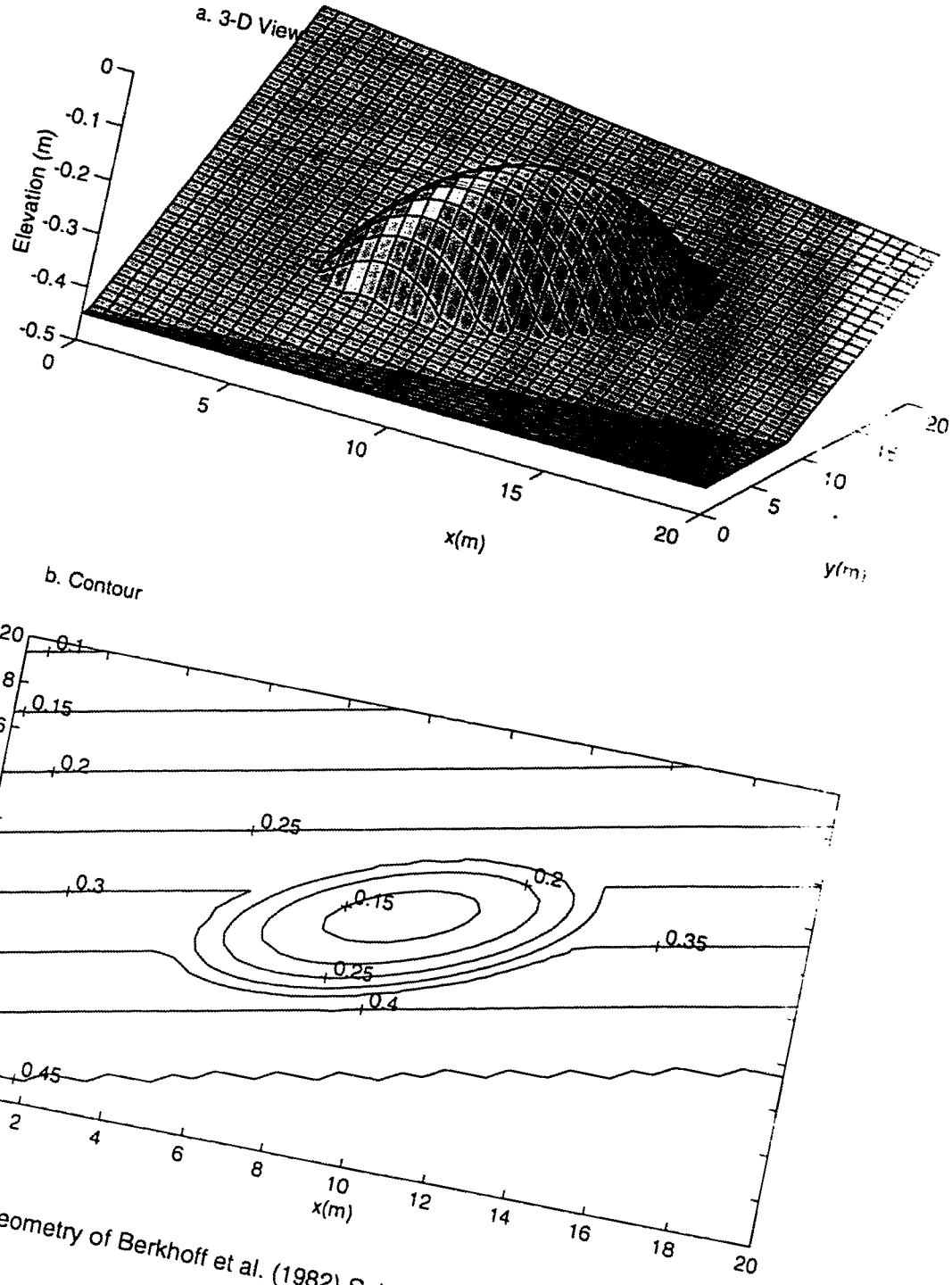

Figure 6.21 Geometry of Berkhoff et al. (1982) Submerged Shoal Experiment

where h_{slope} is the water depth given by Equation (6.40). The resultant depth at the center of the elliptical shoal is 0.1332 m.

Measurements were taken at 8 transects behind the shoal (Berkhoff et al. 1982). Arrays of resistance type wave gages, spaced 0.5 m apart, recorded time series of water surface elevations.

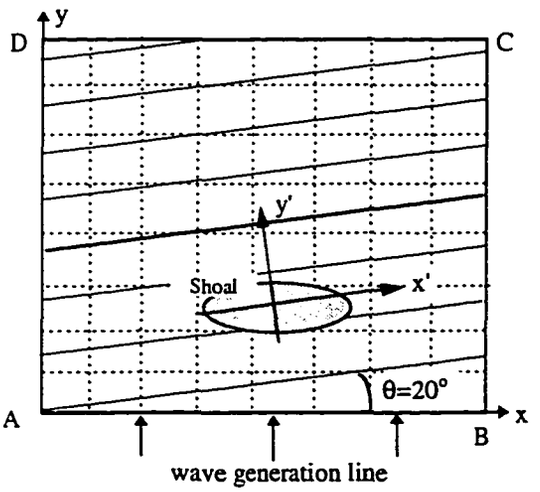

Figure 6.22 Computation Domain

The computational domain is a 20m×20m square domain, as shown in Figure 6.21. The offshore boundary of the computational domain is so chosen that water depth is constant along x=0. A uniform square grid with $\Delta x=\Delta y$ =0.5 m is used. The time step of 0.05s is determined from numerical experiments. The grid lines are so arranged that the grid rows and columns coincide with measurement transects. The interior of the domain is simulated by the numerical algorithm developed in Section 6.3. The wave direction is modeled using Equation (6.28) since in this refraction dominates in the wave transformation process.

Of the four boundaries, AB is an inflow boundary where the wave heights are given, CD is an outflow boundary, and BC and DA are lateral open boundaries. At the inflow

boundary AB, a constant wave height H=0.0464 m is imposed at each boundary point. Three additional constraints are the outgoing wave characteristic equation in the direction $\theta=\pi/2$, Equation (6.16) which is derived by combining the wave characteristic equations in the directions $\theta=0$ and $\theta=\pi$, and the Hedstrom approximate boundary condition of incoming wave characteristics in the direction $\theta=\pi/2$.

At the outgoing boundary CD, four boundary conditions have to be specified. The four boundary conditions are the outgoing wave characteristic equation, energy characteristic equation in the direction of the local wave number vector, Equation (6.16) and the Hedstrom extra condition along the incoming wave characteristics in the local wave propagation direction.

At the lateral boundaries BC and DA, four boundary conditions are specified in the same manner as for the outflow boundary, except that Equation (6.17) is used instead of Equation (6.16).

The computed wave height surfaces at six times are shown in Figure (6.23). From these figures, waves focusing is very obvious waves pass over the shoal. Wave field approaches steady state in about 40 seconds since the entrance at Boundary AB. Detailed comparison between numerical results and experimental data will be incorporated in the future study.

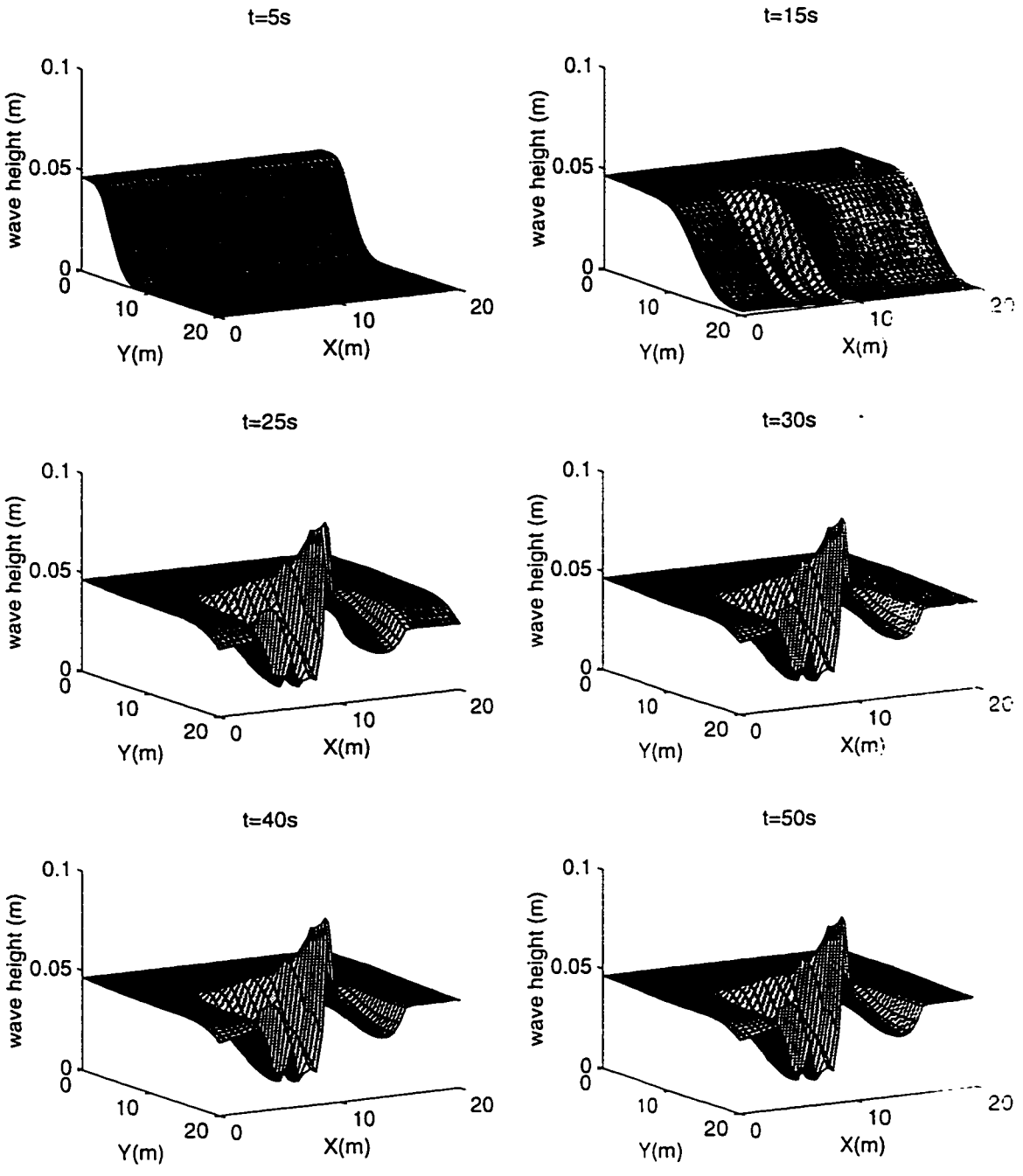

Figure 6.23 Wave Height Surfaces

7 MODELING WAVE REFLECTION AND SEDIMENT TRANSPORT

In this chapter, discussions center on the conceptual aspects of the use of phase-averaged models for simulating wave reflection and sediment transport.

7.1 Modeling of Wave Reflection

Wave reflection is an important wave transformation process in coastal regions. It may occur when the wave propagation is hindered by structures such as breakwaters or simply by steep beach.

As outlined in Chapter 4, the use of progressive wave theory in the apparent stress closure specifically excludes wave reflection. To consider wave reflection, a reflection coefficient (the ratio of incident wave energy to reflected wave energy) should be used. Unfortunately, the reflection coefficient is unknown in most situations. The closure of wave apparent stresses becomes more complicated because the apparent stresses depend on the reflection coefficient. Given a reflection coefficient, a set of solution surfaces similar to those in Chapter 4 may be established using partial standing wave theory, i.e. such as the fourth order theory of Goda (1967). In this case, the solution surfaces would be defined by three parameters: dimensionless water depth, normalized wave height, and reflection coefficient. Since the reflection coefficient itself is unknown, an iteration procedure will be inevitably employed.

Nonlinearity significantly complicates the definition of the reflection coefficient because the wave motion includes not only progressive wave modes and reflective modes, also a third component-interactive mode (or wave-wave interaction) between the progressive waves and reflected waves.

An alternative approach is to compute wave field separately. Wave field (wave height and direction) may be computed from the linear mild-slope equations (Berkhoff 1972, Dingemans 1985) or from the nonlinear Boussinesq equations (Peregrine 1967). Once the wave field is known, the mean-flow mass and momentum equations may be solved for wave setup and mean flow currents under the trough. The trade-off in this approach is that the wave-current interaction is absent in each computation cycle. This can be partially remedied by an iteration procedure.

Any one of these approaches would demand much more computing effort than does the case without wave reflection, the iteration procedure significantly compromising the advantage of phase-averaged models. Application of phase-averaged models must be based on a particular problem at hand.

7.2 Sediment Transport Modeling

Sediment transport process may be divided into three stages (Van der Velden 1989): suspension, horizontal displacement and re-sedimentation. Each stage depends on water movement and sediment characteristics. Waves predominantly loosen material on the bottom and stir it up, while currents mainly transport material to another place. The amount of sediment transport is largely determined by waves, while the transport velocity depends on current. The wave-driven currents typically exist as undertow currents for shore-normal wave propagation, rip currents resulting from edge waves. and longshore currents owing to the spatial gradients of wave apparent stresses.

The combination of waves and currents can intensify sediment transport (van der Velden 1989). For currents only, the average transport velocity is high but the amount of

sediment is low. For waves only, the resulting transport velocity is small but the amount of the suspended sediment is large.

Nonlinearity plays a significant role in coastal sediment transport. If waves are symmetrical, there will hardly be any net transport, the sediment being moved backwards and forwards over the same distance. Wave profiles in shallow water are peaked around the wave crest and flat near the wave trough. Since the shear stress is proportional to the square of the velocity, a peaked crest and flat trough may determine the direction of the wave-averaged shear stresses. Hence the direction of cross-shore sediment transport critically depends on wave nonlinearity (Thieke 1988). Sediment could be transported in a direction opposite to the wave propagation. Clearly, use of nonlinear wave theory is preferable in sediment transport modeling.

Phase-averaged models may find many applications in simulating coastal processes because the mean flow parameters are essential to net sediment transport, which in turn is responsible for seasonal or long-term coastal evolution. It should be fully recognized, however, that the initiation of sediment motion from the sea bed is mainly due to the wave motion which is generally much greater than the mean flow current in magnitude. Other factors including sediment characteristics and bottom boundary layer are also very important to sediment suspension or the amount of sediment available for transport. The prediction of sediment transport can be divided into two parts: bed load and suspended load. The bed load is the transport of sediment which rolls or jumps along the bottom within a thin layer above the bottom. In contrast, suspended transport is only affected by the friction of the grains themselves in water. The difference between the bed load transport and the suspended sediment transport is often not clear. The computation of

sediment transport by far remains largely empirical.

Bijker (1971) developed a bedload transport formula for current and wave combined by modifying the transport formula for currents and for waves. The key issue is the time-averaged bottom shear stress. In integral models, the magnitude of the particle orbital velocity near the bed due to wave motion may be evaluated using the closure procedure described in Chapter 4.

Bed load is confined to a thin layer. The thickness of the layer should be in the same order of the boundary layer thickness. Nielsen (1985) suggested that the boundary layer thickness in a wave-dominated environment be of order

$$\delta = \frac{1}{2} f_{\omega} a_0 \tag{7.1}$$

where f_ω is a friction factor and a_o is the maximum water particle displacement at the bottom. For typical wind waves, the boundary thickness is thin in comparison with water depth.

The suspended sediment transport can be computed by integrating the product of sediment concentration and mean flow velocity from the top of the bed load layer to the water surface. To carry out the integration, the vertical distribution of both velocity and the concentration must be known.

The vertical distribution of the sediment concentration depends on diffusion coefficient and sediment characteristics. Normally, the sediment concentration is not uniform over the water depth due to gravity and the variation of the diffusion coefficient. the distribution of sediment concentration may be formulated by (van der Velden 1989)

$$c(z) = C_a \exp(-w\int_a^z \frac{dz}{\varepsilon_s(z)} \tag{7.2}$$

where C_a is a reference concentration at level z=a, w is the fall velocity of the sediment and ε_z the diffusion coefficient. The reference level is at the top of the bed-load layer and the reference concentration is normally estimated by dividing the bed load transport by the thickness of the bed load layer.

In the present integral model, it is reasonable to assume that the suspended sediment transport takes place only in the bottom layer (from the sea bed to wave trough) because the sediment concentration near the water surface is normally much less than that in the bottom layer. Since the present model assumes a uniform flow velocity in the bottom layer, the integration process is reduced to the integration of the sediment concentration alone.

In summary, sediment transport modeling can be integrated with present mean flow model.

8. CONCLUSIONS

In this study, a wave-averaged depth-integrated wave transformation model was developed. This model represents the major physical phenomena in the coastal wave evolution, including wave shoaling, refraction, diffraction, wave-current interaction and surf beat. General approaches for using phase-averaged models in the simulation of wave reflection and sediment transport have also been discussed. Though these discussions were conceptual, they showed promise in applying the integral model in coastal engineering practice.

With the focus on mean wave parameters, wave height, wave setup and wave-driven currents, the wave apparent stresses were closed using relationships from high-order Fourier approximation wave theory. Numerical solutions adopted the method of characteristics. The information propagation in the system was fully revealed by the characteristics of the system, which were especially beneficial in the construction of open boundary conditions. The importance of appropriate open boundary conditions can not be over emphasized because spurious numerical reflection at the boundary will significantly distort the transient behavior of system. Case studies both in one spatial dimension and two spatial dimensions demonstrated the excellent performances of the numerical schemes and the open boundary conditions. Nearly non-reflecting conditions were achieved in every case.

It was clearly shown in this study that transient dynamics may be important for coastal evolution. The wave-driven current and mean water surface variation are significantly greater than the respective steady state values. Since the wave conditions in deep water are rarely invariant, the simulation of transient behavior is a significant feature

of this model.

In principle, the mean flow integral model developed here is valid throughout the entire coastal area, including the surf zone. The wave transformation and mean flow problem addressed here is very complex. and many complicating effects have been ignored to make the problem tractable. The main simplification is the use of a specific wave theory for wave-apparent-stress closure. Specifically, the use of the Fourier approximation wave theory in the present model excludes wave reflection. However, the computational framework of the integral model is independent of the closure hypotheses, and the present closure can be readily updated or replaced. The assumption of a horizontal bottom in the Fourier approximation wave theory may also influence the numerical solutions when applying the model for wave propagation over an uneven bathymetry.

The present model focuses on the large picture of wave transformation in coastal regions. On the basis of this model, addition of local physics can further enpower the integral model. The local dynamics are significant in the surf zone. The mass and momentum fluxes due to wave breaking needs additional attention. But these phenomena are far from fully understood, and their quantification is insecure. These terms can be easily incorporated into the mathematical model once they can be reasonably well formulated in future.

The limitations of this model aside, it is still a valuable frame work for simulating the evolution of mean wave parameters. In addition, the developed numerical scheme and the approaches for dealing with open boundary conditions can be used for a quasi-linear hyperbolic system of any order.

BIBLIOGRAPHY

Bagnold, R. A., 1940. *Beach Formation By Waves; Some Model Experiments In a Wave Tank.* J. Inst. Civ. Eng., 15: 27-52.

Battjes, J.A., 1974. *Surf Similarity.* Proc. 14th Confc. Coastal Eng., 1, 466-479.

Battjes, J.A. and Janssen, J.P.F.M, 1978. *Energy Loss And Setup Due To Breaking Of Random Waves.* Proc. 16th Confc. Coastal Eng., Hamburg, ASCE, 1, 569-587.

Battjes, J.A. and Stive, M.J.F., 1985. *Calibration And Verification Of A Dissipation Model For Random Breaking Waves.* Journal of Geophysical Research, 90, 9159-9167.

Battjes, J.A., Sobey, R.J. and Stive, M.J.F., 1990. *Nearshore Circulation.* Chapter 13 , pp.467-487.

Battjes J.A., 1994. *Shallow Water Wave Modeling.* International Symposium: Waves-Physical and Numerical Modeling, pp.1-23

Berkhoff, J.C.W., 1972. *Computation Of Combined Refraction-Diffraction.* Proc. 13th Conf. Coastal Eng., ASCE, Vancouver.

Berkhoff, J.C.W., Booij, N. and Radder, A.C., 1982. *Verification of Numerical Wave Propagation Models For Simple Harmonic Linear Water Waves.* Coastal Eng., 6: 255-279.

Bijker, E.W., 1971 *Longshore Transport Computations.* Journal of Waterways, Harbors and Coastal Engineering Division, ASCE, Vol.97, WW4, pp 687-701.

Bode, L. and Sobey, R.J., 1984. *Initial Transient In Long Wave Computations.* Journal of Hydraulic Engineering, Vol.10, No. 10, pp.1371-1397.

Book, D.L., Boris, J.P. and Hain, K., 1975 *Flux-Corrected Transport II: Generalization of The Method.* Journal of Computational Physics, 18, pp. 248-283.

Bradshaw, P., 1972. *The Understanding and Prediction of Turbulent Flow.* Aeronautical Journal, 76, 403-418.

Bretherton, F.P. and Garrett, C.J.R., 1968. *Wave Trains In Inhomogeneous Moving Media*, Proc. Royal Soc. London, Series A302, pp.529-554.

Bulter, D.S., 1960. *The Numerical Solution of Hyperbolic Systems of Partial Differential Equations in Three Independent Variables.* Proc. Royal Soc.(London), 255A, pp.232-252

Chapman, David., 1985 *Numerical Treatment of Cross-Shelf Open Boundaries In a Barotropic Coastal Ocean Model.* Journal of Physical Oceanography, pp.1060-1075.

Courant, R., Friedrichs, K.O., and Lewy, H., 1928. *Uber Die Partellen Differentialgleichungen der Mathematischen Physik.* Math Ann. Vol. 100, pp.32-74

Daubert, A. and Graffe, M.O., 1967. *Some Aspects of Near-Horizontal Unsteady Flow and Their Application to Estuaries.* Communication Presentee au Comite Technique de la Societe Hydrotechnique de France, Juin.

De Vriend, H.J. and Stive, M.J.F., 1987. *Modeling Of Nearshore Currents.* Coastal Eng., 11: 565-601.

Dean, R.G. and Dalrymple, R.A., 1984. *Water Waves Mechanics For Engineers and Scientists.* Prince-Hall, Englewood Cliffs, N.J.

Deleaney, R.A. and Kavangh, P., 1976. *Transonic Flow Analysis in Axial-Flow Turbomachinery Cascades by a Time-Dependent method of Characteristics.* Journal of Engineering for Power, July, pp.356-364.

Derks, H. and Stive, M.J.F., 1984. *Field Investigation in the TOW Study Programme for Coastal Sediment Transport in the Netherlands:* . Proc. 19th Confc. Coastal Eng., Houston, Volume II, Chapter 123, pp. 1830-1845.

Dingemans, M.W., 1985. *Evaluation of Two-Dimensional Horizontal Wave Propagation Models.* Delft Hydraulics Lab. Rep. W301, part5, 117 pp.

Dingemans, M.W., 1987. *Verification Of Numerical Wave Propagation Models With Laboratory Measurements.* Delft Hydraulics.

Engquist B. and Majda A., 1977. *Absorbing Boundary Conditions for the Numerical Simulation of Waves.* Mathematics of Computation, 31: 629-651.

Fenton, J.D., 1988. *Nonlinear Wave Theories*, pp.3-25.

Fox, G. Douglas, 1970. *Forced Plume in a Stratified Fluid.* Journal of Geophysical Research. Vol.75, 33: 6818-6831.

Garcia, R. and Kahawita, R., 1986. *Numerical Solution of the St. Venant Equations with the MacCORMACK Finite-Difference Scheme.* International Journal for Numerical Methods in Fluids, Vol.6, pp. 259-274

Greenwood, B. and Osborne, P.D., 1990. *Vertical and Horizontal Structure in Cross-shore Flows: An Example of Undertow and Wave Setup On a Barred Beach.* Coastal Eng., 14: 543-580.

Hamm, L., Madsen, Per A., and Peregrine, D. H., 1993. *Wave Transformation in the Nearshore Zone: A Review.* Coastal Eng., 21: 5-39.

Harper B.A. and Sobey, R.J., 1983. *Open Boundary Conditions For Open Coast Hurricane Storm Surge.* Coastal Eng., 7: 41-60.

Hedstrom, G.W., 1979. *Non-reflecting Boundary Conditions for Nonlinear Hyperbolic Systems.* Computational Physics, Vol.30, pp.222-237.

Hirsch, Charles, 1986. *Numerical Computation of Internal and External Flows, Volume 1: Fundamentals of Numerical Discretization.* John Wiley & Sons.

Holt, M., 1964. *Recent Contribution to the Method of Characteristics for Three-Dimensional Problems in Gas Dynamics.* Report FM-74-2, College of Engineering, University of California, Berkeley.

Horikawa, K., 1989. *Nearshore Dynamics and Coastal Processes.* University of Tokyo Press.

Hoskin, N.E., 1964. *Solution by Characteristics of the Equations of One-Dimensional Unsteady Flow.* Methods in Computational Physics, edited by B. Alder, Vol.3, pp.265-293

Jonsson, I.G., 1966. *Wave Boundary Layers And Friction Factors.* Proceedings 10th Conference Coastal Engineering, 1: 127-144.

Katopodes, N. and Strelkoff, T., 1979. *Two Dimensional Shallow Water-Wave Models.* Journal of Engineering Mechanics, Vol.105, No. EM2. pp. 317-334.

Larsen J. and Henry, D., 1983. *Open Boundaries in Short Wave Simulation- A New Approach.* Coastal Eng., 7: 285-297.

Lax, P.D., 1958. *Differential Equations, Difference Equations and matrix Theory.* Commun. Pure Appl. Math. Vol. 11, pp.175-194

Le Mehaute, B., 1962. *On Non-Saturated Breakers And The Wave Run-Up.* Proc. 8th Conf. Coastal Eng. 1, 77-92.

Longuet-Higgins, M.S. and Stewart, R.W., 1964. *Radiation Stress in Water Waves; a Physical Discussion, with Applications.* Deep Sea Research, 11, 529-562.

Longuet-Higgins, M.S., 1964. *Breaking Waves -In Deep Or Shallow Water.* Proceedings, Tenth Symposium on Naval Hydrodynamics. pp.597-605.

Massel, Stanislaw R., 1989. *Hydrodynamics Of Coastal Zones.* Elsevier Oceanography Series, 48.

Mei, C. C., 1983. *The Applied Dynamics of Ocean Surface Waves.* Wiley, New York.

Mei, C.C., 1985. *Resonant Reflection of Surface Waves by periodic Sandbars.* Journal of Fluid Mechanics., 152; 315-335.

Miche, R., 1951. *Le pouvoir reflechissant des ouvrages maritime exposes à l'action de la houle,* Annales Ponts et Chaussees, 121^{e} Annee, pp. 285-319.

Munk, W.H., 1949. *Surf Beats.* Trans. Am. Geophys. Union, 30: 849-854.

Nadaoka, K. and Kondoh, T., 1982. *Laboratory Measurements of Velocity Field Structure in The Surf Zone By LDV.* Coastal Engineering in Japan, 25, 125-145.

Nielsen, P., 1985. *A Short Manual of Coastal Bottom Boundary Layers and Sediment Transport.* Public Works Dept., N.S. Wales, Coastal Eng. Branch, TM 85, pp.1-56.

O'Brien, M.P., 1931. *A Report on Sand Movement and Beach Erosion Along the Pacific Coast of the United States.* Beach Erosion Board.

Osher, S. and Solomon, F., 1982. *Upwind Schemes for Hyperbolic Systems of Conservation Laws.* Mathematics of Computation, 38: 339-377.

Peregrine, D.H., 1967. *Long Waves on a Beach.* Jour. Fluid Mech., 27: 815-827.

Potters, D., 1973. *Computational Physics.* John Wiley & Sons.

Phillips, O.M., 1977. *Dynamics of the Upper Ocean.* 2nd Edition, Cambridge University Press, Cambridge.

Ransom, V.H., 1970. *A Second-Order Numerical Method of Characteristics for Three Dimensional Supersonic Flow.* Ph.D. Dissertation, Purdue Univ., West Lafayette, Ind.

Ransom,V.H., Hoffman,J.D. and Thompson, H.D., 1972. *A Second-Order Bicharacteristics Method for Three-Dimensional Steady, Supersonic Flow.* AIAA Journal, Vol. 10, N0.12 , pp.1573-1581.

Reymond, W.H., and Kuo, H.L., 1984. *A Radiation Boundary Condition For Multi-Dimensional Flows.* Quart. J. Roy. Met. Soc., 110: 197-207.

Richardson, D.J., 1964. *The Solution of Two-Dimensional Hydrodynamic Equations by the Method of Characteristics.* Methods in Computational Physics, edited by B. Alder Vol.3, pp.295-318.

RØed, L.P. and Cooper, C.K., 1986. *A Study of Various Open Boundary Conditions For Wind-Forced Barotropic Numerical Ocean Models.* 18th International Colloquium on Ocean Hydrodynamics, Liege, Belgium.

Rudy, D.H. and Strikwerda, J.C., 1980. *A Nonreflecting Outflow Boundary Condition for*

Subsonic Navier-Stokes Calculations. Journal of Computational Physics, 36, pp.55-70.
Sauerwein, H. and Sussman, Mark., 1964. *Numerical Stability of the Three-Dimensional Method of Characteristics.* AIAA Journal, Vol.2, pp.387-389.

Shepard, F.P. and Inman, D.L., 1950. *Nearshore Circulation Related to Bottom Topography and Wave Refraction.* Trans. Am. Geophys. Union, Vol.3, No.2, pp. 196-212.

Sobey, R. J., 1989. *Variations on Fourier Wave Theory.* Int. J. Numerical Methods in Fluids, 9: 1453-1467.

Sobey, R.J. and Thieke, R.J., 1989. *Mean Flow Circulation Equations For Shoaling And Breaking Waves.* Journal of Engineering Mechanics. 115: 285-303.

Sobey, R.J. and Bando, K., 1991. *Variations on Higher-Order Shoaling.* Journal of Waterways, Port, Coastal, and Ocean Engineering, Vol 117, N0.4, pp 348-368.

Spekreijse, S.P., 1980. *Multigrid Solution of the Steady Euler Equations.* CWI Tract 46, Center for Mathematics and Computer Science.

Skjebreia, J.E., 1987. *Observations of Breaking Waves on Sloping Bottoms by Use of Laser Doppler Velocimetry.* Report KH-R-48, W.M. Keck Laboratory of Hydraulics and Water Resources, California Institute of Technology, Pasadena.

Stive, M.J.F., 1984. *Energy Dissipation In Waves Breaking On Gentle Slopes.* Publication No.321, Delft Hydraulics Lab.

Stive, M.J.F. and Wind, H.G., 1986. *Cross-Shore Mean Flow In The Surf Zone.* Coastal Eng. 10, pp. 325-340.

Stive, M.J.F. 1988. *Cross-Shore Flow In Waves Breaking On A Beaching.* Delft Hydraulics, Publication No.395.

Svendsen, I.A. and J. Buhr Hansen., 1977. *The Wave Height Variation For Regular Waves In Shoaling Water.* Coastal Eng. pp.261-279.

Svendsen, I.A. and Hansen, J.B., 1978. *On Deformation of Periodic Long Waves Over a Gently Slopping Bottom.* Jour. Fluid Mech., 87: 433-448.

Svendsen, I.A., 1984a. *Wave Attenuation And Set-up On A Beach.* Proc. 19th Confc. Coastal Eng., 1: 54-69.

Svendsen, I.A., 1984b. *Wave Heights and Set-up In a Surf Zone.* Coastal Eng., 8: 303-329.

Svendsen, I.A., 1984c. *Mass Flux and Undertow in a Surf Zone.* Coastal Eng., 8: 347-365.

Svendsen, I.A., 1987. *Analysis of Surf Zone Turbulence.* J. Geophy. Res. 92: 5115-5124.

Tennekes, H. and Lumley, J.L., 1973. *A first Course in Turbulence.* The MIT Press, Cambridge, Massachusetts.

Thieke, R.J., 1988. *Mean Flow Integral Model For Shoaling And Surf Zone Waves.* Dissertation, U.C. Berkeley.

Thieke, R.J. and Sobey, R.J., 1990. *Cross-Shore Wave Transformation and Mean Flow Circulation.* Coastal Eng., 14: 387-415.

Thornhill, C. K., 1948. *The Numerical Method of Characteristic for Hyperbolic problems in Three Independent Variables.* A.R.E Report 29/48. No.2615.

Thornton, E.B. and Guza, R.T., 1986. *Surf Zone Currents and Random Waves: Models and Field Data.* J. Phys. Oceanogr., 16: 1165-1178.

Townson, J.M., 1974. *An Application of the Method of Characteristics to Tidal Calculation in (x-y-t) Space.* Journal of Hydraulic Research, Vol.12. pp.499-525.

Tsuchiya Y., Yamashita T. and Uemoto, M., 1988. *A Model Of Undertow In the Surf Zone.* Coastal Engineering In Japan, Vol. 30, No.2. pp.63-73.

Tucker, M.J., 1950. *Surf Beats: Sea Waves of 1 to 5 Min. Period.* Proc. Roy. Soc. London, A202: 563 - 573.

Van der Velden, 1989. *Coastal Engineering.* Delft University of Technology.

Verboom, G.K., Stelling, G.S. and Officier. M.J., 1983. *Boundary Conditions for the Shallow Water Equations.* In: M.B. Abbott and J.A. Cunge (Editors) Engineering Applications of Computational Hydraulics I. Pitman, London, pp.230-262.

Williams, J.M., 1981. *Limiting Gravity Waves in Water of Finite Depth.* Phil. Trans. Roy. Soc. London, A302: 139-188.

Webster, J.A., 1968. *An Application of the Method of Characteristics to Tidal Computation.* published Ph.D. thesis, University of Aberdeen, 1968.

Wylie, C.R. and Barrett, L.C., 1982. *Advanced Engineering Mathematics.* McGraw-Hill Book Company.

Yee, H.C. and Warming, R.F., 1985. *Implicit Total Variation Diminishing (TVD) Schemes for Steady State Calculations.* Journal of Computational Physics, 57: 327-360.

Yoo, D. and O'Connor, B.A., 1986. *Mathematical Modeling of Wave-Induced Nearshore Circulation.* Coastal Eng., pp.1667-1681.

APPENDIX A QUASI-LINEAR GOVERNING EQUATIONS FOR MEAN WAVE PARAMETERS IN A ONE SPATIAL DIMENSION

To derive the compatibility equations, the closed integral equations (Equations 4.32 through 4.34) for mean wave parameters in a one spatial dimension must be written in a quasilinear form. First these equations are written into non-conservative forms, then through linear combination they are transformed into a set of three quasilinear equations each with the time derivative of one dependent variable.

In addition to the general notations for dependent variables and closure variables, the following are also used to simplify the equations:

$H_* =$ dimensionless ordinate on the closure surfaces, $= H/H_{Miche.}$

$h_* =$ dimesionless abscissa on the closure surfaces, $= h + \overline{\eta}$.

$$T_h = \frac{1}{0.88\tanh(h_*)}$$

$$S_h = \frac{-1}{0.88\sinh^2(h_*)}$$

Wave Energy Equation:

$$A(1,1)\frac{\partial H}{\partial t} + A(1,2)\frac{\partial \overline{\eta}}{\partial t} + A(1,3)\frac{\partial U_b}{\partial t} + B(1,1)\frac{\partial H}{\partial x} + B(1,2)\frac{\partial \overline{\eta}}{\partial x} + B(1,3)\frac{\partial U_b}{\partial x} = D(1)$$

where

$$A(1,1) = \frac{1}{2}\left[T_h \frac{\partial \eta^2}{\partial H_*} + W_s + HT_h \frac{\partial W_s}{\partial H_*} + W_b T_h \frac{\partial \eta_{tr}}{\partial H_*} + (h + \overline{\eta} + \eta_{tr})T_h \frac{\partial W_b}{\partial H_*} \right]$$

$$A(1,2)=\frac{1}{2}[\ HS_h\frac{\partial\eta^2}{\partial H.}+\frac{\partial\eta^2}{\partial h.}+W_b+H(HS_h\frac{\partial W_s}{\partial H.}+\frac{\partial W_s}{\partial h.})\ +$$

$$W_b(HS_h\frac{\partial\eta_{tr}}{\partial H.}+\frac{\partial\eta_{tr}}{\partial h.})+(h+\overline{\eta}+\eta_{tr})(HS_h\frac{\partial W_b}{\partial H.}+\frac{\partial W_b}{\partial h.})\ ]$$

$$A(1,3)=0$$

$$B(1,1)=F_s+K_s+HT_h(\frac{\partial F_s}{\partial H.}+\frac{\partial K_s}{\partial H.}+N_s\frac{\partial U_s}{\partial H.})+(h+\overline{\eta}+\eta_{tr})T_h\frac{\partial F_b}{\partial H.}$$

$$+(\frac{U_bW_b}{2}+F_b)T_h\frac{\partial\eta_{tr}}{\partial H.}+\frac{U_b}{2}(h+\overline{\eta}+\eta_{tr})T_h\frac{\partial W_b}{\partial H.}$$

$$B(1,2)=(h+\overline{\eta}+\eta_{tr})[\ HS_h\frac{\partial F_b}{\partial H.}+\frac{\partial F_b}{\partial h.}+\frac{U_b}{2}(HS_h\frac{\partial W_b}{\partial H.}+\frac{\partial W_b}{\partial h.})\ ]$$

$$+H[\ HS_h(\frac{\partial F_s}{\partial H.}+\frac{\partial K_s}{\partial H.}+N_s\frac{\partial U_s}{\partial H.})+\frac{\partial F_s}{\partial h.}+\frac{\partial K_s}{\partial h.}+N_s\frac{\partial U_s}{\partial h.}\ ]$$

$$+(\frac{U_bW_b}{2}+F_b)(1+HS_h\frac{\partial\eta_{tr}}{\partial H.}+\frac{\partial\eta_{tr}}{\partial h.})$$

$$B(1,3)=(h+\overline{\eta}+\eta_{tr})(\frac{W_b}{2}+N_b)$$

$$D(1)=-B(1,2)\frac{\partial h}{\partial x}-D_{bf}-D_{bw}$$

Continuity Equation:

$$A(2,1)\frac{\partial H}{\partial t}+A(2,2)\frac{\partial\overline{\eta}}{\partial t}+A(2,3)\frac{\partial U_b}{\partial t}+B(2,1)\frac{\partial H}{\partial x}+B(2,2)\frac{\partial\overline{\eta}}{\partial x}+B(2,3)\frac{\partial U_b}{\partial x}=D(2)$$

where

$A(2,1)=0$

$A(2,2)=1$

$A(2,3)=0$

$$B(2,1)=\hat{U}+HT_h\frac{\partial\hat{U}}{\partial H.}+T_hU_b\frac{\partial\eta_{tr}}{\partial H.}$$

$$B(2,2) = H\ (HS_h \frac{\partial \hat{U}}{\partial H_*} + \frac{\partial \hat{U}}{\partial h_*}) + U_b(1 + HS_h \frac{\partial \eta_{tr}}{\partial H_*} + \frac{\partial \eta_{tr}}{\partial h_*})$$

$$B(2,3) = h + \overline{\eta} + \eta_{tr}$$

$$D(2) = -B(2,2)\frac{\partial h}{\partial x}$$

Momentum Conservation Equation:

$$A(3,1)\frac{\partial H}{\partial t} + A(3,2)\frac{\partial \overline{\eta}}{\partial t} + A(3,3)\frac{\partial U_b}{\partial t} + B(3,1)\frac{\partial H}{\partial x} + B(3,2)\frac{\partial \overline{\eta}}{\partial x} + B(3,3)\frac{\partial U_b}{\partial x} = D(3)$$

where

$$A(3,1) = B(2,1)$$

$$A(3,2) = B(2,2)$$

$$A(3,3) = B(2,3)$$

$$B(3,1) = \hat{U}^2 - S_s + HT_h(\frac{\partial \hat{U}^2}{\partial H_*} - \frac{\partial S_s}{\partial H_*}) - (h + \overline{\eta} + \eta_{tr})T_h \frac{\partial S_b}{\partial H_*} + (U_b^2 - S_b)T_h \frac{\partial \eta_{tr}}{\partial H_*}$$

$$B(3,2) = h + \overline{\eta} - (h + \overline{\eta} + \eta_{tr})(HS_h \frac{\partial S_b}{\partial H_*} + \frac{\partial S_b}{\partial h_*}) + H(HS_h \frac{\partial \hat{U}^2}{\partial H_*} + \frac{\partial \hat{U}^2}{\partial h_*})$$
$$- H(HS_h \frac{\partial S_s}{\partial H_*} + \frac{\partial S_s}{\partial h_*}) + (U_b^2 - S_b)(1 + HS_h \frac{\partial \eta_{tr}}{\partial H_*} + \frac{\partial \eta_{tr}}{\partial h_*})$$

$$B(3,3) = 2\ (h + \overline{\eta} + \eta_{tr})U_b$$

$$D(3) = -(B(3,2) - h + \overline{\eta})\frac{\partial h}{\partial x} - \tau_{bx}$$

To derive characteristic equations, the above equations need to be further transformed into a system of equations each with the time derivative of one variable only, with the form:

$$[I\frac{\partial}{\partial t}+A_x\frac{\partial}{\partial x}]R=Q$$

in which I is a unit 3×3 matrix, $R=[H,\ \overline{\eta},\ U_b]^T$, A_x is a 3×3 coefficient matrix, and Q is a 1×3 column vector of non-homogeneous terms. A_x and Q are given below.

$$A_x(1,1)=\frac{B(1,1)-B(2,1)*A(1,2)}{A(1,1)}$$

$$A_x(1,2)=\frac{B(1,2)-B(2,2)*A(1,2)}{A(1,1)}$$

$$A_x(1,3)=\frac{B(1,3)-B(2,3)*A(1,2)}{A(1,1)}$$

$$A_x(2,1)=B(2,1)$$

$$A_x(2,2)=B(2,2)$$

$$A_x(2,3)=B(2,3)$$

$$A_x(3,1)=\frac{B(3,1)-A_x(1,1)*A(3,1)-A_x(2,1)*A(3,2)}{A(3,3)}$$

$$A_x(3,2)=\frac{B(3,2)-A_x(1,2)*A(3,1)-A_x(2,2)*A(3,2)}{A(3,3)}$$

$$A_x(3,3)=\frac{B(3,3)-A_x(1,3)*A(3,1)-A_x(2,3)*A(3,2)}{A(3,3)}$$

$$Q(1)=\frac{D(1)-D(2)*A(1,2)}{A(1,1)}$$

$$Q(2)=D(2)$$

$$Q(3)=\frac{D(3)-Q(1)*A(3,1)-Q(2)*A(3,2)}{A(3,3)}$$

APPENDIX B QUASI-LINEAR GOVERNING EQUATIONS FOR MEAN WAVE PARAMETERS IN TWO SPATIAL DIMENSIONS

To derive characteristic equations, the closed integral equations are written in a quasilinear form. This appendix gives the complete procedure and exact expressions for the quasilinear equations. In the following equations, θ is the angle between the local wave direction and x axis, and $H_\cdot$, $h_\cdot$, S_h and T_h are as defined in Appendix A.

Energy Conservation Equation:

$$\begin{aligned} &A(1,1)\frac{\partial H}{\partial t}+A(1,2)\frac{\partial \overline{\eta}}{\partial t}+A(1,3)\frac{\partial U_b}{\partial t}+A(1,4)\frac{\partial V_b}{\partial t}\\ &+B(1,1)\frac{\partial H}{\partial x}+B(1,2)\frac{\partial \overline{\eta}}{\partial x}+B(1,3)\frac{\partial U_b}{\partial x}+B(1,4)\frac{\partial V_b}{\partial x}\\ &+C(1,1)\frac{\partial H}{\partial y}+C(1,2)\frac{\partial \overline{\eta}}{\partial y}+C(1,3)\frac{\partial U_b}{\partial y}+C(1,4)\frac{\partial V_b}{\partial y}=D(1) \end{aligned} \tag{B.1}$$

where

$$A(1,1)=\frac{1}{2}\left[\ T_h\frac{\partial \eta^2}{\partial H_\cdot}+W_s+HT_h\frac{\partial W_s}{\partial H_\cdot}+W_bT_h\frac{\partial \eta_{tr}}{\partial H_\cdot}+(h+\overline{\eta}+\eta_{tr})T_h\frac{\partial W_b}{\partial H_\cdot}\ \right]$$

$$\begin{aligned} A(1,2)=\frac{1}{2}\Big[\ &HS_h\frac{\partial \eta^2}{\partial H_\cdot}+\frac{\partial \eta^2}{\partial h_\cdot}+W_b+H(HS_h\frac{\partial W_s}{\partial H_\cdot}+\frac{\partial W_s}{\partial h_\cdot})\ +\\ &W_b(HS_h\frac{\partial \eta_{tr}}{\partial H_\cdot}+\frac{\partial \eta_{tr}}{\partial h_\cdot})+(h+\overline{\eta}+\eta_{tr})(HS_h\frac{\partial W_b}{\partial H_\cdot}+\frac{\partial W_b}{\partial h_\cdot})\ \Big] \end{aligned}$$

$A(1,3)=0$

$A(1,4)=0$

$$\begin{aligned} B(1,1)=&(F_s+K_s)\cos\theta+H\cos\theta\,T_h(\frac{\partial F_s}{\partial H_\cdot}+\frac{\partial K_s}{\partial H_\cdot}+N_s\frac{\partial \hat{U}}{\partial H_\cdot})\\ &+(\frac{U_bW_b}{2}+F_b\cos\theta)T_h\frac{\partial \eta_{tr}}{\partial H_\cdot}+(h+\overline{\eta}+\eta_{tr})T_h(\frac{U_b}{2}\frac{\partial W_b}{\partial H_\cdot}+\cos\theta\frac{\partial F_b}{\partial H_\cdot}) \end{aligned}$$

$$B(1,2) = H\cos\theta\Big[\ HS_h\Big(\frac{\partial F_s}{\partial H.} + \frac{\partial K_s}{\partial H.} + N_s\frac{\partial \hat{U}}{\partial H.}\Big) + \frac{\partial F_s}{\partial h.} + \frac{\partial K_s}{\partial h.} + N_s\frac{\partial \hat{U}}{\partial h.}\ \Big]$$
$$+ (h + \overline{\eta} + \eta_{tr})\Big[\ \cos\theta\,(HS_h\frac{\partial F_b}{\partial H.} + \frac{\partial F_b}{\partial h.}) + \frac{U_b}{2}(HS_h\frac{\partial W_b}{\partial H.} + \frac{\partial W_b}{\partial h.})\ \Big]$$
$$+ \Big(\frac{U_b W_b}{2} + F_b\cos\theta\Big)\Big(1 + HS_h\frac{\partial \eta_{tr}}{\partial H.} + \frac{\partial \eta_{tr}}{\partial h.}\Big)$$

$$B(1,3) = (h + \overline{\eta} + \eta_{tr})\Big(\frac{W_b}{2} + N_b\cos^2\theta\Big)$$

$$B(1,4) = \frac{\sin 2\theta}{2}(h + \overline{\eta} + \eta_{tr})N_b$$

$$C(1,1) = (F_s + K_s)\sin\theta + H\sin\theta\,T_h\Big(\frac{\partial F_s}{\partial H.} + \frac{\partial K_s}{\partial H.} + N_s\frac{\partial \hat{U}}{\partial H.}\Big)$$
$$+ \Big(\frac{V_b W_b}{2} + F_b\sin\theta\Big)T_h\frac{\partial \eta_{tr}}{\partial H.} + (h + \overline{\eta} + \eta_{tr})T_h\Big(\frac{V_b}{2}\frac{\partial W_b}{\partial H.} + \sin\theta\frac{\partial F_b}{\partial H.}\Big)$$

$$C(1,2) = H\sin\theta\Big[\ HS_h\Big(\frac{\partial F_s}{\partial H.} + \frac{\partial K_s}{\partial H.} + N_s\frac{\partial \hat{U}}{\partial H.}\Big) + \frac{\partial F_s}{\partial h.} + \frac{\partial K_s}{\partial h.} + N_s\frac{\partial \hat{U}}{\partial h.}\ \Big]$$
$$+ (h + \overline{\eta} + \eta_{tr})\Big[\ \sin\theta\,(HS_h\frac{\partial F_b}{\partial H.} + \frac{\partial F_b}{\partial h.}) + \frac{V_b}{2}(HS_h\frac{\partial W_b}{\partial H.} + \frac{\partial W_b}{\partial h.})\ \Big]$$
$$+ \Big(\frac{V_b W_b}{2} + F_b\sin\theta\Big)\Big(1 + HS_h\frac{\partial \eta_{tr}}{\partial H.} + \frac{\partial \eta_{tr}}{\partial h.}\Big)$$

$$C(1,3) = \frac{\sin(2\theta)}{2}(h + \overline{\eta} + \eta_{tr})N_b$$

$$C(1,4) = (h + \overline{\eta} + \eta_{tr})\Big[\ \frac{W_b}{2} + N_b\sin^2\theta\ \Big]$$

$$D(1) = -D_{bf} - D_{wb} - B(1,2)\frac{\partial h}{\partial x} - C(1,2)\frac{\partial h}{\partial y}$$
$$+ \Big[\ H(F_s + K_s) + (h + \overline{\eta} + \eta_{tr})F_b\ \Big]\Big(\sin\theta\frac{\partial \theta}{\partial x} - \cos\theta\frac{\partial \theta}{\partial y}\Big)$$

Continuity Equation:

$$\begin{aligned} &A(2,1)\frac{\partial H}{\partial t}+A(2,2)\frac{\partial \overline{\eta}}{\partial t}+A(2,3)\frac{\partial U_b}{\partial t}+A(2,4)\frac{\partial V_b}{\partial t} \\ &+B(2,1)\frac{\partial H}{\partial x}+B(2,2)\frac{\partial \overline{\eta}}{\partial x}+B(2,3)\frac{\partial U_b}{\partial x}+B(2,4)\frac{\partial V_b}{\partial x} \\ &+C(2,1)\frac{\partial H}{\partial y}+C(2,2)\frac{\partial \overline{\eta}}{\partial y}+C(2,3)\frac{\partial U_b}{\partial y}+C(2,4)\frac{\partial V_b}{\partial y}=D(2) \end{aligned} \qquad \text{(B.2)}$$

where

$A(2,1)=0$

$A(2,2)=1$

$A(2,3)=0$

$A(2,4)=0$

$$B(2,1)=\hat{U}\cos\theta+H\cos\theta\,T_h\frac{\partial \hat{U}}{\partial H_*}+T_hU_b\frac{\partial \eta_{tr}}{\partial H_*}$$

$$B(2,2)=H\cos\theta\ (HS_h\frac{\partial \hat{U}}{\partial H_*}+\frac{\partial \hat{U}}{\partial h_*})+U_b(1+HS_h\frac{\partial \eta_{tr}}{\partial H_*}+\frac{\partial \eta_{tr}}{\partial h_*})$$

$$B(2,3)=h+\overline{\eta}+\eta_{tr}$$

$$B(2,4)=0$$

$$C(2,1)=\hat{U}\sin\theta+H\sin\theta\,T_h\frac{\partial \hat{U}}{\partial H_*}+T_hV_b\frac{\partial \eta_{tr}}{\partial H_*}$$

$$C(2,2)=H\sin\theta\ (HS_h\frac{\partial \hat{U}}{\partial H_*}+\frac{\partial \hat{U}}{\partial h_*})+V_b(1+HS_h\frac{\partial \eta_{tr}}{\partial H_*}+\frac{\partial \eta_{tr}}{\partial h_*})$$

$$C(2,3)=0$$

$$C(2,4)=h+\overline{\eta}+\eta_{tr}$$

$$D(2)=-B(2,2)\frac{\partial h}{\partial x}-C(2,2)\frac{\partial h}{\partial y}+H\hat{U}\ (\sin\theta\frac{\partial \theta}{\partial x}-\cos\theta\frac{\partial \theta}{\partial y})$$

Momentum Equation In x Direction:

$$A(3,1)\frac{\partial H}{\partial t}+A(3,2)\frac{\partial \overline{\eta}}{\partial t}+A(3,3)\frac{\partial U_b}{\partial t}+A(3,4)\frac{\partial V_b}{\partial t}$$
$$+B(3,1)\frac{\partial H}{\partial x}+B(3,2)\frac{\partial \overline{\eta}}{\partial x}+B(3,3)\frac{\partial U_b}{\partial x}+B(3,4)\frac{\partial V_b}{\partial x} \qquad \text{(B.3)}$$
$$+C(3,1)\frac{\partial H}{\partial y}+C(3,2)\frac{\partial \overline{\eta}}{\partial y}+C(3,3)\frac{\partial U_b}{\partial y}+C(3,4)\frac{\partial V_b}{\partial y}=D(3)$$

where

$A(3,1) = B(2,1)$

$A(3,2) = B(2,2)$

$A(3,3) = B(2,3)$

$A(3,4) = 0$

$$B(3,1)=\hat{U}^2\cos^2\theta-S_s-N_s\sin^2\theta+HT_h(\cos^2\theta\frac{\partial\hat{U}^2}{\partial H.}-\frac{\partial S_s}{\partial H.}-\sin^2\theta\frac{\partial N_s}{\partial H.})$$
$$-(h+\overline{\eta}+\eta_{tr})T_h(\frac{\partial S_b}{\partial H.}+\sin^2\theta\frac{\partial N_b}{\partial H.})+(U_b^2-S_b-N_b\sin^2\theta)T_h\frac{\partial\eta_{tr}}{\partial H.}$$

$$B(3,2)=h+\overline{\eta}-(h+\overline{\eta}+\eta_{tr})[\,HS_h\frac{\partial S_b}{\partial H.}+\frac{\partial S_b}{\partial h.}+\sin^2\theta(HS_h\frac{\partial N_b}{\partial H.}+\frac{\partial N_b}{\partial h.})\,]$$
$$+H[\,\cos^2\theta(HS_h\frac{\partial\hat{U}^2}{\partial H.}+\frac{\partial\hat{U}^2}{\partial h.})-HS_h\frac{\partial S_s}{\partial H.}-\frac{\partial S_s}{\partial h.}-\sin^2\theta(HS_h\frac{\partial N_s}{\partial H.}+\frac{\partial N_s}{\partial h.})\,]$$
$$+(U_b^2-S_b-N_b\sin^2\theta)(1+HS_h\frac{\partial\eta_{tr}}{\partial H.}+\frac{\partial\eta_{tr}}{\partial h.})$$

$B(3,3) = 2(h+\overline{\eta}+\eta_{tr})U_b$

$B(3,4) = 0$

$$C(3,1)=\frac{\sin 2\theta}{2}(\hat{U}^2+N_s)+HT_h\frac{\sin 2\theta}{2}(\frac{\partial \hat{U}^2}{\partial H.}+\frac{\partial N_s}{\partial H.})$$
$$+(h+\overline{\eta}+\eta_{tr})\frac{\sin 2\theta}{2}T_h\frac{\partial N_b}{\partial H.}+(U_bV_b+N_b\frac{\sin 2\theta}{2})T_h\frac{\partial \eta_{tr}}{\partial H.}$$

$$C(3,2)=U_bV_b+\frac{\sin 2\theta}{2}N_s+H\frac{\sin 2\theta}{2}[\ HS_h(\frac{\partial \hat{U}^2}{\partial H.}+\frac{\partial N_s}{\partial H.})+\frac{\partial \hat{U}^2}{\partial h.}+\frac{\partial N_s}{\partial h.}\ ]+$$
$$(h+\overline{\eta}+\eta_{tr})\frac{\sin 2\theta}{2}(HS_h\frac{\partial N_b}{\partial H.}+\frac{\partial N_b}{\partial h.})+(U_bV_b+N_b\frac{\sin 2\theta}{2})(HS_h\frac{\partial \eta_{tr}}{\partial H.}+\frac{\partial \eta_{tr}}{\partial h.})$$

$$C(3,3)=V_b(h+\overline{\eta}+\eta_{tr})$$

$$C(3,4)=U_b(h+\overline{\eta}+\eta_{tr})$$

$$D(3)=-\tau_{bx}-(B(3,2)-h-\overline{\eta})\frac{\partial h}{\partial x}-C(3,2)\frac{\partial h}{\partial y}$$
$$+[\ H(N_s+\hat{U}^2)+(h+\overline{\eta}+\eta_{tr})N_b\ ](\sin 2\theta\frac{\partial \theta}{\partial x}-\cos 2\theta\frac{\partial \theta}{\partial y})$$

Momentum Equation In y Direction:

$$A(4,1)\frac{\partial H}{\partial t}+A(4,2)\frac{\partial \overline{\eta}}{\partial t}+A(4,3)\frac{\partial U_b}{\partial t}+A(4,4)\frac{\partial V_b}{\partial t}$$
$$+B(4,1)\frac{\partial H}{\partial x}+B(4,2)\frac{\partial \overline{\eta}}{\partial x}+B(4,3)\frac{\partial U_b}{\partial x}+B(4,4)\frac{\partial V_b}{\partial x} \qquad (B.4)$$
$$+C(4,1)\frac{\partial H}{\partial y}+C(4,2)\frac{\partial \overline{\eta}}{\partial y}+C(4,3)\frac{\partial U_b}{\partial y}+C(4,4)\frac{\partial V_b}{\partial y}=D(4)$$

where

$$A(4,1)=C(2,1)$$

$$A(4,2)=C(2,2)$$

$$A(4,3)=0$$

$$A(4,4)=C(2,4)$$

B(4,1)=C(3,1)

B(4,2)=C(3,2)

B(4,3)=C(3,3)

B(4,4)=C(3,4)

$$C(4,1) = \hat{U}^2 \sin^2\theta - S_s - N_s \cos^2\theta + HT_h(\sin^2\theta \frac{\partial \hat{U}^2}{\partial H.} - \frac{\partial S_s}{\partial H.} - \cos^2\theta \frac{\partial N_s}{\partial H.})$$
$$-(h+\overline{\eta}+\eta_{tr})T_h(\frac{\partial S_b}{\partial H.} + \cos^2\theta \frac{\partial N_b}{\partial H.}) + (V_b^2 - S_b - N_b \cos^2\theta)T_h \frac{\partial \eta_{tr}}{\partial H.}$$

$$C(4,2) = h + \overline{\eta} - (h+\overline{\eta}+\eta_{tr})[\ HS_h \frac{\partial S_b}{\partial H.} + \frac{\partial S_b}{\partial h.} + \cos^2\theta\,(HS_h \frac{\partial N_b}{\partial H.} + \frac{\partial N_b}{\partial h.})\ ]$$
$$+H[\ \sin^2\theta\,(HS_h \frac{\partial \hat{U}^2}{\partial H.} + \frac{\partial \hat{U}^2}{\partial h.}) - HS_h \frac{\partial S_s}{\partial H.} - \frac{\partial S_s}{\partial h.} - \cos^2\theta\,(HS_h \frac{\partial N_s}{\partial H.} + \frac{\partial N_s}{\partial h.})\ ]$$
$$+(V_b^2 - S_b - N_b \cos^2\theta)(1 + HS_h \frac{\partial \eta_{tr}}{\partial H.} + \frac{\partial \eta_{tr}}{\partial h.})$$

$$C(4,3) = 0$$

$$C(4,4) = 2\,(h+\overline{\eta}+\eta_{tr})V_b$$

$$D(4) = -\tau_{by} - B(4,2)\frac{\partial h}{\partial x} - (C(4,2) - h - \overline{\eta})\frac{\partial h}{\partial y}$$
$$-[\ H(N_s + \hat{U}^2) + (h+\overline{\eta}+\eta_{tr})N_b\ ](\cos 2\theta \frac{\partial \theta}{\partial x} + \sin 2\theta \frac{\partial \theta}{\partial y})$$

Equations (B.1) through (B.4) are further transformed into a system with equations each containing only time derivative of one variable, i.e.

$$[\ I\frac{\partial}{\partial t} + A_x \frac{\partial}{\partial x} + A_y \frac{\partial}{\partial y}\ ]R = Q \qquad (B.5)$$

in which I is a unit 4×4 matrix, $R = [H.\ \overline{\eta},\ U_b,\ V_b]^T$, A_x and A_y are 4×4 coefficient matrices corresponding respectively to the x- and y-derivative terms, and Q is a column

vector comprised by non-homogeneous source terms.

The entries of A_x , A_y and Q are given below

$$A_x(1,1) = \frac{B(1,1) - B(2,1) * A(1,2)}{A(1,1)}$$

$$A_x(1,2) = \frac{B(1,2) - B(2,2) * A(1,2)}{A(1,1)}$$

$$A_x(1,3) = \frac{B(1,3) - B(2,3) * A(1,2)}{A(1,1)}$$

$$A_x(1,4) = \frac{B(1,4) - B(2,4) * A(1,2)}{A(1,1)}$$

$$A_x(2,1) = B(2,1)$$

$$A_x(2,2) = B(2,2)$$

$$A_x(2,3) = B(2,3)$$

$$A_x(2,4) = B(2,4)$$

$$A_x(3,1) = \frac{B(3,1) - A_x(1,1) * A(3,1) - B(2,1) * A(3,2)}{A(3,3)}$$

$$A_x(3,2) = \frac{B(3,2) - A_x(1,2) * A(3,1) - B(2,2) * A(3,2)}{A(3,3)}$$

$$A_x(3,3) = \frac{B(3,3) - A_x(1,3) * A(3,1) - B(2,3) * A(3,2)}{A(3,3)}$$

$$A_x(3,4) = \frac{B(3,4) - A_x(1,4) * A(3,1) - B(2,4) * A(3,2)}{A(3,3)}$$

$$A_x(4,1) = \frac{B(4,1) - A_x(1,1) * A(4,1) - B(2,1) * A(4,2)}{A(4,4)}$$

$$A_x(4,2) = \frac{B(4,2) - A_x(1,2) * A(4,1) - B(2,2) * A(4,2)}{A(4,4)}$$

$$A_x(4,3) = \frac{B(4,3) - A_x(1,3) * A(4,1) - B(2,3) * A(4,2)}{A(4,4)}$$

$$A_x(4,4) = \frac{B(4,4) - A_x(1,4) * A(4,1) - B(2,4) * A(4,2)}{A(4,4)}$$

$$A_y(1,1) = \frac{C(1,1) - C(2,1) * A(1,2)}{A(1,1)}$$

$$A_y(1,2) = \frac{C(1,2) - C(2,2) * A(1,2)}{A(1,1)}$$

$$A_y(1,3) = \frac{C(1,3) - C(2,3) * A(1,2)}{A(1,1)}$$

$$A_y(1,4) = \frac{C(1,4) - C(2,4) * A(1,2)}{A(1,1)}$$

$$A_y(2,1) = C(2,1)$$

$$A_y(2,2) = C(2,2)$$

$$A_y(2,3) = C(2,3)$$

$$A_y(2,4) = C(2,4)$$

$$A_y(3,1) = \frac{C(3,1) - A_y(1,1) * A(3,1) - C(2,1) * A(3,2)}{A(3,3)}$$

$$A_y(3,2) = \frac{C(3,2) - A_y(1,2) * A(3,1) - C(2,2) * A(3,2)}{A(3,3)}$$

$$A_y(3,3) = \frac{C(3,3) - A_y(1,3) * A(3,1) - C(2,3) * A(3,2)}{A(3,3)}$$

$$A_y(3,4) = \frac{C(3,4) - A_y(1,4) * A(3,1) - C(2,4) * A(3,2)}{A(3,3)}$$

$$A_y(4,1) = \frac{C(4,1) - A_y(1,1) * A(4,1) - C(2,1) * A(4,2)}{A(4,4)}$$

$$A_y(4,2) = \frac{C(4,2) - A_y(1,2) * A(4,1) - C(2,2) * A(4,2)}{A(4,4)}$$

$$A_y(4,3) = \frac{C(4,3) - A_y(1,3) * A(4,1) - C(2,3) * A(4,2)}{A(4,4)}$$

$$A_y(4,4) = \frac{C(4,4) - A_y(1,4) * A(4,1) - C(2,4) * A(4,2)}{A(4,4)}$$

$$Q(1) = \frac{D(1) - D(2) * A(1,2)}{A(1,1)}$$

$$Q(2)=D(2)$$

$$Q(3) = \frac{D(3) - Q(1) * A(3,1) - D(2) * A(3,2)}{A(3,3)}$$

$$Q(4) = \frac{D(4) - Q(1) * A(4,1) - D(2) * A(4,2)}{A(4,4)}$$

APPENDIX C CHARACTERISTICS AND CHARACTERISTIC EQUATIONS FOR SHALLOW WATER EQUATIONS

As indicated in Chapters 5 and 6, the integral equations for mean-flow mass conservation and momentum conservation are quite similar to the shallow water wave equations when in deep water or if wave height is small. Thus an analysis on the shallow water wave equations will assist in understanding the current system, and in clarifying the procedure for deriving the characteristics and characteristic equations. In this appendix, the characteristics and characteristic equations for the one- and two-spatial-dimension (1-D and 2-D) shallow water equations are derived, with particular attention directed to the physical interpretation of the eigenvalues and eigenvectors.

C.1 Characteristics For 1-D Shallow Water Equations

To illustrate the basic concept of the method of characteristics, a single homogeneous, quasilinear equation

$$\frac{\partial P}{\partial t} + u\frac{\partial P}{\partial x} = 0 \qquad \text{(C.1.1)}$$

will first be studied. In this equation, t and x are time and space coordinates, P the dependent variable, and u a variable which may be a function of x, t and P, but not of $\frac{\partial P}{\partial t}$ or $\frac{\partial P}{\partial x}$. Along a specific path defined by $\frac{dx}{dt} = u$, Equation (C.1.1) can be written as

$$\frac{dP}{dt} = 0 \qquad \text{(C.1.2)}$$

Equation (C.1.2) is called a characteristic equation for Equation (C.1.1), and the path is

called a characteristic curve. Compared with the original equation, the characteristic equation has the following advantages:

- It is an ordinary differentiation equation.
- P is invariant along the characteristic curve, and moves at a speed equal to u.

The first simplifies the problem. In particular, for a system of many equations, the original partial differential equations are transformed into a set of ordinary differential equations. The second feature assists in the physical interpretation of a system. These features of the characteristic equations make the method of characteristics attractive in dealing with a *quasilinear* system-a system with only derivatives of first order.

A systematic approach to the derivation of the characteristic equations for a quasilinear system in one spatial dimension is now considered for the one-spatial-dimension shallow water wave equations.

The 1-D shallow water wave equations are the continuity equation:

$$\frac{\partial h}{\partial t}+\frac{\partial (hu)}{\partial x}=0 \qquad \text{(C.1.3)}$$

and the momentum conservation equation:

$$\frac{\partial u}{\partial t}+u\frac{\partial u}{\partial x}=-g\frac{\partial h}{\partial x} \qquad \text{(C.1.4)}$$

where h(x,t) is the total water depth, u(x,t) the depth-averaged velocity, and g the gravitational acceleration. The non-homogeneous source terms have been omitted since they are not relevant to the characteristics of the system. By introducing a vector dependent variable $\bar{R}=[h,u]$, Equations (C.1.3) and (C.1.4) can be written as a single vector equation

$$(I\frac{\partial}{\partial t}+A\frac{\partial}{\partial x})\vec{R}=0 \tag{C.1.5}$$

in which I is a unit 2×2 matrix, and A is the coefficient matrix

$$A=\begin{vmatrix} u & h \\ g & u \end{vmatrix} \tag{C.1.6}$$

A characteristic curve S(x,t)=0 for a system will exist if a system of first-order equations can be transformed through a linear combination of the form

$$\vec{\ell}\bullet(\frac{\partial}{\partial t}+A\frac{\partial}{\partial x})\vec{R}=0 \tag{C.1.7}$$

into an equivalent system containing only derivatives along the curve S; $\vec{\ell}$ is an arbitrary vector (ℓ_1, ℓ_2).

Along the characteristic curve, one of the co-ordinates. say t, can be eliminated by differential calculus

$$dS=\frac{\partial S}{\partial x}dx+\frac{\partial S}{\partial t}dt=0 \tag{C.1.8}$$

or, along the curve S, as

$$\frac{\partial t}{\partial x}\Big|_s=-\frac{\partial S/\partial x}{\partial S/\partial t}=-\frac{n_x}{n_t} \tag{C.1.9}$$

where the components (n_t, n_x) of the normal vector $\vec{n}=\vec{\nabla}S$ are introduced. Then the partial derivatives along the line S can be written as

$$\frac{\bar{\partial}}{\partial x}=\frac{\partial}{\partial x}+\frac{\partial t}{\partial x}\frac{\partial}{\partial t}=\frac{\partial}{\partial x}-\frac{n_x}{n_t}\frac{\partial}{\partial t} \tag{C.1.10}$$

$$\frac{\bar{\partial}}{\partial t}=\frac{\partial}{\partial t}-\frac{n_x}{n_t}\frac{\partial}{\partial t}=0 \tag{C.1.11}$$

Introducing these relations into the linear combination (C.1.5) leads to

$$\vec{\ell} \bullet [I\frac{\partial}{\partial t} + A(\frac{\vec{\partial}}{\partial x} - \frac{n_x}{n_t}\frac{\partial}{\partial t})]\vec{R} = 0 \qquad \text{(C.1.12)}$$

A characteristic curve will exist for $\vec{R}$ if the system can be reduced to the form

$$\vec{\ell} \bullet A\frac{\vec{\partial}\vec{R}}{\partial x} = 0 \qquad \text{(C.1.13)}$$

Subtracting Equation (C.1.13) from Equation (C.1.12) gives

$$\vec{\ell} \bullet (n_t I + n_x A) = 0 \qquad \text{(C.1.14)}$$

For non-trivial solutions for $\vec{\ell}$, the determinant of the matrix (n_xA+n_tI) must be equal to zero, i.e.

$$\det(n_x A + n_t I) = 0 \qquad \text{(C.1.15)}$$

By introducing $\lambda = -\frac{n_t}{n_x}$, the above equation is an eigenvalue problem.

$$\det[A - \lambda I] = 0 \qquad \text{(C.1.16)}$$

The vector satisfying equation (C.1.14) is termed as a left eigenvector[1] for the matrix A. Substituting Equation(C.1.6) for A into Equation (C.1.16) gives

$$\det\begin{vmatrix} u-\lambda & h \\ g & u-\lambda \end{vmatrix} = 0 \qquad \text{(C.1.17)}$$

which leads to

$$(u-\lambda)^2 - gh = 0 \qquad \text{(C.1.18)}$$

Equation (C.1.18) gives two roots

---

[1] There are generally two eigenvectors corresponding to a matrix A, the left eigenvector which is defined by $\vec{\ell} \bullet (A - \lambda I) = 0$, and the right eigenvector, defined by $(A - \lambda I) \bullet \vec{\ell} = 0$.

$$\lambda_1 = u + C, \qquad \lambda_2 = u - C \tag{C.1.19}$$

in which $C=\sqrt{gh}$, the gravity wave celerity. Since the two eigenvalues are real and distinct, the 1-D shallow water wave equations are a hyperbolic system.

To derive the eigenvector $\bar{\ell}$, substitute the expressions for λ and A into Equation (C.1.14) giving, for λ_1=u-C,

$$\begin{cases} C\ell_1 + g\ell_2 = 0 \\ h\ell_1 + C\ell_2 = 0 \end{cases} \tag{C.1.20}$$

These equations are linearly dependent because the determinant of the coefficient matrix is zero. So only indefinite solutions for ℓ_1 and ℓ_2 can be obtained. But the ratio of ℓ_2 to ℓ_1 is uniquely given and can be obtained from either of Equations (C.1.20). It is equal to -C/g. Since the eigenvector is only used for linearly combining equations in Equation (C.1.7), only the ratio of its components are important. One component can be set arbitrarily. Setting ℓ_1=1, the eigenvector is then $\bar{\ell}_1 = [1, -\frac{C}{g}]$. Similarly, the eigenvector corresponding to the second eigenvalue $\lambda_2 = u + C$ is $\bar{\ell}_2 = [1, \frac{C}{g}]$.

For each eigenvalue and eigenvector, the corresponding characteristic equation is given by Equation (C.1.5). For λ_1, the characteristic equation is

$$\frac{\partial h}{\partial t} - \frac{C}{g}\frac{\partial u}{\partial t} + (u - C)\frac{\partial h}{\partial x} - (u - C)\frac{C}{g}\frac{\partial u}{\partial x} = 0 \tag{C.1.21}$$

By replacing h by C^2/g (from C^2=gh), and multiplying through by g/C, Equation (C.1.21) becomes

$$\frac{\partial (u - 2C)}{\partial t} + (u - C)\frac{\partial (u - 2C)}{\partial x} = 0 \tag{C.1.22}$$

or

$$\frac{d(u-2C)}{dt}=0 \qquad \text{along} \quad \frac{dx}{dt}=u-C \tag{C.1.23}$$

u-2C is the well-known Riemann invariant along the characteristic. The characteristic equation for the eigenvalue $\lambda_2 = u+C$ is

$$\frac{d(u+2C)}{dt}=0 \qquad \text{along} \quad \frac{dx}{dt}=u+C \tag{C.1.24}$$

The above procedure is valid for a quasiliner system of any number of equations. Since the characteristic path is defined by $\frac{dx}{dt}=\lambda$, the physical meaning of the eigenvalue is clear. It is just the speed at which information propagates along the characteristic curve. For the 1-D shallow water wave equations, there are two distinct eigenvalues, so from a point information propagates along two distinct paths.

C.2 Characteristic Properties For 2-D Shallow Water Equations

The 2-D shallow water wave equations are the continuity equation:

$$\frac{\partial h}{\partial t}+\frac{\partial (hu)}{\partial x}+\frac{\partial (hv)}{\partial y}=0 \tag{C.2.1}$$

and the x- and y-momentum equations:

$$\frac{\partial u}{\partial t}+u\frac{\partial u}{\partial x}+v\frac{\partial u}{\partial y}=-g\frac{\partial h}{\partial x} \tag{C.2.2}$$

$$\frac{\partial v}{\partial t}+u\frac{\partial v}{\partial x}+v\frac{\partial v}{\partial y}=-g\frac{\partial h}{\partial y} \tag{C.2.3}$$

Again all the non-homogeneous terms have been omitted. By introducing a vector dependent variable $\vec{R}=[h,u,v]$, Equations (C.2.1) through (C.2.3) may be grouped into a

single vector equation in quasilinear form:

$$(I\frac{\partial}{\partial t}+A_x\frac{\partial}{\partial x}+A_y\frac{\partial}{\partial y})\vec{R}=0 \qquad \text{(C.2.4)}$$

In which I is a unit 3×3 matrix, and the coefficient matrices are

$$A_x=\begin{vmatrix} u & h & 0 \\ g & u & 0 \\ 0 & 0 & u \end{vmatrix} \qquad \text{(C.2.5)}$$

$$A_y=\begin{vmatrix} v & 0 & h \\ 0 & v & 0 \\ g & 0 & v \end{vmatrix} \qquad \text{(C.2.6)}$$

Following Hirsch (1986), a characteristic surface S(t,x,y) in two spatial dimensions will exist if the first order system of equations, i.e. Equation (C.2.4), can be transformed through a linear combination of the form

$$\vec{\ell}\bullet(I\frac{\partial}{\partial t}+A_x\frac{\partial}{\partial x}+A_y\frac{\partial}{\partial y})\vec{R}=0 \qquad \text{(C.2.7)}$$

into an equivalent system containing only derivatives on the surface S, where $\vec{\ell}$ is an arbitrary vector (ℓ_1,ℓ_2,ℓ_3).

Along the surface S(x, y, t)=0, differential calculus allows one of the co-ordinates, say t, to be eliminated. Total differentiation of the surface function gives:

$$dS=\frac{\partial S}{\partial t}dt+\frac{\partial S}{\partial x}dx+\frac{\partial S}{\partial y}dy=0 \qquad \text{(C.2.8)}$$

Also along the surface S,

$$\frac{\partial t}{\partial x}=-\frac{\partial S/\partial x}{\partial S/\partial t}=-\frac{n_x}{n_t} \qquad \text{(C.2.9)}$$

$$\frac{\partial t}{\partial y} = -\frac{\partial S/\partial y}{\partial S/\partial t} = -\frac{n_y}{n_t} \tag{C.2.10}$$

where(n_t, n_x, n_y) are the components of the normal vector $\vec{n} = \vec{\nabla} S$. The partial derivative with respect to x along the surface S, $\overline{\partial / \partial x}$, is

$$\frac{\overline{\partial}}{\partial x} = \frac{\partial}{\partial x} + \frac{\partial t}{\partial x}\frac{\partial}{\partial t} = \frac{\partial}{\partial x} - \frac{n_x}{n_t}\frac{\partial}{\partial t} \tag{C.2.11}$$

Similar relationships can be established for y and t. For t, the derivative on the surface is equal to zero. Introducing these relations into the linear combination (C.2.7) leads to

$$\vec{\ell} \bullet [-I\frac{\partial}{\partial t} + A_x(\frac{\overline{\partial}}{\partial x} - \frac{n_x}{n_t}\frac{\partial}{\partial t}) + A_y(\frac{\overline{\partial}}{\partial y} - \frac{n_y}{n_t}\frac{\partial}{\partial t})]\vec{R} = 0 \tag{C.2.12}$$

A characteristic surface will exist for $\vec{R}$ if the system can be reduced to the form

$$\vec{\ell} \bullet (A_x\frac{\overline{\partial}}{\partial x} + A_y\frac{\overline{\partial}}{\partial y})\vec{R} = 0 \tag{C.2.13}$$

which requires that the surface S satisfies

$$\vec{\ell} \bullet (n_t I + n_x A_x + n_y A_y) = 0 \tag{C.2.14}$$

For nontrivial solutions for $\vec{\ell}$, the determinant of the matrix $(n_t I + n_x A_x + n_y A_y)$ must be zero, i.e.

$$\det\left| n_t I + n_x A_x + n_y A_y \right| = 0 \tag{C.2.15}$$

Introducing λ=- n_t, the above equation becomes an eigenvalue problem for the matrix ($n_x A_x$+ $n_y A_y$):

$$\det\left| (n_x A_x + n_y A_y) - \lambda I \right| = 0 \tag{C.2.16}$$

Substituting Equations (C.2.5) and (C.2.6) for A_x and A_y into the above equation gives

$$\det\begin{vmatrix} un_x + vn_y - \lambda & hn_x & hn_y \\ gn_x & un_x + vn_y - \lambda & 0 \\ gn_y & 0 & un_x + vn_y - \lambda \end{vmatrix} = 0 \qquad \text{(C.2.17)}$$

which can be expanded to

$$(un_x + vn_y - \lambda)[(un_x + vn_y - \lambda)^2 - gh(n_x^2 + n_y^2)] = 0 \qquad \text{(C.2.18)}$$

or

$$\alpha \cdot \beta = 0 \qquad \text{(C.2.19)}$$

where $\alpha = un_x + vn_y - \lambda$ and $\beta = (n_x u + n_y v - \lambda)^2 - gh(n_x^2 + n_y^2)$.

In the (n_x, n_y, λ) coordinate system, β=0 defines a characteristic normal cone, with apex at $(n_x, n_y, \lambda)_{apex}$=(0,0,0), cutting the planes α=constant in circles. α=0 is a characteristic normal plane. Therefore, there are two families of characteristic normal, a normal cone and a normal plane.

From β=0, there are two distinct eigenvalues:

$$\lambda_{1,2} = un_x + vn_y \pm C \cdot \sqrt{(n_x^2 + n_y^2)} \qquad \text{(C.2.20)}$$

in which $C=\sqrt{gh}$. From α=0, a third eigenvalue is obtained as

$$\lambda_3 = un_x + vn_y \qquad \text{(C.2.21)}$$

By introducing cylindrical coordinates, $n_x = r\cos(\theta)$ and $n_y = r\sin(\theta)$, the eigenvalues can be written as

$$\lambda_{1,2} = r[u\cos(\theta) + v\sin(\theta) \pm C] \qquad \text{(C.2.22)}$$

and

$$\lambda_3 = r[u\cos(\theta) + v\sin(\theta)] \qquad \text{(C.2.23)}$$

Since the eigenvalues are real and distinct, this system is hyperbolic.

Note that λ, n_x, and n_y are all proportional to r, so the value of r can be set arbitrarily. By choosing r=1, the eigenvalues take the form:

$$\lambda_{1,2} = u\cos\theta + v\sin\theta \pm C \tag{C.2.24}$$

and

$$\lambda_3 = u\cos\theta + v\sin\theta \tag{C.2.25}$$

The characteristic normal vectors in (x,y,t) space are

$$\vec{n}_i = (\cos\theta, \sin\theta, \lambda_i) \qquad i=1,2,3 \tag{C.2.26}$$

As in one spatial dimension, the eigenvalue represents the speed at which the information propagates along the characteristic surfaces.

It is further observed that $u\cos(\theta)+v\sin(\theta)$ is the projection of a resultant velocity vector $\hat{U}$ on the θ direction, as denoted by $U(\theta)$ in Figure C.1.

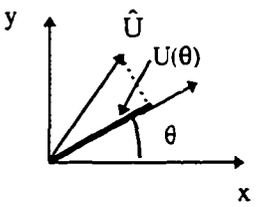

Figure C.1 Velocity Projection On A Directional Line

If using the projected velocity, the eigenvalues can be written more simply as

$$\lambda_{1,2} = U(\theta) \pm C \tag{C.2.27}$$

and

$$\lambda_3 = U(\theta) \tag{C.2.28}$$

Equation (C.2.27) gives exactly the same expression for the eigenvalue as in one spatial dimension except that in two spatial dimensions a nominal velocity is used. The third eigenvalue is always equal to the velocity projection. Along a streamline, say at an angle ϕ with the x-axis, the eigenvalues are $\lambda_{1,2}(\phi) = \hat{U} \pm C$ and $\lambda_3(\phi) = \hat{U}$. Here the velocity is real representing a resultant velocity. The streamline is of special interest because the maximum eigenvalue always occurs on this line. The maximum eigenvalue is important in numerical simulation as it dictates the stability criterion-the CFL condition.

On the x-axis, the three eigenvalues are $\lambda_{1,2}(0) = u \pm C$ and $\lambda_3(0) = u$; and on the y-axis, the eigenvalues are $\lambda_{1,2}(90°) = v \pm C$ and $\lambda_3(90°) = v$.

Corresponding to each eigenvalue, Equation (C.2.14) defines a set of relationships among the components of an eigenvector. For λ_1, Equation (C.2.14) becomes

$$\begin{cases} C\ell_1 + g\cos\theta\ell_2 + g\sin\theta\ell_3 = 0 \\ h\cos\theta\ell_1 + C\ell_2 = 0 \\ h\cos\theta\ell_1 + C\ell_3 = 0 \end{cases} \qquad \text{(C.2.29)}$$

Again these equations are not linearly independent because the determinant of the Jacobian coefficient matrix is always zero. Thus only indefinite solutions can be obtained. By setting ℓ_1=1, ℓ_2 and ℓ_3 can be obtained from any two equations in Equation (C.2.29). The eigenvector for λ_1 is $\vec{\ell}_1 = [1, -\frac{h\cos\theta}{C}, -\frac{h\sin\theta}{C}]$.

Similarly, the eigenvector corresponding to the eigenvalue λ_2 can be obtained as $\vec{\ell}_2 = [1, \frac{h\cos\theta}{C}, \frac{h\sin\theta}{C}]$. And the eigenvector for λ_3 is $\vec{\ell}_3 = [0, 1, -C\tan\theta]$.

Orthogonal to each normal vector defined by Equation (C.2.26), there is a characteristic surface. The characteristics corresponding to λ_1 and λ_2 are termed *wave characteristics* because the eigenvalues are related to the gravity wave speed. And the characteristics corresponding to λ_3 are termed *flow characteristics* because the eigenvalue is only related to flow velocity. The characteristic surfaces of these two families are also significantly different. The characteristic surfaces of the first family are orthogonal to the normal cone (β=0) and are inscribed by a conoid, cutting any plane parallel to the x-y plane in circles, as shown in Figure C.2. The characteristic cone is defined by:

$$(dx - u\,dt)^2 + (dy - v\,dt)^2 = gh\,(dt)^2 \qquad \text{(C.2.30)}$$

The line of tangency between the cone and a characteristic surface is called a bi-characteristics

The characteristic surfaces of the second family consist of surfaces whose normal vectors lie on a common plane, the α=0 plane. The mutual intersection of these surfaces is a curve whose projection on the x-y plane is a streamline. The line is defined by:

$$dx=u\,dt,\ dy=v\,dt,\ dt=dt \qquad \text{(C.2.31)}$$

This line is also the central axis of the characteristic cone of the first family.

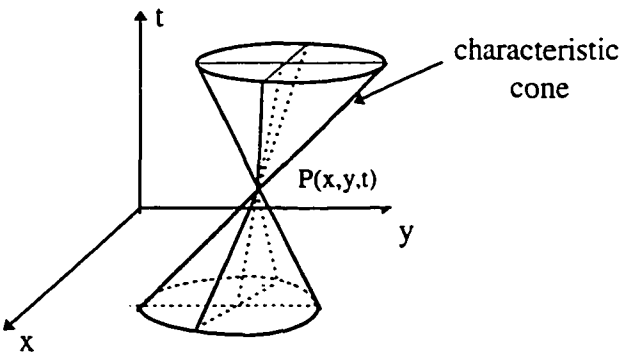

Figure C.2 The Characteristic Cone And Streamline

As shown in Figure C.2, there are two limbs of the characteristic conoid from a point. A disturbance initiated at the point propagates along the bi-characteristics in the positive t direction. Accordingly, no point outside this conoid is influenced by the disturbance. Thus the convex hull of the upper conoid represents the domain of influence for the point. On the other hand, disturbances at an earlier time outside the lower conoid do not influence the point. Thus the convex hull of the lower conoid is the domain of dependence for the solution point.

The eigenvectors, bi-characteristics and characteristic surfaces are all defined in the (x-y-t) solution space. Thus the eigenvector is not a physical vector, nor are the characteristic surfaces physical surfaces. The characteristic surfaces represent wave fronts in the (x-y-t) space.

The characteristic equations can be derived by substituting the expressions for the eigenvectors back into Equation (C.2.7). For λ_1,

$$(1,-\frac{h\cos\theta}{C},-\frac{h\sin\theta}{C})\bullet\begin{bmatrix}\frac{\partial h}{\partial t}\\ \frac{\partial u}{\partial t}\\ \frac{\partial v}{\partial t}\end{bmatrix}+(1,-\frac{h\cos\theta}{C},-\frac{h\sin\theta}{C})\bullet\begin{vmatrix}u & h & 0\\ g & u & 0\\ 0 & 0 & u\end{vmatrix}\bullet\begin{bmatrix}\frac{\partial h}{\partial x}\\ \frac{\partial u}{\partial x}\\ \frac{\partial v}{\partial x}\end{bmatrix}$$
$$+(1,-\frac{h\cos\theta}{C},-\frac{h\sin\theta}{C})\bullet\begin{vmatrix}v & 0 & h\\ 0 & v & 0\\ g & 0 & v\end{vmatrix}\bullet\begin{bmatrix}\frac{\partial h}{\partial y}\\ \frac{\partial u}{\partial y}\\ \frac{\partial v}{\partial y}\end{bmatrix}=0 \qquad (C.2.32)$$

which leads to

$$\frac{\partial h}{\partial t}-\frac{C\cos\theta}{g}\frac{\partial u}{\partial t}-\frac{C\sin\theta}{g}\frac{\partial v}{\partial t}+(u-C\cos\theta)\frac{\partial h}{\partial x}+\frac{C}{g}(C-u\cos\theta)\frac{\partial u}{\partial x}$$
$$-\frac{Cu\sin\theta}{g}\frac{\partial v}{\partial x}+(v-C\sin\theta)\frac{\partial h}{\partial y}-\frac{Cv\cos\theta}{g}\frac{\partial u}{\partial y}+\frac{C}{g}(C-v\sin\theta)\frac{\partial v}{\partial y}=0 \qquad \text{(C.2.33)}$$

Grouping the above equation based on each dependent variable gives

$$\begin{aligned}&\frac{\partial h}{\partial t}+(u-C\cos\theta)\frac{\partial h}{\partial x}+(v-C\sin\theta)\frac{\partial h}{\partial y}\\&-\frac{C\cos\theta}{g}\frac{\partial u}{\partial t}-\frac{C\cos\theta}{g}(u-C\cos\theta)\frac{\partial u}{\partial x}-\frac{C\cos\theta}{g}(v-C\sin\theta)\frac{\partial u}{\partial y}\\&-\frac{C\sin\theta}{g}\frac{\partial v}{\partial t}-\frac{C\sin\theta}{g}(u-C\cos\theta)\frac{\partial v}{\partial x}+\frac{C\sin\theta}{g}(v-C\sin\theta)\frac{\partial v}{\partial y}\\&+\sin\theta\,(C\sin\theta\frac{\partial u}{\partial x}-C\cos\theta\frac{\partial u}{\partial y})-\cos\theta\,(C\sin\theta\frac{\partial v}{\partial x}-C\cos\theta\frac{\partial v}{\partial y})=0\end{aligned} \qquad \text{(C.2.34)}$$

This equation is universally valid since it is just a linear combination of the original equations through the components of the characteristic vector. But it only describes information propagation at a specific speed. By introducing the differentiation along a bi-characteristic curve, Equation (C.2.34) can be further simplified to

$$\frac{dh}{d\tau}-\frac{C\cos\theta}{g}\frac{du}{d\tau}-\frac{C\sin\theta}{g}\frac{dv}{d\tau}+\frac{C\sin\theta}{g}\frac{du}{d\phi}-\frac{C\cos\theta}{g}\frac{dv}{d\phi}=0 \qquad \text{(C.2.35)}$$

where

$$\frac{d}{d\tau}=\frac{\partial}{\partial t}+(u-C\cos\theta)\frac{\partial}{\partial x}+(v-C\sin\theta)\frac{\partial}{\partial y} \qquad \text{(C.2.36)}$$

$$\frac{d}{d\phi}=C\sin\theta\frac{\partial}{\partial x}-C\cos\theta\frac{\partial}{\partial y} \qquad \text{(C.2.37)}$$

The parameter $\tau(x,y,t)$ is a parametric expression for the bi-characteristics. $\phi(x,y,t)$ is a parametric expression for the curves on the characteristic conoid cut by a t=constant plane. The relationship between parameters τ and ϕ will be discussed in detail in

Appendix D.

As in one spatial dimension, the water depth h may be replaced by C^2/g. After some algebraic manipulation, Equation (C.2.37) reduces further to

$$\frac{d(2C-u\cos\theta-v\sin\theta)}{d\tau}-\frac{d(v\cos\theta-u\sin\theta)}{d\phi}=0 \qquad (C.2.38)$$

This equation, in contrast of equation (C.2.34), is only valid along the bi-characteristics. Unlike in one spatial dimension, the characteristic equations still involve derivatives in two independent directions. The characteristic equations are still partial differential equations. Compared to the original equations, the derivatives are in one lower dimensions. Besides, the characteristic equation contains the direction θ which is defined within $(-\pi, \pi)$. So there are an infinite number of characteristic equations for each eigenvalue. These features make numerical solutions by the method of characteristics in two spatial dimensions totally different from that in one spatial dimension.

Similarly, the characteristic equation for the eigenvalue λ_2 can be obtained as

$$\frac{dh}{d\tau}+\frac{C\cos\theta}{g}\frac{du}{d\tau}+\frac{C\sin\theta}{g}\frac{dv}{d\tau}-\frac{C\sin\theta}{g}\frac{du}{d\phi}+\frac{C\cos\theta}{g}\frac{dv}{d\phi}=0 \qquad (C.2.39)$$

or

$$\frac{d(2C+u\cos\theta+v\sin\theta)}{d\tau}+\frac{d(v\cos\theta-u\sin\theta)}{d\phi}=0 \qquad (C.2.40)$$

where

$$\frac{d}{d\tau}=\frac{\partial}{\partial t}+(u+C\cos\theta)\frac{\partial}{\partial x}+(v+C\sin\theta)\frac{\partial}{\partial y} \qquad (C.2.41)$$

and

$$\frac{d}{d\phi} = -C\sin\theta\frac{\partial}{\partial x} + C\cos\theta\frac{\partial}{\partial y} \qquad \text{(C.2.42)}$$

Equation (C.2.38) is equivalent to Equation (C.2.35) since θ ranges from $-\pi$ to π and $\sin(\theta+\pi)=-\sin\theta$, $\cos(\theta+\pi)=-\cos\theta$. Equation (C.2.39) is the most common form of characteristic equations in the literature. It is clear that the derivative $d/d\phi$ in equation (C.2.42) is the directional derivative along the normal of the characteristic surfaces, but multiplied by C. The quantity $v\cos\theta - u\sin\theta$ is the projection of the velocity vector on the normal. Equation (C.2.40) is readily reduced to the Riemann invariant form in one spatial dimension by substituting $\theta=0$ and $v=0$. The variable $2C+u\cos\theta+v\sin\theta$ is invariant along the characteristic surfaces if $(v\cos\theta - u\sin\theta)$ is constant along the normal line to the vector $(\cos\theta, \sin\theta)$ in x-y plane. This is ensured by choosing $\theta=\tan^{-1}(\frac{v}{u})$ or along the streamline. So along the streamline, $\hat{U} \pm 2C = \text{constant}$, where $\hat{U}$ is the resultant velocity. The system in two spatial dimensions along the streamline behaves exactly the same as in one space dimension.

The characteristic equation corresponding to the eigenvalue λ_3 is

$$-\sin\theta\left(\frac{\partial u}{\partial t} + u\frac{\partial u}{\partial x} + v\frac{\partial u}{\partial y} + g\frac{\partial h}{\partial x}\right) + \cos\theta\left(\frac{\partial v}{\partial t} + u\frac{\partial v}{\partial x} + v\frac{\partial v}{\partial y} + g\frac{\partial h}{\partial y}\right) = 0 \qquad \text{(C.2.43)}$$

Equation (C.2.43) is just the y-momentum equation multiplied by $\cos\theta$ minus the x-momentum equation multiplied by $\sin\theta$. This equation can be further simplified by introducing the differentiation along the line defined by Equation (C.2.31):

$$-\sin\theta\frac{d\,u}{d\gamma} + \cos\theta\frac{dv}{d\gamma} + \frac{g}{C}\frac{dh}{d\phi} = 0 \qquad \text{(C.2.44)}$$

Replacing h by C^2/g and combining the first two terms leads to

$$\frac{d(v\cos\theta - u\sin\theta)}{d\gamma} + \frac{d(2C)}{d\phi} = 0 \tag{C.2.45}$$

in which

$$\frac{d}{d\gamma} = \frac{\partial}{\partial t} + u\frac{\partial}{\partial x} + v\frac{\partial}{\partial y} \tag{C.2.46}$$

and $d/d\phi$ is as defined in Equation (C.2.42). Again the characteristic equations, i.e. Eqs. (C.2.45), involve differentiations in two independent directions, one fewer than in the original partial differential equations. Equation (C.2.45) is similar to Equation (47) of Lin and Shen (1984). The characteristic equations for the three eigenvalues involve differentiation in three directions, that is, the line defined by γ, bi-characteristics τ and information front ϕ (to be discussed in detail in Appendix D).

One important fact about the characteristic equations is that there are infinite characteristic equations, but there are only three unknowns. Daubert and Graffe (1967) proved uniqueness of solutions for the shallow water wave equations for a pure initial value problem. Since the solutions are unique, there should be only three independent characteristic equations (Ransom et al. 1972). A simple proof is given here. Denoting the eigenvector in direction θ as $L(\theta)$, then the three eigenvectors are recast as a 3×3 matrix:

$$L(\theta) = \begin{bmatrix} \vec{\ell}_1^{\,\theta} \\ \vec{\ell}_2^{\,\theta} \\ \vec{\ell}_3^{\,\theta} \end{bmatrix} = \begin{bmatrix} 1 & -\frac{h\cos\theta}{C} & -\frac{h\sin\theta}{C} \\ 1 & \frac{h\cos\theta}{C} & \frac{h\sin\theta}{C} \\ 0 & \sin\theta & -\cos\theta \end{bmatrix} \tag{C.2.49}$$

Adding an arbitrary angle ε to θ, the corresponding eigenvectors L(θ+ε) will be

$$L(\theta+\varepsilon)=\begin{bmatrix}\bar{\ell}_1^{\theta+\varepsilon}\\ \bar{\ell}_2^{\theta+\varepsilon}\\ \bar{\ell}_3^{\theta+\varepsilon}\end{bmatrix}=\begin{bmatrix}1 & -\dfrac{h\cos(\theta+\varepsilon)}{C} & -\dfrac{h\sin(\theta+\varepsilon)}{C}\\ 1 & \dfrac{h\cos(\theta+\varepsilon)}{C} & \dfrac{h\sin(\theta+\varepsilon)}{C}\\ 0 & \sin(\theta+\varepsilon) & -\cos(\theta+\varepsilon)\end{bmatrix} \tag{C.2.49}$$

If a eigenvector at the direction θ+ε for an arbitrary ε, L(θ+ε), can be obtained through a linear combination of the component vectors of L(θ), then L(θ+ε) is dependent on L(θ). By inspection, the following relationships always exist:

$$\begin{cases}\bar{\ell}_1^{\theta+\varepsilon}=\dfrac{1}{2}[\bar{\ell}_1^{\theta}+\bar{\ell}_2^{\theta}+\cos\varepsilon(\bar{\ell}_1^{\theta}-\bar{\ell}_2^{\theta})]-\dfrac{h\sin\varepsilon}{C}\bar{\ell}_3^{\theta}\\ \bar{\ell}_2^{\theta+\varepsilon}=\dfrac{1}{2}[\bar{\ell}_1^{\theta}+\bar{\ell}_2^{\theta}-\cos\varepsilon(\bar{\ell}_1^{\theta}-\bar{\ell}_2^{\theta})]+\dfrac{h\sin\varepsilon}{C}\bar{\ell}_3^{\theta}\\ \bar{\ell}_3^{\theta+\varepsilon}=\sin\varepsilon(\bar{\ell}_1^{\theta}-\bar{\ell}_2^{\theta})+\cos\varepsilon\,\bar{\ell}_3^{\theta}\end{cases} \tag{C.2.50}$$

This shows that L(θ+ε) is dependent on L(θ), and proves that there are only three independent characteristic equations, since ε is an arbitrary angle.

It is also interesting to notice that the integral of the characteristic equations of wave characteristics over θ=(0,2π) is exactly the continuity equation and the integral of the characteristic equations of flow characteristic over θ=(0,2π) is trivial.

It can also be shown that the Equations (2.39) in four different directions with uniform π/2 angular spacing constitute an independent set of characteristic equations which is equivalent to the set of characteristic equations along any one of the four

directions. The proof is given here.

Along any given angle θ, the eigenvector for Equation (C.2.39) is $\bar{\ell}_2^{\theta} = [1, \quad \frac{h\cos\theta}{C}, \quad \frac{h\sin\theta}{C}]$. Along the direction θ+π,

$$\bar{\ell}_2^{\theta+\pi} = [1, \quad \frac{h\cos(\theta+\pi)}{C}, \quad \frac{h\sin(\theta+\pi)}{C}] = [1, \quad -\frac{h\cos\theta}{C}, \quad -\frac{h\sin\theta}{C}] \qquad \text{(C.2.51)}$$

which is equal to $\bar{\ell}_1^{\theta}$. Similarly, along θ+π/2 and θ+3π/2, the eigenvectors $\bar{\ell}_2$ are $\bar{\ell}_2^{\theta+\pi/2} = [1, \quad -\frac{h\sin\theta}{C}, \quad \frac{h\cos\theta}{C}]$ and $\bar{\ell}_2^{\theta+3\pi/2} = [1, \quad \frac{h\sin\theta}{C}, \quad -\frac{h\cos\theta}{C}]$. the average of $\bar{\ell}_2^{\theta+\pi/2}$ and $\bar{\ell}_2^{\theta+3\pi/2}$ is equal to $\bar{\ell}_3^{\theta}$. So characteristic equations (Equation C.2.39) in θ=π, 3π/2, 0 and π can be combined into a three linearly independent equations which are exactly the same as the three characteristic equations corresponding to λ_1 λ_2 and λ_3 in any of the four direction.

Thus the characteristic equation corresponding to the flow characteristics can not be used for obtaining numerical solutions, because they can be combined from the characteristic equations for wave characteristics in two perpendicular directions. The most common choices of the directions for setting up characteristic equations are θ=π, 3π/2, 0, π (Townson,1974).

APPENDIX D CHARACTERISTICS IN TWO SPATIAL DIMENSIONS

This appendix will focus on the general properties of characteristic surfaces, the physical meaning of a bi-characteristics, the relationship between the bi-characteristics and other curves on the characteristic surfaces, and finally on how to determine the bi-characteristics if the eigenvalues are known.

D.1. General Properties of Characteristic Surfaces

The following properties of characteristic surfaces are noteworthy:

- Corresponding to each eigenvalue λ, there is a characteristic surface. The normal vector $\bar{N}$ of the characteristic surface is proportional to $(-\lambda(\theta), \cos\theta, \sin\theta)$, where θ is the azimuth at which the eigenvalue is obtained.
- If a vector $\bar{S}(\Delta t, \Delta x, \Delta y)$ on the characteristic surface is not perpendicular to the t axis, Δx and Δy may be interpreted as diplacments in x and y direction during a time interval Δt. In particular, if Δt is equal to unity, the corresponding Δx and Δy take the values of the velocity components in x and y directions, say C^l_x and C^l_y, respectively. Then this vector is expressed by $\bar{S}\ (1, C^l_x, C^l_y)$. This vector is perpendicular to the normal vector $\bar{N}(-\lambda, \cos\theta, \sin\theta)$ to the surface, leading to

$$\bar{S} \cdot \bar{N} = (1, C^l_x, C^l_y) \cdot (-\lambda, \cos\theta, \sin\theta) = 0 \qquad (D.1)$$

or

$$C^l_x \cdot \cos\theta + C^l_y \sin\theta = \lambda \qquad (D.2)$$

This relationship is valid for any line vector on the characteristic surface which is not perpendicular to the t axis.

- The vectors on the characteristic surfaces perpendicular to the t axis may generally expressed by $(0, C^2_x, C^2_y)$. C^2_x and C^2_y can no longer be interpreted as velocity but a vector on (x,y) plane. This vector is also perpendicular to the surface normal vector, such that

$$C^2_x \cdot \cos\theta + C^2_y \cdot \sin\theta = 0 \qquad (D.3)$$

- Bi-characteristics is the line of tangency between a characteristic surface and a characteristic cone, see Figure D.1. The characteristic cone is a cone insecribing the characteristic surfaces for entire azimuth $(0,2\pi)$. The bi-characteristics is important to the numerical simulation with the method of characteristics (MOC) because it is the path normally used for integration of the characteristic equations.

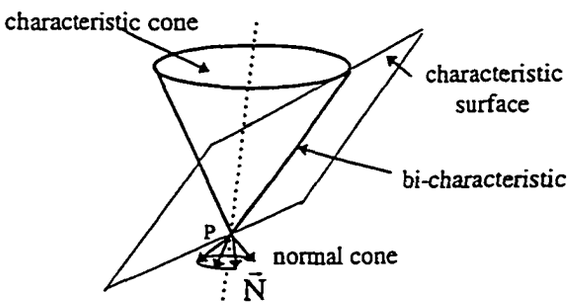

Figure D.1 Relationship among characteristic surfaces, characteristic cone and bi-characteristics.

Different from other lines on the characteristic surface, the bi-characteristics is the linkage among the characteristics in different directions because the characteristic cone is the linkage among the characteristics in all directions. Thus the bi-characteristics can not be determined by the eigenvalue and eigenvector in a specific direction alone. To determine the bi-characteristics, the equation for the characteristic cone must be known. The domain enclosed by the bi-characteristics is the domain of influence or the domain of dependence.

- The derivatives in characteristic equations are only along the characteristic surface. In other words, the derivatives are with respect to two independent variables.

D.2 Integration Paths

For a hyperbolic system with three independent variables, all derivatives in characteristic equations can be written with respect to just two parameters. There are, however, infinite pairs of non-parallel vectors on the characteristic surface which can serve as the dual directions for the derivatives in the characteristic equation.

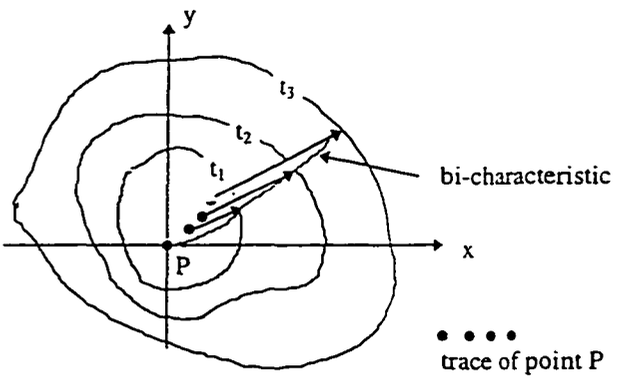

Figure D.2 Information Front Propagation

But only two vectors on the characteristic surface can be associated with the information propagation. One is the t=constant line which is just the front of the information propagation at time t, see Figure D.2. The other is the bi-characteristics whose projection on x-y plane is the trace of information propagation. Hence the t=constant direction and bi-characteristics form a pair of directions which is physically most meaningful. The t=constant vector is normally not perpendicular to the bi-characteristics due to the continuous advection of the apex of the characteristic cone. For

numerical simulation, the derivatives in the characteristic equations should be defined in these two directions.

To determine the bi-characteristics and t=constant vector, the characteristic cone equation should be known first. General expressions for these two vectors can be established by using Equations (D.2) and (D.3). First the eigen-value, $\lambda(\theta)$, is expanded into a Fourier series:

$$\lambda = C + \sum_{i=1,2,\ldots} u_i \cos i\theta + v_i \sin i\theta \tag{D.4}$$

in which the coefficients are

$$C = \frac{1}{2\pi}\int_0^{2\pi} \lambda \, d\theta \tag{D.5}$$

$$u_i = \frac{1}{\pi}\int_0^{2\pi} \lambda \cos i\theta \, d\theta \tag{D.6}$$

$$v_i = \frac{1}{\pi}\int_0^{2\pi} \lambda \sin i\theta \, d\theta \tag{D.7}$$

and u_i, v_i and C are not dependent on the azimuth θ. For the present system, the higher order terms are much smaller than the constant and the first order terms. Thus the terms of second order or higher can be omitted. The subscript "i" will be dropped from now on.

If $|u| \ll |C|$ and $|v| \ll |C|$ at any time and position, the eigenvalue does not vary significantly with the direction, and information radially propagates away in all directions at an almost uniform speed. Such characteristics are non-directional characteristics. On the other hand, if $|u| \gg |C|$ or $|v| \gg |C|$ at any time and position, then the eigenvalue would vary appreciably with the direction. Such characteristics are directional characteristics.

The flow characteristics of the shallow water wave equations (See Appendix C) is a directional characteristics, while the wave characteristics is a non-directional characteristics if the Froude number is much smaller than unity.

Physically (u,v) in Equation (D.4) is the velocity vector of advection of the apex of a characteristic cone, shown as the dotted points in Figure D.2. The center line of the characteristic cone is a line whose projection on x-y plane is a streamline. Let $\vec{U}$ denote the velocity vector at the apex of the characteristic cone, the bi-characteristic vector $\vec{S}_1$ and t=constant vector $\vec{S}_2$ are related as

$$(\vec{S}_1 - \vec{U}) \bullet \vec{S}_2 = 0 \tag{D.8}$$

as shown in Figure D.3

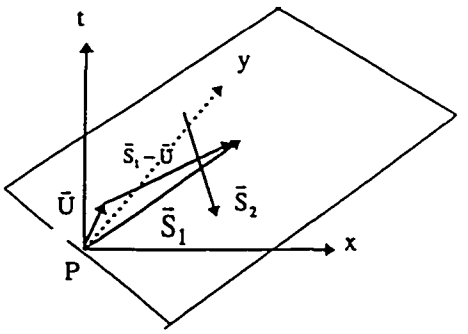

Figure D.3 Illustration of the relationship between bi-characteristics and t=constant vector

If the bi-characteristic is written

$$\frac{dx}{dt} = C_x^b = g_1 \cos\theta + g_2 \sin\theta + g_3 \tag{D.9}$$

$$\frac{dy}{dt} = C_y^b = h_1 \cos\theta + h_2 \sin\theta + h_3 \tag{D.10}$$

Then substituting the above expressions for C_x^b and C_y^b and Equation (D.4) for the eigen-value λ into Equation (D.2) gives

$$\begin{cases} g_3 = u, & h_3 = v \\ g_1 = C, & h_2 = C \\ g_2 = h_1 \end{cases} \tag{D.11}$$

Then C_x^b and C_y^b are

$$C_x^b = u + C\cos\theta + g_2 \sin\theta \tag{D.12}$$

$$C_y^b = v + C\sin\theta - g_2 \cos\theta \tag{D.13}$$

The coefficient g_2 can be determined by substituting C_x^b and C_y^b into the equation for the characteristic cone. Actually Equations (D.12) and (D.13) may be used to define any line vector on the characteristic surface which is not perpendicular to the t-axis. The t=constant line can be defined by setting t=constant in the equation for the characteristic cone.

D.3 Bi-Characteristics And CharacteristicEquations In A Special Case

As indicated in Section D.2, the determination of bi-characteristics depends on the knowledge of the equation of a characteristic cone. In this section, a brief introduction is given about determining the equation for the characteristic cone for a special system in which the characteristics surfaces $x_3(x, y, t)$=constant satisfying

$$A_{ij} \frac{\partial x_3}{\partial x_i} \frac{\partial x_3}{\partial x_j} = 0 \tag{D.14}$$

where x_i=(x,y,t), i=1, 2, 3, and A_{ij} is a 3×3 matrix. Many hydrodynamic and aerodynamic systems, including the shallow water wave equations, satisfy Equation(D.14).

For this special case, Butler (1960) and Richardson (1984) derived expressions for the characteristic cone, the bi-characteristics and characteristic equations. The following presentation is mainly based on Richardson (1984)

(a) Characteristic Cone

First note that to the normal to characteristic surfaces $\dot{x_3}(x,y,t)$=constant is proportional to $\partial \dot{x_3} / \partial x_i$. Equation (D.14) may then be replaced by

$$A_{ij} L_i L_j = 0 \tag{D.15}$$

where L_i are the direction cosines of the normal to the surfaces $\dot{x_3}$ =constant. Equation (D.15) indicates that the surfaces $\dot{x_3}(x,y,t)$=constant satisfying Equation (D.15) touch a quadric cone. Also there may be an infinite number of characteristic surfaces through each point because the normal vector L_i is not uniquely defined. The infinity of the characteristic surfaces may be identified by a parameter ϕ, $0 \le \phi \le 2\pi$; ϕ will also identify the particular surface $\dot{x_3}$=constant.

All surfaces $\dot{x_3}$=constant satisfying (D.14) will be inscribed by a cone, which may be fully described by two independent parameters, ϕ and τ, i.e.,

$$x_i = x_i(\phi, \tau) \tag{D.16}$$

where τ is a measure of time for a point moving from the apex of the cone to a subsequent point, as shown in Figure D.4. ϕ=constant identifies curves on both the characteristic cone and characteristics surfaces. These curves are called bi-characteristics. The surfaces τ=constant are time-constant planes cutting through the characteristic cone.

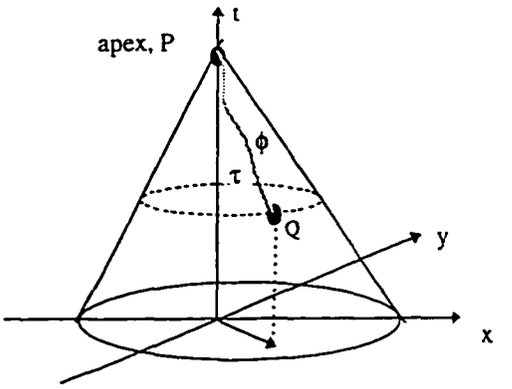

Figure D.4 Parametrization of a Characteristic Cone

The characteristics plane at a point, say P, will satisfy

$$L_i dx_i = 0 \qquad \text{(D.17)}$$

where dx_i are directions within the characteristic surface.

The characteristic cone $x_i=x_i(\phi, \tau)$, being the envelope of the surfaces x_3=constant, will satisfy the eliminant of (D.15) and (D.17), and

$$\frac{\partial L_i}{\partial \phi} dx_i = 0 \qquad \text{(D.18)}$$

Now,

$$L_i \frac{\partial L_i}{\partial \phi} = 0 \qquad \text{(D.19)}$$

and therefore $L_i, \frac{\partial L_i}{\partial \phi}$, *and* dx_i form three mutually orthogonal vectors for each ϕ.

The vector $A_{ij}L_j$ may thus be expressed in terms of $L_i, \frac{\partial L_j}{\partial \phi}$ and dx_i

$$A_{ij}L_j = aL_i + b\frac{\partial L_i}{\partial \phi} + cdx_i \qquad \text{(D.20)}$$

Now

$$A_{ij}L_jL_i = A_{ij}L_j\frac{\partial L_i}{\partial \phi} = 0 \qquad \text{(D.21)}$$

Equation (D.21) essentially states that $A_{ij}L_i$ is perpendicular to the plane of tangency to the normal cone, or it is proportional to the bi-characteristic direction. Hence

$$A_{ij}L_j = c\,dx_i, \qquad \text{(D.22)}$$

giving

$$L_j = cA_{ij}^{-1}dx_i, \qquad \text{(D.23)}$$

The equation of the cone surface at the point P is thus

$$A_{ij}^{-1}dx_i dx_j = 0 \qquad \text{D.24)}$$

(b) Bi-characteristics and Compatibility Equations

If the position at the previous time step is at P, and at the subsequent time step at Q (see Figure D.4), the line vector from P to Q may be expressed as

$$dx_i = \frac{\partial x_i}{\partial \tau}d\tau + \frac{\partial x_i}{\partial \phi}d\phi \qquad \text{(D.25)}$$

let $dx_i = (\zeta_i + \mu_i\cos\theta + \nu_i\sin\theta)d\tau$ be the displacements satisfying the equation of the cone at its apex, where θ is the orientation. and ζ_i, μ_i, and ν_i are the coefficients to be determined. This is so for suitable ζ_i, μ_i, and ν_i for $0 \le \theta \le 2\pi$, which satisfy

$$\begin{aligned} -A_{ij}^{-1}\zeta_i\zeta_j = A_{ij}^{-1}\mu_i\mu_j = A_{ij}^{-1}\nu_i\nu_j \\ A_{ij}^{-1}\nu_i\zeta_j = A_{ij}^{-1}\mu_i\nu_j = A_{ij}^{-1}\zeta_i\nu_j = 0 \end{aligned} \qquad \text{(D.26)}$$

The conditions (D.26) ensure that the directions dx_i satisfy the condition (D.24) and permit ζ to be any vector lying inside the characteristic cone. The direction given by (D.25) will lie on the cone through P only if

$$(\zeta_i + \mu_i \cos\theta + \nu_i \sin\theta)A_{ij}^{-1}(\frac{\partial x_1}{\partial \tau}d\tau + \frac{\partial x_1}{\partial \phi}d\phi) = 0 \qquad \text{at Q.} \tag{D.27}$$

But at Q

$$(\zeta_i + \mu_i \cos\theta + \nu_i \sin\theta)A_{ij}^{-1}\frac{\partial x_i}{\partial \tau} = 0 \tag{D.28}$$

so

$$(\zeta_i + \mu_i \cos\theta + \nu_i \sin\theta)A_{ij}^{-1}\frac{\partial x_1}{\partial \phi} = 0 \tag{D.29}$$

Physically, Equation (D.28) means exactly the same as Equation (D.2), and Equation (D.29) the same as Equation (D.3). Furthermore, in Equations (D.28) and (D.29), $\frac{\partial x_i}{\partial \tau} \propto (1, C_x^1, C_y^1)$ and $\frac{\partial x_i}{\partial \phi} \propto (0, C_x^2, C_y^2)$, and

$$(\zeta_i + \mu_i \cos\theta + \nu_i \sin\theta)A_{ij}^{-1} \propto (\cos\phi, \sin\phi, -\lambda) \tag{D.30}$$

where "$\propto$" denotes proportionality.

Thus $A^{-1}{}_{ij}$ is just a transformation matrix between a line vector on the characteristic cone and a normal vector. Since the two cones, the one through P and the one through Q, touch on a common bi-characteristic, the equation of each bi-characteristic through P is

$$dx_i = (\zeta_i + \mu_i \cos\theta + \nu_i \sin\theta)d\tau \tag{D.31}$$

$$(\zeta_i + \mu_i \cos\theta + \nu_i \sin\theta)A_{ij}^{-1}\frac{\partial x_1}{\partial \phi} = 0 \tag{D.32}$$

$$\theta = \phi \text{ at } \tau = 0 \tag{D.33}$$

For the shallow water wave equations, the above equations become

$$
\begin{aligned}
&dt = d\tau \\
&dx = (u + C\cos\theta)d\tau \\
&dy = (v + C\sin\theta)d\tau \\
&\cos\theta\frac{\partial x}{\partial \phi} + \sin\theta\frac{\partial x}{\partial \phi} = 0 \\
&\theta = \phi \quad \text{at} \quad \tau = 0
\end{aligned}
\tag{D.34}
$$

This relationship can be used to trace bi-characteristic curves. Along these bi-characteristic directions the characteristic conditions take the form,

$$
A_v du_v = \left[B + C_v \left\{ \cos\theta\, \nu_i \frac{\partial u_v}{\partial x_i} - \sin\theta \mu_i \frac{\partial u_v}{\partial x_i} \right\} \right] d\tau \tag{D.35}
$$

where

$$
\begin{aligned}
A_v &= A_{1v} + A_{1v}\cos\theta + A_{2v}\sin\theta \\
B_v &= B_{1v} + B_{1v}\cos\theta + B_{2v}\sin\theta \\
C_v &= C_{1v} + C_{1v}\cos\theta + C_{2v}\sin\theta
\end{aligned}
\tag{D.36}
$$

where all the coefficients A_{1v}, B_{1v}, etc. are independent of θ.

APPENDIX E NUMERICAL DETERMINATION OF BI-CHARACTERISTICS AND INTEGRAL CHARACTERISTIC EQUATIONS

As indicated in Chapter 5 and 6, the coefficient matrices are sufficiently complicated that the characteristics of the system must be computed numerically. The equations linearly combined through the computed eigenvector in the form of Equation (6.11) still include derivatives with respect to x, y and t. To derive the characteristic equations with derivatives only in two directions, the bi-characteristics should first be determined. Since the characteristics are computed numerically, the bi-characteristics and characteristic equations must also be estimated numerically. In this appendix, a procedure is developed to numerically establish characteristic equations along approximate bi-characteristics.

E.1 General Procedure

Linear combination of the quasilinear governing equations gives

$$\sum_{i=1,4} \ell_i \cdot \left(\frac{\partial q_i}{\partial t} + A_x^i \frac{\partial q_i}{\partial x} + A_y^i \frac{\partial q_i}{\partial y} \right) = \sum_{i=1,4} \ell_i \cdot S_i \qquad \text{(E.1)}$$

where $q=(H, \overline{\eta}, U_b, V_b,)$ and ℓ_i is a left eigen-vector. There are four eigen-vectors for the present system, accordingly four equations in the form of Equation (E.1) are available. But any one of them is sufficient to demonstrate the procedure for deriving integral characteristic equations. Equation (E.1) is written out as

$$\begin{aligned} &\ell_1 \frac{\partial H}{\partial t} + a_x \frac{\partial H}{\partial x} + a_y \frac{\partial H}{\partial y} + \ell_2 \frac{\partial \overline{\eta}}{\partial t} + b_x \frac{\partial \overline{\eta}}{\partial x} + b_y \frac{\partial \overline{\eta}}{\partial y} + \\ &\ell_3 \frac{\partial U_b}{\partial t} + c_x \frac{\partial U_b}{\partial x} + c_y \frac{\partial U_b}{\partial y} + \ell_4 \frac{\partial V_b}{\partial t} + d_x \frac{\partial V_b}{\partial x} + d_y \frac{\partial V_b}{\partial y} \;=\; S \end{aligned} \qquad \text{(E.2)}$$

where $a_x = \ell_1 A_x(1,1) + \ell_2 A_x(2,1) + \ell_3 A_x(3,1) + \ell_4 A_x(4,1)$, and a_y, b_x,... are similarly

derived.

The fact that Equation (E.2) can always be transformed to an equation with derivatives only in two directions suggests a hypothetical equation:

$$\begin{aligned}
&m_1(C_t^1\frac{\partial H}{\partial t}+C_x^1\frac{\partial H}{\partial x}+C_y^1\frac{\partial H}{\partial y})+m_2(C_t^1\frac{\partial \overline{\eta}}{\partial t}+C_x^1\frac{\partial \overline{\eta}}{\partial x}+C_y^1\frac{\partial \overline{\eta}}{\partial y})\\
&+m_3(C_t^1\frac{\partial U_b}{\partial t}+C_x^1\frac{\partial U_b}{\partial x}+C_y^1\frac{\partial U_b}{\partial y})+m_4(C_t^1\frac{\partial V_b}{\partial t}+C_x^1\frac{\partial V_b}{\partial x}+C_y^1\frac{\partial V_b}{\partial y})\\
&+n_1(C_t^2\frac{\partial H}{\partial t}+C_x^2\frac{\partial H}{\partial x}+C_y^2\frac{\partial H}{\partial y})+n_2(C_t^2\frac{\partial \overline{\eta}}{\partial t}+C_x^2\frac{\partial \overline{\eta}}{\partial x}+C_y^2\frac{\partial \overline{\eta}}{\partial y})\\
&+n_3(C_t^2\frac{\partial U_b}{\partial t}+C_x^2\frac{\partial U_b}{\partial x}+C_y^2\frac{\partial U_b}{\partial y})+n_4(C_t^2\frac{\partial V_b}{\partial t}+C_x^2\frac{\partial V_b}{\partial x}+C_y^2\frac{\partial V_b}{\partial y})=S
\end{aligned} \tag{E.3}$$

where (C_t^1, C_x^1, C_y^1) and (C_t^2, C_x^2, C_y^2) are two vectors in (x-y-t) space, and m_i and n_i are coefficients to be determined. Equation (E.3) is equivalent to

$$\ell_1\frac{dh}{ds}+\ell_2\frac{d\eta}{ds}+\ell_3\frac{du}{ds}+\ell_4\frac{dv}{ds}+n_1\frac{dh}{dz}+n_2\frac{d\eta}{dz}+n_3\frac{du}{dz}+n_4\frac{dv}{dz}=S \tag{E.4}$$

where

$$\frac{d}{ds}=C_t^1\frac{\partial}{\partial t}+C_x^1\frac{\partial}{\partial x}+C_y^1\frac{\partial}{\partial y} \tag{E.5}$$

and

$$\frac{d}{dz}=C_t^2\frac{\partial}{\partial t}+C_x^2\frac{\partial}{\partial x}+C_y^2\frac{\partial}{\partial y} \tag{E.6}$$

Comparing the terms in Equation (E.2) with their counterparts in Equation (E.3) gives

$$\begin{aligned}
&m_1C_t^1+n_1C_t^2=\ell_1,\quad m_1C_x^1+n_1C_x^2=a_x,\quad m_1C_y^1+n_1C_y^2=a_y\\
&m_2C_t^1+n_2C_t^2=\ell_2,\quad m_2C_x^1+n_2C_x^2=b_x,\quad m_2C_y^1+n_2C_y^2=b_y\\
&m_3C_t^1+n_3C_t^2=\ell_3,\quad m_3C_x^1+n_3C_x^2=c_x,\quad m_3C_y^1+n_3C_y^2=c_y\\
&m_4C_t^1+n_4C_t^2=\ell_4,\quad m_4C_x^1+n_4C_x^2=d_x,\quad m_4C_y^1+n_4C_y^2=d_y
\end{aligned} \tag{E.7}$$

Eequation (E.7) gives 12 constraints for 14 unknowns, i.e. C_t^1, C_x^1, C_y^1, C_t^2, C_x^2, C_y^2, m_1, m_2, m_3, m_4, n_1, n_2, n_3, and n_4. But some of the unknowns can be absorbed into other unknowns, for example, m_1 may be absorbed by C_t^1, and n_1 by C_t^2, or vice versa. This would lead to 12 constraints for the same number of unknowns.

As indicated in Appendix D, there are infinite pairs of directions on a characteristic surface which could satisfy Equation (E.3). This implies that the 12 constraints in Equation (E.7) are not linearly independent. In this study, the pair consisting of bi-characteristic direction and the t=constant direction on the characteristic surface is of interest.

Let the bi-characteristic vector from a point be denoted by (C_t^1, C_x^1, C_y^1), and the t=constant vector by (C_t^2, C_x^2, C_y^2). By definition (see Appendix D), $C_t^2=0$.

Setting C_t^2 equal to zero and factoring C_t^1 into m_i (This is equivalent of setting $C_t^1=1$, then C_x^1 and C_y^1 physically represent the information propagation speeds in the x and y directions; see Appendix D for details), the four constraints in the first column of Equation (E.7) become: $m_1=\ell_1$, $m_2=\ell_2$, $m_3=\ell_3$, and $m_4=\ell_4$. Substituting the values for m_i into the remaindering constraints in Equation (E.7) gives

$$\begin{aligned}
&\ell_1 C_x^1 + n_1 C_x^2 = a_x, \quad \ell_1 C_y^1 + n_1 C_y^2 = a_y \\
&\ell_2 C_x^1 + n_2 C_x^2 = b_x, \quad \ell_2 C_y^1 + n_2 C_y^2 = b_y \\
&\ell_3 C_x^1 + n_3 C_x^2 = c_x, \quad \ell_3 C_y^1 + n_3 C_y^2 = c_y \\
&\ell_4 C_x^1 + n_4 C_x^2 = d_x, \quad \ell_4 C_y^1 + n_4 C_y^2 = d_y
\end{aligned} \tag{E.8}$$

By inspection, one of n_1, n_2, n_3 and n_4 may be factored into C_x^2 and C_y^2. This would

further eliminate one unknown and leave a total of 7 unknowns. This also implies that the eight constraints in Equations (E.8) are not linearly independent. Only a nontrivial unknown can be factored into other unknowns. Since the current system is partially similar to the shallow water wave equations, a careful examination about the characteristicequations for the shallow water wave equations suggests that n_4 be set at unity.

As established in Appendix D, the following relationships exist for the bi-characteristics vector and t=constant vector:

$$C_x^1 \cos\theta + C_y^1 \sin\theta = \lambda \tag{E.9}$$

$$C_x^2 \cos\theta + C_y^2 \sin\theta = 0 \tag{E.10}$$

where λ is an eigenvalue for a direction θ. Since λ and θ are known, Equations (E.9) and (E.10) are linear, and preferable to those in Equation (E.8) which are usually nonlinear. By using Equations (E.9) and (E.10), it can be shown that the constraints on the two columns in Equation (E.8) are linearly dependent. A brief proof is given here.

According to the definition for a left eigen-vector

$$\vec{\ell} \cdot (A_x \cos\theta + A_y \sin\theta) = \lambda \cdot \vec{\ell} \tag{E.11}$$

where A_x and A_y are the coefficient matrices, as in Equation (E.1). Writing out Equation (E.11) results in four equations:

$$\lambda = (a_x \cos\theta + a_y \sin\theta) / \ell_1 \tag{E.12}$$

$$\lambda = (b_x \cos\theta + b_y \sin\theta) / \ell_2 \tag{E.13}$$

$$\lambda = (c_x \cos\theta + c_y \sin\theta) / \ell_3 \tag{E.14}$$

$$\lambda = (d_x \cos\theta + d_y \sin\theta) / \ell_4 \tag{E.15}$$

Now the two constraints on the fourth row in Equation (E.8) are used to prove that they are linearly dependent. Notice that n_4 is set at unity. By expressing C_y^1 as a function of C_x^1 from Equation (E.9) and C_y^2 as a function of C_x^2 from Equation (E.10), and substituting the functions for C_y^1 and C_y^2 into the constraint on the second column gives

$$\ell_4 \frac{\lambda - C_x^1 \cos\theta}{\sin\theta} + \frac{C_x^2 \cos\theta}{\sin\theta} = d_y \tag{E.16}$$

which can be organized as

$$\ell_4 C_x^1 + C_x^2 = \frac{\lambda \ell_4 - d_y \sin\theta}{\cos\theta} \tag{E.17}$$

The right side of the above equation is d_x according to Equation (E.15). Hence these two constraints are linearly dependent. Similarly, the two constraints on the other rows can be proven linearly dependent.

Equations (E.8) through (E.10) give six linearly independent equations for seven unknowns. By choosing C_x^1 as a free parameter, the six other unknowns can be related to C_x^1 as

$$C_y^1 = (\lambda - C_x^1 \cos\theta) / \sin\theta \tag{E.18}$$

$$C_x^2 = d_x - \ell_4 C_x^1 \tag{E.19}$$

$$C_y^2 = -c \tan\theta (d_x - \ell_4 C_x^1) \tag{E.20}$$

$$n_1 = \frac{a_x - \ell_1 C_x^1}{d_x - \ell_4 C_x^1} \tag{E.21}$$

$$n_2 = \frac{b_x - \ell_2 C_x^l}{d_x - \ell_4 C_x^l} \tag{E.22}$$

$$n_3 = \frac{c_x - \ell_3 C_x^l}{d_x - \ell_4 C_x^l} \tag{E.23}$$

One more constraint must be introduced in order to have unique solutions. The equation of the characteristic cone would provide this necessary constraint. Since the characteristic cone differs significantly for different families of characteristics, it is necessary to discuss each family individually. The flow characteristics is not used in the numerical scheme proposed in Chapter 6, so it will not be discussed.

E.2 Approximate Equation For The Wave Characteristic Cone

Since the wave characteristics of the current system is very similar to those of the shallow water wave equations, it is assumed that the cone of the wave characteristics can be expressed in the form

$$(dx - udt)^2 + (dy - vdt)^2 = (C\ dt)^2 \tag{E.24}$$

where C, u and v are determined by Equations (D-5) through (D-7) in Appendix D. With C_x =dx/dt and C_y =dy/dt, the above equation can also be written as

$$(C_x - u)^2 + (C_y - v)^2 = C^2 \tag{E.25}$$

Since the bi-characteristics also lies on the cone, C_x^l and C_y^l salso atisfy Equation (E.25). Approximating the eigenvalue λ by C+ucosθ+vsinθ. and solving for C_x^l and C_y^l from Equations (E.25) and (E.9) gives

$$C_x^l = u + C\cos\theta \tag{E.26}$$

$$C_y^l = v + C\sin\theta \tag{E.27}$$

Once C_x^l and C_y^l are solved, the rest of unknowns can be obtained from Equations (E.18) through (E.23).

Numerically, C, u and v can be computed by using the eigen-values in four directions, normally in 0, $\pi/2$, π, $3\pi/2$:

$$C = (\lambda_{\theta=0} + \lambda_{\theta=\pi/2} + \lambda_{\theta=\pi} + \lambda_{\theta=3\pi/2}) / 4 \tag{E.28}$$

$$u = [(\lambda\cos\theta)_{\theta=0} + (\lambda\cos\theta)_{\theta=\pi/2} + (\lambda\cos\theta)_{\theta=\pi} + (\lambda\cos\theta)_{\theta=3\pi/2}) / 4 \tag{E.29}$$

$$v = [(\lambda\sin\theta)_{\theta=0} + (\lambda\sin\theta)_{\theta=\pi/2} + (\lambda\sin\theta)_{\theta=\pi} + (\lambda\sin\theta)_{\theta=3\pi/2}) / 4 \tag{E.30}$$

E.3 Approximate Equation For The Energy Characteristic Cone

A typical characteristic cone of wave energy propagation is shown in the Figure E.1. In contrast to wave characteristics, there is no backward transmission for wave energy in this model.

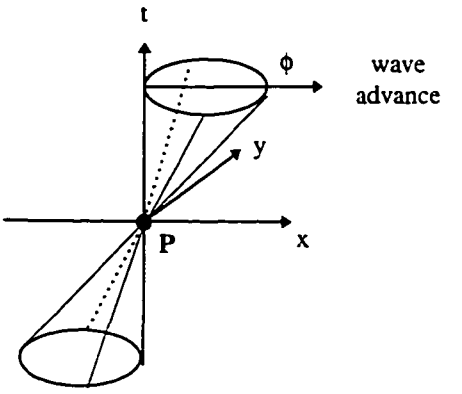

Figure E.1 Sketch Of The Energy Characteristic Cone

The equation of the energy characteristic cone is:

$$(dx)^2 + (dy)^2 = [C_e \cdot dt]^2 \tag{E.31}$$

and C_e may be approximated by

$$C_e(\theta) = \lambda_e \cdot f(\theta - \varphi) \tag{E.32}$$

where λ_e is the computed eigenvalue corresponding to wave energy propagation, and $f(\theta-\phi)$ is a function taking account of the fact that there is no backward propagation, in form:

$$f(\theta-\varphi) = \frac{|\cos(\theta-\varphi)| + \cos(\theta-\varphi)}{2\cos(\theta-\varphi)} = \begin{cases} 1 & \text{for } |\theta-\varphi| \le \frac{\pi}{2} \\ 0 & \text{Otherwise} \end{cases} \tag{E.33}$$

Then C_x^l and C_y^l can be determined from the equation of the characteristic cone and Equation (E.18). Under normal wave conditions, the eigen-value for the energy characteristic can be approximated by $C_g\cos(\theta-\varphi)$, as supported by Figure 6.1, where C_g is the wave group speed. Substituting $\lambda_e = C_g\cos(\theta-\varphi)$ into Equations (E.33) and (E.18), and solving C_x^l and C_y^l gives

$$\begin{aligned} C_x^l &= \lambda^e \cos\theta = C_g \cos(\theta-\varphi)\cos\theta \\ C_y^l &= \lambda^e \sin\theta = C_g \cos(\theta-\varphi)\sin\theta \qquad \text{for } |\theta-\varphi| \le \frac{\pi}{2} \end{aligned} \tag{E.34}$$